Dynamics of Extreme-Mass-Ratio binaries

d'Ambrosi, G.

2016

document version
Publisher's PDF, also known as Version of record

VRIJE UNIVERSITEIT

Dynamics of Extreme-Mass-Ratio binaries

Extraction of gravitational waves beyond Last Stable Orbit and introduction of spin in the particle limit

ACADEMISCH PROEFSCHRIFT

ter verkrijging van de graad Doctor aan
de Vrije Universiteit Amsterdam,
op gezag van de rector magnificus
prof.dr. V. Subramaniam,
in het openbaar te verdedigen
ten overstaan van de promotiecommissie
van de Faculteit der Exacte Wetenschappen
op donderdag 21 april 2016 om 11.45 uur
in de aula van de universiteit,
De Boelelaan 1105

door

Giuseppe D'Ambrosi

geboren te Ascoli Piceno, Italië

promotoren: prof.dr. J.F.J. van den Brand
prof.dr. J.W. van Holten

A man may be attracted to science for all sorts of reasons. Among them are the desire to be useful, the excitement of exploring new territory, the hope of finding order, and the drive to test established knowledge. These motives and others besides also help to determine the particular problems that will later engage him. Furthermore, though the result is occasional frustration, there is good reason why motives like these should first attract him and then lead him on. The scientific enterprise as a whole does from time to time prove useful, open up new territory, display order, and test long-accepted belief. Nevertheless, the individual *engaged on a normal research problem* is almost never doing any one of these things. *Once engaged, his motivation is of a rather different sort. What then challenges him is the conviction that, if only he is skillful enough, he will succeed in solving a puzzle that no one before has solved or solved so well. Many of the greatest scientific minds have devoted all of their professional attention to demanding puzzles of this sort. On most occasions any particular field of specialization offers nothing else to do, a fact that makes it no less fascinating to the proper sort of addict.*

-T.S. Kuhn, The Structure of Scientific Revolutions

Reading committee:	prof.dr. R. Fleischer (Vrije Universiteit Amsterdam) prof.dr. P.J.G. Mulders (Vrije Universiteit Amsterdam) prof.dr. G. Nelemans (Radboud Universiteit Nijmegen) Dr. H.J. Bulten (Vrije Universiteit Amsterdam) Dr. M. van de Meent (University of Southampton)
English title:	Dynamics of Extreme Mass Ratio binaries
Printed by:	Gildeprint Drukkerijen - The Netherlands
Front cover:	Figure designed by Maura Graziani

This work is part of the research programme of the Foundation for Fundamental Research on Matter (FOM), which is part of the Netherlands Organisation for Scientific Research (NWO).

* *

Contents

* *

* *

Motivations and Outline

* *

After one century from its first formulation, General Relativity (GR) is still the most credited theory of the gravitational interaction having found many direct and indirect experimental confirmations [1]. Among the theoretical predictions of General Relativity that until this year lacked direct experimental evidence there were Gravitational Waves (GWs), local perturbations of the spacetime metric travelling through spacetime itself [2]. First the discovery of the binary pulsar PS 1913+16 [3] provided a strong indirect evidence of their existence. Then direct evidence of GWs came early this year when the waves produced by a binary coalescence of black holes have been detected for the first time [4]. Moreover other cosmic processes produce gravitational waves, but with different wavelengths of the same radiative spectrum. This is an example of how gravitational radiation can inform us about many different astrophysical phenomena.

GWs can help us constrain competitive theories of gravity or extensions of GR, which predict different gravitational signals for a variety of sources [5, 6]. Moreover they represent a completely unexplored realm for astrophysical research [7], which can complement current observations based on the electromagnetic spectrum. The direct detection of GWs opens a new era of astrophysical research and provides new tests of GR [8] and possibly quantum gravity tests [9]. Therefore the experimental detection of Gravitational Waves was long expected [10, 11, 12], and it is naturally coupled to theoretical source modelling and waveform prediction. The research work and the topics discussed in this thesis contribute to the latter and to a better understanding of the general relativistic dynamics of compact objects.

Astrophysical research makes extensive use of GR calculations, whenever the Newtonian mechanics is not sufficient for the desired level of accuracy and when non-Newtonian phenomena appear. In particular the search for *strong gravity* has acquired a lot of relevance. Strong Gravity can be seen in opposition to weak gravity, but a quantitative threshold between the two scales is given by the ratio [1]

$$\epsilon \sim \frac{GM}{Rc^2},$$

where R is a typical dimension of the phenomenon under consideration, and M its characteristic mass scale. For a non-rotating black-hole horizon this is $\epsilon \sim 1$, for neutron stars $\epsilon \sim 0.2$. These are considered in the regime of strong gravity. Solar system is at $\epsilon < 10^{-5}$,

this is no strong gravity[1]. Since GR is so effective in weak-field regime, investigating strong gravity, i.e. when gravitational fields are strong and spacetime curvature is large, can also give insight into modifications of GR [13]. However, the recent discovery by the joint aLIGO and aVirgo collaborations of the black-hole binary emitting GWs [4] is the first test we have for GR in the strong regime, and no deviation from GR predictions has been measured yet [8]. The computational and theoretical techniques employed in the regime of strong gravity differ from those of weak field dynamics and the Extreme Mass Ratio systems discussed in this thesis are considered within this regime.

Extreme-Mass-Ratio compact binaries

Prominent sources of Gravitational Waves are compact binary coalescences [14], two-star systems such as Neutron Star-Black Hole (NS-BH) or Black Hole-Black Hole (BH-BH). While comparable-mass binaries are already accessible for the ground-based interferometers aLIGO and aVIRGO, space-based detectors such as eLISA will probe the frequency range of signals from Extreme-Mass-Ratio binaries (EMR) [15]. The latter consist of a central Supermassive Black Hole ($10^5 - 10^7 M_\odot$, $M_\odot$ being the mass of Sun) with a smaller companion inspiralling around it until the eventual plunge and merge. The best theoretical description of EMR inspirals is given in terms of Black Hole perturbation theory, i.e. the smaller companion is taken to be a probe in the central body's background metric. We have investigated the simplest case for non-spinning Black Holes, along the path started by Regge and Wheeler [16], devising a solution of the geodesic equations, fully known analytically, that models the plunge phase.

One way of improving the description of the inspiralling orbit of the minor companion in an EMR binary is by considering deviations from a known geodesic orbit. As the motion is mainly driven by the bigger central body, it is expected to be quasi-geodesic and small deviations from this can account for non-conservative effects, such as gravitational radiation. This idea has been successfully implemented for eccentric orbits already in [17, 18], giving insight in the adiabatic inspiral phase of the coalescence. The method consists mainly in solving the Regge-Wheeler equations for a body in an orbit deviated from an analytically known geodesic, in this case circular orbits in Schwarzschild background.

In order to extend this method to the final phases of EMR coalescences, in [19] we developed first the analytical orbit for the plunge phase, so-called "ballistic orbits". This provided insight into a new sector of geodesic motion in Schwarzschild metric beyond the Last Stable Orbit $r = 6M$. Subsequently a numerical solution of the Regge-Wheeler equations based on these orbits has been evaluated using Lousto-Price algorithm [20]. The radiative results obtained in this way agree with the expectations from quasi-geodesic motion [21, 22].

Moreover we have extended our analysis to include the first-order deviations from these orbits, in order to successfully overcome the limits of the aforementioned ballistic orbits. This became a valid tool to model plunging orbits for EMR binaries, tuning

[1] Another definition refers to the region where spacetime curvature, represented by the Riemann tensor, is comparable to the inverse length squared of a typical dimension $\frac{GM}{R^3c^2} \sim \frac{1}{\ell^2}$.

their parameters, such as orbital energy and angular momentum, according to the desired criteria.

Compact spinning objects in curved spacetime

Another interesting case to consider is when the companion body is spinning, which would account for EMR binaries with rotating Neutron Stars, for instance. The equations of motion for a classical spinning object in Special (and General) Relativity are well-known [23, 24]. They employ different spin supplementary conditions to make the system mathematically determined and solvable [25]. Within the particle approximation and to first order in spin they simplify such that the issue of choosing the supplementary condition can be easily overcome.

We introduced a different road to derive dynamics within this framework based on an effective symplectic structure with no need of supplementary conditions, valid for general Hamiltonians, that allows to obtain constants of motion, and consequently develop the kinematical description of a spinning particle -representative of a compact object- in a curved background [26, 27]. This construction returns the usual equations of motion with a minimal Hamiltonian, and gives way to several generalizations [28] as well. Establishing the formalism for this and other applications is the content of the last part of this thesis.

Outline of this thesis: in chapter 1 a self-contained introduction to General Relativity and Gravitational Waves is presented, together with a brief overview of the current experimental efforts to detect GWs. Black-Hole binaries are also discussed at the end of the chapter.

In the second chapter an introduction to Black Holes and to Black-Hole perturbation theory is given, necessary for the study of Extreme Mass Ratio systems, followed by basic concepts of geodesic deviations, which are used here as an orbit perturbation method.

In chapter 3 the study of a particular solution of the geodesic equations in Schwarzschild metric is presented. This is used as a model for the plunge phase of an Extreme Mass Ratio binary and gravitational radiation is extracted for this system. Strong points and limitations of the model are discussed. In the fourth chapter improvements of the methods presented in chapter 3 are discussed, together with their limits. These new orbits take advantage of the geodesic deviation method to obtain new results.

In chapter 5 we establish the formalism to extend the results obtained in the previous chapters to the case of spinning particles. These constitute a model for rotating compact objects such as neutron stars in a binary system. We compare the method with existing literature and track the future directions for its application.

The last part is the Conclusion of this thesis. After that a summary accessible to a broader audience is provided.

Notation

Before diving into the core of this dissertation, we wish to give some useful remarks about the notation and units used throughout this work.

If not explicitly stated, the used units are the geometrized ones, in this case $c = G = 1$. In order to restore the usual units one has to multiply the quantity of interest by the appropriate powers and factors of the speed of light c and the universal gravitational constant G. For instance, with these units, length and time have the same dimensions as mass, therefore velocity is dimensionless and it must be multiplied by $c \sim 3 \cdot 10^8 \frac{m}{s}$ to have it in meters per second.

For all the vectors and tensors appearing in the following, every Greek index refers to a quadri-dimensional Lorentz index, $\rho = 0 \dots 3$, where the 0-component refers to time, and the other three are the spatial ones, corresponding to the Cartesian coordinates (x, y, z) or more often to the spherical ones (r, θ, φ) as will be mentioned explicitly. For only the spatial components a latin index will be used, i.e. $j = 1, 2, 3$. Repeated indices are summed over, as for Einstein convention.

Common partial differentiation can be indicated in subscripts with a comma symbol, as it is conventional in General Relativity, while covariant differentiation will be indicated by a semicolon, namely

$$\partial_\nu A^\mu = \frac{\partial A^\mu}{\partial x^\nu} = A^\mu{}_{,\nu} \qquad \text{while} \qquad \nabla_\nu A^\mu = A^\mu{}_{;\nu} = A^\mu{}_{,\nu} + \Gamma^\mu_{\nu\lambda} A^\lambda .$$

The convention (same as Weinberg [29]) about signature of the Minkowski metric is

$$(ds)^2 = \eta_{\mu\nu} dx^\mu dx^\nu = -(dx^0)^2 + (\mathbf{dx})^2$$

and the sign of the Riemann tensor

$$R^\mu{}_{\nu\lambda\kappa} = \partial_\kappa \Gamma^\mu_{\nu\lambda} - \partial_\lambda \Gamma^\mu_{\nu\kappa} + \Gamma^\mu_{\rho\kappa} \Gamma^\rho_{\nu\lambda} - \Gamma^\mu_{\rho\lambda} \Gamma^\rho_{\nu\kappa} .$$

Finally symmetrization and antisymmetrization on a couple of indices will be indicated in the following way:

$$A_{(\mu\nu)} = \frac{1}{2} \left(A_{\mu\nu} + A_{\nu\mu} \right) \qquad\qquad A_{[\mu\nu]} = \frac{1}{2} \left(A_{\mu\nu} - A_{\nu\mu} \right) .$$

* *

1 Introduction

* *

Newtonian mechanics represented a revolution in modern science, also for the contributions to gravity and astronomy. Every other astronomical observation back since has been interpreted in the light of Newton's ideas, until a new paradigm stepped forward a hundred years ago. This is currently the most credited theory of the gravitational interaction and the leading interpretation of astrophysical phenomena and our universe: General Relativity, formulated by Einstein in a series of works between 1907-1916 [30].

During this century several discoveries have confirmed General Relativity (GR) as an effective theory for the gravitational interaction, making it a full-fledged field in physics research. The classical proofs date back to the beginning of the century and were suggested by Einstein himself: the perihelium shift in the orbit of Mercury, a well-known phenomenon discovered by Le Verrier[1] which could find a precise explication through GR [32], and the deflection of light around a massive object, such as the Sun, which Einstein regarded as necessary to prove, as he would "feel very sorry for the dear Lord, for the theory *is* correct!", if such experiment would have failed to prove GR right [33]. These are the so-called "classical proofs" of GR.

Other proofs came later, like observations of gravitational lensing by NASA [34] and the famous gravitational time-delay experiment by Pound and Rebka [35]. Finally, the Global Positioning System (GPS) would not be so effective and precise (positional accuracies of around 15 meters and 50 nanoseconds in time transfer accuracy everywhere on Earth[2]) without GR corrections. The same applies to navigation using Earth-orbiting atomic clocks and to overall satellites' motion; most of the wonderful possibilities and apps of our personal smartphones owe their existences to General Relativity.

After the initial phase (late 19th century- 1919) when the foundations of Special and General Relativity were laid down and the classical proofs of GR mentioned above were performed, there was a period during which technology and experiments could not catch up with the theoretical advancements in the fields. This ended in 1960 with many measurements and verifications of GR predictions, such as the gravitational redshift and the soundest indirect proof we have of the existence of Gravitational Waves, the orbital period of the Hulse-Taylor binary pulsar [36]. Many alternative theories of gravity were

[1] He also recognized that the phenomenon could not be explained solely on the basis of Newtonian mechanics and with the perturbations of the known planets [31], suggesting the existence of a hypothetical planet even closer to the Sun than Mercury, i.e. "Vulcan". No such planet has ever been found.

[2] And military applications can reach even higher accuracies.

unable to fit the experimental results and therefore discarded, turning GR into the leading theory of gravity.

This chapter is an introduction to general relativity and gravitational waves in particular. The chapter opens up with a summary of the main ideas behind General Relativity and the concept of spacetime, giving way afterwards to the equations of motion in a gravitational field and their symmetries. In the second section the concept of gravitational waves and how we detect them are made clear. Finally a brief description of the sources of gravitational radiation is presented, with an emphasis on Extreme Mass Ratio binaries, which are the main object of investigation of this work.

1.1 Gravity and General Relativity

General Relativity is the leading theory for the gravitational interaction and a growing field in Physics. This is possible mainly because of the abundance of astrophysical observations that we have been able to make from the '60s onwards (so-called "golden era" of GR [1]). The discovery of gravitational waves also adds another valid tool to inspect astrophysical sources and to study limits and validity of GR itself.

The conceptual basis and the key starting concept of GR is in the *Equivalence Principle* and its different formulations. The first historical formulation is related to Newton's investigations about the difference between the inertial mass m_i and the gravitational mass m_g. The first one is the one appearing in the kinematics as representative of the inertia of a body, the second one is the source of gravity and the "charge" experiencing gravity, in the same way as the electric charge is for the electromagnetic interactions. Newton could establish that every form of matter gravitates in the same manner, because pendula of different materials, but with the same length, oscillate with the same periods. To this one has to add the Universality of Free Fall, tested by Galilei as well [37] from the leaning tower of Pisa (Italy)[3], and get to the conclusion that inertial mass and gravitational mass are, if not equal, proportional to each other. The famous Eötvös experiment and following ones have shown that the ratio $\frac{m_i}{m_g}$ between the two kinds of mass is 1 up to a sensitivity of 10^{-13} [38, 1], with current experiments being developed to push this limit even further down, as MICROSCOPE, to be launched within this year [39].

The fact that the bodies with different composition and internal structure fall independently of these properties when not acted upon by any other force than gravity, is the main content of the *Weak Equivalence Principle* (WEP), certainly true in the Newtonian

[3] Actually the reported experiments of falling bodies contrasting Aristotle's principle that heavier bodies fall faster and showing the universality of free fall were performed at Delft (the Netherlands) in 1586, by S. Stevin and J. C. de Groot. Not far from where Galilei's manuscript was first published (Leiden) with similar results by using inclined planes and more mathematical rigour. It is generally accepted by historians that Galilei's experiment from Pisa tower is only a thought experiment.

limit. Adding local Lorentz invariance and local position invariance to the WEP sets up the *Einstein Equivalence Principle* (EEP):

- the Weak Equivalence Principle is always valid;
- the results of any local non-gravitational experiment performed in a freely falling frame are independent of the motion of the reference frame;
- the results of any local non-gravitational experiment are independent of the position in spacetime in which the experiment is performed.

The EEP is often exemplified saying that an observer cannot distinguish locally between a constant gravitational field or an accelerated frame. Clearly if $m_i \neq m_g$, if the WEP were not valid in the first place, this equivalence of accelerated frames could not be possible at all.

Asking that these principles are valid for all fundamental physics, including gravity, is often called the *Strong Equivalence Principle* (SEP), i.e. even when the experiments are performed with some background gravitational field, it is always possible to find an observer in absence of gravity obtaining locally the same results. The EEP is the driving principle of the theory of General Relativity, because it entails a metric theory of gravity, where spacetime is endowed with a symmetric metric, the trajectories of freely falling bodies are geodesics of that metric, and that the non-gravitational laws of physics are those of Special Relativity in a local freely falling frame. Such is GR.

Therefore it is a consequence of the Equivalence Principle to interpret space and time as a manifold and gravitational fields as a manifestation of its geometry. A different interpretation of the EEP or a different application, even to a minor level, might lead to competing theories of gravitation, be they metric theories like GR, or not [40].

The strong connection between the physics of gravitation and geometry, and in particular the Riemannian geometry, was repeatedly remarked by Poincaré and Einstein and it is the core concept of GR. In the following section we describe the fundamental equations of GR, relying on the language of differential geometry.

1.1.1 The geodesic equations

Already with the advent of *Special Relativity* more than a hunded years ago [41] the concepts of absolute space and time were replaced by the more complicated structure of spacetime. The idea is that there is no preferred inertial reference system, all inertial frames are equivalent and there are no absolute concepts of space and time. Rather, time and space have the same dignity as coordinates. Special Relativity establishes the relative character of velocity and the relations among different reference frames comply with Lorentz transformations, rather than Galilei's. The geometry of such spacetime can be conveniently described in Cartesian coordinates by Minkowski metric

$$\eta_{\mu\nu} = \begin{pmatrix} -1 & 0 & 0 & 0 \\ 0 & 1 & 0 & 0 \\ 0 & 0 & 1 & 0 \\ 0 & 0 & 0 & 1 \end{pmatrix}, \qquad (ds)^2 = -(d\tau)^2 = \eta_{\mu\nu} dx^\mu dx^\nu, \tag{1.1.1}$$

where $(d\tau)$ is the proper time element, invariant to any coordinate transformation. A particle's trajectory in space is replaced by the particle's worldline in spacetime, described by an affine parameter, here the proper time τ, i.e. the time as measured by the particle itself. The line element ds represents the spacetime separation between two events with a temporal distance $dt = dx^0$ and a spatial distance dx^i. All the results of Special Relativity can be derived from Minkowski metric.

The word "general" in *General theory of Relativity* shows that the theory has been introduced as a generalisation of the Special theory of Relativity. Although there has been some confusion in the past about what exactly is being generalised [42, 43], originally, i.e. in Einstein's views, it was the extension of the principle of relativity from inertial frames to accelerated frames, and virtually to all frames in arbitrary motion. That is the consequence of the Strong Equivalence Principle making an accelerated frame locally indistinguishable from one within a constant gravitational field. Independently of whether this holds or not and to which extent "locally" [40], General Relativity surely generalises the geometrical concepts behind spacetime, extending them to the gravitational interaction. It is a metric theory of gravity, where rather than using a field behaving in the same way regardless of the different bodies, a geometric description is preferred and thought more convenient.

In GR spacetime is a manifold whose geometry is modified by the masses and the gravitational fields, therefore the line element (1.1.1) is still a covariant quantity, irrespective of the reference frame used, but the underlying metric is not necessarily Minkowskian, it can be any symmetric 2-tensor $g_{\mu\nu}$ satisfying metric requirements [44]. So the metric, from an elegant geometrical tool to derive the relativity laws and transformations, turns to be one of the key concepts in the theory of gravitation.

Another important concept is coordinate invariance. Since there is no privileged reference frame, the laws of physics must be formulated in a way, using covariant indices and tensors, that is invariant under regular coordinate transformations. More precisely every diffeomorphism $x^\mu \to x'^\mu(x)$, with $x'^\mu(x)$ an arbitrary smooth function of the position, has to leave the line element (1.1.1) invariant, and this is achieved if the metric tensor transforms accordingly

$$(1.1.2) \quad g_{\mu\nu}(x) \to g'_{\mu\nu}(x') = \frac{\partial x^\rho}{\partial x^\mu}\frac{\partial x^\sigma}{\partial x^\nu} g_{\rho\sigma}(x), \qquad (ds)^2 = g_{\mu\nu}dx^\mu dx^\nu = g'_{\mu\nu}dx'^\mu dx'^\nu.$$

Clearly everytime that Lorentz indices in a quantity are fully contracted and summed over, the quantity under consideration is invariant to such coordinate transformations. Otherwise tensors and vectors transform accordingly, as the metric tensor $g_{\mu\nu}(x)$ did in (1.1.2).

The metric tensor $g_{\mu\nu}$ describes the geometry of the spacetime as it is modified by mass distributions[4]. A constant gravitational field gives back a flat spacetime, perfectly matching the original Minkowski metric, consistently with the Equivalence Principle. In a common laboratory on Earth the gravitational field can be neglected with very good approximation, therefore for many physical applications in different fields the metric is the flat one (1.1.1) and one needs not to employ the laws of GR. This is clearly not the case for astrophysical scales and for every time gravity is studied on its own.

[4] The metric inverse is given by $g^{\mu\nu}$, such that the product $g_{\mu\rho}g^{\rho\nu} = \delta^\mu{}_\nu$.

The introduction of a curved -rather than flat- spacetime modifies the equations of motion accordingly. If in flat spacetime Newton's law of inertia states that a free body in an inertial frame, with no external field involved, will keep its motion along a straight line with the same constant velocity, in curved space this image changes. The free body will keep its motion, but along a path determined by the underlying geometry, which is determined by the global gravitational field. This is summarised in the equations of motion for a free particle in GR, or *geodesic equations*

$$\frac{dx^\mu}{d\tau^2} + \Gamma^\mu_{\nu\lambda}\frac{dx^\nu}{d\tau}\frac{dx^\lambda}{d\tau} = 0, \tag{1.1.3}$$

where τ is the proper time along the particle's worldline, so $u^\mu = \frac{dx^\mu}{d\tau}$ is its 4-velocity vector and $\Gamma^\mu_{\nu\lambda}$ are the connection coefficients, or Christoffel symbols, related to the metric of the spacetime manifold where the particle is living.

A metric spacetime is defined through a metric tensor $g_{\mu\nu}$ and a connection. Whenever the latter is compatible with the metric, it can be induced from the metric itself,

$$\Gamma^\mu_{\nu\lambda} = \frac{1}{2}g^{\mu\rho}\left(g_{\rho\nu,\lambda} + g_{\rho\lambda,\nu} - g_{\nu\lambda,\rho}\right), \tag{1.1.4}$$

making it symmetric $\Gamma^\mu_{\nu\lambda} = \Gamma^\mu_{\lambda\nu}$. The same equations of motion (1.1.3) can be derived via variational principles from a free particle's gravitational action [29]

$$S = -m\int d\tau = -m\int \sqrt{-dx^\mu dx^\nu g_{\mu\nu}}. \tag{1.1.5}$$

The geodesic equations (1.1.3) lie at the heart of General Relativity's interpretation of geometry and gravity. In fact the motion of a free particle $\xi^\mu(\tau)$ in an inertial frame (Newtonian mechanics) is

$$\frac{d^2\xi^\mu}{d\tau^2} = 0, \tag{1.1.6}$$

and the trajectory a straight line with constant velocity. If we look at the same motion from a constantly accelerated frame, one can derive the law of motion by a transformation to curvilinear coordinates $\xi^\mu \to \frac{\partial\xi^\mu}{\partial x^\nu}x^\nu$, obtaining back Eq. (1.1.3). Since the acceleration is constant in the second frame, an observer there cannot tell the difference between accelerated motion and homogeneous gravitational field with strength[5] $\Gamma^\mu_{\nu\lambda}$: another formulation of the Equivalence Principle.

In the case of a massless particle, like a photon, the geodesic equations are still valid, if one indicates with x^μ the position of such particle, but the worldline's description changes: derivatives are taken with respect to an affine parameter different from τ, say λ, because the line element (1.1.1) is identically null $(ds)^2 = -(d\tau)^2 = 0$ as required for light-like trajectories. One needs just to replace λ to τ in (1.1.3), using it as an affine parameter, but not as a proper time.

[5]Notice that this transformation implies that $\Gamma^\mu_{\nu\lambda} = \frac{\partial x^\mu}{\partial\xi^\alpha}\frac{\partial^2\xi^\alpha}{\partial x^\nu\partial x^\lambda}$, which shows manifestly through Lorentz transformation how the connection, despite its indices, is not a tensor.

Another observation [45] can be made from Eq. (1.1.3) multiplying both terms with the mass density of dust ρ,

$$\rho\frac{d^2x^\mu}{d\tau^2}+\rho\Gamma^\mu_{\nu\lambda}\frac{dx^\nu}{d\tau}\frac{dx^\lambda}{d\tau}=0 \quad \Rightarrow \quad \rho\frac{d^2x^\mu}{d\tau^2}=-\Gamma^\mu_{\nu\lambda}t^{\nu\lambda}, \tag{1.1.7}$$

with $t^{\nu\lambda}=\rho u^\nu u^\lambda$ the Energy-Momentum tensor density of dust. The non-tensorial force $f^\mu=t^{\nu\lambda}\Gamma^\mu_{\nu\lambda}$ is analogous to the Lorentz force $f^\mu_{Lorentz}=\rho_{el}u^\nu F^\mu{}_\nu$ acting on a charged particle, the Christoffel symbols playing the role of the electromagnetic field-strength, and the force being quadratic in the velocities, rather than linear. This shows how the Energy-Momentum tensor density of matter plays the role of the source of gravitational interaction, thus leading to the next section, where the equations for the gravitational field are displayed.

1.1.2 Einstein field equations

The geodesic equations (1.1.3) account for motion in a spacetime curved by gravitational fields and masses, but the interaction between these is given by the Einstein field equations [46]. These are at the basis of practically any calculation in General Relativity, as ideally solving them provides the geometric description of the spacetime and the distribution of gravitational fields in it.

They show exactly the interplay between mass and geometry: on the left-hand side one has the Einstein tensor $G^{\mu\nu}$ given by the curvature of the spacetime. This depends strictly on the underlying geometry, for it is built on the "Riemann curvature tensor", which expresses how the spacetime curves locally[6]. Besides, the presence of a non-constant gravitational field implies non-zero curvature; spacetimes such as Minkowski's are flat spacetimes because the corresponding Riemann and Ricci tensors vanish identically at every point, signalling the absence of gradients in the gravitational field. This can be recognized by the definition itself of the Riemann tensor and the Christoffel symbols (1.1.4), where second and first derivatives of the metric appear:

$$R^\mu{}_{\nu\lambda\kappa}=\partial_\kappa\Gamma^\mu_{\nu\lambda}-\partial_\lambda\Gamma^\mu_{\nu\kappa}+\Gamma^\mu_{\rho\kappa}\Gamma^\rho_{\nu\lambda}-\Gamma^\mu_{\rho\lambda}\Gamma^\rho_{\nu\kappa}. \tag{1.1.8}$$

As first derivatives of the metric $g_{\mu\nu,\lambda}$ appear also in a flat spacetime in an accelerated frame, and they can be put to zero with a suitable choice of coordinates, only non-vanishing second or higher derivatives give information about real gravitational fields, hence the importance of the Riemann curvature tensor as in Eq. (1.1.8).

Considering that the equations describing the gravitational interaction must reduce to the well-known $\frac{1}{r^2}$ universal gravitation formula in the Newtonian limit of slow motion or weak-field approximation, the following Einstein field equations were established, combining the curvature of spacetime with the mass (and after Special Relativity also energy) distribution,

$$G_{\mu\nu}=R_{\mu\nu}-\frac{1}{2}Rg_{\mu\nu}=\frac{8\pi G}{c^4}T_{\mu\nu}, \tag{1.1.9}$$

[6] The Riemann curvature tensor $R^\mu{}_{\nu\kappa\lambda}$ gives the displacement caused by a curved spacetime when one tries to parallel-transport a vector along a closed path [43]. In a flat spacetime any vector parallel-transported along any closed path does not experience any change in direction, and its curvature is null throughout the spacetime.

where $R_{\mu\nu} = R^{\kappa}{}_{\mu\kappa\nu}$ is the contraction of the Riemann tensor, or "Ricci tensor", $R = R^{\mu}{}_{\mu}$ is its contraction, the "Ricci scalar", and $T_{\mu\nu}$ is the Energy-Momentum tensor defined on the spacetime manifold with metric $g_{\mu\nu}$. The Eqs. (1.1.9) in vacuum would read the same but with an identically null EM-tensor $T_{\mu\nu} = 0$. Taking the trace of both terms one can draw the following relation

$$R - \frac{4}{2}R = -R = \frac{8\pi G}{c^4}T, \tag{1.1.10}$$

with $T = T^{\mu}{}_{\nu}$, and rewrite (1.1.9) in a different form,

$$R_{\mu\nu} = \frac{8\pi G}{c^4}\left(T_{\mu\nu} - \frac{1}{2}Tg_{\mu\nu}\right), \tag{1.1.11}$$

which is for instance more convenient for weak-field calculations, where the metric on the right-hand side of (1.1.11) can be replaced by the flat Minkowski metric $\eta_{\mu\nu}$. Both the Einstein and the Energy-Momentum tensors are symmetric 2-tensors, $T_{\mu\nu} = T_{\nu\mu}$ and therefore the 16 possible combinations of indices in (1.1.9) actually reduce to 10 different equations. The symmetries of the Riemann tensor and the Bianchi identities provide a null covariant derivative of the Einstein tensor at the left-hand side, in agreement with the conservation of the EM-tensor for isolated systems,

$$G^{\mu\nu}{}_{;\nu} = T^{\mu\nu}{}_{;\nu} = 0. \tag{1.1.12}$$

The 4 equations (1.1.12) reduce the degrees of freedom of the original field equations to only 6 independent equations. These, together with appropriate initial conditions, are a system of differential equations of the second order to be solved in the metric coefficients $g_{\mu\nu}(x^{\lambda})$.

Just as the geodesic equation (1.1.3), also the field equations for gravity can be derived via variational methods from an action,

$$S_G = -\frac{1}{16\pi G}\int d^4x\sqrt{-g}R, \tag{1.1.13}$$

with $g = -det(g_{\mu\nu})$ and R the Ricci scalar. This provides the left-hand side of the field equations (1.1.9), while the right-hand side is given by the corresponding action for matter, which depends on the particular system under study, for instance (1.1.5) is the one for a single particle. This is often the starting point for competing theories of gravity, such as scalar-tensor theories or $f(R)$ theory, to mention a few.

One needs to provide the matter and energy distribution of space for a specific system, be it a star, a planetary system, or a portion of the universe, and then solve the coupled differential equations and find the metric $g_{\mu\nu}$, from which the connection and the equations of motion are derived. On the other hand one can ask for solutions satisfying particular symmetry requirements and then solve, hence finding out all the possible physically sensible spacetimes and theorems about them [47]. The task of solving (1.1.9) is not an easy one and only particular cases are completely integrable in closed form. The rest is left to approximations and numerical methods.

1.1.3 Killing vectors

A considerable help in obtaining the solutions of the equations of motion in a given spacetime comes from the Killing vectors, namely from the knowledge of the symmetries of the underlying spacetime. A Killing vector is a vector ξ^μ satisfying the following relation

$$\xi_{\mu;\nu} + \xi_{\nu;\mu} = 0, \tag{1.1.14}$$

i.e. it is antisymmetric with respect to covariant differentiation. These vectors define a coordinate transformation leaving the metric invariant. If $x^\mu \to x'^\mu = x^\mu + \xi^\mu(x)$, then the metric changes accordingly in $g'_{\mu\nu}(x')$ as in Eq. (1.1.2). To first order in the displacement vector $\xi^\mu(x)$ the metric is invariant $g'_{\mu\nu}(x') = g_{\mu\nu}(x)$ if

(1.1.15)

$$\begin{aligned} g'_{\mu\nu}(x') &= \frac{\partial x^\rho}{\partial x^\mu}\frac{\partial x^\sigma}{\partial x^\nu} g_{\rho\sigma}(x') = \left(\delta^\rho{}_\mu + \partial_\mu \xi^\rho\right)\left(\delta^\sigma{}_\nu + \partial_\nu \xi^\sigma\right)\left(g_{\rho\sigma}(x) + g_{\rho\sigma,\lambda}\xi^\lambda\right) + o(|\xi|^2) \\ &= g_{\mu\nu}(x) + g_{\mu\nu,\lambda}\xi^\lambda + \partial_\mu\xi^\rho g_{\rho\nu} + \partial_\nu \xi^\sigma g_{\mu\sigma} + o(|\xi|^2) \\ &\qquad\qquad \left(\text{using } g_{\mu\nu,\lambda} = g_{\mu\rho}\Gamma^\rho_{\nu\lambda} + g_{\nu\sigma}\Gamma^\sigma_{\mu\lambda}\right) \\ &= g_{\mu\nu}(x) + \left(\partial_\mu\xi^\rho + \Gamma^\rho_{\mu\lambda}\xi^\lambda\right) g_{\rho\nu} + \left(\partial_\nu\xi^\sigma + \Gamma^\sigma_{\nu\lambda}\xi^\lambda\right) g_{\sigma\mu} + o(|\xi|^2) \\ &= g_{\mu\nu}(x) + \nabla_\mu\xi_\nu + \nabla_\nu\xi_\mu + o(|\xi|^2), \end{aligned}$$

so the metric is unchanged if (1.1.14) holds. So Killing vectors are connected to "isometries" in the metric. Moreover a given metric allows manifestly for a Killing vector every time $g_{\mu\nu}$ is independent of a given coordinate, say x^0, for that coordinate system. In fact let $T^{\alpha\ldots}{}_{\beta\ldots}$ be any tensor which has a cyclic coordinate x^0, so that $T^{\alpha\ldots}{}_{\beta\ldots,0} = 0$, then the vector $\xi^\mu = \delta^\mu{}_0$ indicates a direction along which the Lie derivative of $T^{\alpha\ldots}{}_{\beta\ldots}$ is null, namely [48]

$$\pounds_\xi T^{\alpha\ldots}{}_{\beta\ldots} = 0 \quad \Longleftrightarrow \quad \exists \xi^\alpha = \delta^\alpha{}_0 \,:\, T^{\alpha\ldots}{}_{\beta\ldots,0} = 0, \qquad \forall T^{\alpha\ldots}{}_{\beta\ldots} \text{ tensor} \tag{1.1.16}$$

where $\pounds_\xi(\ldots)$ indicates the Lie derivative along the vector ξ^μ. Applying this theorem to the metric tensor gives back exactly the Killing equation (1.1.14).

Identification of Killing vectors for a given metric allows for conserved quantities along a geodesic. Suppose that u^α is tangent to the geodesic affinely parametrized by λ, then

$$\begin{aligned} \frac{d}{d\lambda}(u^\alpha\xi_\alpha) &= (u^\alpha\xi_\alpha)_{;\beta}u^\beta \\ &= u^\alpha{}_{;\beta}u^\beta\xi^\alpha + u^\alpha u^\beta \xi_{\alpha;\beta} = 0, \end{aligned} \tag{1.1.17}$$

upon using the geodesic equation (1.1.3) and antisymmetry of the gradient of Killing vectors (1.1.14). $u_\alpha\xi^\alpha$ is a conserved quantity for motion along the geodesic with tangent u^α in the spacetime with Killing vector ξ^α, in that coordinate system. In the next chapter we will apply these theorems to motion in Schwarzschild spacetime to find conserved quantities for geodesic motion.

1.2 Gravitational Waves

In addition to laying down the foundations of GR, Einstein derived many experimental predictions of his intuitions. Most of them have been nowadays verified, as we have amply mentioned at the beginning of this chapter, but one important prediction eluded full experimental evidence until this year: Gravitational Waves (GWs). Remarkably gravitational radiation is a fully relativistic phenomenon that can be derived in different ways within GR, and in this section we will show in some detail the simplest derivation, i.e. linearising Einstein field equations, and the most important properties of Gravitational Waves.

Before that, it is appropriate to stress that, although we directly detected GWs, we gathered several indirect proofs of their existence, as relativistic corrections to astrophysical phenomena, justifying the GW hunt during previous years [10, 11, 12, 49]. Calculations show that the existence of gravitational radiation and the consequent loss of energy and angular momentum by their sources fits very well with many astrophysical observations. Without them we would not be able to explain these. The most famous one is the period shift in pulsar binaries due to the emission of gravitational radiation. The first one to be detected was PSR B1913+16, which was worth a joint Nobel prize to Hulse and Taylor in 1993 [36]. Fig. 1.1 reports 30 years of observations at the Arecibo (Puerto Rico) observatory, showing the perfect fit of the time shift in the periastron position to the GR prediction. After 100 years from their first prediction [30], gravitational waves have fi-

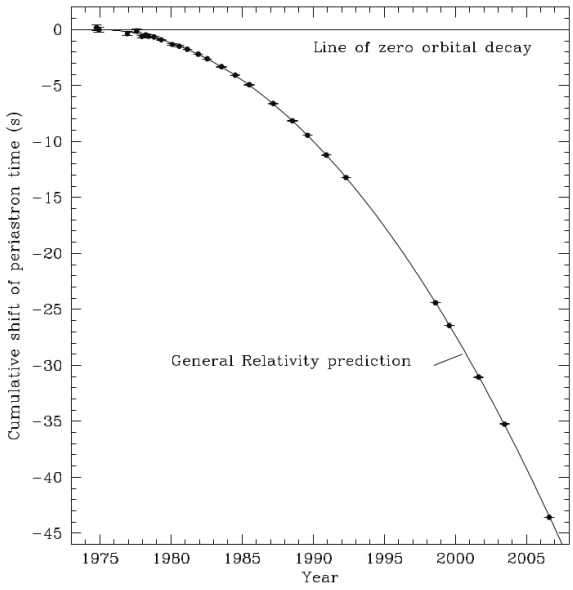

Figure 1.1: Orbital decay of pulsar binary PSR B1913+16. The points are the change in the periastron period, the continuous curve is the corresponding GR prediction. In the late '90s the Arecibo observatory was closed for upgrading, hence the lack of points in that period. Diagram credit to [2].

nally been detected by the aLIGO laser interferometers [4]. The data analysed by the joint collaborations of aLIGO and aVirgo show the gravitational radiation produced by two comparable-mass black holes merging together; the detection has been called GW150914. The detected waveforms agree with the GR prediction for the inspiral and merger of a pair of black holes and for the ringdown of the resulting single black hole, see Fig. 1.2. Many other detections of similar events are expected to come in the next years.

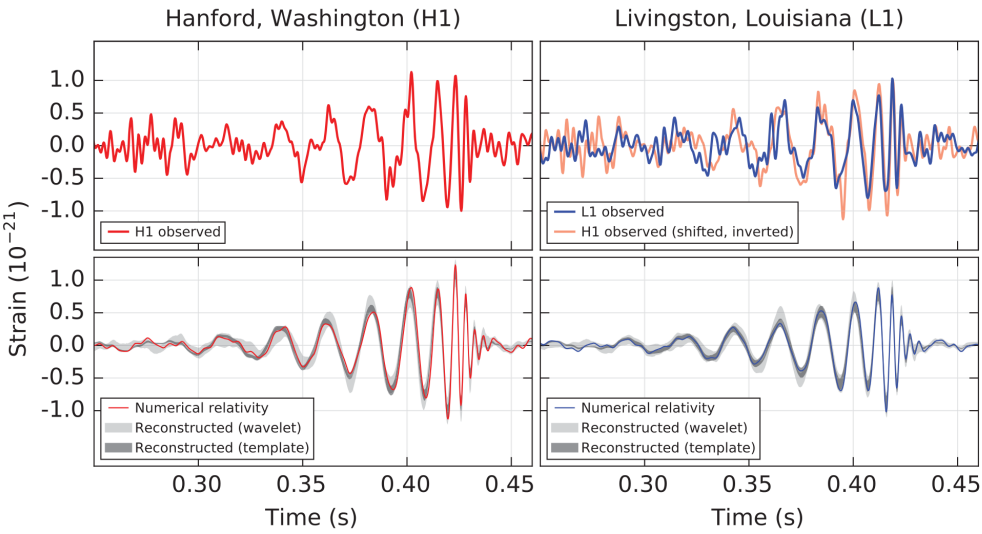

Figure 1.2: The observed gravitational-wave event GW150914 observed by the two aLIGO interferometers in Hanford and Livingston. The top panels show the measured signal. The bottom panels show the expected signal produced by the merger of two black holes, based on numerical relativity simulations. Plot credit to [4].

Gravitational waves are the radiation associated with the gravitational field. They are "ripples" of spacetime, propagating through spacetime itself, interacting with it. This is a direct consequence of the non-linearity of the gravitational interaction, as we will shortly show. The simplest way to show the existence of waves of the gravitational field is considering a small perturbation $h_{\mu\nu}$ on a flat background, represented by Minkowski metric $\eta_{\mu\nu}$

$$g_{\mu\nu} = \eta_{\mu\nu} + h_{\mu\nu}, \qquad |h_{\mu\nu}| \ll 1, \tag{1.2.1}$$

with $g_{\mu\nu}$ the overall metric[7]. One can always choose a reference frame where (1.2.1) holds, thanks to the invariance of GR to coordinate transformations. After a straightforward calculation, one can substitute (1.2.1) into the Einstein field equations (1.1.9) and retain only terms to first order in the perturbation $h_{\mu\nu}$. One is left with the *linearised field equations*,

$$\Box\bar{h}_{\mu\nu} + \eta_{\mu\nu}\partial^\rho\partial^\sigma\bar{h}_{\rho\sigma} - \partial^\rho\partial_\nu\bar{h}_{\mu\rho} - \partial^\rho\partial_\mu\bar{h}_{\nu\rho} = -16\pi T_{\mu\nu}, \tag{1.2.2}$$

[7] In linearised theory indices are raised and lowered with the background metric, which is $\eta_{\mu\nu}$ Minkowski metric.

with $\bar{h}_{\mu\nu} = h_{\mu\nu} - \frac{1}{2}\eta_{\mu\nu}h$ and $h = \eta^{\mu\nu}h_{\mu\nu}$, the alternative version and the trace of the perturbation $h_{\mu\nu}$, respectively. Further insight can be gained considering that for an infinitesimal coordinate transformation $x^\mu \to x'^\mu = x^\mu + \zeta^\mu(x)$, the perturbation transforms as

$$h_{\mu\nu}(x) \to h'_{\mu\nu}(x') = h_{\mu\nu}(x) - (\partial_\mu\zeta_\nu + \partial_\nu\zeta_\mu), \tag{1.2.3}$$

The function $\zeta^\mu(x)$ can be chosen arbitrarily (provided that $|h_{\mu\nu}| \ll 1$, i.e. it is still a small perturbation), allowing for some gauge freedom in the perturbation. Therefore it is very convenient to move to the harmonic gauge $\partial^\nu\bar{h}_{\mu\nu} = 0$. This simplifies Eq. (1.2.2) considerably, resulting into

$$\Box\bar{h}_{\mu\nu} = -16\pi T_{\mu\nu}, \tag{1.2.4}$$

which is manifestly a wave equation for the perturbation $h_{\mu\nu}$. Gravitational radiation is possible. Notice that the harmonic gauge condition takes off 4 degrees of freedom, reducing again the 10 independent components of $\bar{h}_{\mu\nu}$ to 6, as for the original Einstein field equations (1.1.9).

Another derivation of GW can be obtained in a more general way defining the inverse "gothic metric"

$$\mathfrak{g}^{\alpha\beta} = \sqrt{-g}g^{\alpha\beta}, \quad \text{and the field} \quad \mathrm{h}^{\alpha\beta} = \eta^{\alpha\beta} - \mathfrak{g}^{\alpha\beta}, \tag{1.2.5}$$

This is an exact definition, no approximation or assumption about the smallness of $\mathrm{h}^{\alpha\beta}$ has been made[8]. With these definitions and this time harmonic gauge on $\mathrm{h}^{\alpha\beta}$, the Einstein field equations take the so-called Landau-Lifshitz form [50]

$$\Box\mathrm{h}^{\alpha\beta} = -16\pi\tau^{\alpha\beta}, \tag{1.2.6}$$

with $\tau^{\alpha\beta} = \tau^{\alpha\beta}[\mathrm{h}]$ the effective Energy-Momentum pseudotensor, that can be further decomposed into

$$\tau^{\alpha\beta} = (-g)\left(T^{\alpha\beta} + t^{\alpha\beta}_{LL} + \partial_\nu\mathrm{h}^{\alpha\mu}\partial_\mu\mathrm{h}^{\beta\nu} - \mathrm{h}^{\mu\nu}\partial_\mu\partial_\nu\mathrm{h}^{\alpha\beta}\right), \tag{1.2.7}$$

with $t^{\alpha\beta}_{LL}$ the Landau-Lifshitz Energy-Momentum pseudotensor [2], also depending on $\mathrm{h}^{\alpha\beta}$. Eq. (1.2.6) shows once again the wave propagation of the gravitational field, this time making clear the non-linearity of the field equations. The right-hand side depends quadratically on the field $\mathrm{h}^{\alpha\beta}$ itself, thus telling that the gravitational field generates gravity. This formulation of the Einstein field equations is the starting point for Post-Newtonian theory and other iterative methods, see [51] and references therein. In fact Eqs. (1.2.6) can be solved formally without specifying the motion of the source, giving

$$\mathrm{h}^{\alpha\beta}(t,\mathbf{x}) = -4\int \frac{d^3x'}{|\mathbf{x}-\mathbf{x}'|}\tau^{\alpha\beta}\left(t - |\mathbf{x}-\mathbf{x}'|, \mathbf{x}'\right), \tag{1.2.8}$$

[8] Actually $\mathrm{h}^{\alpha\beta}$ reduces to the perturbation $\bar{h}^{\alpha\beta}$ used in linearised theory, by replacing $g^{\alpha\beta} = \eta^{\alpha\beta} + h^{\alpha\beta}$ into the definition of the gothic metric and $\mathrm{h}^{\alpha\beta}$, for small $h^{\alpha\beta}$.

where the integration is performed over the past null cone of the point $(t, \mathbf{x})$. Since $\tau^{\alpha\beta}$ still depends on $\mathrm{h}^{\alpha\beta}$, this is nothing but rephrasing the original differential equation into an integral one. Motion of the source is retrieved imposing the harmonic gauge condition on (1.2.8) and a solution is found via iterative methods in a weak-field and slow-motion regime.

1.2.1 Transverse-Traceless gauge

In order to see how gravitational waves propagate in spacetime, it is convenient to start again with the linearised Einstein field equations (1.2.4) outside the source, for the sake of simplicity in vacuum. This allows one to examine how the gravitational wave itself curves spacetime and to analyse its effect on other distributions of mass far from the source or to eventual detectors.

Outside the source $T_{\mu\nu} = 0$, therefore

$$\Box \bar{h}_{\mu\nu} = 0, \qquad \text{with} \qquad \partial^\nu \bar{h}_{\mu\nu} = 0, \tag{1.2.9}$$

the imposed gauge condition. This choice still leaves some freedom and if one performs a change of coordinates $x^\mu \to x^\mu + \zeta^\mu$, with $\zeta^\mu(x)$ an arbitrary smooth $\mathcal{C}^2(\mathbb{R}^4)$ function, the gravitational perturbation $\bar{h}_{\mu\nu}$ changes as

$$\begin{aligned} \bar{h}_{\mu\nu} \to \bar{h}'_{\mu\nu} &= \bar{h}_{\mu\nu} - (\partial_\mu \zeta_\nu + \partial_\nu \zeta_\mu - \eta_{\mu\nu} \partial_\rho \zeta^\rho) \\ \partial^\nu \bar{h}_{\mu\nu} \to (\partial^\nu \bar{h}_{\mu\nu})' &= \partial^\nu \bar{h}_{\mu\nu} - \Box \zeta_\mu, \end{aligned} \tag{1.2.10}$$

and the harmonic gauge condition is preserved, provided that ζ^μ satisfies $\Box \zeta^\mu = 0$. Also Eq. (1.2.9) is preserved, because $\Box \left(\partial_\mu \zeta_\nu + \partial_\nu \zeta_\mu - \eta_{\mu\nu} \partial_\rho \zeta^\rho\right) = 0$ as well. One can then choose ζ^0 so that $\bar{h} = \eta^{\mu\nu} \bar{h}_{\mu\nu} = 0$, i.e. the gravitational perturbation is traceless. Then $\bar{h}_{\mu\nu} = h_{\mu\nu}$, we go back to the original formulation. With the left components of ζ^i one can impose that $h^{0i}(x) = 0$ everywhere. From the harmonic condition then one gets $\partial^0 h_{00} + \partial^i h_{0i} = 0 = \partial^0 h_{00}$. This implies that we can put $h_{00} = 0$ without loss of generality. Summarising, one can always change to a reference frame equivalent to an infinitesimal coordinate transformation with vector ζ^μ satisfying $\Box \zeta^\mu = 0$, obtaining

$$h^{0\mu} = 0, \qquad h = h^i_i = 0, \qquad \partial^j h_{ij} = 0. \tag{1.2.11}$$

The first property tells that the perturbation is given only by the spatial parts, the second that it is traceless, and the third one that it is divergence free. The original field equation is conserved and we can solve it formally, obtaining

$$\Box h_{\mu\nu} = 0 \quad \Rightarrow \quad h_{\mu\nu} = \Re \left[A_{\mu\nu} e^{i k_\alpha k^\alpha} \right], \tag{1.2.12}$$

with $k^\alpha = (\omega, \mathbf{k})$ the wave-vector and $A_{\mu\nu}$ the polarization vector. The Einstein field equations and the harmonic gauge further constrain to

$$k_\alpha k^\alpha = 0, \qquad \text{and} \qquad A_{\mu\nu} k^\nu = 0, \tag{1.2.13}$$

namely that gravitational waves travel at the speed of light (so $\omega = |\mathbf{k}|$) and the wave is contained in a plane orthogonal to the direction of propagation, i.e. they are transverse

waves. For these reasons the whole gauge procedure is called *Transverse-Traceless gauge* (TT-gauge hereafter).

For a convenient representation one can choose the direction $\mathbf{k}$ along the z-axis of a Cartesian coordinate system and the complete wave solution reads

$$h^{TT}_{\mu\nu}(t,z) = \begin{pmatrix} 0 & 0 & 0 & 0 \\ 0 & h_+ & h_\times & 0 \\ 0 & h_\times & -h_+ & 0 \\ 0 & 0 & 0 & 0 \end{pmatrix} \cos\left[\omega\,(t-z)\right], \tag{1.2.14}$$

with the two independent polarization modes $h_+, h_\times$ called "plus" and "cross" polarizations respectively. Two are the degrees of freedom of a GW in linearised theory, and the line element of spacetime where such gravitational wave is passing through is

$$\begin{aligned}(ds)^2 = &-(dt)^2 + (1 + h_+ \cos\left[\omega\,(t-z)\right])\,(dx)^2 + (1 - h_+ \cos\left[\omega\,(t-z)\right])\,(dy)^2 \\ &+ 2h_\times \cos\left[\omega\,(t-z)\right] dxdy + (dz)^2.\end{aligned} \tag{1.2.15}$$

If one considers a homogeneously massive ring in the (x,y)-plane getting hit by the gravitational wave (1.2.14) orthogonal to them, it lies in the spacetime (1.2.15) and gets stretched over time like in Fig. 1.3, justifying the names of the polarizations.

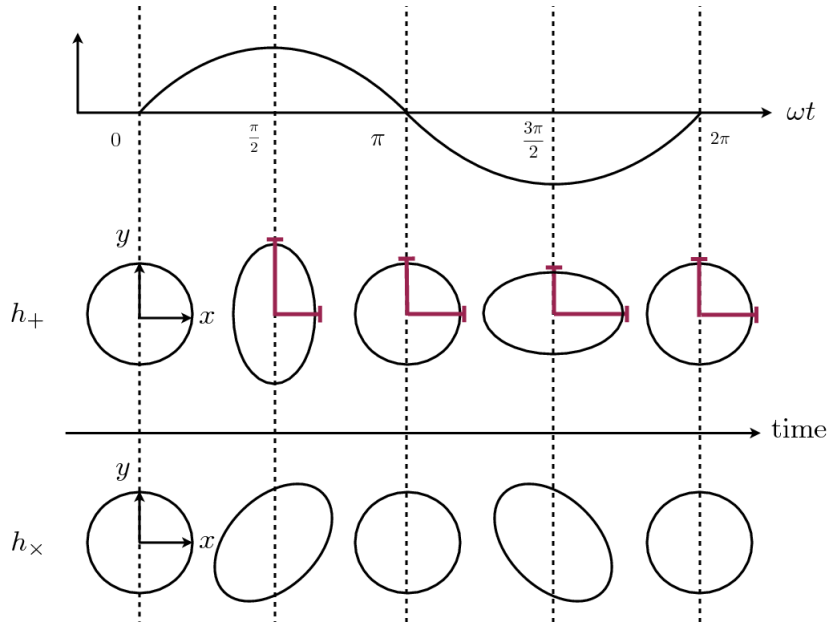

Figure 1.3: Deformations of a massive ring traversed by an orthogonal gravitational wave as in (1.2.14). The effects of the two polarizations take place along the coordinate axes (+) and their diagonals (×). Diagram credit to [52].

From Fig. 1.3 and the aforementioned effects, it is clear that GWs carry energy and angular momentum along, so in the next section we are going to discuss what produces gravitational radiation and how energy is associated to them.

1.2.2 Energy of Gravitational Waves

We have seen how to obtain a solution to the linearised Einstein field equations in vacuum. One can build a formal solution also for more general cases, where $T_{\mu\nu} \neq 0$,

$$\bar{h}_{\mu\nu}(t, |\mathbf{x}|) = \frac{4G}{c^4} \int d^3x' \frac{1}{|\mathbf{x} - \mathbf{x}'|} T_{\mu\nu} \left(t - \frac{|\mathbf{x} - \mathbf{x}'|}{c}, \mathbf{x}' \right), \tag{1.2.16}$$

which is found employing the retarded Green's function, just like for the electromagnetic case of the Maxwell equations. The expression (1.2.16) can be reduced to the TT-gauge using a projector operator $h^{TT}_{\mu\nu} = \Lambda_{\mu\nu,\rho\sigma} \bar{h}_{\rho\sigma}$, see [2] for details. We have also restored the G, c factors in this section, in order to give a better sense of the orders of magnitude at play with gravitational radiation.

However, the solution (1.2.16) is not really useful unless one is able to solve the integral in closed form, knowing the EM-tensor $T_{\mu\nu}$, or one has to make some approximations or assumptions. Since the gravitational wave is observed far away from the sources emitting it, one can approximate the distance in (1.2.16) as

$$|\mathbf{x} - \mathbf{x}'| = r - \frac{\mathbf{x} \cdot \mathbf{x}'}{r} + o\left(\frac{d^2}{r} \right), \tag{1.2.17}$$

with $r = |\mathbf{x}|$ the distance from the source to the detection point -where we want to know the wave $\bar{h}_{\mu\nu}(t, \mathbf{x})$- and d a typical dimension of the source, such that $r \gg d$.

Further insight can be gained considering non-relativistic sources, whereby the typical velocities inside the sources are much smaller than the speed of light, so $v \ll c$, and therefore the reduced wavelength of the radiation is considerably bigger than the size of the system $\lambda\!\!\!^{-} \sim \frac{c}{v} d \gg d$. With these assumptions the gravitational field outside the source (1.2.16) can be rewritten in the TT-gauge as

$$h^{TT}_{ij}(t, \mathbf{x}) = \frac{4G}{c^4} \frac{1}{r} \Lambda_{ij,kl} \int d^3x' T^{kl} \left(t - \frac{r}{c} + \frac{\mathbf{x} \cdot \mathbf{x}'}{r}, \mathbf{x}' \right). \tag{1.2.18}$$

One can see from the expression above how the amplitude of the field decreases like $\sim \frac{1}{r}$ and how small a GW is on the whole, thanks to the $\frac{G}{c^4}$ multiplying factor.

The far-distance assumption and the non-relativistic velocities assumption pave the way to a multipole expansion, similar to the one performed in electrodynamics. After a straightforward calculation one can show that the leading term in such expansion is the quadrupole moment, namely the gravitational wave results in

$$h^{TT}_{ij}(t, \mathbf{x}) = \frac{2G}{c^4} \frac{1}{r} \ddot{Q}^{TT}_{ij}(t - \frac{r}{c}) + \text{ higher moments}, \tag{1.2.19}$$

the second derivative with respect to time of the quadrupole moment

$$Q^{ij} = \int d^3x \rho(t, \mathbf{x}) \left(x^i x^j - r^2 \delta^{ij} \right), \tag{1.2.20}$$

where $\rho(t, \mathbf{x})$ is the mass-energy density of the source. From these results we learn that there is no monopole or dipole radiation, that radiation depends on the time derivative

of the quadrupole moment, at the lowest order, and therefore that static and completely symmetric sources do not emit GWs. The same results can be obtained in a rigorous way also within the Landau-Lifshitz formalism, confirming that the quadrupole is the leading term in the multipole expansion of the gravitational field.

In order to calculate the energy and the angular momentum carried by a gravitational wave, we have to take into account the Energy-Momentum tensor associated to gravitational radiation. This can be found extending to second order the linearisation of Einstein field equations. In this case one starts from a non-trivial background metric $\bar{g}_{\mu\nu}$ and adds two orders of perturbations, $h^{(1)}_{\mu\nu}$ and $h^{(2)}_{\mu\nu}$, so

$$g_{\mu\nu} = \bar{g}_{\mu\nu} + h^{(1)}_{\mu\nu} + h^{(2)}_{\mu\nu}, \tag{1.2.21}$$

the background $\bar{g}_{\mu\nu}$ is now allowed to be curved. The EM-tensor of GWs, far away from the original source, is then defined as

$$T^{GW}_{\mu\nu} = \frac{c^4}{8G\pi}\langle R^{(2)}_{\mu\nu} - \frac{1}{2}\bar{g}_{\mu\nu}R^{(2)}\rangle, \tag{1.2.22}$$

where $R^{(2)}_{\mu\nu}$ is the Ricci tensor obtained from the second order contributions of the perturbations, and $R^{(2)}$ is its associated scalar. The brackets indicate an average over a region big compared to the dynamical scales of the gravitational wave, like its reduced wavelength λ, which has to be smaller than the region of variation of the background, say R_B, in order to keep being considered as a perturbation. So the average is taken on a region of scale l such that $\lambda \ll l \ll R_B$. The fact that an EM-tensor can be associated to GWs, and that it is sourcing Einstein field equations to second order of the perturbation, shows manifestly that these waves interact with the background spacetime, modifying it. Momentum and angular momentum can be derived from their EM-tensor, showing that they can modify the distance in space of other masses, as it happens for the massive ring in Fig. 1.3.

From the Eq. (1.2.22), one can obtain the energy density which, in TT-gauge, reads as

$$T^{00} = \frac{c^2}{16\pi G}\langle \dot{h}^2_+ + \dot{h}^2_\times\rangle, \qquad \Rightarrow \qquad \frac{dE}{dt} = \frac{c^3 r^2}{32\pi G}\int d\Omega \langle \dot{h}^{TT}_{ij}\dot{h}^{TT}_{ij}\rangle, \tag{1.2.23}$$

where also the power emitted is indicated. By using the quadrupole moment (1.2.20) as leading term in the multipole expansion into the power expression above, one obtains the power emitted through gravitational waves to the quadrupole level, the so-called "quadrupole formula"

$$P_{quad} = \left(\frac{dE}{dt}\right)_{quad} = \frac{G}{5c^5}\langle \dddot{Q}_{ij}\dddot{Q}^{ij}\rangle. \tag{1.2.24}$$

The factor $\frac{1}{c^5}$ damps considerably the power emitted, hence the difficulty of detecting GWs as we will see in the next section, and the reason's why Post-Newtonian expansions are needed at least up to 2.5 order, for then corrections up to $\left(\frac{v}{c}\right)^5$ are first available [51, 53].

1.2.3 Looking for Gravitational Waves

Spacetime is very stiff, as the powers of c in the Einstein equations and in the power expression indicate. Therefore detection of GWs is as non-trivial as a necessary task. Historically two broad kinds of detectors have been developed to succeed in this: resonant bars and interferometers [14].

Resonant bars represent the first attempt at a detection of GWs. They are based on the principle that a gravitational wave stretches apart and then compresses again a mechanical system. One can think of two masses separated by a string, if the characteristic frequency of the wave is near the resonance frequency of the spring, the response is magnified. Such systems were realized as metal cylinders and one looks for changes in the amplitude of the thermal motion of these bars.

These systems were pioneered by Weber in the '60s [54], and although he claimed detection of waves, following experiments denied the discovery. Different similar experiments have been set up in the years and the resonant-bars epoch gave way to another kind of experiments allowing to reach higher sensitivities: laser interferometers.

Gravitational-wave interferometers are based on a different idea: measuring the travel time of light along different paths (the arms of the interferometer). A gravitational wave modifies locally the proper distance and therefore an interferometer with orthogonal arms will experience a stretch in one direction and a shrink in the other. The light signal is reflected by the mirrors at the end of each arm and there will be a phase difference between the light returning from one arm and the other. This can be measured and provides the proof of the passage of the wave.

The original idea is the same of a Michelson-Morley interferometer, which was supposed to prove the existence of aether. A monochromatic light signal is first separated by a beam-splitter into two different arms at 90°, of lengths L_x, L_y respectively, reflected by mirrors at the end of each arm, and then recombined again at beam-splitter location. Here part of the recombined signal goes to a photodetector measuring the intensity. If we call E_0 the initial amplitude of the electromagnetic signal (laser light), with frequency ω_L, the power detected at the photodetector will be proportional to the amplitude of the output

$$|E_{out}|^2 = E_0^2 \sin^2 \left[\omega_L \left(L_y - L_x\right)\right], \tag{1.2.25}$$

and to the difference in the lengths. The passage of a GW causes a variation of these and therefore in the measured signal. Clearly the actual interferometers employ more advanced systems than a simple Michelson-Morley interferometer. However, the length of the arms determines the scale of frequencies that one will be able to see with the experimental setup. The use of Fabry-Perot cavities in the arms allows to reach higher sensitivities and lower frequencies ($\sim 10^2 Hz$) in the modern ground-based interferometers, as GEO (Germany - $600m$ arm length), aLIGO (US - $4km$ arm length), and aVIRGO (Italy - $3km$ arm length) [10, 49].

Currently GEO is collecting data, together with aLIGO, which has still to reach its nominal sensitivity, while aVirgo is under upgrade. Once the upgrade is finished we will have more than one second-generation detectors available and even weaker and farther

sources will become detectable, increasing the number of detectable events to a significant level. After the analysis of the first series of data from aLIGO has proven direct evidence of GWs, further detections are expected in the next years by aLIGO and aVirgo, but also by other ground-based detectors which are under construction in Japan (KAGRA), or proposed to be constructed (Ligo-India) [11], extending the worldwide network of ground-based interferometers. However, to reach much lower frequencies one needs to put interferometers into space, such as the eLISA project aims to do (launch expected by 2034). In this case the interferometer employs a triangular configuration of three satellites moving in space with a considerably bigger arm distance ($\sim 10^6 km$).

Instead very low frequency waves ($\sim 10^{-9} Hz$) can be detected with a different technique, employing **pulsar timing**. Pulsars are fast-rotating stars with strong magnetic fields which emit radiation in a preferred direction; their axis of rotation precesses fast and the Earth is illuminated periodically only when the cone of emission is in the right direction. This turns pulsars into very regular clocks, so monitoring pulsars over years allows one to measure variations due to the change in the distance from the pulsar to the Earth. This is due to a stochastic GW background at very low frequency. Currently an International Pulsar Timing Array of different experimental collaborations is set up to make their first detection [55].

1.3 Sources of Gravitational Waves

As we have shown previously, gravitational waves are generated by accelerating asymmetric distributions of mass, and our universe is drenched in GWs. Unfortunately gravitational radiation is a very weak signal on the whole, so in order to obtain some detection in this ocean of waves, one has to look at the biggest ones, authentic tsunamis and storms brought about by the most violent phenomena. The sources of gravitational radiation have to produce a strong enough gravitational field, before we can detect them. This reduces to a variety of astrophysical events, with different frequencies corresponding to different kind of sources. An overview of the frequencies and sources is given in Fig. 1.4, showing the gravitational spectrum, analogous to the electromagnetic one.

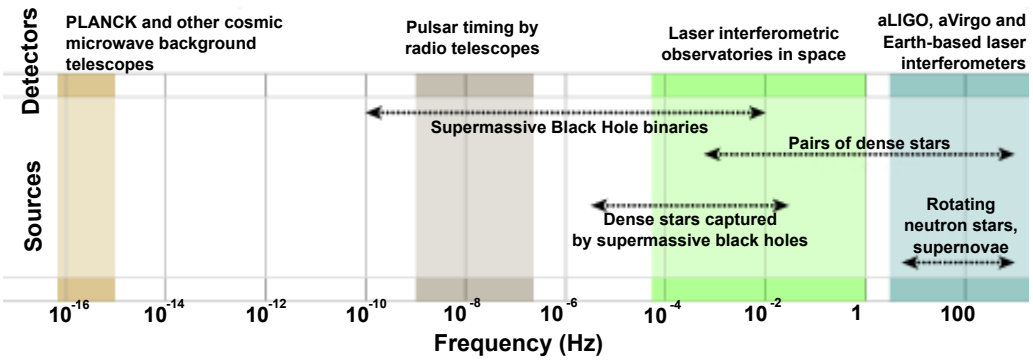

Figure 1.4: Gravitational spectrum. The frequency of the wave is indicated in the bottom row. Above one finds the sources and the detectors and experiments looking in that range of frequency.

Sources of GWs can be divided according to the kind of signal they are believed to emit. In fact one can have a wide variety of sources with two extreme behaviours: continuous and long-lived waves emitted with roughly constant frequency and amplitude, or very short-lived and rapidly changing signal (here both "constant" and "changing" are considered with respect to the observation time). The experimental technique for detection changes accordingly.

Among the most prominent candidates for GW detection, **Compact Binary Coalescences** are sources of GWs formed by two compact objects orbiting around each other [56]. This particular system forms under certain conditions, like both stars have to be massive enough to undergo collapse into a compact object (Neutron Star or Black Hole), but without destroying its companion or tearing so much mass apart that the orbit is no longer bound. Of all the binary star systems, common in our galaxy, only a fraction satisfies these requirements. Binary coalescences are further distinguishable in binaries with only Neutron Stars (NS-NS) or a Neutron Star and a Black Hole (NS-BH), and only Black Holes (BH-BH). The first direct detection of GWs GW150914 belongs to this category.

Continuous wave sources are produced by rotating non-axisymmetric Neutron Stars (NS) [57]. They emit in the highest frequency range of the spectrum, as one can see from Fig. 1.4, and their GWs can provide valuable information to determine their properties and structure, especially when combined with electromagnetic measurements. Neutron stars are dense objects endowed with strong magnetic fields and they can be found isolated or in binaries, orbiting together with other objects, such as another star or a black hole. A neutron star whose emission points periodically to Earth's direction is what is commonly called a "pulsar".

Another kind of source of radiation is represented by astronomical violent and **transient phenomena**, such as supernovae, instabilities in Neutrons Stars, or gamma-ray bursts. Supernovae are violent events on the evolutionary path of massive stars. These collapse under the influence of gravity, exhibiting some asymmetry that gives rise to GWs. After this collapse very dense objects such as neutron stars or black holes are formed. Instead the processes behind the emission of gamma-ray bursts are still uncertain, and they could be events like the explosion of supernovae. Another transient source can be the sudden release of energy from highly magnetized Neutron Stars (Magnetar) or bursts from cosmic string cusps [58, 59]. The dynamics of these various mechanisms is not easily modeled and therefore it is complicated to calculate waveforms or templates for the expected GW signal. Eventually supernovae should already be in the range of detection of interferometers such as aVIRGO or aLIGO.

On a different note GWs can come from the superposition of incoherent sources, forming a so-called **stochastic background**. This can be a cosmological background of primordial GWs, produced during Big Bang and early stages of the universe, which occupy the lowest part of the gravitational spectrum and were claimed to be indirectly discovered by the BICEP2 experiment [60, 61] a year ago. Also cosmological models other than the standard one predict the existence of primordial GWs, although with different strengths of the predicted background. Another possibility is from astrophysical events such as cosmic strings or superposition of many distant events, like binary coalescences

from compact stars too far away to be seen individually. The detection of such stochastic background is not easy to distinguish from instrumental noise, so its measurement relies considerably on cross-correlation techniques between many detectors.

As we will see in the next chapters, a binary coalescence undergoes different stages, emitting correspondingly different kind of gravitational radiation. During the first stage, the "inspiral", the two bodies spiral towards each other loosing energy and angular momentum into radiation, emitting a weak signal, slowly increasing in amplitude and frequency for hundreds of millions of years. In this phase the motion is slow and the gravitational field weak, the perfect playground for Post-Newtonian methods. Analytic expressions for gravitational waveforms can be calculated accurately.

The phase when the signal is strong enough for detection for ground-based interferometers is when they get very close to each other, they "merge" into a final compact object, and they emit with great luminosity for a short period of time. This stage is better understood in terms of perturbations of the Einstein field equations or numerical relativity. We are in the strong gravity regime. Eventually a remaining object radiates away the deformations of the previous stage in a superposition of particular frequencies, so-called quasi-normal modes. This is the "ringdown" phase, studied through perturbation theory.

The mass ratio between the two objects in a binary coalescence determines its life and the shape of the gravitational waveform, but also other factors like the spin of the single components contribute. When the difference of mass is several orders of magnitude ($\sim 10^5$), the major body is a Supermassive Black Hole, and we are dealing with an "Extreme Mass Ratio binary". In this case the minor companion can be treated as a probe in the spacetime generated by the more massive body, and the frequencies at which they emit are considerably lower, in the range for space-based detectors, such as eLISA. It is commonly believed that a supermassive black hole lies right at the center of the Milky Way.

* *

2 Black Hole perturbation theory

* *

Coalescences of compact binary systems are among the most prominent sources of Gravitational Waves. These are usually a couple of Black Hole-Black Hole or Black Hole-Neutron Star. In the case of an Extreme Mass Ratio binary, which is the kind of binary we are most interested in this thesis, the central black hole is a supermassive one ($M \geq 10^6 M_\odot$).

The two bodies orbit around each other, or better around their mutual center of mass, and gravitational radiation is released during this process, influencing the motion of the binary system. This goes through different stages, from an initial weak-field motion, where the two objects are still far from each other, all the way to the final strong-field stage, where the two merge together. The shape of the gravitational signal changes and the techniques employed for their prediction vary accordingly.

Different theoretical frameworks have been devised in the last years in order to describe the motion of a binary coalescence and consequently predict the emitted gravitational signal. They mainly vary in their range of applicability, but thanks to the collective efforts of the gravitational community, we are able nowadays to extend our understanding to various kinds of compact binaries.

The best way to have a synoptical view of all these techniques is comparing binary coalescences by the mutual distance of the two orbiting bodies and their mass ratio. A pictorial representation of this idea is given in Fig. 2.1. One has to keep in mind that a single binary system goes through different areas in this plot as time goes by, because the mutual distance shrinks -an effect of the emission of energy and momentum through gravitational waves.

Post-Newtonian (PN) theory is based on an approximation in General Relativity that applies when the gravitational field is weak and the motion of the matter is slow. It describes successfully the gravitational field of the solar system, but it can also be applied to situations involving compact bodies with strong internal gravity, provided that the mutual gravity between bodies is weak. This is the case for binaries with comparable masses still orbiting far away from each other. The PN-theory relies on the relaxed form of the Einstein field equations in the Landau-Lifshitz formulation [50]. In this formulation the equations for the perturbation of the metric are solved iteratively and the truncation is the main source of approximation. Once the potentials $h_{\alpha\beta}$ are obtained

in terms of undetermined matter variables, those are finally determined by enforcing the conservation equation of the energy-momentum tensor. Then an expansion in retarded time is performed, and this generates a Post-Newtonian expansion in powers of c^{-1}. Commonly a correction of order $(\frac{v}{c})^n$ to a Newtonian expression is said to be of $\frac{n}{2}$ PN-order. For instance, two iterations of the relaxed field equations are needed to produce the leading-order 0PN expression for the gravitational-wave field. The interested reader can find more details in [51, 53].

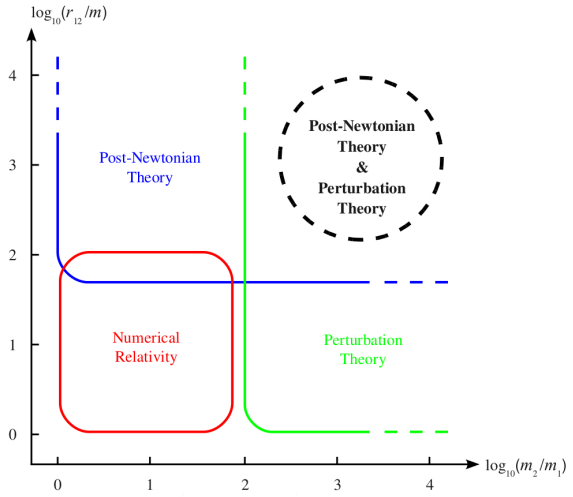

Figure 2.1: Mutual distance r_{12} in a coalescing binary of masses m_1, m_2 vs mass ratio.
Diagram credit to [62].

These years have seen a considerable enhancement in the availability of computational power and this led to the development of Numerical Relativity, allowing to explore regions of the parameter space that are not available to PN-methods [63, 64]. The idea is basically to solve the Einstein field equations for specific situations with numerical techniques, for instance transforming the involved differential equations in finite-difference equations and solving these throughout spacetime. A similar way to discretize spacetime is also used in this thesis to solve the radiative equations of the gravitational field, as we will amply describe in the following sections (Lousto-Price algorithm). Sometimes entire regions of spacetime are excluded from these computation, like the interior of a BH horizon in excision methods [65, 66]. However Numerical Relativity allows to treat several other astrophysical problems, not just the computation of gravitational radiation [67, 68].

Another method that encompasses all these regimes of different mass ratios and mutual distances is the so-called Effective One Body approach [69]. In this approach the dynamics of two masses m_1, m_2 is mapped into the dynamics of one particle with reduced mass $\mu = \frac{m_1 m_2}{m_1+m_2}$ moving in an effective metric. The hamiltonian defined by the geodesic action of this metric can be mapped to the relative-motion PN hamiltonian, thus recovering the PN equations of motion. However in the test-particle limit geodesic motion is retrieved exactly, and not just the PN truncation. This method can treat comparable mass ratio binaries all the way to the merger and has given already many results for the description of coalescences and the relative gravitational radiation [70, 71, 72].

Last but not least come the perturbative methods. In this case the motion is calculated from a perturbation of the background non-trivial metric [16, 73]. This is how binary systems with high mass ratio are most naturally explored. The Einstein field equations are

first written including this perturbation on the metric and the energy-momentum tensor, then solved with the means available. At zeroth order in the mass ratio one retrieves the usual geodesic motion, then corrections are added. The perturbation allows to use fully GR and to study the background spacetime and its properties. The back-reaction from this perturbation gives rise to gravitational self-force, which changes gradually the particle's motion and is also studied in these perturbative schemes [74, 75].

In this chapter we will focus on BH perturbation theory, for this allows to describe best the Extreme Mass Ratio binaries (down-right corner of Fig. 2.1) and to use GR fully, giving an unique opportunity to test the background spacetime itself and to explore its properties. First a self-contained description of the Schwarzschild spacetime is given. Then, in the second section, the mathematical formalism and the main results of Schwarzschild Black Hole perturbation theory are recalled, with a short derivation of the Regge-Wheeler radiative equations. The third section is dedicated to these equations and to the methods of solution employed in this thesis. In the last section another perturbation method, the geodesic deviations method, is described.

2.1 Black Holes in General Relativity

The first appearance of a black hole dates back to 1783, when reverend Mitchell calculated, within purely Newtonian mechanics, the escape velocity of a particle at the surface of a body with mass M and radius R, equating kinetic energy and Newtonian gravitational potential,

$$v_{escape}^2 = \frac{2GM}{R}.$$

If $v_{escape} > c$ then light cannot escape from this object. Therefore a star with mass M and radius R such that

$$\frac{2GM}{c^2R} \geq 1,$$

emits light that cannot go farther than $\frac{2GM}{c^2}$, hence it is a dark star. Since its birth as "dark star", the concept of black bole has developed into one of the most fascinating topics in General Relativity. It did not take long for its discovery in GR, considering that the first BH solution - the Schwarzschild solution- has been found just one year after the first Einstein's publication regarding the general theory of relativity in 1915 [76]. Research on BHs developed quite a lot since and nowadays they appear as common objects not just in GR, but in other theory and models in high-energy physics as well, such as string theory and AdS/CFT correspondence. In fact, starting from the Bekenstein-Hawking formulation it is possible to give a thermodynamical interpretation of BH solutions [77, 78]. Thanks to this, higher-dimensional black holes become interesting objects to study in order to derive properties of their dual counterparts in Field Theories with one dimension less. Without the link provided by the AdS/CFT correspondence it would not be possible to address such problems, due to the strong coupling of the dual field theory and lack of alternative efficient theoretical tools [79, 80].

Black holes occupy also quite a role in the astrophysical research, as we are gaining more and more proofs of their existence, and eventually the detection of Gravitational Waves will be a further confirmation of this. In fact, among the predictions we expect to be able to do with GWs, there is the possibility of distinguishing from the gravitational signal itself whether it has been emitted by a BH or another astrophysical object.

Nevertheless we need to make clear which kind of BH are the ones we are interested in when looking at an EMR binary system, and which GR solutions are avalaible and being studied to address them. To this end, we will leave the various BH solutions appearing in many theoretical models aside and stick to the GR ones. We will make a clear distinction between the astrophysical BHs and the corresponding solutions in the classical theory of General Relativity, and focus on the latter.

It is commonly believed that black holes are the result of gravitational collapse of stars; in most star formation models with more than $10M_\odot$ one obtains a "Black Hole" [43, 81]. Needless to say, if black holes stem out of collapsing stars and big aggregates of matter, they are more likely to be in the centers of galaxies. Although there are no *direct* proofs of the existence of black holes, we suspect the universe to be quite populated with them; our own galaxy, the Milky Way, has a supermassive BH ($M > 10^6 M_\odot$) at its center $SgrA^*$ [82]. A series of experimental evidences shows that such regions in the galaxy with a SuperMassive BH at their center, among which "Active Galactic Nuclei", are best and simplest explained through BH existence and BH accretion models. These are the observation of orbits of other stars around them[1], gravitational lensing, indirect observation of BH horizons [83], relativistic jets from microquasars, or the formation of the accretion disks [82], to name a few.

Historically, black holes have been found as particular solutions of the Einstein field equations in vacuum, asymptotically flat, and provided with an event horizon screening the singularity inside from the rest of the universe. This means that the metric $g_{\mu\nu}$ describing what is commonly called a "Black Hole" is a solution of the Einstein field equations $R_{\mu\nu} - \frac{1}{2}Rg_{\mu\nu} = 0$ that tends to the Minkowski metric $\eta_{\mu\nu}$ as the observer moves infinitely far away from the center of reference frame. There is where the black hole is situated, in this description, with its mass M, surrounded by one (or more) *event horizon(s)*. The horizon is a particular boundary in the BH spacetime beyond which events cannot affect an outside observer. This means, for instance, that a particle moving on a geodesic in the BH spacetime that crosses this horizon will not be able to come back on its path, no matter what the particle is. Not even if it is a photon. This is what makes Black Holes black, they do not let light itself escape to the outer region beyond the horizon, hence the name. This concept will be more clear when we address the Schwarzschild solution in the following section.

Black holes as solutions of the Einstein field equations have other common features, independently of their derivation and peculiarities. They all "hide" a curvature singularity behind the horizon, meaning that every BH solution has at least one singularity in the region of spacetime precluded by the BH horizon(s). This quite general fact is

[1] The study of the Keplerian orbits around a suspected BH is used to estimate its mass.

believed to be a conjectured principle, not yet proven, that physicists call the *cosmic censorship hypothesis*. All singularities in the universe, with the exception of a possible initial singularity are covered by horizons [84]. BHs do not make an exception.

Another remarkable property is that all BH solutions in GR are members of the same class in the Petrov classification of spacetimes [47] in the Newman-Penrose formalism relying on the use of tetrads. In this formalism the ten independent components of the Weyl tensor can be represented by five complex scalars $\Psi_i, i = 0 \dots 4$. The transformation of these scalars under rotations of the tetrad vectors defines classes of spacetime, generally called Petrov-Pirani classification [85, 86]. One of the reasons of the success of the Newman-Penrose formalism is that all BH solutions in GR are Petrov type D, meaning that all the Weyl scalars vanish but Ψ_2, making the analysis of BH spacetimes a lot easier in this way.

While BHs have no naked singularity, i.e. what the cosmic censorship says, they also have *no hair*. A general stationary black hole can be ultimately characterized by three quantities only, its mass M, the angular momentum J, and the charge Q. These features are inherited by the black hole from the original collapsing star, all the other features are not present in the final black hole [81].

As we deem BHs are created out of gravitational collapse of a star, it is reasonable to think that after some time it settles down to a stationary state and that the resulting Black Hole is stationary (it is temporal invariant). Therefore it can be proved that a stationary black hole is also axially symmetric [47]. Any stationary and axially symmetric black hole without electrical charge Q can be described by the Kerr solution. This represents the most used BH model for astrophysical black holes, as it has all the symmetries required and fits to a rotating object too, having non-null angular momentum J. The Kerr-Newman solution is the generalization with nonvanishing electric charge and electromagnetic fields.

Moreover if one asks for spherical symmetry and a static solution (not time-dependent), one ends up with a Schwarzschild Black Hole[2]. Its generalization with nonvanishing charge is also known, it is the Reissner-Nordstrøm solution. Although many BH solutions are known, few are astrophysically relevant, and this means that the same solution can be applied to many different situations, which is rather convenient. In fact, if an astrophysical Black Hole had electric charge, it would likely loose it in little time by interactions with surrounding bodies, becoming electrically neutral, as all major macroscopic objects are. This leaves us with the Kerr solution as the most general and astrophysically relevant model, together with the Schwarzschild solution. The latter is still important because of the *Birkhoff's theorem*, stating that any spherically symmetric geometry of spacetime which is solution of the Einstein field equations in vacuum is necessarily Schwarzschild geometry [87]. This entails that in order to describe geometries outside stars, planets and other spherical distributions of matter, Schwarzschild BH fits very well[3]. Moreover it is just a simpler solution to study than the Kerr BH, making it the first playground where to test models, even for GW emission. This is among the reasons we will address

[2] Equally it can be proven that any static Black Hole solution has necessarily spherical symmetry [47].

[3] Schwarzschild solution is also the unique solution of Einstein's equations describing nonrotating black holes in empty space, this statement is known as *Israel's theorem*.

EMR binaries with a Schwarzschild geometry in this thesis, and a description of the main features of this geometry is presented next.

2.1.1 Schwarzschild spacetime

Taking the origin of the reference frame at the center of the Black Hole, in spherical coordinates, the Schwarzschild solution can be written, in its most common form, as

$$ds^2 = -\left(1 - \frac{2M}{r}\right) dt^2 + \frac{1}{1 - \frac{2M}{r}} dr^2 + r^2(d\theta^2 + \sin^2\theta d\varphi^2). \tag{2.1.1}$$

One can see that for $r \to +\infty$ the Minkowski limit is obtained. The positive parameter M represents the mass of the Black Hole, in fact in the weak field approximation, for r large, the motion of the body is described by Newton's laws with gravitational potential $U(r) = -\frac{M}{r}$, i.e. the central gravitational potential outside a body with mass M.

The Schwarzschild metric is spherically symmetric and static, it is therefore invariant for temporal translations and for time reversal $t \leftrightarrow -t$. The metric does not depend on t or φ. As such, the metric admits a timelike Killing vector ξ_0^μ for the time translation, and three spacelike Killing vectors corresponding to the symmetries of the rotation group $SO(3)$. More specifically,

- $\xi_0^\mu = (1, 0, 0, 0) \qquad \xi_0^\mu \partial_\mu = \partial_t,$
- $\xi_1^\mu = (0, 0, \sin\varphi, \cot\theta\cos\varphi) \qquad \xi_1^\mu \partial_\mu = \sin\varphi\partial_\theta + \cot\theta\cos\varphi\partial_\varphi,$
- $\xi_2^\mu = (0, 0, -\cos\varphi, \cot\theta\sin\varphi) \qquad \xi_2^\mu \partial_\mu = -\cos\varphi\partial_\theta + \cot\theta\sin\varphi\partial_\varphi,$
- $\xi_3^\mu = (0, 0, 0, 1) \qquad \xi_4^\mu \partial_\mu = \partial_\varphi.$

In GR every Killing vector corresponds to a constant of motion for free geodesic motion. If ξ^μ is a Killing vector, then the quantity

$$\xi_\alpha \frac{dx^\alpha}{d\tau} = \xi_\alpha u^\alpha = constant,$$

when x^α is the particle worldline coordinate. The corresponding conserved quantities for the four Killing vectors above are the energy per unit mass ε, the angular momentum per unit mass components J_i, with $i = 1, 2, 3$, i.e.

$$\varepsilon = -u_\alpha \xi_0^\alpha, \qquad J_i = u_\alpha \xi_i^\alpha, \tag{2.1.2}$$

Since every orbit in Schwarzschild spacetime can be chosen to be equatorial, by putting $\theta = \frac{\pi}{2}$, the angular momentum does not precess and one can choose constants $J_1 = J_2 = 0$ and $J_3 = \ell$, such that the angular momentum is along the z-axis, or always perpendicular to the ∂_φ vector and the plane of the orbit. Not surprising, for the Schwarzschild metric has perfect spherical symmetry, so there is no preferred direction in space.

Moreover Schwarzschild solution is completely conservative, the energy is conserved and it cannot account by itself alone for dissipating phenomena like the emission of gravitational waves. At the same time, by Birkhoff's theorem [87], as we mentioned previously,

the Schwarzschild solution is the ideal description for the exterior of any spherically symmetric star or distribution of matter. The two conclusions we can draw immediately from these facts are that spherically symmetric objects cannot be sources of Gravitational Waves, and that in order to obtain radiation from a Schwarzschild BH one needs to introduce perturbations to the metric (2.1.1), which we are going to do in the next section.

Before that, we first focus on some other important properties of the Schwarzschild BH. The metric is singular in $r = 0$ and $r = 2M$. While the first one is a real singularity, the second one is an artifact of the coordinate choice and can be removed by changing coordinates, as it was first recognized by LeMaître [88, 89]. The fact that only $r = 0$ is a curvature singularity can be shown by computing the Kretschmann curvature scalar

$$R_{\alpha\beta\gamma\delta}R^{\alpha\beta\gamma\delta} = 48\frac{M^2}{r^6}, \tag{2.1.3}$$

where $R_{\alpha\beta\gamma\delta}$ is the Riemann tensor associated to Schwarzschild metric (2.1.1). The scalar (2.1.3) diverges at $r = 0$ anyway, while for different systems of coordinates the metric (2.1.1) can be regular at $r = 2M$, and the curvature scalar (2.1.3) would still diverge at $r = 0$. An easy way to observe this is to switch to the Eddington-Finkelstein and Kruskal coordinates [90, 91]. Just define the variables

$$u \equiv t - r_*, \qquad v \equiv t + r_*, \tag{2.1.4}$$

with the "tortoise" coordinate

$$r_* \equiv r + 2M \ln\left(\frac{r}{2M} - 1\right). \tag{2.1.5}$$

The tortoise coordinate tends to $-\infty$ as $r \to 2M$, and for every $r > 2M$ then $(u, v) \in \mathbb{R}^2$. With these definitions, the metric (2.1.1) becomes

$$\begin{aligned} ds^2 &= -\left(1 - \frac{2M}{r}\right)(dt^2 - dr_*^2) + r^2(d\theta^2 + \sin^2\theta d\varphi^2) \\ &= -\left(1 - \frac{2M}{r}\right) du dv + r^2(d\theta^2 + \sin^2\theta d\varphi^2). \end{aligned} \tag{2.1.6}$$

Moreover, defining

$$U \equiv -e^{-\frac{u}{4M}}, \qquad V \equiv e^{\frac{v}{4M}}, \tag{2.1.7}$$

one has the Kruskal metric

$$ds^2 = -\frac{32M^3}{r}e^{-\frac{r}{2M}} dU dV + r^2(d\theta^2 + \sin^2\theta d\varphi^2), \tag{2.1.8}$$

with $U < 0, V > 0$, which clearly shows how the $r = 2M$ singularity can be visually removed from the metric. In the Kruskal coordinates (2.1.7) the maximal extension of the Schwarzschild BH (when $(U, V) \in \mathbb{R}^2$ and $UV < 1$) is performed and the coordinate singularity $r = 2M$ is eliminated. A graphical representation of the different regions in

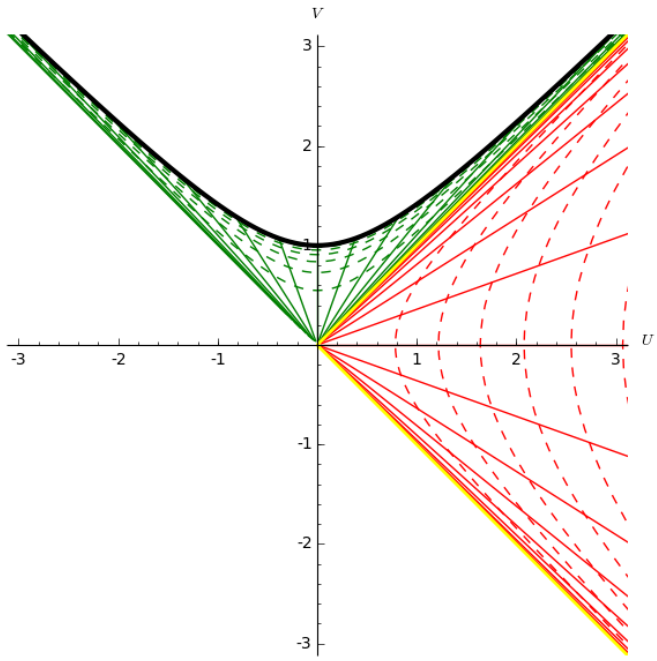

Figure 2.2: Kruskal diagram of Schwarzschild spacetime. The red region is the exterior of the BH, $r > 2M$. The green region the interior. The yellow line represents the BH horizon $r = 2M$. Dashed lines are $r = const$ lines, straight lines are $t = const$ lines, the black curve is the curvature singularity $r = 0$ or $UV = 1$. The maximal extension of the Schwarzschild BH occupies symmetrically the other two quadrants of the plot, here left intentionally blank. The maximal extension of Schwarzschild spacetime has no meaning if one considers a BH as an astrophysical object. Diagram credit to http://sagemanifolds.obspm.fr/index.html.

which the Schwarzschild spacetime is divided is given by the Kruskal diagram in Fig. (2.2).

Although it is a coordinate singularity, the hypersurface $r = 2M$ represents what is commonly called an event horizon. It divides Schwarzschild spacetime into two regions. An object crossing the horizon can never come back, and therefore the regions $r < 2M$ and $r > 2M$ are not causally connected. This is valid for light- and time-like geodesics, so for the geodesics of a possible physical observer or signal, like a photon. Once the horizon is crossed, the object can only decrease its radial distance towards the center of the BH. This can be seen evaluating how the light-cones of an infalling body tilt towards the BH, showing that the only possible future directions for the observer are all directed towards the origin (see Fig. 2.3).

Any observer takes a finite amount of proper time τ to reach the BH horizon, but in terms of the time t of an observer situated infinitely far away, this approaching process takes infinite time. If we were to send a probe into a Schwarzschild BH emitting a periodic laser signal back to us, then this signal would be redshifted more and more as the probe approaches the horizon and its luminosity diminishes, as the signal fights against the

gravitational potential to reach us. The time between one repeated signal and the next one inflates so much until it takes infinite time for the next signal to be received by us. At this point the probe disappears from our detector screens and we say that it has been swallowed by the black hole.

The BH horizon screens the curvature singularity at the origin, preventing any causal contact with it, complying with the cosmic censorship conjecture. No signal from the observer reaching the singularity can be sent outside the black hole. This is the picture in General Relativity, therefore any calculation that we are going to show has the BH horizon as natural physical limit, for $t \to +\infty$. Any investigation of what happens in the interior region is beyond the purposes of our work and anyway involves a region with high curvature and high energies, where a quantum-gravitational description might suit better, rather than just classical GR.

2.1.2 The Innermost Stable Circular Orbit

The symmetries of Schwarzschild spacetime and the associated conservation laws help defining the motion of massless and massive particles. For an exhaustive and detailed discussion of all the possible bound and unbound orbits in Schwarzschild spacetime, we refer to [47]; here only a short recap of the motions most relevant to us is given, emphasizing in particular the role of the Innermost Stable Circular Orbit $r = 6M$, as this is an important orbit for coalescing binaries as well. This concept will become clear at the end of this section and in the next chapter.

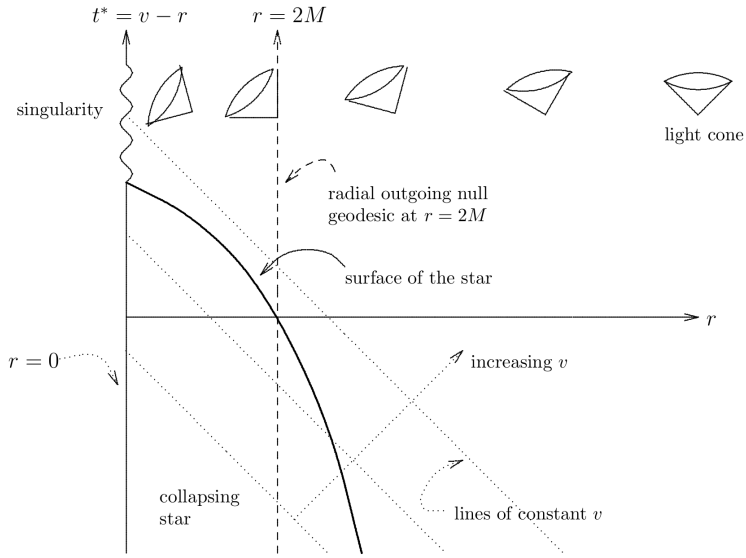

Figure 2.3: Finkelstein diagram of Schwarzschild spacetime. The light-cones distort as $r \to 2M$, so that no future-directed timelike or null worldline can escape the $r \leq 2M$ region. Diagram credit to [81].

The geodesic equations in Schwarzschild spacetime can be derived from the associated Lagrangian $\mathcal{L} = \frac{1}{2} g_{\mu\nu} u^\mu u^\nu$, where $u^\mu = \frac{dx^\mu}{d\tau}$ is the four-velocity of the particle of unit mass ($m = 1$). The equations for time t and azimuthal angle φ just reaffirms what we know from the Killing vectors (2.1.2), namely

$$\left(1 - \frac{2M}{r}\right) u^t = \varepsilon, \qquad r^2 \sin^2\theta u^\varphi = \ell, \tag{2.1.9}$$

with the energy and angular momentum per unit mass ε and ℓ. Instead, the equation for the latitude angle θ is

$$\frac{du^\theta}{d\tau} = -\frac{2}{r} u^r u^\theta + \sin\theta\cos\theta \left(u^\varphi\right)^2 . \tag{2.1.10}$$

As we anticipated discussing the Killing relations, this can be solved choosing $\theta = \frac{\pi}{2}$, because the polar axes can be chosen in an arbitrary way, due to the spherical symmetry, and all the orbits are confined to the equatorial plane, $u^\theta = 0$.

The radial equation can be derived from the constraint on the four-velocity $u^\mu u_\mu = -1[0]$ for massive (respectively massless) particles. This equation relates together the two constants appearing in (2.1.9), i.e. the energy and the angular momentum per unit mass. Respectively for a massive (massless) particle one has

$$g_{\mu\nu} u^\mu u^\nu = -\left(1 - \frac{2M}{r}\right)(u^t)^2 + \frac{(u^r)^2}{\left(1 - \frac{2M}{r}\right)} + r^2 (u^\theta)^2 + r^2 \sin^\theta (u^\varphi)^2 = -1[0], \tag{2.1.11}$$

which becomes, upon replacing (2.1.9) and $\theta = \frac{\pi}{2}$,

$$(u^r)^2 + \left(1 - \frac{2M}{r}\right)\left(1 + \frac{\ell^2}{r^2}\right) = \varepsilon^2, \tag{2.1.12}$$

for a massive particle, and

$$(u^r)^2 + \frac{\ell^2}{r^2}\left(1 - \frac{2M}{r}\right) = \varepsilon^2 \tag{2.1.13}$$

for a massless one[4]. Summarizing, the equations of motion are

$$\begin{aligned} \theta &= \frac{\pi}{2}, & u^\varphi &= \frac{\ell}{r^2}, \\ u^t &= \frac{\varepsilon}{\left(1 - \frac{2M}{r}\right)}, & (u^r)^2 &= \varepsilon^2 - V(r), \end{aligned} \tag{2.1.14}$$

with $V(r)$ an "effective potential" given by

$$V_{massive}(r) = \left(1 - \frac{2M}{r}\right)\left(1 + \frac{\ell^2}{r^2}\right) \qquad \text{or} \qquad V_{massless}(r) = \frac{\ell^2}{r^2}\left(1 - \frac{2M}{r}\right), \tag{2.1.15}$$

[4]For a massless particle the line element $(ds)^2 = 0$ and the geodesic is described using an affine parameter, say λ, different from proper time, such that $u^\mu = \frac{dx^\mu}{d\lambda}$. Also the interpretation of the constants of motion ε, ℓ changes to energy and angular momentum of the massless particle, because $m^2 = 0$.

respectively for massive and massless particles. While for the latter ℓ is just a multiplicative constant, for massive particles the dynamics is influenced by a nontrivial dependence on the angular momentum. A qualitative study of the effective potential (2.1.15) can inform us about the possible orbits in Schwarzschild spacetime, in an analogue way as it is done in Newtonian mechanics.

Geodesics for a massless particle -such as a photon- describe open orbits, the deflection of the ingoing particle. The only closed orbit is possible at $r = 3M$, and it is an unstable circular orbit [47], commonly referred to as *light ring*.

Geodesics for a massive particle instead show much more variety, bound and unbound motion is possible. Eccentric orbits are possible, although they are generically not closed orbits, due to periastron advance (a purely GR phenomenon), but the position is anyway oscillating between a minimum (periastron) and a maximum distance (apastron). This happens because of the potential well exhibited by (2.1.15), so a body with given initial energy E can be trapped in a bound orbit. Together with elliptical orbits, circular orbits are possible as well. As a matter of fact, one can study the effective potentials in (2.1.15), writing down

(2.1.16)
$$V(r) = \left(1 - \frac{2M}{r}\right)\left(\delta_1 + \frac{\ell^2}{r^2}\right), \qquad \text{with} \qquad \delta_1 = \begin{cases} 1, & \text{if massive particle,} \\ 0, & \text{if massless.} \end{cases}$$

Then the condition for circular orbits is $\partial_r V = 0$ and yields

(2.1.17)
$$\ell^2(r - 3M) = \delta_1 M r^2,$$

and one deduces immediately that circular geodesics exist only for $r \geq 3M$ and the only null circular orbit ($\delta_1 = 0$) is the light ring $r = 3M$. Taking a closer look at the second derivative $\partial_r^2 V$ for circular orbits, so using the expression (2.1.17),

(2.1.18)
$$\frac{\partial^2 V}{\partial r^2} = \frac{2\delta_1 M(r - 6M)}{r^3(r - 3M)},$$

one realizes that $r = 6M$ is a flex point and stable circular orbit; the circular orbits between this and the light ring $3M \leq r < 6M$ are necessarily unstable, while for $r \geq 6M$ Eq.(2.1.18) is positive and the orbits are stable. Summarizing, one can draw the following conclusions for timelike motion:

- bound orbits are allowed only for $r > 3M$;
- circular orbits with $3M \leq r < 6M$ are unstable;
- circular orbits with $r \geq 6M$ are stable.

All these considerations can be easily visualized in the plot of the effective potential as in Fig. 2.4. A great role is played by the last stable orbit, $r = 6M$, commonly referred to as the *Innermost Stable Circular Orbit* or ISCO. This can be recognized by minimizing the potential (2.1.15) while looking for a circular orbit $r = R$. The resulting expression gives

(2.1.19)
$$R = \frac{\ell^2}{2M}\left(1 + \sqrt{1 - \frac{12M^2}{\ell^2}}\right),$$

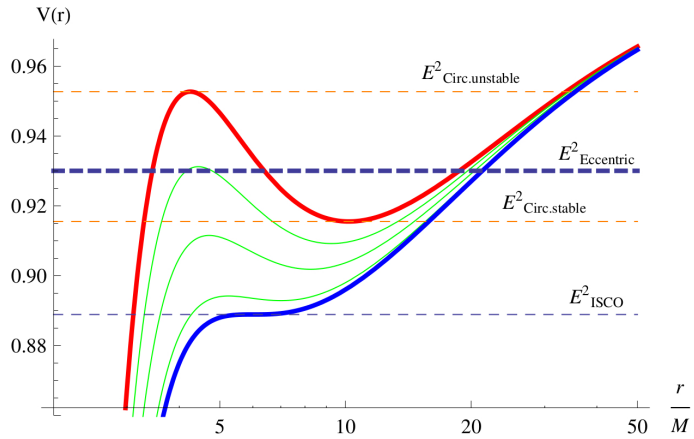

Figure 2.4: Effective potential $V(r)$ for decreasing values of angular momentum L (red and green curves). A particle with energy E can move along an eccentric orbit between periastron and apastron. For different energies circular orbits are possible, respectively at the maximum and minimum of the potential (orange dashed lines). For the special value $L = 2\sqrt{3}M$ the potential allows only a flex point at $r = 6M$ (blue curve). There the only possible closed orbit is the ISCO (blue dashed line).

strongly dependent on the angular momentum per unit mass ℓ. Minimizing this last expression (2.1.19), one finds the minimal circular orbit, i.e. the ISCO. This happens for a special value of the angular momentum $\ell = 2\sqrt{3}M$. Reminding that energy and angular momentum are connected via the normalization condition on the velocity $u^\mu u_\mu = -1$ that, for a circular orbit, reads

(2.1.20)
$$\varepsilon^2 = \left(1 - \frac{2M}{R}\right)\left(1 + \frac{\ell^2}{R^2}\right),$$

(one just needs to replace $u^r = 0$ in (2.1.14)). Finally, one can obtain the following solution for the ISCO of a unit-mass particle:

(2.1.21)
$$t(\tau) = \sqrt{2}\tau, \qquad r = 6M, \qquad \theta = \frac{\pi}{2}, \qquad \varphi(\tau) = \frac{\sqrt{3}}{18M}\tau, \qquad \varepsilon = \frac{2\sqrt{2}}{3}, \qquad \ell = 2\sqrt{3}M.$$

2.2 Perturbations of Schwarzschild spacetime

A small body μ orbiting in the background metric $g_{\mu\nu}$ of a major companion with mass M introduces a perturbation to its spacetime. This perturbation allows to study the properties of the background spacetime and eventually results in gravitational radiation. In this section we will discuss the perturbation of a Schwarzschild Black Hole and establish the master equations that are needed to describe the Gravitational Waves produced. In general there are two approaches to BH perturbations, one can study the perturbation of the metric coefficients, moving from the linearised Einstein field equations, or study the

perturbations in the Weyl scalar using the Newman-Penrose formalism [47]. For the case of Schwarzschild Black Holes the first approach will be followed.

Just as Gravitational Waves have two polarizations, there are two wave equations derived by BH perturbation theory, for even and odd parity modes, bearing the name of the people who first derived them, namely the "Regge-Wheeler and Zerilli-Moncrief equations" [16, 92, 93]. Different derivations of these equations can be found commonly in textbooks like [47] or in works like [94, 95, 96]. Here we will just recall the main elements of the fully covariant derivation given in [97].

However different the derivation of the Regge-Wheeler/Zerilli-Moncrief equations can be, the common path is to linearise the Einstein field equations, expand its main terms in spherical harmonics, and then apply gauge transformations. Eventually two wave equations are obtained, together with the procedure to retrieve physical quantities like energy and angular momentum fluxes, or the connection with Gravitational Waves in more common gauges, notably the Transverse-Traceless gauge.

2.2.1 Separation in Tensor Spherical Harmonics

Schwarzschild spacetime enjoys spherical symmetry, therefore one can separate already the angular part from time and radial distance in the metric,

$$(ds)^2 = g_{ab}dx^a dx^b + r^2\Omega_{AB}d\theta^A d\theta^B, \tag{2.2.1}$$

where g_{ab} is the metric of a two-dimensional Lorentzian space with coordinates $(x^0, x^1) = (t, r)$, and Ω_{AB} is the metric of the unit two-sphere $\mathcal{S}^2$, namely $\Omega_{AB}d\theta^A d\theta^B = (d\theta)^2 + \sin^2\theta(d\varphi)^2$. These spheres are orthogonal to the Lorentzian two-dimensional space and the full Schwarzschild spacetime is given by the product of the two-spere with the two-dimensional Lorentzian manifold. The connection with the usual form of Schwarzschild metric given in Eq. (2.1.1) is evident.

The importance of such separation (2.2.1) lies in the spherical symmetry that, as we will see, prevents different angular components from mixing with each other, therefore the study of a single angular component can be performed independently of the others. The background (2.2.1) satisfies the Einstein field equations in vacuum, and adding a point particle of mass μ is adding a perturbation to the Schwarzschild metric,

$$g_{\mu\nu}^{pert.} = g_{\mu\nu}^{Schwa.} + h_{\mu\nu}, \tag{2.2.2}$$

with $h_{\mu\nu}$ being the small perturbation. Perturbations of the Einstein field equations are then described by a variation of the equations themselves and the addition of an energy-momentum tensor $T_{\mu\nu}$

$$\delta G_{\mu\nu} = \delta(R_{\mu\nu} - \frac{R}{2}g_{\mu\nu}) = 8\pi T_{\mu\nu}. \tag{2.2.3}$$

The perturbing energy-momentum tensor for a pointlike particle is

$$T_{\mu\nu} = \mu \int \frac{d\tau}{\sqrt{-g}} u_\mu u_\nu \delta^4(x^\alpha - x_p^\alpha(\tau)), \tag{2.2.4}$$

with $x_p^\alpha(\tau)$ the particle's geodesic, $u^\nu = \frac{dx_p^\nu}{d\tau}$ the 4-velocity in the proper time τ, and $g = det(g_{\mu\nu})$ the metric determinant. Perturbations are considered only to first order in $h_{\mu\nu}$, therefore the inverse metric of (2.2.2) is simply $g^{\mu\nu}_{pert.} = g^{\mu\nu} - h^{\mu\nu}$. With these results in mind, the left-hand side of (2.2.3) can be cast in the form

$$\delta G_{\mu\nu} = \delta R_{\mu\nu} - \frac{g_{\mu\nu}}{2} g^{\alpha\beta}\delta R_{\alpha\beta}, \tag{2.2.5}$$

and the variation of the Ricci tensor can be calculated in normal coordinates thanks to the Palatini identity [29]

$$\delta R_{\mu\nu} = \delta\Gamma^\lambda_{\mu\nu;\lambda} - \delta\Gamma^\lambda_{\mu\lambda;\nu}, \quad \text{with} \quad \delta\Gamma^\lambda_{\mu\nu} = \frac{g^{\lambda\rho}}{2}\left(h_{\mu\rho,\nu} + h_{\nu\rho,\mu} - h_{\mu\nu,\rho}\right). \tag{2.2.6}$$

Being tensorial equations (such difference of Christoffel symbols is a tensor), Eqs. (2.2.6) are valid in any coordinate system and covariant. Therefore the regular derivatives can be replaced by covariant derivatives and one obtains the global variation

$$2\delta G_{\mu\nu} = h_{\lambda\mu;\nu}{}^{\lambda} + h_{\lambda\nu;\mu}{}^{\lambda} - \Box h_{\mu\nu} - h^{\lambda}{}_{\lambda;\mu\nu} - g_{\mu\nu}\left(h^{\lambda\rho}{}_{;\lambda\rho} - \Box h^{\lambda}{}_{\lambda}\right). \tag{2.2.7}$$

Now one can take advantage of the spherical symmetry introducing a multipole decomposition for the perturbation $h_{\mu\nu}$ and for the energy-momentum tensor $T_{\mu\nu}$. Such decomposition is based on the spherical harmonic functions, a complete orthonormal basis for the two-space $\mathcal{S}^2$ defined through the equation

$$\Omega^{AB}\frac{d^2Y^{lm}}{d\theta^A d\theta^B} + l(l+1)Y^{lm} = 0, \tag{2.2.8}$$

with (l, m) integer numbers, with $l \geq 0$ and $m = -l, -l+1 \ldots 0 \ldots l, l-1, l$. A more extended description of the spherical harmonics, their properties, identities, and mutual relations can be found in textbooks such as [98]. Here we just recall the basic terms that we need for the decomposition of (2.2.7). It is a well-known fact that every scalar $S(\theta, \varphi)$ that is function of only angular variables, i.e. that is defined completely on $\mathcal{S}^2$, can be decomposed in spherical harmonics as

$$S(\theta,\varphi) = \sum_{l=0}^{+\infty}\sum_{m=-l}^{l} s_{lm}Y^{lm}(\theta,\varphi), \quad \text{with} \quad s_{lm} = \int S(\theta,\varphi)Y^*_{lm}(\theta,\varphi)d\Omega. \tag{2.2.9}$$

Such expansion can be extended to vectors and tensors through the derivatives of the harmonics Y^{lm}. For instance a vector field is normally decomposed as

$$V_A(\theta,\varphi) = \sum_{l=0}^{+\infty}\sum_{m=-l}^{l}\left(v_{lm}Z^{lm}_A(\theta,\varphi) + \tilde{v}_{lm}X^{lm}_A(\theta,\varphi)\right), \text{with } Z^{lm}_A = \frac{dY^{lm}}{d\theta^A},\ X^{lm}_A = \varepsilon_A{}^B\frac{dY^{lm}}{d\theta^B}, \tag{2.2.10}$$

ε^{AB} being the antisymmetric Levi-Civita tensor in two dimensions. For our purposes we also need symmetric rank-2 tensor harmonics, which are

$$U_{AB} = \Omega_{AB}Y^{lm}, \qquad V_{AB} = \frac{d^2Y^{lm}}{d\theta^A d\theta^B} + \frac{l(l+1)}{2}\Omega_{AB}Y^{lm}, \qquad W_{AB} = \frac{1}{2}\left(X^{lm}_{A,B} + X^{lm}_{B,A}\right); \tag{2.2.11}$$

these definitions do not agree with those originally used by Regge and Wheeler [16] in the normalization conditions and names, rather they follow the detailed work of Martel [95].

The parity of a spherical harmonic, either scalar, or tensor one, is given by l, following the key properties that

$$\begin{aligned} Y^{lm}(\pi-\theta,\varphi+\pi) &= (-1)^l Y^{lm}(\theta,\varphi), \\ Y^{*lm}(\theta,\varphi) &= (-1)^m Y^{l,-m}(\theta,\varphi), \end{aligned} \tag{2.2.12}$$

for a change of the angular variables that is symmetric with respect to the origin of the coordinate system. A spherically symmetric spacetime preserves the parity of the spherical (l,m)-modes and the derivation of the equations can be performed for every mode separately. Thus we have for the *even parity modes* $(l+m=2n)$

$$h^e_{\mu\nu}(x^c,\theta^A) = \sum_{lm} \begin{pmatrix} p^{lm}_{ab} Y^{lm}(\theta,\varphi) & q^{lm}_a Z^{lm}_A(\theta,\varphi) \\ q^{lm}_a Z^{lm}_A(\theta,\varphi) & r^2\left[K^{lm}U^{lm}_{AB}(\theta,\varphi) + G^{lm}V^{lm}_{AB}(\theta,\varphi)\right] \end{pmatrix}, \tag{2.2.13}$$

while for the *odd parity modes*

$$h^o_{\mu\nu}(x^c,\theta^A) = \sum_{lm} \begin{pmatrix} 0 & h^{lm}_a X^{lm}_A(\theta,\varphi) \\ h^{lm}_a X^{lm}_A(\theta,\varphi) & h^{lm}_2 W^{lm}_{AB}(\theta,\varphi) \end{pmatrix}, \tag{2.2.14}$$

where p_{ab}, q_a, K, G, h_a, and h_2 are functions of $x^c=(t,r)$ only, components of the perturbation $h_{\mu\nu}$ along the different harmonics. In the same way one can write the expansion for the energy-momentum tensor, which comprehensively looks like

$$T^{\mu\nu} = \sum_{lm} \frac{4\pi}{r^2} \begin{pmatrix} 2r^2 Q^{ab}_{lm} Y^{lm}(\theta,\varphi) & Q^a_{lm} Z^A_{lm}(\theta,\varphi) + P^a_{lm} X^A_{lm} \\ Q^a_{lm} Z^A_{lm}(\theta,\varphi) + P^a_{lm} X^A_{lm} & Q^\flat U^{AB}_{lm}(\theta,\varphi) + \frac{Q^\sharp}{r^2} V^{AB}_{lm}(\theta,\varphi) + \frac{P}{r^2} W^{AB}_{lm}(\theta,\varphi) \end{pmatrix}, \tag{2.2.15}$$

with, again, $Q^{ab}, Q^a, Q^\flat, Q^\sharp$ non-zero for the even modes, and P^a, P non-zero for the odd modes; all together functions of $x^c=(t,r)$ only.

2.2.2 The Regge-Wheeler and Zerilli-Moncrief equations

After the angular decomposition given in Eqs. (2.2.13), (2.2.14), and (2.2.15) has been established, one can reduce further the problem exploiting gauge transformations. In GR a general coordinate transformation $x^\mu \to x^\mu + \xi^\mu$ is also a gauge transformation, and the perturbation $h_{\mu\nu}$ transforms accordingly as

$$h_{\mu\nu} \to h_{\mu\nu} - 2\xi_{(\mu;\nu)}. \tag{2.2.16}$$

The gauge vector ξ^μ can be decomposed along spherical harmonics and its components divided into even and odd modes as well. This decomposition allows to determine six gauge invariant quantities. Referring to the expansion coefficients defined in the previous section (2.2.13), the following ones are six covariant quantities (denoted by a "$\sim$")

$$\begin{aligned} \tilde{p}_{ab} &= p_{ab} - 2v_{(a;b)}, & \tilde{K} &= K + \frac{l(l+1)}{2}G - 2\frac{r_{,a}v^a}{r}, \\ \tilde{h}_a &= h_a - \frac{1}{2}h_{2,a} - \frac{r_{,a}}{r}h_2, & &\text{with } v_a = q_a - \frac{r^2}{2}G_{,a}. \end{aligned} \tag{2.2.17}$$

The first line shows four gauge invariants for the even modes, and the second line presents two gauge invariants for the odd modes ($a = t, r$). Calculations are then easily performed in the Regge-Wheeler gauge [16], whereby ξ is chosen so that $\tilde{p}_{ab} = p_{ab}$, $\tilde{K} = K$, and $\tilde{h}_a = h_a$. For any calculation in this gauge one simply needs to replace the Regge-Wheeler quantities with the corresponding invariants in order to be fully covariant.

The linearised Einstein field equations (2.2.3) can be enforced, mode by mode, together with the contracted Bianchi identities, which reduce the number of independent equations by 4, leaving only 6 independent equations. Such identities come from the evaluation of the following terms:

$$\int T^{a\mu}{}_{;\mu} Y^{lm*} d\Omega = 0, \qquad \int T^{A\mu}{}_{;\mu} Z^{lm*}_A d\Omega = 0, \qquad \int T^{A\mu}{}_{;\mu} X^{lm*}_A d\Omega = 0. \tag{2.2.18}$$

There are 10 perturbation expansion coefficients to be solved for (2.2.13), but four of the metric perturbations (three even and one odd) can be fixed via arbitrary gauge functions in ξ^μ. There remain 6 metric perturbations to be found, just as there are 6 gauge invariants (2.2.17) and 6 independent equations available. Therefore the system is fully determined.

The next step is to solve the equations mode by mode. Since one is interested in the gravitational radiation, one neglects the non-radiative modes, i.e. the useful modes are for $l \geq 2$. In [92] Zerilli first showed that the monopole term $l = 0$ can be solved for, using gauge freedom, and it reduces to a mass perturbation. Namely the perturbed metric of a free-falling body of mass μ onto a black hole with mass M is still a Schwarzschild metric, but with mass $M + \mu\varepsilon$. In the same paper it is shown that the perturbation due to the $l = 1$ mode can be partly gauged away, and partly accounts for a correction of the angular momentum. Both monopole and dipole terms in the spherical harmonics' expansion in Schwarzschild spacetime are not radiative modes.

Finally the even and odd modes can be successfully decoupled by introducing [93] the scalar field

$$\psi_{ZM} = \frac{r}{\lambda + 1}\left[\tilde{K} + \frac{1}{\Lambda}\left(r_{,a} r_{,b} \tilde{p}^{ab} - r r_{,a} \tilde{K}^{,a}\right)\right], \tag{2.2.19}$$

with $\lambda = (l+2)(l-1)/2$ and $\Lambda = \lambda + 3M/r$. One can combine the terms together and write down the inhomogeneous Zerilli-Moncrief equation for the even modes $l + m = 2n$

$$g^{ab}\psi^{ZM}_{;ab}(x^c) - V^l_{ZM}(r)\psi^{ZM}(x^c) = S^{ZM}(x^c), \tag{2.2.20}$$

with the "potential"

$$V^l_{ZM}(r) = \frac{1}{r^2\Lambda^2}\left[2\lambda^2\left(\lambda + 1 + \frac{3M}{r}\right) + \frac{18M^2}{r^2}\left(\lambda + \frac{M}{r}\right)\right], \tag{2.2.21}$$

and the inhomogeneous term, so-called "source term" given by

$$\begin{aligned} S^{ZM} = {} & \frac{2}{\Lambda} r^a Q_a - \frac{Q^\sharp}{r} + \frac{r}{(\lambda+1)\Lambda^2}\left(\lambda(\lambda-1) + \frac{3M}{r}(2\lambda - 3) + \frac{21M^2}{r^2}\right) Q^a{}_a \\ & + \frac{r^2}{(\lambda+1)\Lambda}\left(\frac{6M}{r^2\Lambda} Q^{ab} r_{,a} r_{,b} + \frac{1 - \frac{2M}{r}}{r} Q^\flat - (Q^a{}_a)_{,b} r^{,b}\right), \end{aligned} \tag{2.2.22}$$

for every even (l,m)-mode. Similarly for the odd modes $l+m=2n+1$ one can define [16] the scalar field

$$\psi_{RW} = -\frac{\tilde{h}_a r^{,a}}{r}, \tag{2.2.23}$$

and the resulting wave equation is

$$g^{ab}\psi^{RW}_{;ab}(x^c) - V^l_{RW}(r)\psi^{RW}(x^c) = S^{RW}(x^c), \tag{2.2.24}$$

with the potential and source term given respectively by

$$V^l_{RW} = \frac{1}{r^2}\left(l(l+1) - \frac{6M}{r}\right), \qquad S^{RW} = \frac{2}{r^2}\left(1-\frac{3M}{r}\right)P + \frac{r^{,a}}{r}(P_a - P_{,a}). \tag{2.2.25}$$

In Schwarzschild coordinates $g^{ab}\psi^{lm}_{;ab}(x^c) = -\left(\frac{\partial^2}{\partial t^2} - \frac{\partial^2}{\partial r^2}\right)\psi^{lm}(t,r)$ and the covariant wave equations (2.2.20) (2.2.24) reduce to their most common form

$$\begin{aligned}\left(-\frac{\partial^2}{\partial t^2} + \frac{\partial^2}{\partial r^2} - V^l_{ZM}(r)\right)\psi^{lm}_{ZM}(t,r) &= S^{lm}_{ZM}(t,r),\\ \left(-\frac{\partial^2}{\partial t^2} + \frac{\partial^2}{\partial r^2} - V^l_{RW}(r)\right)\psi^{lm}_{RW}(t,r) &= S^{lm}_{RW}(t,r),\end{aligned} \tag{2.2.26}$$

where the potentials $V^l_{RW/ZM}$ were given by (2.2.21), (2.2.25). The source terms in Schwarzschild coordinates take the following form

(2.2.27)

$$\begin{aligned} S^{lm}_{ZM} = \frac{1}{(\lambda+1)\Lambda}\Bigg[& r^2(1-\frac{2M}{r})\Big((1-\frac{2M}{r})^2 Q^{tt}{}_{,r} - Q^{rr}{}_{,r}\Big) + r\left(\frac{\Lambda}{1-\frac{2M}{r}} - 1\right)Q^{rr}\\ &+ (1-\frac{2M}{r})Q^{\flat} - \frac{1-\frac{2M}{r}}{r\Lambda}\Big(\lambda(\lambda-1)r^2 + (4\lambda-9)Mr + 15M^2\Big)Q^{tt}\Bigg]\\ &+ \frac{2Q^r}{\Lambda(r)} - \frac{Q^\sharp}{r},\\ S^{lm}_{RW} = \frac{1}{r}&\left(\frac{2}{r}(1-\frac{3M}{r})P - (1-\frac{2M}{r})P_{,r} + P^r\right). \end{aligned}$$

Thus, moving from Droste's to tortoise coordinates (useful for the numerical resolution of the RW/ZM equations, as it will be explained in the next section), the RW/ZM equation changes accordingly into

$$\left(\partial^2_{r^*} - \partial^2_t - \bar{V}^l_{RW/ZM}(r^*)\right)\psi^{lm}_{RW/ZM} = \bar{S}^{lm}_{RW/ZM} \tag{2.2.28}$$

with $\bar{V}^l = \left(1-\frac{2M}{r}\right)V^l$ and $\bar{S}^{lm}_{RW/ZM} = \left(1-\frac{2M}{r}\right)S^{lm}_{RW/ZM}$. The so-called "tortoise coordinates" (t,r^*) are defined through the relation

$$r^* = r + 2M\log\left(\frac{r}{2M} - 1\right), \tag{2.2.29}$$

with the same observer's time t.

If we now evaluate the angular expansion coefficients of the energy-momentum tensor (2.2.15) in Schwarzschild coordinates for a point particle with mass μ, with the subscript "p" indicating the particle's position, we obtain

(2.2.30)
$$Q^{tt} = \frac{8\pi\mu}{r^2}u^t\delta(r-r_p(\tau))Y^{*lm}(\theta_p,\varphi_p), \qquad P^r = \frac{16\pi\mu}{l(l+1)}\frac{u^r}{u^t}u^A X_A^{*lm}(\theta_p,\varphi_p)\delta(r-r_p(\tau)),$$
$$Q^{rr} = \frac{8\pi\mu}{r^2}\frac{u^{r2}}{u^t}\delta(r-r_p(\tau))Y^{*lm}(\theta_p,\varphi_p), \quad Q^r = \frac{16\pi\mu}{l(l+1)}\frac{u^r}{u^t}u^A Z_A^{*lm}(\theta_p,\varphi_p)\delta(r-r_p(\tau)),$$
$$Q^\flat = 8\pi\mu\frac{u^A u^B}{u^t}U_{AB}^{*lm}(\theta_p,\varphi_p)\delta(r-r_p(\tau)),$$
$$Q^\sharp = 32\pi\mu\frac{(l-2)!}{(l+2)!}r^2\frac{u^A u^B}{u^t}V_{AB}^{*lm}(\theta_p,\varphi_p)\delta(r-r_p(\tau)),$$
$$P = 16\pi\mu\frac{(l-2)!}{(l+2)!}r^2\frac{u^A u^B}{u^t}W_{AB}^{*lm}(\theta_p,\varphi_p)\delta(r-r_p(\tau)).$$

One then notices immediately that they are all multiples of the Dirac delta distribution of the particle position. This is a natural consequence of the pointlike nature of the energy-momentum tensor (2.2.4). The derivatives appearing in the definitions of the source terms introduce the derivatives of the Dirac distribution and the source terms get divided into two main functions, one multiple of the delta function, and one multiple of its derivative. Therefore one can rewrite [18] the source terms (2.2.27) as

$$\bar{S}^{lm}_{RW/ZM} = \left(1-\frac{2M}{r}\right)\left(F^{lm}_{RW/ZM}\partial_r\delta(r-r_p) + G^{lm}_{RW/ZM}\delta(r-r_p)\right). \tag{2.2.31}$$

Here the following relations hold for $F^{lm}_{RW/ZM}, G^{lm}_{RW/ZM}$ in terms of orbital velocities:

(2.2.32)
$$F^{lm}_{ZM} = \frac{8\pi\mu Y^{*lm}}{\Lambda(\lambda+1)}\left[\left(1-\frac{2M}{r}\right)^2 u^t - \frac{u^{r2}}{u^t}\right],$$
$$G^{lm}_{ZM} = \frac{8\pi\mu Y^{*lm}}{\Lambda(\lambda+1)}\left[\left(1-\frac{2M}{r}\right)^2 (u^t{}_{,r} - \frac{2u^t}{r}) + \frac{u^{r2}}{ru^t} - \frac{2u^r u^r_{,r}}{u^t} + \frac{u^{r2}u^t{}_{,r}}{u^{t2}} + \left(\frac{\Lambda}{1-\frac{2M}{r}}\right)\frac{u^{r2}}{ru^t}\right.$$
$$\left. - \left(1-\frac{2M}{r}\right)\frac{u^t}{r^3\Lambda}(\lambda(\lambda-1)r^2 + (4\lambda-9)Mr + 15M^2)\right] + \frac{32\pi\mu}{l(l+1)\Lambda}\frac{u^r}{u^t}u^A Z_A^{*lm}$$
$$+ \frac{8\pi\mu}{\Lambda(\lambda+1)}\left(1-\frac{2M}{r}\right)\frac{u^A u^B}{ru^t}U_{AB}^{*lm} - 32\pi\mu\frac{(l-2)!}{(l+2)!}r\frac{u^A u^B}{u^t}V_{AB}^{*lm};$$
$$F^{lm}_{RW} = -16\pi\mu\left(1-\frac{2M}{r}\right)\frac{(l-2)!}{(l+2)!}r\frac{u^A u^B}{u^t}W_{AB}^{*lm},$$
$$G^{lm}_{RW} = \frac{16\pi\mu}{u^{t2}}\frac{(l-2)!}{(l+2)!}\left[u^A\left(\left(u^t + ru^t{}_{,r}\right)\left(1-\frac{2M}{r}\right) - u^t\right) - 2r\left(1-\frac{2M}{r}\right)u^t u^A_{,r}\right]u^B W_{AB}^{*lm}$$
$$+ \frac{16\pi\mu u^r u^A}{l(l+1)ru^t}X_A^{*lm}.$$

Before deriving how the Regge-Wheeler and Zerilli-Moncrief equations relate to other gauges or how to extract physical quantities from them, it is worth noticing that we started from ten independent equations (the linearised Einstein field equations (2.2.3)) and ended with just two wave equations. As we already said, this is to be expected as the independent polarizations of gravitational waves, which are the outcome of the BH perturbation, are two as well, so there has been no extra degree of freedom introduced.

Another interesting property of the Zerilli-Moncrief and Regge-Wheeler functions $\psi^{lm}_{RW/ZM}$ can be recognized if we look at the Schwarzschild metric as a special case of a stationary axisymmetric spacetime [47], which in spherical coordinates and in its most general form is

$$(ds)^2 = e^{2\nu}(dt)^2 - e^{2\psi}(d\varphi - \omega dt)^2 - e^{2\mu_2}(dr)^2 - e^{2\mu_3}(d\theta)^2, \tag{2.2.33}$$

with ν, ψ, ω, and μ_i functions of (r, θ) only, as required by stationarity and symmetry about a spatial direction. Schwarzschild metric is a special case of this with the requirements

$$e^{2\nu} = e^{-2\mu_2} = 1 - \frac{2M}{r}, \qquad e^{\mu_3} = r, \qquad e^{\psi} = r\sin\theta, \qquad \omega = 0. \tag{2.2.34}$$

Therefore a general perturbation of (2.2.33) will result in $\omega \neq 0$, a small quantity, the adding of a term $-q_2 dr - q_3 d\theta$ to ωdt, to account for non-stationarity, and small increments in the functions ν, ψ, μ_i. If one then performs a reversal in sign of φ, the signs of ω, q_2, q_3 are to be reversed as well to keep the metric unchanged. For this reason perturbations of this kind, i.e. changing ω and adding q_2, q_3 are called *axial*, while the other perturbations in ν, ψ, μ_2, μ_3 are called *polar*.

These two kinds of perturbations decouple and can be considered independently from each other. In fact it can be shown that the polar ones lead to the Zerilli-Moncrief equation, while axial perturbations lead to the Regge-Wheeler equation [47]. Therefore the difference between even and odd modes acquires yet another meaning: they represent respectively the polar and the axial perturbations of Schwarzschild spacetime.

2.2.3 Physical meaning of the Regge-Wheeler wave functions

The solutions of the Regge-Wheeler equations (2.2.26) give information about the gravitational radiation, but it is necessary to perform a gauge transformation in order to relate them to the more common form of the transverse-traceless gauge. To this end a complex null-tetrad is introduced which defines the so-called "radiation gauge". This gauge allows to calculate the gravitational radiation towards infinity (very far away from the source region), in which case it is called *outgoing* radiation gauge, or towards the BH horizon, namely *ingoing* radiation gauge. As far as the observed gravitational waves are concerned, one is more interested in the outgoing radiation, not in the one absorbed by the black hole, so we will deal with that one mainly. However in both cases the Regge-Wheeler functions are the starting point and in this section we recall briefly what the link between these, the gravitational waves $h_\times, h_+$, the emitted energy, and the emitted angular momentum is.

A complex null-tetrad [47] is a set of complex vectors l^μ, n^μ, and m^μ satisfying the following properties: l^μ, n^μ are null vectors tangent to outgoing and ingoing light rays respectively, the vector m^μ has complex conjugate $\bar{m}^\mu$ on the two-sphere $\mathcal{S}^2$. Moreover,

$$l^\mu l_\mu = 0 = n^\mu n_\mu, \qquad m^\mu m_\mu = 0 = \bar{m}^\mu \bar{m}_\mu, \qquad l^\mu n_\mu = -1 = -m^\mu \bar{m}_\mu, \tag{2.2.35}$$

and the spacetime metric can be rewritten in terms of this tetrad (completeness relation)

$$g_{\mu\nu} = 2[m_{(\mu}\bar{m}_{\nu)} - l_{(\mu}n_{\nu)}]. \tag{2.2.36}$$

For instance, in Schwarzschild coordinates one choice for the tetrad vectors is

(2.2.37)
$$l_\mu = (-1, \frac{1}{1-\frac{2M}{r}}, 0, 0), \qquad n_\mu = -\frac{1}{2}(1 - \frac{2M}{r}, 1, 0, 0), \qquad m_\mu = \frac{r}{\sqrt{2}}(0, 0, 1, i\sin\theta).$$

As was mentioned, one introduces the Outgoing Radiation Gauge (ORG) conditions:

$$\begin{aligned} &h^{ORG}_{\mu\nu} n^\mu n^\nu = 0, \\ &h^{ORG}_{\mu\nu} n^\mu m^\nu = 0 = h^{ORG}_{\mu\nu} n^\mu \bar{m}^\nu, \\ &h^{ORG}_{\mu\nu} n^\mu l^\nu = 0 = h^{ORG}_{\mu\nu} m^\mu \bar{m}^\nu. \end{aligned} \tag{2.2.38}$$

With the definitions (2.2.35) and the conditions (2.2.38), the metric perturbation (2.2.2) in the ORG becomes

$$\begin{aligned} h^{ORG}_{\mu\nu} =& l^\lambda l^\rho h_{\lambda\rho} n_\mu n_\nu + 2(l^\lambda \bar{m}^\rho h_{\lambda\rho} n_{(\nu} m_{\mu)} + l^\lambda m^\rho h_{\lambda\rho} n_{(\mu} \bar{m}_{\nu)}) \\ &+ \bar{m}^\lambda \bar{m}^\rho h_{\lambda\rho} m_\mu m_\nu + m^\lambda m^\rho h_{\lambda\rho} \bar{m}_\mu \bar{m}_\nu. \end{aligned} \tag{2.2.39}$$

After some calculations involving the metric decomposition given in eqs. (2.2.13), (2.2.14) in the outgoing radiation gauge, to leading order $\frac{1}{r}$, it is possible [97] to write down the following useful relation

(2.2.40)
$$h_+(r,t,\theta,\phi) - ih_\times(r,t,\theta,\phi) = \frac{1}{2r}\sqrt{\frac{(l+2)!}{(l-2)!}} \sum_{l,m} \left(\psi^{lm}_{ZM}(r,t) - 2i \int_{-\infty}^{t} \psi^{lm}_{RW}(r,t')dt' \right) {}_{-2}Y^{lm}(\theta,\phi),$$

where the spin-weighted spherical harmonics are introduced with spin-weight $s = -2$

$$V^{lm}_{AB} \bar{m}^A \bar{m}^B = \frac{1}{2}\sqrt{\frac{(l+2)!}{(l-2)!}} \cdot {}_{-2}Y^{lm}(\theta,\phi). \tag{2.2.41}$$

Once the RW/ZM wave functions are known, they can be used to calculate the radiative part of the gravitational field far away from the source, as it is given in (2.2.40) in the transverse-traceless gauge. Eq. (2.2.40) is the main equation relating the RW/ZM-waveforms to the more common form of gravitational radiation.

2.2.4 Emitted energy and angular momentum

In order to evaluate the emitted energy and angular momentum we have to turn back to the energy-momentum tensor of a gravitational wave and write this in terms of the metric perturbation in the outgoing radiation gauge (2.2.39).

The energy-momentum tensor of a gravitational wave, namely the tensor containing the information about the gravitational field radiated away has been first formulated in a gauge-invariant fashion by Isaacson [99],

$$T^{GW}_{\mu\nu} = \frac{1}{64\pi}\langle h^{\lambda\rho}{}_{;\mu} h_{\lambda\rho;\nu}\rangle, \tag{2.2.42}$$

where $\langle\cdots\rangle$ indicates an average over a region of spacetime. This has to be large compared to radiation wavelength, and typically in the radiation zone the GW wavelength is small compared to the radius of curvature, so the energy-momentum tensor is well-defined there. Notice also that (2.2.42) is of second order in the perturbation $h_{\mu\nu}$, so it does not sum up to the source energy-momentum tensor on the right-hand side of the variation of the linearised Einstein field equation (2.2.3); a GW back-reaction calculation is not yet included at the level of Regge-Wheeler equations.

In Schwarzschild spacetime there are two fundamental Killing vectors, the time direction and the azimuthal angle φ direction, which give birth to the conserved energy and angular momentum, therefore the flow of energy and angular momentum are related to the projections of the energy-momentum tensor (2.2.42) upon these vectors. If $\xi^\mu_t = \delta^\mu_t, \xi^\mu_\varphi = \delta^\mu_\varphi$ are the two Killing vectors, then the corresponding projections are $T^\mu{}_\nu \xi^\nu_t = T^\mu{}_t$ and $T^\mu{}_\nu \xi^\nu_\varphi = T^\mu{}_\varphi$ respectively, and they are divergence-free, from Killing's equation and energy conservation $T^{\mu\nu}{}_{;\nu} = 0$. From Gauss theorem applied to a 4-volume V in Schwarzschild spacetime with border a 3-surface ∂V, one can infer that

$$\begin{aligned} \int_V T^\mu{}_{t;\mu} dV = \oint_{\partial V} T^\mu{}_t dS_\mu = 0 \qquad &\to \quad \Delta E = \int_S T^\mu{}_t dS_\mu, \\ \int_V T^\mu{}_{\varphi;\mu} dV = \oint_{\partial V} T^\mu{}_\varphi dS_\mu = 0 \qquad &\to \quad \Delta L = \int_S T^\mu{}_\varphi dS_\mu, \end{aligned} \tag{2.2.43}$$

with dS_μ the oriented surface element on ∂V. The flows of energy and angular momentum through a closed 3-surface ∂V vanish, therefore the difference in energy and angular momentum at a fixed radial distance r is given by the surface integral on open 3-surfaces with $r = constant$, denoted by S (expressions on the right in (2.2.43) above). Replacing the surface element in Schwarzschild metric by a sphere $r = constant$, i.e. $dS = \eta_\mu \sqrt{1 - \frac{2M}{r}} r^2 \sin\theta dt d\Omega$, one eventually obtains

$$\begin{aligned} \Delta E = -\epsilon r^2 \left(1 - \frac{2M}{r}\right) \int T_{rt} dt d\Omega \qquad &\to \quad \frac{dE}{dt} = -\epsilon r^2 \left(1 - \frac{2M}{r}\right) \int T_{tr} d\Omega, \\ \Delta L = \epsilon r^2 \left(1 - \frac{2M}{r}\right) \int T_{r\varphi} dt d\Omega \qquad &\to \quad \frac{dL}{dt} = \epsilon r^2 \left(1 - \frac{2M}{r}\right) \int T_{r\varphi} d\Omega, \end{aligned} \tag{2.2.44}$$

with η_μ the normal vector to the S-surface, and $\epsilon = 1$ for dS_μ pointing toward increasing r, $\epsilon = -1$ for dS_μ pointing toward decreasing r.

Now one needs to calculate the needed energy-momentum components from its expression (2.2.42), using the decomposition along the tetrad (2.2.39) for the gravitational perturbation. Eventually one gets the following expression for the far-zone fluxes over time of emitted energy (power) and radiated angular momentum (ang. mom. rate):

(2.2.45)
$$\frac{dE}{dt} = \frac{1}{64\pi}\sum_{l,m}\frac{(l+2)!}{(l-2)!}\left(|\dot{\psi}^{lm}_{ZM}(r,t)|^2 + 4|\psi^{lm}_{RW}(r,t)|^2\right),$$
$$\frac{dL}{dt} = 2\Re\left[\frac{i}{128\pi}\sum_{l,m} m\frac{(l+2)!}{(l-2)!}\left(\dot{\psi}^{lm}_{ZM}(r,t)\psi^{*lm}_{ZM}(r,t) + 4\psi^{*lm}_{RW}(r,t)\int_{-\infty}^{t}\psi^{*lm}_{RW}(r,t')dt'\right)\right].$$

These are the equations that relate the RW/ZM functions to the emitted energy and angular momentum radiated far away from the source of gravitational waves (calculated through the outgoing radiation gauge). Every scalar function has to be evaluated at the desired location (the observer's distance r_{obs}). Remarkably a similar calculation [97] for the fluxes towards the BH horizon, performed in the ingoing radiation gauge, shows that the final expressions for the fluxes are the same as in the far-zone, with the difference in the location r.

2.3 The Lousto-Price algorithm

The Regge-Wheeler equations (2.2.26) presented in the previous section are a list of second order partial differential equations for every (l,m)-mode of the tensorial spherical harmonic expansion of the perturbed metric and source terms in the original Einstein field equations. They give birth to wave-like solutions influenced by the potential at the left-hand side, which depends on the Schwarzschild background, and the source terms on the right-hand side, which depend on the orbit of the minor body perturbing the background.

Nevertheless the procedure to obtain such solutions is not analytic and relies on numerical methods, unless one studies special regimes, such as in the neighbourhood of the horizon, when inquiring for quasi-normal modes [100, 101, 102], where an approximated version of the RW/ZM-equations is solved instead of the full problem. Similarly, a Green's function of the differential operator in (2.2.26) can be used [103] and results obtained in the far-zone approximation $r \to +\infty$.

Here a numerical algorithm is presented that will be used for the results summarized in this thesis, the Lousto-Price algorithm [20]. It is a general algorithm passing the original differential equation into finite-difference equations, dividing the spacetime into finite-size regions, or cells. In this section we describe the main features of this algorithm, independently of its implementation.

The idea behind the algorithm is quite simple: evolving given initial conditions for the functions $\psi^{lm}_{RW/ZM}$ in time and in many positions in Schwarzschild spacetime. Eventually only the values at a reference position, the observer's position, are collected. These represent the evolution of the even and odd modes $\psi^{lm}_{RW/ZM}(r_{obs},t)$ in time.

The starting point is the RW/ZM-equation for a general (l,m)-mode (with $l \geq 2$), which is more conveniently rewritten in tortoise coordinates, i.e.

$$\left(\partial_{r^*}^2 - \partial_t^2 - \bar{V}^l_{RW/ZM}(r^*)\right)\psi^{lm}_{RW/ZM} = \bar{S}^{lm}_{RW/ZM}, \tag{2.3.1}$$

where the source term S^{lm} and the potential V^l get multiplied by a Schwarzschild factor $\left(1-\frac{2M}{r}\right)$, as we showed in (2.2.28). Treating the equation in the variables (t,r^*) makes it easier to solve numerically. In fact the tortoise-coordinate transformation (2.2.29) stretches the curved light-cone lines (where the line element $(d\tau)^2 = 0$) into straight lines as the Schwarzschild metric now reads

$$(d\tau)^2 = \left(1-\frac{2M}{r}\right)(dt)^2 - \left(1-\frac{2M}{r}\right)(dr^*)^2 - r^2\left((d\theta)^2 + \sin^2\theta(d\varphi)^2\right) \tag{2.3.2}$$

and is symmetric in the time and radial component, therefore a Schwarzschild light-cone in these coordinates is represented by

$$t = \pm r^* + constant, \tag{2.3.3}$$

namely straight lines forming $\frac{\pi}{4}$ angles with the (t,r^*)-coordinate axes. In this way the BH horizon present at $r = 2M$ in Schwarzschild spacetime can be mapped to $r^* \to -\infty$ and Schwarzschild spacetime can be divided in squared cells of equal area and with user-defined size (Δ) as in Fig. 2.5. Suppose two such lines depart from the origin $(t,r^*) = (0,0)$ of a (t,r^*) spacetime diagram and then at every $r^* = \pm 2\Delta$ two similar light-cone lines depart from the horizontal axis $t = 0$, in this way all of Schwarzschild spacetime is paved with square cells of area $2\Delta^2$.

The finite-difference algorithm steps in when instead of considering a continuous solution for the waveform $\psi^{lm}_{RW/ZM}(t,r^*)$ known throughout spacetime, one is limited to the knowledge of $\psi^{lm}_{RW/ZM}$ only at specific locations, i.e. the vertices of the cells that pave the time-radius spacetime diagram. The parameter Δ represents half width of any cell and the sampling step for the time evolution of the solution $\psi^{lm}_{RW/ZM}(t,r^*)$, namely two immediately subsequent values of $\psi^{lm}_{RW/ZM}$ are separated by a time difference $t = \Delta$. It goes without saying that the continuity is retrieved in the limit $\Delta \to 0$, where the cells become infinitesimal and the solution continuous.

With this grid of cells in mind, one takes as initial conditions the values for the waveform function $\psi^{lm}_{RW/ZM}(r^*,0)$ and its derivative in time $\dot{\psi}^{lm}_{RW/ZM}(r^*,0)$ at $t = 0$, to be known at every position r^* in space. From the equations (2.3.1) it is clear that the $\psi^{lm}_{RW/ZM}$ functions are continuous[5] everywhere but at the particle's location [97, 96], due to the Dirac delta discontinuity in the source terms (2.2.31). So, writing down the Taylor expansion of the $\psi^{lm}_{RW/ZM}$ function at $t = \Delta$

$$\psi^{lm}_{RW/ZM}(r^*,\Delta) = \psi^{lm}_{RW/ZM}(r^*,0) + \dot{\psi}^{lm}_{RW/ZM}(r^*,0)\Delta + o(\Delta^2), \tag{2.3.4}$$

we know already the values for $\psi^{lm}_{RW/ZM}$ at every event position (r^*,t) in the first two lines. These are sufficient to determine the complete evolution up to a user-defined time

[5] As mentioned in [104] the Zerilli function $\psi^{lm}_{RW/ZM}$ is a function of continuity class $C^{-1}(\mathbb{R}^2)$, i.e. a function that is continuous $(C^0(\mathbb{R}^2))$ after integration.

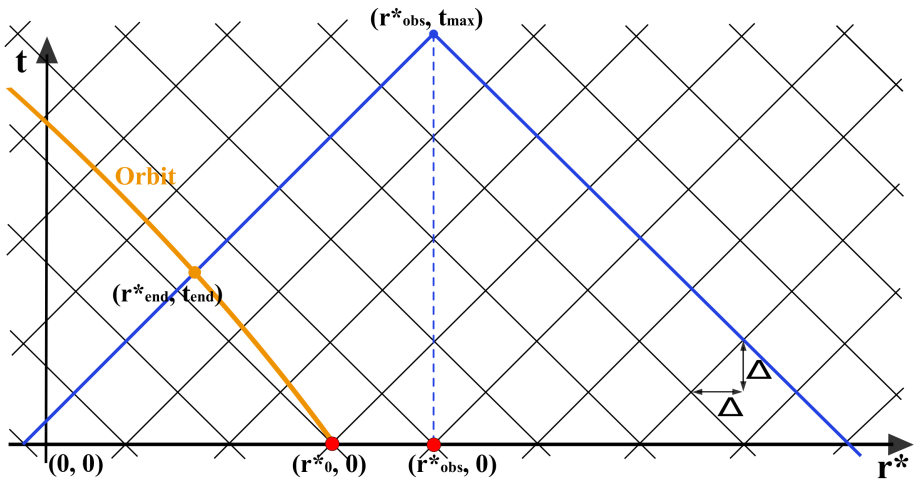

Figure 2.5: Schwarzschild spacetime divided in cells. The area in the blue triangle represents the past light-cone where $\psi^{lm}_{RW/ZM}$ points are evaluated. The orbit of the body traverses only a subset of cells within the causality triangle. Starting from the values on two rows, one retrieves the following ones.

$t = t_{max}$. This time determines the size of the area of points needed to build the solution. In fact only the points contained in the past light-cone of (r^*_{obs}, t_{max}) determine causally the values $\psi^{lm}_{RW/ZM}(r^*_{obs}, t)$, for every $0 < t < t_{max}$. The total number of time steps is given by $\frac{t_{end}}{2\Delta}$ and only the couples (r^*, t) in the area inside the causality triangle really need to be taken into account and evaluated.

The body's trajectory is represented by curve in the diagram, and the cells which are traversed by this curve have to be evaluated differently from the non-traversed ones. For the latter ones the source terms (2.2.31) are identically zero, the opposite happens in the traversed cells. The traversed cell gets split into four different areas, depending on the way the cell is traversed (which is strictly depending on the orbit of the smaller body in (t, r^*)-coordinates). Just as the waveform function $\psi^{lm}_{RW/ZM}$ has been discretized over the cells, also the orbit is evaluated only in different representative points (the intersections with the cell's borders) and therefore discretized. Since no body is moving faster than light, not every combination of trajectory crossing the cell is allowed, in fact there are four categories of traversed cells, as Fig. 2.6 shows.

Knowing the values of $\psi^{lm}_{RW/ZM}$ at two subsequent times t and $t + \Delta$ allows one to evaluate the following value at time $t = t + 2\Delta$, and so on until the final time. From the first two lines obtained with the initial conditions, the third one can be evaluated and from there the fourth and so on. In this way, knowing the values of the waveform functions $\psi^{lm}_{RW/ZM}$ at time t means knowing a list of values for $\psi^{lm}_{RW/ZM}$ at different r^* locations on the same row. This being done, one proceeds from row to row using the values at the cells' corners to evaluate the missing corner of every cell. Eventually one stores only the values of $\psi^{lm}_{RW/ZM}$ at the observer's tortoise coordinate, and these values constitute the time evolution of the solution of the Regge-Wheeler equations.

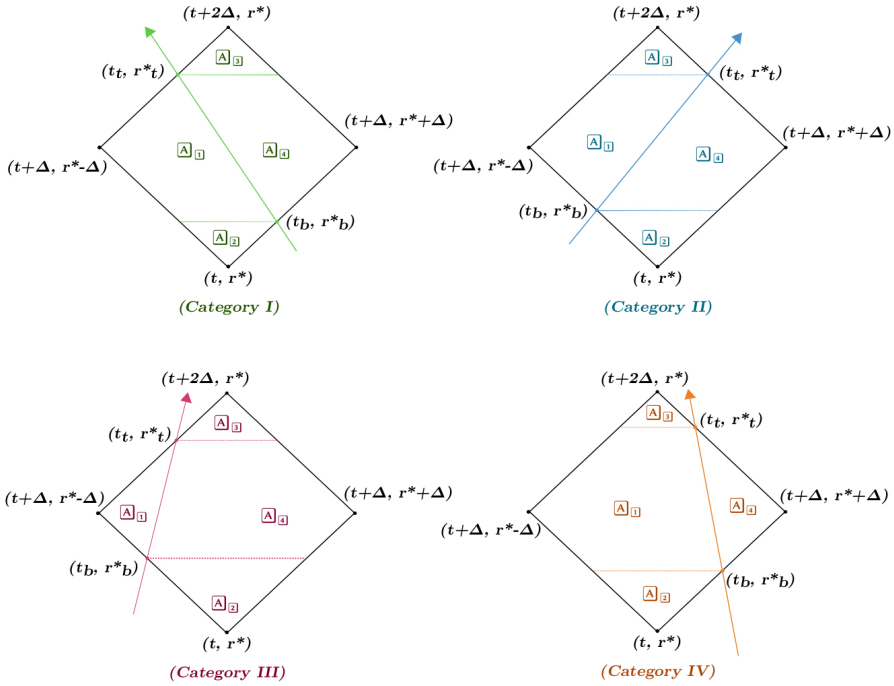

Figure 2.6: The four kinds of traversed cells that can occur, with the separation into four different areas A_i, for $i = 1 \dots 4$ for every cell. The waveform function solution to the RW/ZM-equations is known in the three low corners of the cell, the remaining top corner is to be evaluated.

The actual algorithm acts by integrating the equation (2.3.1) on both sides of the equation. Through this, one recovers a finite-difference expression for values of $\psi^{lm}_{RW/ZM}$ at a certain time depending on the values of the same $\psi^{lm}_{RW/ZM}$ at previous times and different locations, as we just explained,

(2.3.5)

$$\psi^{lm}_{RW/ZM}(t+2\Delta, r^*) = -\psi^{lm}_{RW/ZM}(t, r^*) + \frac{1 - \frac{\Delta^2}{4}\bar{V}^l_{RW/ZM}(r^* - \Delta)}{1 + \frac{\Delta^2}{4}\bar{V}^l_{RW/ZM}(r^*)}\psi^{lm}_{RW/ZM}(t+\Delta, r^* - \Delta) + \frac{1 - \frac{\Delta^2}{4}\bar{V}^l_{RW/ZM}(r^* + \Delta)}{1 + \frac{\Delta^2}{4}\bar{V}^{lm}_{RW/ZM}(r^*)}\psi^{lm}_{RW/ZM}(t+\Delta, r^* + \Delta),$$

(2.3.6)

$$\begin{aligned}\psi^{lm}_{RW/ZM}(t+2\Delta,r^*) = &-\psi^{lm}_{RW/ZM}(t,r^*)\frac{1+\frac{A_2}{4}\bar{V}^{lm}_{RW/ZM}(r^*)}{1+\frac{A_3}{4}\bar{V}^{lm}_{RW/ZM}(r^*)} - \frac{\int_{cell}\bar{S}^{lm}_{RW/ZM}(t,r)dtdr^*}{4+\bar{V}^{l}(r^*)A_4}\\ &+\frac{1-\frac{A_1}{4}\bar{V}^{l}_{RW/ZM}(r^*-\Delta)}{1+\frac{A_3}{4}\bar{V}^{l}_{RW/ZM}(r^*)}\psi^{lm}_{RW/ZM}(t+\Delta,r^*-\Delta)\\ &+\frac{1-\frac{A_4}{4}\bar{V}^{l}_{RW/ZM}(r^*+\Delta)}{1+\frac{A_3}{4}\bar{V}^{lm}_{RW/ZM}(r^*)}\psi^{lm}_{RW/ZM}(t+\Delta,r^*+\Delta).\end{aligned}$$

The two expressions above refer to the two possibilities that one evaluates values of $\psi^{lm}_{RW/ZM}$ on corners of a regular empty cell (2.3.5) or those of a cell traversed by the orbit itself (2.3.6). In the latter case an integral of the source term adds up to the result. The barred quantities are the usual potentials and source terms multiplied by a $\left(1-\frac{2M}{r}\right)$ factor, as required by the coordinate transformation from Droste to tortoise coordinates. The $A_i, i=1\ldots4$ are areas inside the cell (whose total area is $2\Delta^2$) defined by the path drawn in the diagram by the orbit. For details about the calculation of such expressions see [20, 18], the main used assumption being to consider the involved functions $\bar{V}^l, \bar{S}^{lm}$, and $\psi^{lm}_{RW/ZM}$ constant on a single A_i region.

The calculation of the integral of the source terms $\bar{S}^{lm}$ (2.2.31) present in the traversed-cell expression (2.3.5) for $\psi^{lm}_{RW/ZM}(t+2\Delta,r^*)$ exploits the sampling property of Dirac's delta distributions $\delta(r-r_p(t))$ and integration by parts. More detailed calculations can be found in [97, 105] whose final result is

$$\begin{aligned}\int_{cell}\bar{S}^{lm}dr^*dt = &\int_{t_b}^{t_t}dt\left[\frac{G^{lm}(r)}{1-\frac{2M}{r}} - \partial_r\left(\frac{F^{lm}(r)}{1-\frac{2M}{r}}\right)\right]\Bigg|_{r=r_p(t)}\\ &\pm\frac{F^{lm}(r_p(t_b))}{\left(1-\frac{2M}{r_p(t_b)}\right)^2}\frac{1}{1\mp\dot{r}_p(t_b)}\\ &\pm\frac{F^{lm}(r_p(t_t))}{\left(1-\frac{2M}{r_p(t_t)}\right)^2}\frac{1}{1\pm\dot{r}_p(t_t)},\end{aligned} \tag{2.3.7}$$

where $\dot{r}_p(t)$ is the particle's radial velocity at the times when the particle enters or leaves the cell (t_b or t_t respectively). The $\pm$ sign is determined out of one of the four possible crossing categories, as in Fig. 2.6 (as four are the combinations of 2 $\pm$ signs).

This concludes the brief description of the Lousto-Price algorithm. Later on it will be applied to a specific kind of orbits in Schwarzschild spacetime. So far, other results obtained with this method include the straight plunge [20, 106, 95], circular, parabolic and eccentric orbits [97, 95, 17, 18, 96].

2.4 Perturbation of the orbit: geodesic deviations

Perturbing the BH background metric is not the only technique to access the information of an EMR binary emitting gravitational radiation. So far we have seen how to obtain

the Gravitational Waves as a result of the perturbation of a given spacetime (specifically Schwarzschild spacetime), but one can also consider to take into account deviations on a given geodesic orbit, which is a solution of the geodesic equations (1.1.3) for the unperturbed background spacetime, in order to obtain more general orbits. The effects of GW emission can then be included in these new orbits, for instance tuning accordingly the energy and angular momentum of the body following the deviated orbit.

In this section we present a possible method of generalising an initially simple geodesic orbit that will be applied later on to specific orbits in Schwarzschild spacetime in order to describe the last phases of an EMR coalescence.

In flat Minkowski spacetime two test bodies (with ideally no mass) moving on straight lines initially parallel to each other will keep being on such parallel paths if no external force is applied, thus satisfying Newton's inertial principle. In a curved spacetime this is not always the case, rather two bodies moving on two generically different geodesics, separated by a distance vector n^μ, will undergo a change of their original mutual separation. A *geodesic deviation* will take place, obeying the geodesic deviation equation [43]

$$\frac{D^2 n^\mu}{D\tau^2} = R^\mu{}_{\nu\rho\lambda} n^\rho \frac{dx^\nu}{d\tau}\frac{dx^\lambda}{d\tau}, \tag{2.4.1}$$

where $x^\mu(\tau)$ is the geodesic trajectory, depending on the affine parameter or proper time τ, and $R^\mu{}_{\nu\rho\lambda}$ is Riemann curvature tensor associated to the background metric. This equation joins covariantly the effect of a non-trivial curvature to a change in the original geodesic path, when no external field is involved. The operator on the left-hand side is the usual covariant derivative along the geodesic x^μ, i.e.

$$\frac{DA^\mu}{D\tau} = \frac{dA^\mu}{d\tau} + \Gamma^\mu_{\nu\lambda}\frac{dx^\nu}{d\tau}A^\lambda, \quad \forall A^\mu \text{ tensor}. \tag{2.4.2}$$

The geodesic deviation equation (2.4.1) is the key to a perturbation method of an original geodesic orbit first devised in [107, 108], and then further developed and put to use in practice for eccentric orbits in [17, 18]. Here we will describe the salient features and master equations of this procedure.

If $\bar{x}^\mu(\tau)$ is an analytically known geodesic in a given spacetime $g_{\mu\nu}$, it is possible to build a family of such geodesics within the spacetime, a *congruence*, that can be distinguished by a dummy parameter allowing one to move from one geodesic to the other. For instance in Schwarzschild spacetime all the circular solutions $r = constant$ of the geodesic equations

$$\frac{d^2\bar{x}^\mu}{d\tau^2} + \Gamma^\mu_{\nu\lambda}\frac{d\bar{x}^\nu}{d\tau}\frac{d\bar{x}^\lambda}{d\tau} = 0 \tag{2.4.3}$$

are parametrized by the value of the constant radius. Should we decide to measure the radius in units of the BH mass M, every such circular orbit would be $r = nM$ times distant from the central black hole, and changing continuously the value of $n \in \mathbb{R}$ would allow one to span the whole congruence of circular geodesics. Similarly $x^\mu(\tau;\sigma)$ can indicate a family of geodesics in a given spacetime.

Let $\bar{x}^\mu(\tau) = x^\mu(\tau;0)$ be the reference geodesic, the next geodesic in the family is given by a vector displacement n^μ off the original $\bar{x}^\mu$,

$$x^\mu(\tau;\sigma) = \bar{x}^\mu(\tau;0) + \sigma n^\mu. \tag{2.4.4}$$

This newly built orbit has to satisfy the geodesic equation (2.4.3) as well to first order in σ and this requirement gives back the geodesic deviation equation for n^μ, namely (2.4.1). In fact one can always ask that, at a given proper time $\tau = \tau_0$, the point $\bar{x}^\mu(\tau_0)$ be corresponding to another point on the other geodesic $x^\mu(\tau_0;\sigma)$ at the *same* proper time. This implies that n^μ varies with proper time too and that it changes along the original geodesic as this is swept through by the affine parameter τ. The evolution equation of $n^\mu(\tau)$ is simply the geodesic deviation equation (2.4.1).

The deviation vector n^μ gives the geodesic separation from a point on the reference geodesic to a point on the nearby geodesic characterized by the same value of the affine parameter τ. Extending this correspondence to all values of the proper time, thus sweeping the whole geodesic, it is possible to construct the world-lines having the deviation vector as tangent vector (purple curves in Fig. 2.7). In this way, $n^\mu(\sigma)$ plays the same role that the tangent vector $u^\mu(\tau) = \frac{dx^\mu}{d\tau}(\tau)$ does for the congruence of geodesics $x^\mu(\tau;\sigma)$. With this respect one can regard σ as an affine parameter sweeping the geodesic whose tangent is $n^\mu(\sigma;\tau)$, and $u^\mu(\sigma;\tau)$ as its deviation vector.

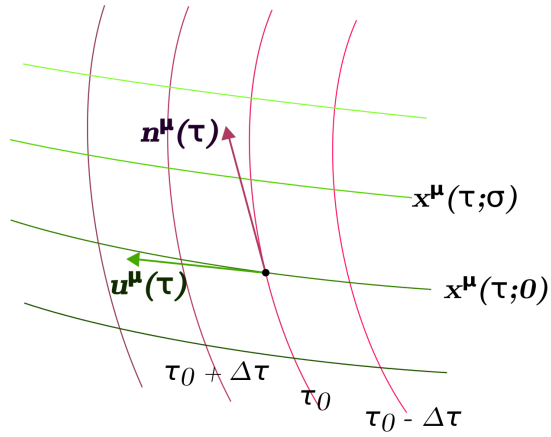

Figure 2.7: Congruence of geodesics x^μ in proper time τ (green curves), with tangent vector u^μ and deviation vector n^μ.

All this accounts for the definition of the deviation vector as

$$n^\mu = \frac{Dx^\mu}{D\sigma}, \tag{2.4.5}$$

and the interchange between n^μ and u^μ is confirmed by the remarkable property

$$\frac{Dn^\mu}{D\tau} = \frac{D^2x^\mu}{D\tau D\sigma} = \frac{d^2x^\mu}{d\tau d\sigma} + \Gamma^\mu_{\nu\lambda}\frac{dx^\lambda}{d\tau}\frac{dx^\nu}{d\sigma} = \frac{Du^\mu}{D\sigma}, \tag{2.4.6}$$

or, stated differently

$$(u\cdot\nabla n)^\mu = u_\nu\nabla^\nu n^\mu = n^\nu\nabla_\nu u^\mu = (n\cdot\nabla u)^\mu \Rightarrow u\cdot\nabla n = n\cdot\nabla u. \tag{2.4.7}$$

Now the key point to understand is that one can use this connection among different geodesics to build new orbits out of an analytically known one. Eq. (2.4.4) is just an approximation to first order in the deviation parameter σ of the difference between neighbouring geodesics within the same congruence, the complete expression is as follows

$$x^\mu = \bar{x}^\mu + \sigma\frac{dx^\mu}{d\sigma}\bigg|_{\sigma=0} + \frac{\sigma^2}{2!}\frac{d^2x^\mu}{d\sigma^2}\bigg|_{\sigma=0} + \mathcal{O}(\sigma^3), \tag{2.4.8}$$

which can be rewritten in fully covariant fashion as

$$x^\mu = \bar{x}^\mu + \sigma n^\mu + \frac{1}{2}\sigma^2\left(k^\mu - \Gamma^\mu_{\nu\lambda} n^\lambda n^\nu\right) + \mathcal{O}(\sigma^3), \tag{2.4.9}$$

provided the following covariant definitions have been given at $\sigma = 0$:

$$n^\mu = \frac{\partial x^\mu}{\partial \sigma}, \qquad k^\mu = \frac{\partial n^\mu}{\partial \sigma} + \Gamma^\mu_{\nu\lambda} n^\lambda n^\nu. \tag{2.4.10}$$

The Christoffel symbols in (2.4.9) and (2.4.10) are evaluated along the original geodesic $\bar{x}^\mu$, the deviation parameter σ is defined as the physical distance between the final orbit and the original geodesic at $\tau = 0$,

$$(d\sigma)^2 = g_{\mu\nu} dx^\mu dx^\nu \Big|_{\tau=0}. \tag{2.4.11}$$

The evolution equations for the deviation vectors (2.4.10) are to be found by demanding that the perturbed orbit satisfy the geodesic equation (2.4.3), resulting in

$$\begin{aligned} \frac{D^2 n^\mu}{D\tau^2} &= R^\mu{}_{\lambda\nu\kappa} u^\lambda n^\nu u^\kappa, \\ \frac{D^2 k^\mu}{D\tau^2} &= R^\mu{}_{\lambda\nu\kappa} u^\lambda k^\nu u^\kappa + R^\mu{}_{\kappa\nu\lambda;\rho}\left(u^\kappa u^\lambda n^\nu n^\rho - u^\nu u^\rho n^\kappa n^\lambda\right) + 4R^\mu{}_{\kappa\nu\lambda} u^\lambda n^\nu \frac{Dn^\kappa}{D\tau}. \end{aligned} \tag{2.4.12}$$

The curvature terms are evaluated along the known geodesic $\bar{x}^\mu$, and the equation to first order in σ is nothing but the geodesic deviation equation (2.4.1) we started from. The equations (2.4.12) are more conveniently used in their non-covariant form,

$$\begin{aligned} &\frac{d^2 n^\mu}{d\tau^2} + 2u^\lambda \Gamma^\mu_{\lambda\nu} \frac{dn^\mu}{d\tau} + u^\kappa u^\lambda \Gamma^\mu_{\kappa\lambda,\nu} n^\nu = 0, \\ &\frac{d^2 m^\mu}{d\tau^2} + 2u^\lambda \Gamma^\mu_{\lambda\nu} \frac{dm^\mu}{d\tau} + u^\kappa u^\lambda \Gamma^\mu_{\kappa\lambda,\nu} m^\nu = S^\mu(n), \end{aligned} \tag{2.4.13}$$

where $m^\mu = k^\mu - \Gamma^\mu_{\lambda\nu} n^\lambda n^\nu$ and $S^\mu(n)$ is a source term depending on the deviation vector n^μ,

$$S^\mu(n) = -2\Gamma^\mu_{\lambda\nu} \frac{dn^\lambda}{d\tau}\frac{dn^\nu}{d\tau} - 4\Gamma^\mu_{\lambda\nu,\kappa} u^\lambda n^\kappa \frac{dn^\nu}{d\tau} - \Gamma^\mu_{\lambda\nu,\rho\kappa} u^\lambda u^\nu n^\rho n^\kappa. \tag{2.4.14}$$

This procedure allows to write down the geodesic deviation equations at all orders, in manifestly covariant form (2.4.12) or not (2.4.13). At any order the same left-hand side structure of (2.4.13) occurs again. Therefore if $n^\mu = 0 \to S^\mu(n) = 0$, also m^μ and subsequent orders' deviation vectors will be null. However, for the purposes of this thesis we will never go beyond the first order in geodesic deviation when tackling practical applications.

The advantages offered by an expansion like Eq. (2.4.9) are that one can always build a new (perturbed) orbit out of an analytically known one just by truncating the

series, which is effectively a Taylor series. The newly obtained orbit can in principle be formulated analytically, once the corresponding deviation equations (2.4.13) have been solved, and it is still a geodesic solution of the given background metric.

One can use this new orbit in order to tune some parameters, such as energy and angular momentum to the desired values, taking into account effects such as gravitational emission. The next step is to reconstruct the binary coalescence moving from an initial orbit $\bar{x}^\mu$ to new perturbed orbits, each time adjusting the relevant parameters. The whole picture is an approximation of the actual gradual orbit deformation due to the GW emission and the back-reaction of these with the background.

* *

3 Plunge along ballistic orbits

* *

Binary coalescences go through three different stages, which are commonly referred to as the inspiral, plunge and merger-ringdown [21]. During the *inspiral* of an EMR binary, the smaller companion μ follows bound quasi-periodic orbits, such as those studied in [17, 18, 105]. Loss of energy through GWs generally translates in a loss of eccentricity (*circularisation*) in this phase, although the eccentricity may increase again just before plunging [109], depending on the parameters of the orbit and its evolution[1]. However, the region of the ISCO is where the *plunge* sets in and unstable plunging orbits in some range of parameters can be used in the description of this phase and the following.

Analytical results for the orbits of test masses in Schwarzschild spacetime are found in standard textbooks [47, 43, 110]. Complete geodesics –meaning the full spacetime position as a function of (proper) time– are less easy to compute, and usually given only in the form of implicit expressions [111, 112]. For practical applications several perturbative schemes have been developed to construct satisfactory approximations, see refs. [113, 2] and work cited there. In refs. [107, 17, 18, 105] a different, fully relativistic scheme has been developed based on covariant deformation of known (circular) orbits. This last method, developed to second order in the deformation parameter, was also shown to give very good results for the gravitational signals from quasi-periodic bound orbits with moderate eccentricities.

In the present chapter we extend the relativistic calculations to include a particular class of unstable orbits, describing test masses falling towards the horizon in the regime where the motion is no longer quasi-periodic. A well-known extreme case of infall is the straight plunge along a radial orbit, which was dealt with extensively in refs. [97, 95]. Here we focus on the opposite extreme, infall from a periodic orbit, in particular circular orbits close to the innermost stable circular orbit (ISCO), which we name *ballistic* orbits, because of their behaviour, as will become clear in the next section.

Such unstable orbits are interesting on their own and shed light on the dynamics of EMR binaries, so they can also be used for the evaluation of gravitational radiation. In particular they show that an EMR plunge can follow an almost-circular path at the beginning, up to a radial value $r \sim 4.3M$, when $\dot{r} \sim r\dot{\varphi}$ and the radial velocity becomes comparable to the transverse velocity, after which the radial motion becomes dominant. Moreover, the ballistic orbits are the starting point for a geodesic deviation expansion

[1] However, the relative increase of the eccentricity is modest: $e \ll 1$, while during previous stages of the inspiral e can drop by several orders of magnitude.

[17, 18] which can give an even more realistic description of the final plunge of an EMR system, as will be shown in the next chapter.

The chapter is structured as follows: first an explanation is given of how to build such orbits, of their properties, and of how to use them to derive gravitational radiation. In the next section we show the problems inherent to the calculation of waveforms and the following results. At the end of this chapter we discuss the results and how they fit in the existing literature on this topic.

3.1 Ballistic orbits

3.1.1 Circular orbits in Schwarzschild spacetime

Physical trajectories of bodies orbiting in a non-spinning EMR binary can be described by time-like geodesics in Schwarzschild spacetime. This represents a well-known solution [76] of the Einstein field equations of General Relativity and it is as old as GR itself[2] .

Schwarzschild metric is the physical solution to the Einstein field equations in vacuum around any spherical distribution of mass[3] such as stars or Black Holes. Actually a Black Hole is first defined as a spherical distribution of mass contained within its Schwarzschild radius $r = \frac{2GM}{c^2}$, which is the BH *horizon*, a threshold that not even light can escape from. That makes the star contained within the horizon a "black" star, appearing in astrophysical observations as a gap, a "hole" in space where other objects orbit around. Adding a rotation, or spin, to a Black Hole would require a different solution of the same Einstein field equations, namely a Kerr-Newman spacetime solution [47, 117], which is currently the most complete description of astrophysical Black Holes and reduces back to the Schwarzschild solution as its non-rotating limit.

Nevertheless we will first address the case of non-spinning Black Holes, and for these the Schwarzschild solution is the best description. Taking the origin of the reference frame centered in the Black Hole position in spherical coordinates -so that r is the radial distance away from the BH, θ and φ are latitude and longitude angles respectively- the Schwarzschild solution has the following aspect

$$d\tau^2 = \left(1 - \frac{2M}{r}\right) dt^2 - \frac{dr^2}{1 - \frac{2M}{r}} - r^2 d\theta^2 - r^2 \sin^2\theta d\varphi^2. \tag{3.1.1}$$

Due to the spherical symmetry of the background geometry, Droste coordinates can be chosen in such way that any specific orbit lie in the equatorial plane ($\theta = \frac{\pi}{2}$). Motion in the equatorial plane of Schwarzschild spacetime is characterized by two constants [47], and for a body with mass μ moving in this metric, the energy and the angular momentum

[2] Schwarzschild's paper was communicated to the Berlin Academy by Einstein about two months after the publication of his field equations in a short communication [47]. For a more complete tale about the discovery of Schwarzschild's solution, refer to [114, 115, 116]

[3] Thanks to Birkhoff's theorem [87], which affirms that any spherically symmetric solution of the Einstein field equations in vacuum must be static and asymptotically flat, Schwarzschild metric is of fundamental importance.

are, respectively

$$E = \mu\left(1 - \frac{2M}{r}\right)u^t \qquad L = \mu r^2 \sin^2\theta u^\varphi, \tag{3.1.2}$$

where u^t and u^φ are the time and azimuthal component of the 4-vector velocity u^μ. From now on we will refer just to the energy per unit mass $\varepsilon = \frac{E}{\mu}$ and the angular momentum per unit mass $\ell = \frac{L}{\mu}$ (also called "specific" energy and angular momentum). In terms of these the four-velocity constraint $u_\mu u^\mu = -1$ is equivalent to

$$\varepsilon^2 = \left(\frac{dr}{d\tau}\right)^2 + V_\ell(r), \tag{3.1.3}$$

with the effective potential

$$V_\ell = \left(1 - \frac{2M}{r}\right)\left(1 + \frac{\ell^2}{r^2}\right). \tag{3.1.4}$$

The angular momentum is orthogonal to the plane of the orbit, so along the z-direction, and it is conserved, together with the energy. As long as the motion is geodetic, its dynamics is completely conservative. From the Einstein field equations in vacuum we can write down the geodesic equations

$$\begin{aligned}
\frac{d^2t}{d\tau^2} &= -\frac{2M}{r^2\left(1-\frac{2M}{r}\right)}\left(\frac{dr}{d\tau}\right)\left(\frac{dt}{d\tau}\right)\\
\frac{d^2r}{d\tau^2} &= -\frac{M}{r^2}\left(1-\frac{2M}{r}\right)\left(\frac{dt}{d\tau}\right)^2 + \frac{M}{r^2\left(1-\frac{2M}{r}\right)}\left(\frac{dr}{d\tau}\right)^2\\
&\quad + r\left(1-\frac{2M}{r}\right)\left(\frac{d\theta}{d\tau}\right)^2 + r\left(1-\frac{2M}{r}\right)\sin^2\theta\left(\frac{d\varphi}{d\tau}\right)^2\\
\frac{d^2\theta}{d\tau^2} &= -\frac{2}{r}\left(\frac{dr}{d\tau}\right)\left(\frac{d\theta}{d\tau}\right) + \sin\theta\cos\theta\left(\frac{d\varphi}{d\tau}\right)^2\\
\frac{d^2\varphi}{d\tau^2} &= -\frac{2}{r}\left(\frac{dr}{d\tau}\right)\left(\frac{d\varphi}{d\tau}\right) - 2\frac{\cos\theta}{\sin\theta}\left(\frac{d\theta}{d\tau}\right)\left(\frac{d\varphi}{d\tau}\right).
\end{aligned} \tag{3.1.5}$$

As already mentioned, motion in Schwarzschild geometry is planar when L is conserved, so one can put $\theta = \frac{\pi}{2}$ and constant in time, without loss of generality. If we now look at circular orbits $r = R > 2M$, the equations (3.1.5) read

$$\frac{d^2t}{d\tau^2} = 0 \quad \frac{d^2\varphi}{d\tau^2} = 0 \quad \frac{M}{R^3}\left(\frac{dt}{d\tau}\right)^2 = \left(\frac{d\varphi}{d\tau}\right)^2. \tag{3.1.6}$$

From the normalization of the four-velocity condition (3.1.3) we get the following relations

$$1 - \frac{\varepsilon^2}{1-\frac{2M}{R}} + \frac{\ell^2}{R^2} = 0 \quad \text{with} \quad \varepsilon = \frac{1-\frac{2M}{R}}{\sqrt{1-\frac{3M}{R}}}, \quad \ell = \sqrt{\frac{RM}{1-\frac{3M}{R}}}, \tag{3.1.7}$$

which in turn imply that for circular orbits $r = R$

$$t(\tau) = \frac{\varepsilon}{1 - \frac{2M}{R}}\tau = \frac{\tau}{\sqrt{1 - \frac{3M}{R}}}, \quad \varphi(\tau) = \frac{\ell}{R^2}\tau = \sqrt{\frac{MR}{1 - \frac{3M}{R}}}\frac{\tau}{R^2}. \tag{3.1.8}$$

In the region beyond the BH horizon $r > 2M$ it is possible for a body to orbit around a Schwarzschild BH on a circular orbit. This orbit will be stable as long as $r \geq 6M$, and $r = 6M$ is commonly referred to as the Innermost Stable Circular Orbit, meaning that for $r < 6M$ only unstable orbits are possible (like the "light-ring" orbit $r = 3M$ for photons). To see this, consider again the effective potential (3.1.4) and plot it against the radial variable r for different values of the specific angular momentum ℓ, as shown in Fig. 3.1. It has the typical well potential behaviour where circular orbits represent the extremal points of the curves, minima and maxima.

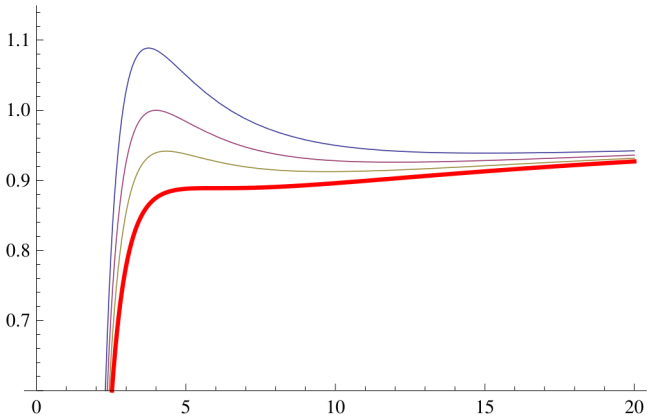

Figure 3.1: Effective potential for different values of angular momentum ℓ. The red thick line corresponds to $\ell^2 = 12M^2$, the one giving rise to the ISCO orbit.

Minimizing the effective potential V_ℓ, it follows that for $\ell^2 > 12M^2$ there always exist circular orbits. In fact, there are two types of circular orbits, a stable one at $r = R_+$ in the minimum of V_ℓ, and an unstable one at $r = R_-$ in its maximum, with

$$R_\pm = \frac{\ell^2}{2M}\left(1 \pm \sqrt{1 - \frac{12M^2}{\ell^2}}\right). \tag{3.1.9}$$

For $R = 6M$ and $\ell^2 = 12M^2$ the effective potential V_ℓ has only a point of inflection, and these two solutions coincide; this is the well-known innermost stable circular orbit (ISCO). For $\ell^2 < 12M^2$ the potential V_ℓ has no stable points for any ℓ, and no circular orbits exist.

The ISCO allows us to distinguish two regions in Schwarzschild spacetime, an "outer" region, for $r > 6M$ and an "inner" region. In terms of binary system coalescences it is known that the last phases of the evolution, plunge and merger, both take place in the inner region, while the inspiral ends at the proximity of the ISCO [21].

Solving the geodesic equations (3.1.5) for $r = 6M$ gives the ISCO orbit in detail

$$t(\tau) = \pm\sqrt{2}\tau, \qquad \varphi(\tau) = \pm\frac{\sqrt{3}}{18}\tau, \tag{3.1.10}$$
$$R = 6M, \quad \theta = \frac{\pi}{2}, \qquad \varepsilon^2 = \frac{8}{9}, \quad \ell^2 = 12M^2.$$

The sign of energy determines whether we have a body, or particle, moving back in time or not. For instance, this makes the difference between particle and antiparticle. The sign in the angular momentum indicates whether it is moving clockwise or counterclockwise with proper time. This is true for general planar orbits, and in the following we will choose positive signs for both the energy and the angular momentum.

The expression for V_ℓ for different circular orbits is conveniently parametrized by

$$\xi = \sqrt{1 - \frac{12M^2}{\ell^2}} \quad \Rightarrow \quad \varepsilon_\pm^2 = V_\ell[R_\pm] = \frac{2}{9}\frac{(2 \pm \xi)^2}{1 \pm \xi}. \tag{3.1.11}$$

Note that for orbits near the ISCO (small ξ), both the energy and angular momentum of circular orbits vary only as ξ^2. As a result, for orbits near the ISCO the effective potential is very flat between R_- and R_+; in fact, in the domain $\xi < 0.3$ the difference between maximum and minimum of V_ℓ is less than 1 percent.

3.1.2 Ballistic orbits in Schwarzschild spacetime

In order to describe motion of a body in the final phases of a binary coalescence, we need orbits in the inner region. To this purpose we consider this kind of orbit

$$r = \frac{R}{1 + e\cot^2(A\varphi/2)}. \tag{3.1.12}$$

Here (R, e, A) are constants fixed by the values of ε and ℓ, as will be shortly shown. As one can see, the orbits (3.1.12) are periodic trajectories going from an apastron R towards the BH and then coming back, therefore we refer to them as *ballistic* orbits. This means that the orbit lies entirely inside a region $r < R$, and taking $R \leq 6M$ places the orbit completely in the inner region beyond the ISCO. Moreover this implies that φ is allowed to change in a limited range in order to describe a one-way motion towards the BH horizon $r = 2M$. An example is shown in Fig. 3.2.

Such orbits exist (3.1.12) for specific values of the constants e, A and R. First, moving from the normalization condition of the four-velocity (3.1.3) and using the Killing relations, one gets [47]

$$\frac{\varepsilon^2 - 1}{2} = \frac{1}{2}\left(\frac{dr}{d\tau}\right)^2 + \frac{1}{2}\left(1 - \frac{2M}{r(\tau)}\right)\left(1 + \frac{\ell^2}{r^2(\tau)}\right) - \frac{1}{2},$$

and this relation can be stated in terms of potential terms showing the existence of minima/maxima of the orbit (respectively periastron and apastron), and of the ISCO itself, as we already discussed in the previous section. Using the chain rule we calculate $\frac{dr}{d\tau}$ in terms of the angle φ and get:

$$\frac{dr}{d\tau}(\tau) = \frac{dr}{d\varphi}(\varphi)\frac{d\varphi}{d\tau} = \frac{\ell}{r^2(\varphi)}\frac{dr}{d\varphi}(\varphi)$$

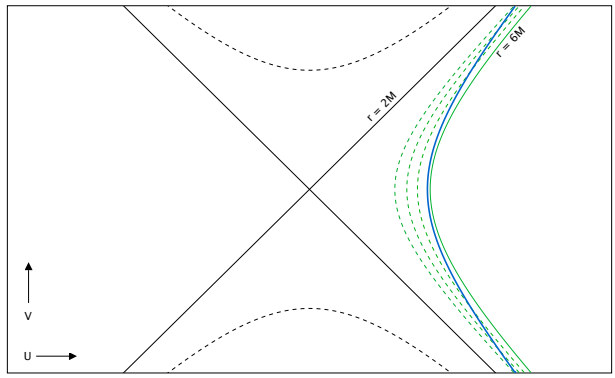

Figure 3.2: Kruskal diagram showing a ballistic orbit crossing lines of constant $r < 6M$ (dotted curves). The ISCO ($r = 6M$) is the ultimate limit of ballistic orbits.

with the angle depending on proper time $\varphi = \varphi(\tau)$, we obtain

$$\frac{\ell^2}{r^4}\left(\frac{dr}{d\varphi}\right)^2 = \varepsilon^2 - \left(1 - \frac{2M}{r}\right)\left(1 + \frac{\ell^2}{r^2}\right). \tag{3.1.13}$$

The left-hand side of the latter can be evaluated to be, thanks to the ansatz (3.1.12),

$$\frac{d}{d\varphi}\frac{1}{r} = -\frac{eA}{R}\frac{\cos(A\varphi/2)}{\sin^3(A\varphi/2)} \quad \Rightarrow \quad \ell^2\left(\frac{d}{d\varphi}\frac{1}{r}\right)^2 = \frac{\ell^2 e^2 A^2}{R^2}\frac{\cos^2(A\varphi/2)}{\sin^6(A\varphi/2)}, \tag{3.1.14}$$

while the right-hand side (3.1.13) becomes

$$\varepsilon^2 - 1 + \frac{2M}{R}\left(1 + e\cot^2 y\right) - \frac{\ell^2}{R^2}\left(1 + e\cot^2 y\right)^2 + \frac{2M\ell^2}{R^3}\left(1 + e\cot^2 y\right)^3, \tag{3.1.15}$$

where we have introduced the notation $y = A\varphi/2$. Multiplying both sides of the equation by $\sin^6 y$, it takes the form

$$\begin{aligned} \frac{e^2A^2\ell^2}{R^2}\cos^2 y \;=\; & \left(\varepsilon^2 - \left(1 - \frac{2M}{R}\right)\left(1 + \frac{\ell^2}{R^2}\right)\right)\sin^6 y \\ & + \left(\frac{2M}{R} - \frac{2\ell^2}{R^2} + \frac{6M\ell^2}{R^3}\right) e\cos^2 y \sin^4 y \\ & - \left(\frac{\ell^2}{R^2} - \frac{6M\ell^2}{R^3}\right) e^2\cos^4 y \sin^2 y + \frac{2M\ell^2}{R^3}\, e^3\cos^6 y. \end{aligned} \tag{3.1.16}$$

Finally we use the identity $\sin^2 y = 1 - \cos^2 y$, and equate powers of $\cos y$ on both sides, with the following results: from the constant terms ($\cos^0 y$) we retrieve the usual energy conservation relation for circular orbits (3.1.7)

$$\varepsilon^2 = \left(1 - \frac{2M}{R}\right)\left(1 + \frac{\ell^2}{R^2}\right); \tag{3.1.17}$$

from the coefficients of $\cos^2 y$

$$eA^2\ell^2 = 2MR - 2\ell^2 + \frac{6M\ell^2}{R}; \tag{3.1.18}$$

from the coefficients of $\cos^4 y$

$$2e\left(\frac{2M}{R} - \frac{2\ell^2}{R^2} + \frac{6M\ell^2}{R^3}\right) + e^2\left(\frac{\ell^2}{R^2} - \frac{6M\ell^2}{R^3}\right) = 0; \tag{3.1.19}$$

and finally from the coefficients of $\cos^6 y$

$$e\left(\frac{2M}{R} - \frac{2\ell^2}{R^2} + \frac{6M\ell^2}{R^3}\right) + e^2\left(\frac{\ell^2}{R^2} - \frac{6M\ell^2}{R^3}\right) + e^3\frac{2M\ell^2}{R^3} = 0. \tag{3.1.20}$$

The last two equations can be simplified using (3.1.18)

$$\frac{e^2\ell^2}{R^2}\left(2A^2 + 1 - \frac{6M}{R}\right) = 0, \qquad \frac{e^2\ell^2}{R^2}\left(A^2 + 1 - \frac{6M}{R} + \frac{2eM}{R}\right) = 0, \tag{3.1.21}$$

from which an expression for the amplitude A follows as

$$A^2 = \frac{2eM}{R} = \frac{1}{2}\left(\frac{6M}{R} - 1\right). \tag{3.1.22}$$

Substitution of these results back into Eq. (3.1.18) then determines the angular momentum:

$$\ell^2 = \frac{16M^2}{\left(1 - \frac{2M}{R}\right)\left(1 + \frac{6M}{R}\right)}. \tag{3.1.23}$$

As a consequence we find for the energy per unit of mass (specific energy)

$$\varepsilon^2 = \left(1 - \frac{2M}{r}\right)\left(1 + \frac{\ell^2}{R^2}\right) = \frac{\left(1 + \frac{2M}{R}\right)^2}{1 + \frac{6M}{R}}. \tag{3.1.24}$$

Also note, that positivity of A^2 requires $R < 6M$; for $R \to 6M$ the solution transforms smoothly to the ISCO:

$$r = R = 6M, \quad \ell^2 = 12M^2, \quad e = A = 0. \tag{3.1.25}$$

Note that r reaches its maximum $r = R$ for $A\varphi = \pi$. It follows immediately that the complete orbit lies within the ISCO, as required.

More precisely, just like for circular orbits, there is only one independent parameter fixing a ballistic orbit, which we can choose to be the extremal point (apastron) $r = R$. The correspondence with circular orbits is not limited to this fact, as we will show shortly.

Summarizing the results obtained so far, these orbits lie completely within the ISCO, starting from and falling back into the horizon; therefore we refer to them as ballistic orbits. The constants defining the ballistic orbits are

$$A^2 = \frac{1}{2}\left(\frac{6M}{R} - 1\right), \qquad e = \frac{3}{2}\left(1 - \frac{R}{6M}\right),$$

$$\varepsilon^2 = \frac{\left(1 + \frac{2M}{R}\right)^2}{1 + \frac{6M}{R}}, \qquad \ell^2 = \frac{16M^2}{\left(1 - \frac{2M}{R}\right)\left(1 + \frac{6M}{R}\right)}. \tag{3.1.26}$$

For these orbits the value of the parameter ξ, defined in (3.1.11), is

$$\xi = A^2 = \frac{1}{2}\left(\frac{6M}{R} - 1\right), \tag{3.1.27}$$

and as a consequence

$$\varepsilon^2 = \frac{2}{9}\frac{(2+\xi)^2}{1+\xi}. \tag{3.1.28}$$

Thus it is clear that these ballistic orbits inside the ISCO are degenerate in energy and angular momentum with the stable circular orbits outside the ISCO. We can establish in this way a 1-1-correspondence with the circular geodesics. This correspondence is evident if you look at the effective potential term (3.1.4) and the possible orbits, see Fig. 3.3.

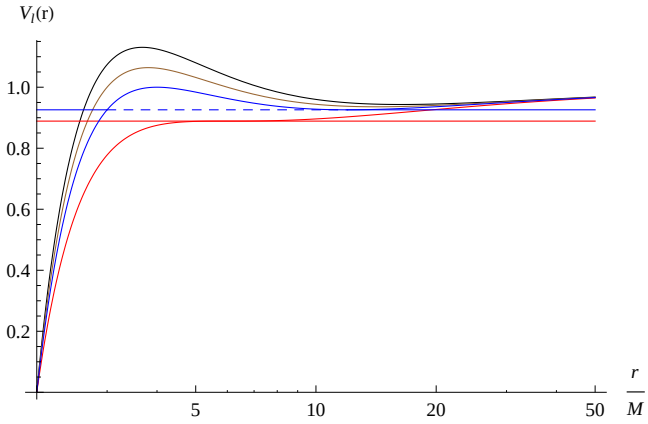

Figure 3.3: $V_\ell(r)$ for several $\ell^2 \geq 12M^2$, where the equality sign determines the ISCO (lowest curve). The horizontal lines indicate the energy levels of the stable circular orbits (dashed) and corresponding ballistic orbits (continuous).

There are analytic representations for three kinds of special geodesics: stable and unstable circular orbits with respectively

$$R_+ = \frac{6M}{1-\xi}, \qquad R_- = \frac{6M}{1+\xi}, \tag{3.1.29}$$

and special ballistic orbits with apastron

$$R = \frac{6M}{1+2\xi}. \tag{3.1.30}$$

These ballistic orbits are always degenerate in energy and angular momentum with the stable circular orbit for the same ξ, whilst the unstable circular orbit at this ξ has a slightly higher energy; however, all three of them become degenerate at the ISCO where $\xi = 0$. Other ballistic orbits exist; an analytic representation for these can be obtained from the ones given in Eqs. (3.1.12) and (3.1.26) by the method of geodesic deviations [118, 107].

However observe that the energy of a body on a ballistic orbit is always slightly higher than the ISCO energy. In fact, the Taylor expansion of the energy (3.1.28) is

$$\varepsilon^2 = \varepsilon_{ISCO} + 2\frac{\xi^2}{9} - 2\frac{\xi^3}{9} + o(\xi^4),$$

showing that any variation of order ξ from the ISCO energy is towards increasing the energy of the test-particle. The degeneracy in energy and angular momentum of the ballistic orbits and circular orbits implies that in both cases these quantities are greater than those of the ISCO. Thus it follows that when a test particle in stable motion on the ISCO is slightly boosted with the correct angular momentum, it can either move up to a larger distance from the horizon on a stable circular orbit, or move down to such an infalling ballistic orbit of the same ε and ℓ.

In real systems such a small boost could happen for instance by interaction with a third body passing by. A ballistic geodesic is the kind of orbit a body would follow when accelerating from the ISCO towards the horizon, or when being captured by the central BH in the ISCO region, while being on his way on an outbound orbit. Just as it is, (3.1.12) represents a first order approximation of the real plunging orbit of the smaller companion in a Supermassive Black Hole Binary Coalescence. Further improvements can be obtained pursuing the geodesic deviation scheme [107, 18].

3.1.3 Infall on a ballistic orbit

As equation (3.1.12) is invariant under $\varphi \to -\varphi$, the ballistic orbit is symmetric about the apastron $r = R$. The second half of the orbit describes the infall of a test mass from the apastron to the horizon, so we have to consider a definite range of values for φ in order to use the interesting branch of this solution, as was already mentioned.

We describe now the infalling orbit in some more detail. Firstly Eq. (3.1.12) expresses the radial co-ordinate r as a function of φ. By using the constants of motion (3.1.26) one can also determine the explicit functional dependence of the coordinate time t and the proper time τ on the angle φ. The expression for proper time is the simplest one, obtained by integrating the relation

$$\frac{d\varphi}{d\tau} = \frac{\ell}{r^2} = \frac{\ell}{R^2}\left(1 + e\cot^2\frac{A\varphi}{2}\right)^2, \tag{3.1.31}$$

with the result

$$\begin{aligned}\left(\frac{1-e}{(3-e)(3-2e)}\right)^{3/2}\frac{\tau-\tau_0}{2M} &= \frac{A\varphi}{(3-e)\sqrt{e}} - \arctan\left(\frac{1}{\sqrt{e}}\tan\frac{A\varphi}{2}\right) \\ &\quad + \frac{\sqrt{e}(1-e)}{3-e}\,\frac{\cot\frac{A\varphi}{2}}{1+e\cot^2\frac{A\varphi}{2}}.\end{aligned} \tag{3.1.32}$$

Here τ_0 is a constant of integration fixing the zero point of proper time. A convenient choice will be to take $\tau = 0$ at $r = R$. Similarly, we can solve for t as a function of φ by

integrating

(3.1.33)
$$\begin{aligned}\frac{dt}{d\varphi} &= \frac{\varepsilon}{\ell}\frac{r^3}{r-2M}\\ &= \frac{2MR\varepsilon}{\ell}\left(\frac{R}{2M}\frac{1}{\left(1+e\cot^2\frac{A\varphi}{2}\right)^2}+\frac{1}{1+e\cot^2\frac{A\varphi}{2}}+\frac{1}{\frac{R}{2M}-1-e\cot^2\frac{A\varphi}{2}}\right).\end{aligned}$$

The result is

(3.1.34)
$$\begin{aligned}\frac{1}{(2-e)}\sqrt{\frac{e}{2(1-e)}}\frac{t-t_0}{4M} &= \frac{(3-2e)^2A\varphi}{2(2-e)(1-e)^2}+\frac{e(3-2e)}{2(1-e)}\frac{\operatorname{cotan}\frac{A\varphi}{2}}{1+e\operatorname{cotan}^2\frac{A\varphi}{2}}\\ &\quad-\frac{(11-11e+2e^2)\sqrt{e}}{2(1-e)^2}\arctan\left(\frac{1}{\sqrt{e}}\tan\frac{A\varphi}{2}\right)\\ &\quad-\frac{1}{(2-e)}\sqrt{\frac{e}{2(1-e)}}\operatorname{arccoth}\left(\sqrt{\frac{2(1-e)}{e}}\tan\frac{A\varphi}{2}\right).\end{aligned}$$

Finally, this result can be translated to a result for t as a function of r:

(3.1.35)
$$\begin{aligned}\frac{2}{(2-e)}\sqrt{\frac{e}{2(1-e)}}\frac{t-t_0}{4M} &= \frac{\left(11-11e+2e^2\right)\sqrt{e}}{(1-e)^2}\arctan\sqrt{\frac{r}{(6-4e)M-r}}\\ &\quad-\frac{2(3-2e)^2}{(1-e)^2(2-e)}\arctan\sqrt{\frac{er}{(6-4e)M-r}}-\frac{\sqrt{er\left((6-4e)M-r\right)}}{2M(1-e)}\\ &\quad+\frac{1}{2-e}\sqrt{\frac{2e}{1-e}}\operatorname{arccoth}\sqrt{\frac{2(1-e)r}{(6-4e)M-r}}.\end{aligned}$$

A typical ballistic orbit close to the ISCO, with $e = 1.5\times10^{-3}$ is shown in Fig. 3.4. This orbit encircles the black hole about 20 times before crossing the horizon. Moreover, the radial motion is seen to be small compared to the transverse motion until the radial coordinate gets in the domain $4M < r < 5M$. Once the cross-over to radially dominated motion is made, only a few turns remain. These observations will be made more precise in the last section of this chapter.

As one can see from the time relations (3.1.34), (3.1.35), the orbital parameters depend on the central mass M and the eccentricity e (or equivalently R, using relations (3.1.26)). In the following applications the choice will be on the observer's time in terms of the radial variable (3.1.35), so treating the radial distance r as independent parameter, because of computational simplicity[4]. This requires to invert the initial relation (3.1.12) as well, and a discussion about the domains of all these functions is necessary.

[4] A more physically sensible choice would be to have the coordinates $x^\mu(\tau)$ as function of proper time, but the inversion of (3.1.34) is not possible in closed form and analytically, so the best option, also in view of numerical applications, is to take r or φ as independent variable and let the orbit be described by that.

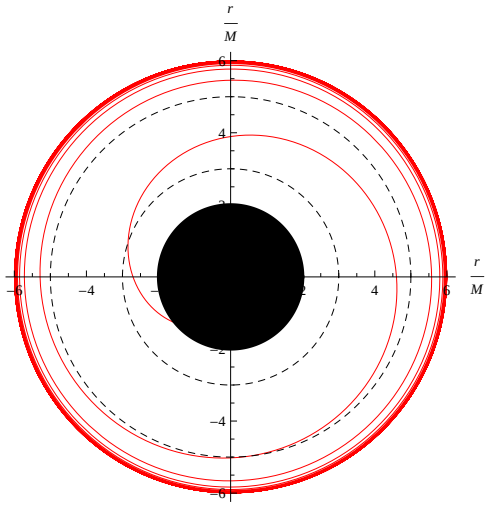

Figure 3.4: The inspiraling ballistic orbit towards the Schwarzschild horizon for $e = 0.0015$.

We are looking for an orbit that starts from the ISCO and then drives the body all the way beyond it down to the BH horizon, in the inner region. This means that there is a starting angle φ^* that corresponds to the body located in the ISCO region. Nevertheless, one can see that putting $R = 6M$ in all the preceding relations just gives back the stable ISCO orbit, where $r = 6M$ all the time and $A = e = 0$, so neither oscillation nor fall of the body towards the Black Hole. The only possibility is that $R < 6M$ and in order to conveniently parametrize this requirement, we introduce the parameter δ through the following definition

$$R = 6M(1-\delta) \quad \rightarrow \quad \delta = \frac{2}{3}e, \tag{3.1.36}$$

such that δ is a small dimensionless number. This clearly recognizes that R is the point of closest approach to the ISCO ($r = 6M$) of any ballistic orbit. The smaller δ is, the closer to the ISCO the orbit will start. If we now rewrite energy and angular momentum in terms of the new parameter δ,

$$\ell = \frac{4\sqrt{3}M(1-\delta)}{\sqrt{4-8\delta+3\delta^2}} \tag{3.1.37}$$

$$\varepsilon = \frac{4-3\delta}{3\sqrt{2-3\delta+\delta^2}}, \tag{3.1.38}$$

one can see -as was expected- that in the limit $\delta \to 0$ the values for energy and angular momentum on the ISCO orbit are retrieved with continuity. Analyzing more carefully the specific energy, one can see that we have limits on the values for the parameter δ, due to the square roots present in the expressions above, and precisely $0 < \delta < \frac{2}{3}$. These limits match exactly the ones for the eccentricity $0 < e < 1$.

For instance, the expression (3.1.33) $\tau(\varphi)$ for the proper time becomes

(3.1.39)

$$\tau(\varphi) = -\frac{12\sqrt{6}M(\delta-1)}{(2-3\delta)^2}\sqrt{\frac{4}{\delta}+11\delta-3\delta^2-12}\left[\sqrt{\frac{\delta}{2-2\delta}}\varphi\right.$$
$$+\frac{3}{2}\sqrt{\frac{3}{2}}(\delta-2)\sqrt{\delta}\arctan\left(\frac{\sqrt{\frac{2}{3}}\tan\left(\frac{1}{2}\sqrt{\frac{\delta}{2-2\delta}}\varphi\right)}{\sqrt{\delta}}\right)-\left.\frac{3\delta(3\delta-2)\tan\left(\frac{1}{2}\sqrt{\frac{\delta}{2-2\delta}}\varphi\right)}{6\delta+4\tan^2\left(\frac{1}{2}\sqrt{\frac{\delta}{2-2\delta}}\varphi\right)}\right]$$
$$+\,constant.$$

The inverse relation for (3.1.12) reads

$$\varphi(r) = \pm\frac{\arctan\sqrt{\frac{er}{R-r}}}{b} = \pm\sqrt{\frac{8(1-\delta)}{\delta}}\arctan\sqrt{\frac{3\delta r}{2(6M(1-\delta)-r)}}. \tag{3.1.40}$$

As one can see, there is a choice of sign to make. Since it deals with an odd function, this will decide the orientation the body's trajectory. At the two endpoints of the ballistic orbit, namely $r = 2M$ and $r = 6M$ the following relations hold

$$r(\varphi_1) = 2M \Rightarrow \varphi_1 = \pm 2\frac{\arctan\sqrt{\frac{4}{3\delta}-2}}{\sqrt{\frac{\delta}{2-2\delta}}} + \frac{2k\pi}{\sqrt{\frac{\delta}{2-2\delta}}} \tag{3.1.41}$$
$$r(\varphi_2) = R \quad \Rightarrow \varphi_2 = \pm\frac{\pi}{\sqrt{\frac{\delta}{2-2\delta}}} + \frac{2k'\pi}{\sqrt{\frac{\delta}{2-2\delta}}}.$$

Since the argument of the cotangent term in (3.1.12) is $\frac{A}{2}\varphi$ and periodic with period π, we have to take into account solutions for φ with periodicity $\frac{2k\pi}{A}, k \in \mathbb{Z}$. The ballistic orbits are symmetric about the apastron, so if φ_i is any solution of these requirements, $-\varphi_i$ is a solution as well. Since we need $r = R$ as starting point and not the other way around, we pick up a period granting this order. The simplest choice would be to have $\varphi \in (\varphi_1, \varphi_2)$ with $k = k' = 0$,

$$-\frac{\pi}{\sqrt{\frac{\delta}{2-2\delta}}} \leqslant \varphi \leqslant -2\frac{\arctan\sqrt{\frac{4}{3\delta}-2}}{\sqrt{\frac{\delta}{2-2\delta}}}. \tag{3.1.42}$$

After inverting the relation used for $r(\varphi)$, one can find how the angle changes with respect to the radial distance from the black hole. The range of angles wherein the orbit is considered for a very small δ, say $\delta = 0.001$ becomes -140.43 rad $> \varphi > -2.45$ rad so the particle orbits around the black hole several times, roughly $\left[\frac{140.43-2.45}{2\pi}\right] = 21 \sim 22$ revolutions in a region very close to the ISCO, for the radius does not vary much, and then there is a fast plunge towards the horizon.

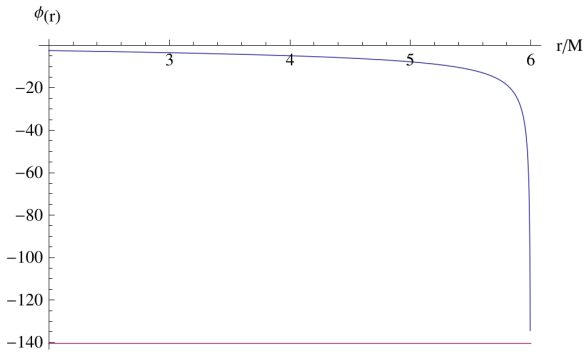

Figure 3.5: Angle evolution with radial distance, from the ISCO to the horizon, for $\delta = 0.001$

Eventually one can draw the conclusion of choosing negative angles and the minus sign in the inverted relation (3.1.40). In this way we have chosen a unique period for the angle φ, there is no need to add cumbersome $k\pi$ periodicity terms anywhere, and it is clear how relations $\tau(r), t(r)$ such as (3.1.35) have been derived.

Proper time $\tau(r;\delta)$ in terms of radial distance and the new parameter δ is again

(3.1.43)

$$\tau(r,\delta) = \frac{1}{A(e-1)^2}\left[-2\arctan\sqrt{\frac{er}{R-r}} - (e-3)\sqrt{e}\arctan\sqrt{\frac{r}{R-r}} + \frac{(e-1)\sqrt{\frac{er}{R-r}}}{1+\frac{r}{R-r}} + \pi\left(1+\frac{(e-3)\sqrt{e}}{2}\right)\right],$$

where we have also made explicit the value of the constant of integration that has been found by demanding that $\lim_{r\to R}\tau(r;\delta) = 0$. In the same way the relation for the observer's time $t(r;\delta)$ in terms of the radial distance from the BH follows automatically from replacing (3.1.40) into (3.1.35),

(3.1.44)

$$
\begin{aligned}
t(r,\delta) = {} & \frac{\sqrt{r+6M(\delta-1)(3\delta-2)}}{\sqrt{6r\delta^3}(2-3\delta)^2}\times \\
& \Bigg[2\sqrt{6}M\sqrt{\frac{r\delta}{6M(1-\delta)-r}}\left(88\delta+135\delta^3-198\delta^2-27\delta^4\right)\arctan\left(\sqrt{\frac{r}{6M(1-\delta)-r}}\right) \\
& -\delta\left(288M\sqrt{\frac{r}{6M(1-\delta)-r}}(\delta-1)^2\arctan\left(\sqrt{\frac{3}{2}}\sqrt{\frac{r\delta}{6M(1-\delta)-r}}\right)\right) \\
& +\sqrt{6}(3\delta-2)\left(r\sqrt{\delta}(3\delta-4)+2M\sqrt{\frac{r\delta(3\delta-2)}{6M(1-\delta)-r}}\log\left(\frac{\sqrt{\frac{r\delta}{6M(1-\delta)-r}}+\sqrt{\frac{\delta}{2-3\delta}}}{\sqrt{\frac{r\delta}{6M(1-\delta)-r}}-\sqrt{\frac{\delta}{2-3\delta}}}\right)\right)\Bigg] \\
& +\frac{M\pi\sqrt{\frac{2}{\delta}-3}}{\sqrt{6}(2-3\delta)^2}\left(144-88\sqrt{6\delta}-288\delta+198\sqrt{6\delta}\delta+144\delta^2-135\sqrt{6\delta}\delta^2+27\sqrt{6\delta}\delta^3\right).
\end{aligned}
$$

The value for the constant of integration, i.e. $t_0 = t(R)$, has been recovered by asking again that $\lim_{r\to R} t(r;\delta) = 0$ (demanding $\lim_{\varphi\to\varphi_2} t(\varphi;\delta) = 0$ from (3.1.35) would give the same result) .

3.1.4 Source terms for the Regge-Wheeler equations

From all the expressions listed in the section above the orbital velocities u^μ can be derived straightforwardly. These will feed the source terms (2.2.32) in the Regge-Wheeler equations (2.2.26), which have to be solved to extract gravitational radiation from a ballistic orbit. As we explained in the preceding chapter, one usually moves from Droste's to tortoise coordinates (2.2.29), which are useful for the sampling of Schwarzschild spacetime in the numerical implementation of Lousto-Price's algorithm. Once again the RW/ZM equation changes accordingly into

$$
(\partial^2_{r^*} - \partial^2_t - \bar{V}^l_{RW/ZM}(r^*))\psi^{lm}_{RW/ZM} = \bar{S}^{lm}_{RW/ZM} \tag{3.1.45}
$$

with $\bar{V}^l = \left(1-\frac{2M}{r}\right)V^l$ and $\bar{S}^l_{RW/ZM} = \left(1-\frac{2M}{r}\right)S^l_{RW/ZM}$. A further decomposition of the source terms is the following [97, 105]

$$
\bar{S}^{lm}_{RW/ZM} = \left(1-\frac{2M}{r}\right)\left(F^{lm}_{RW/ZM}\partial_r\delta(r-r_p) + G^{lm}_{RW/ZM}\delta(r-r_p)\right). \tag{3.1.46}
$$

So all the coefficients in the spherical harmonics expansion can be evaluated through the orbital velocity u^μ. From them we derive the general (lm) term in the sum for the source terms $\bar{S}^l_{RW/ZM}$ and then the F, G functions mentioned beforehand (2.2.32) which will be directly put into the code when required. The result of this are the following expressions for the even modes (Zerilli-Moncrief modes)

(3.1.47)

$$F^{lm}_{ZM}(r,\delta,\varphi)=\frac{-24\pi\mu Y^{*lm}(\frac{\pi}{2},\varphi)}{(\lambda+1)\Lambda}\Big[\frac{(2M-r)^2\sqrt{2-3\delta+\delta^2}(48M^2(\delta-1)^2+r^2(4-8\delta+3\delta^2))}{r^4(9\delta^3-36\delta^2+44\delta-16)}\Big],$$

and

(3.1.48) $$G^{lm}_{ZM}(r,\delta,\varphi)=g_1Y^{*lm}(\frac{\pi}{2},\varphi)+g_2Z^{*lm}_{\varphi}(\frac{\pi}{2},\varphi)+g_3U^{*lm}_{\varphi}(\frac{\pi}{2},\varphi)+g_4V^{*lm}_{\varphi\varphi}(\frac{\pi}{2},\varphi),$$

with $g_i=\frac{N_i}{D_i}, i=1,2,3$ having the following meaning

(3.1.49)

$$\begin{aligned}N_1=&-8\pi\mu\big(1-\frac{2M}{r}\big)(3\delta-4)\sqrt{2-3\delta+\delta^2}\Bigg[3M(5M-3r)r^2(4-3\delta)^2(3\delta-2)+\\&(4M-r)r^3(4-3\delta)^2(3\delta-2)\lambda+r^4(4-3\delta)^2(3\delta-2)\lambda^2+\\&\Lambda\Bigg(8640M^4(\delta-1)^3-6912M^3r(\delta-1)^3+2Mr^3(112-336\delta+306\delta^2-81\delta^3)\\&+108M^2r^2(15\delta^3-47\delta^2+48\delta-16)+r^4(54\delta^3-189\delta^2+204\delta-68)\Bigg)\\&-r(r+6M(\delta-1))(12M(1-\delta)+r(3\delta-2))^2\Lambda^2\Bigg],\\D_1=&\,3(2M-r)r^4(4-3\delta)^2(\delta-2)(\delta-1)(3\delta-2)(1+\lambda)\Lambda^2,\end{aligned}$$

(3.1.50)

$$\begin{aligned}N_2=&-128\sqrt{3}\pi\mu(r-2M)M\sqrt{(r+6M(\delta-1))(\delta-2)}(\delta-1)\left(12(1-\delta)M+r(3\delta-2)\right),\\D_2=&\,l(l+1)r^3\sqrt{r^3}(3\delta-4)(4-8\delta+3\delta^2)\Lambda,\\N_3=&-1152M^2\pi\mu(r-2M)^2(\delta-1)^3,\\D_3=&\,r^6(1+\lambda)\Lambda(3\delta-4)(3\delta-2)sqrt2-3\delta+\delta^2,\\N_4=&-4608M^2\pi\mu(2M-r)(\delta-1)^3,\\D_4=&\,r^4(3\delta-4)(3\delta-2)\sqrt{2-3\delta+\delta^2}\frac{(l-2)!}{(l+2)!}.\end{aligned}$$

The odd counterparts (Regge-Wheeler modes) are instead

(3.1.51) $$F^{lm}_{RW}(r,\delta,\varphi)=\frac{2304M^2\pi\mu(\delta-1)^2\sqrt{2-3\delta+\delta^2}(r-2M)^2(l-2)!}{r^5(9\delta^3-36\delta^2+44\delta-16)(l+2)!}W^{*lm}_{\varphi\varphi}(\frac{\pi}{2},\varphi)$$

(3.1.52)

$$\begin{aligned}G^{lm}_{RW}(r,\delta,\varphi)=-M\pi\mu\Bigg[&\frac{9216M(r-3M)(r-2M)(\delta-1)^2(l-2)!}{r^6(9\delta^3-36\delta^2+44\delta-16)(l+2)!}W^{*lm}_{\varphi\varphi}(\frac{\pi}{2},\varphi)\\&+\frac{64\sqrt{3}(r-2M)(\delta-1)^2(12M(1-\delta)+r(3\delta-2))\sqrt{\frac{r+6M}{r^3(\delta-2)(\delta-1)}})}{l(l+1)r^4(3\delta-4)(3\delta-2)}X^{*lm}_{\varphi}(\frac{\pi}{2},\varphi)\Bigg].\end{aligned}$$

Now that the ballistic orbits have been constructed, their properties established, and the resulting source terms in the Regge-Wheeler equations derived, we move to the next section where the numerical solution of the Regge-Wheeler equations (3.1.46) is shown and the gravitational waveforms obtained.

3.2 Gravitational Waveforms

Although there exist attempts [119] to build an analytical solution of the Regge-Wheeler equations (3.1.45), or semi-analytical in the last phases of the evolution and quasi-normal modes, [100, 120, 101, 102], the best way to obtain a solution is through numerical methods. In works such as [121, 22] an explicit assumption is made about the form of the final solution and integration techniques such as Runge-Kutta methods can be employed. In our case however we will not rely on any assumption concerning the shape of $\psi^{lm}_{RW/ZM}$ in (3.1.45), albeit we will see eventually that it meets the expectations one could get from pre-existing literature. We will rely on the simple Lousto-Price algorithm, first introduced in [20], and previously utilized for straight plunge [20, 106, 95], parabolic and eccentric orbits [97, 95, 17, 18, 96]. The following work, based on [19], represents the first instance where this method is applied to plunging orbits beyond the ISCO.

In this section a brief description of how the Lousto-Price algorithm[5] (hereafter LP algorithm) is used for the ballistic orbits is given, followed by the obtained results about the potential functions $\psi^{lm}_{RW/ZM}$ for the relevant modes, and the subsequent physical gravitational waves.

3.2.1 The Lousto-Price algorithm implemented for ballistic orbits

For our purposes the LP algorithm has been implemented in C++ programming language; at every run of the program different values of (l, m) were used, starting from $l = 2$ modes to $l = 4$ modes. The $l = 0, 1$ modes are not radiative modes [2], due to energy and momentum conservation, so were not considered. The code[6] can be found in the following public folder: https://dl.dropboxusercontent.com/u/38427324/Code_ballistic.zip.

Although the LP algorithm is conceptually simple and its code implementation requires neither particular C++ structures nor detailed explanations, a few words about its robustness are necessary. More specifically it is interesting to see how the obtained waveforms are modified by the change of user-defined parameters in the code, such as the grid step Δ, as this helps selecting the physical content of the output. In fact, all the relevant information ideally should not depend on numerical issues raised by the implementation itself.

Likewise, the ballistic orbit (3.1.12) ends at the BH horizon, which is a singularity of Schwarzschild spacetime, in Droste coordinates. This leads to factors and functions that will blow up as soon as the particle comes closer to the horizon. Numerically there is a limit to this procedure: numbers too small will be treated like zero by the code with all

[5] The general idea and concept of the algorithm have been explained in the previous chapter.

[6] Further details about the code itself can be found upon login request following the link https://wiki.nikhef.nl/gravwav/Code_files .

its consequences. Therefore we have developed a way to describe the body approaching the horizon, without getting into this problem. This, together with the issues raised in the previous paragraph, are the object of this subsection.

There are basically three features that influence the waveform output and that help in understanding the physical content obtainable from the LP algorithm applied to the Regge-Wheeler equations. These are the tuning of initial conditions, so the values for $\psi^{lm}_{RW/ZM}$ and $\dot{\psi}^{lm}_{RW/ZM}$ needed for $t = 0$, the observer's distance from the central Black Hole r_{obs}, and the grid step Δ. We will show how these influence the output and what can be done to avoid it.

Behaviour changing user-defined parameters

The LP algorithm evolves the function $\psi^{lm}_{RW/ZM}$ in time in a limited spacetime region, represented by the past light-cone of the last evaluated point $\psi^{lm}_{RW/ZM}(r^*_{obs}, t_{max})$. As was previously mentioned, values for $\psi^{lm}_{RW/ZM}$ and its time derivative are needed at time $t = 0$ for every position. Thanks to the Taylor expansion,

$$\psi^{lm}_{RW/ZM}(r^*, \Delta) = \psi^{lm}_{RW/ZM}(r^*, 0) + \dot{\psi}^{lm}_{RW/ZM}(r^*, 0)\Delta + o(\Delta^2), \tag{3.2.1}$$

values for $\psi^{lm}_{RW/ZM}$ are known at the following time $t = \Delta$ as well. Now the question is, which initial conditions should be imposed in the solution of the Regge-Wheeler equations?

Claiming $\psi^{lm}_{RW/ZM}(r^*, t = 0) = 0$ is saying that there was no initial gravitational wave present before time $t = 0$, which is physically not reasonable, so initial conditions reflecting the knowledge of previously radiated gravitational waves would be the most reasonable assumption. Choosing initial conditions in General Relativity has been and still is a much debated problem [64], for this as for other interesting situations.

Despite all this, we show that for our case this is irrelevant, for the initial conditions influence only the beginning part of the signal and get soon replaced by the relevant information coming from the ballistic orbit. This is similar to what happens for periodic motions, such as eccentric orbits [18], where the initial radiation represents a transient totally dependent on the numerics of the solving algorithm or the initial conditions [97, 22, 105].

As one can see from the plots in Fig. 3.6, the amplitudes of the Zerilli-Moncrief function share the same behaviour after the same time. Before this time the evolution is only influenced by the initial conditions, which are, respectively, null initial conditions $\psi^{(2,2)}_{ZM} = 0$, constant initial conditions $\psi^{(2,2)}_{ZM} = 3\times10^{-7}$, and gaussian distributed, centered around 0, initial conditions. The same is assumed for the time derivative, and the order of magnitude is taken to be comparable with the source terms (3.1.46) for that mass ratio ν, in order not to overcome the contribution from the source.

This answers the question: the best initial conditions are those that reflect the physical situation, but they are not relevant for the physical signal coming from the ballistic orbit. In the rest of the analysis the particle will be let to orbit on the ISCO for a sufficiently long period, in order to mimic the last stages of the inspiral in a BH binary coalescence, then it will follow a ballistic orbit.

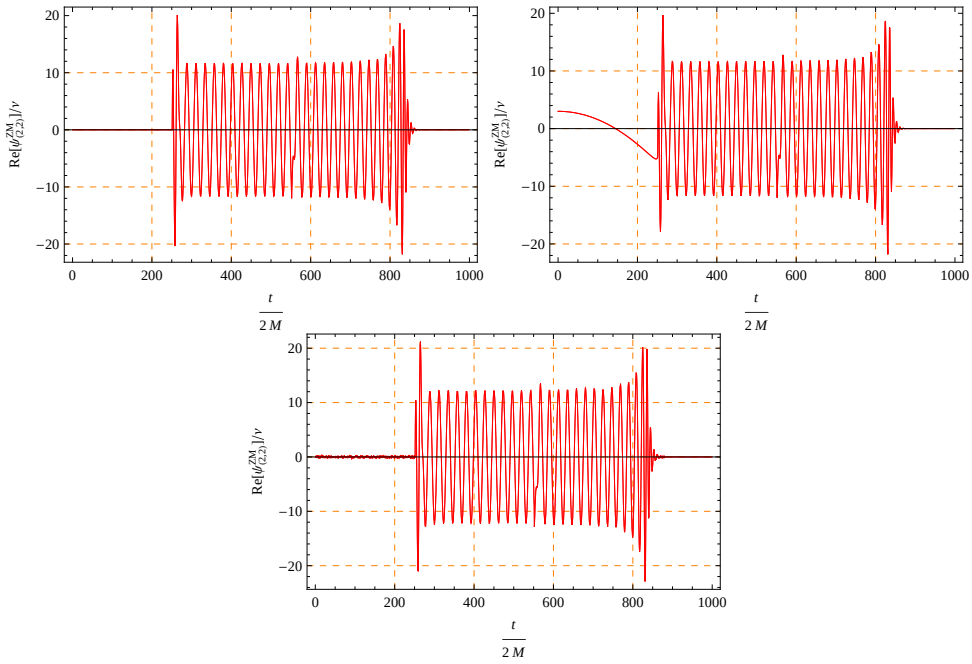

Figure 3.6: Real part of $\psi^{(2,2)}_{ZM}/\nu$ amplitudes for $\delta = 0.01$ with different initial conditions. After $\frac{t}{2M} = 250$ the signal is the same.

Once the complete evaluation of the various $\psi^{lm}_{RW/ZM}$ is performed, only the values at the observer's position are collected. This parameter, namely r^*_{obs}, can be chosen as one of the initial parameters of the algorithm. Clearly the whole procedure leading to the Regge-Wheeler equations is valid in the Regge or radiation gauge, which in turn implies that the observer is already quite distant from the source of gravitational perturbation. The question is how to quantify this "distant". The plots in Fig. 3.7 show the same waveform, for different values of observer's distance. One can deduce that only in the case where the distance is comparable with the dimensions of the orbit (remind that the ballistic orbit begins at a distance $r \sim 6M$) the signal changes considerably, then staying the same, provided that other parameters do not change.

These plots have been realized with non-trivial initial conditions, namely letting the particle orbit on the ISCO at $r = 6M$ for a time $\frac{t}{2M} = 300$, and then jumping on the ballistic orbit (3.1.12). This allows to recognize two other important phenomena, valid for all waveforms.

Everytime there is a change in the orbit, the waveforms undergo "jumps", just like the signal originated by the initial conditions is replaced by that influenced by the source terms (3.1.46), as it was clear in the previous plots as well. This is a downside of the algorithm, which solves a finite-difference differential equation, but it helps singling out the physical reliable signal from the rest. More about this will be said in the next section. Another physical interpretation of it is that it originates from a sudden change like a collision of the inspiraling body with a third one, shifting it to another orbit.

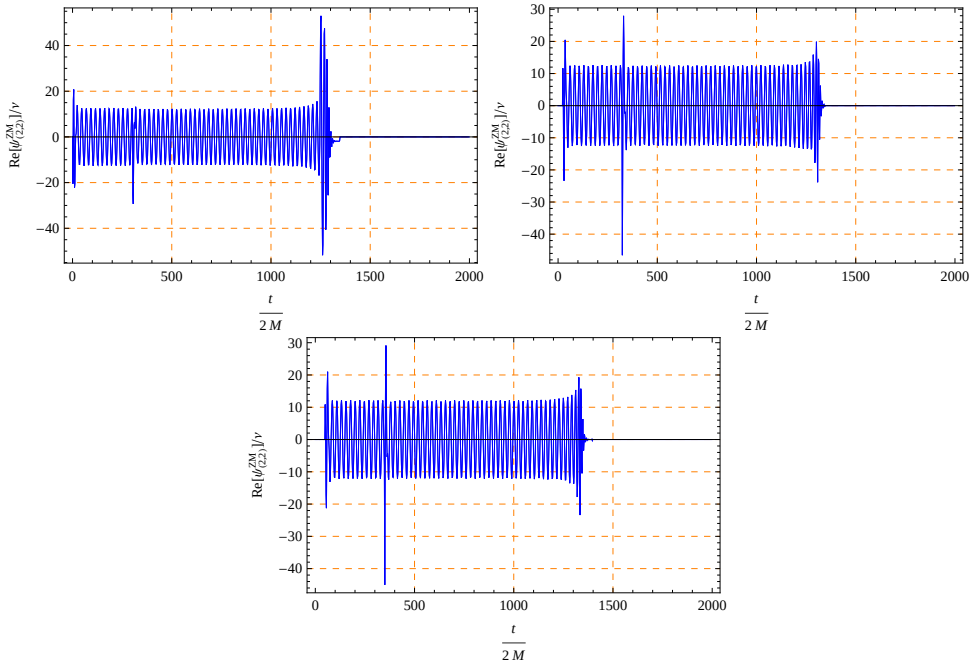

Figure 3.7: Real part of $\psi^{(2,2)}_{ZM}/\nu$ amplitudes for $\delta = 0.005$ observed from different distances, from left to right respectively $r_{obs} = 10M, 50M, 100M$.

Secondly, the effect of the source terms on the waveform starts at a time which is directly depending on the observer's position relative to the beginning of the ballistic orbit (3.1.12), namely $R = 6M(1-\delta)$. In fact the points calculated including the source terms appear in the future light-cone of the points along the orbit, as one can check looking at the scheme in Fig. 2.5. Therefore, in any run of the program, no relevant signal coming from the ballistic orbit is going to be expected before a time $\frac{t}{2M} = \frac{r^*_{obs} - r^*_0}{2\Delta}$.

Finally another user-defined parameter, which influences the final output, is the grid step Δ. Clearly the smaller this is, the better the continuity limit is achieved, at the expenses of computational time (more points are evaluated for the same final time t_{max}). Thus, provided that Δ is small enough to give a reasonable number of values for $\psi^{lm}_{RW/ZM}$ (this number is given by $\frac{t_{max}}{2\Delta}$), what is the error given by the discreteness of the grid?

Without entering the details of the calculations, the various quadratures leading to the evolution algorithm (2.3.5), (2.3.6) already introduce an overall error of the order $o(\Delta^4)$ for the cells traversed by the particle trajectory, and of order $o(\Delta^3)$ for non-traversed ones, for a more detailed discussion about these error estimates, see [20, 106]. These errors are equivalent errors of order $o(\Delta^2)$ for the final waveform $\psi^{lm}_{RW/ZM}$, matching the truncation error in the Taylor expansion (3.2.1) used for the initial conditions. Therefore any result coming from the LP algorithm has to be taken with an error of $o(\Delta^2)$.

Behaviour in the near-horizon region

Thanks to the ballistic orbits (3.1.12) one can describe the motion of the particle all the way down to the BH horizon. This will be reached in a finite proper time τ but in an infinite observer time t. This means that if we plot the observer's time $t(r)$ as in (3.1.44), the BH horizon represents a vertical asymptote for this time, as one can see in Fig. 3.8.

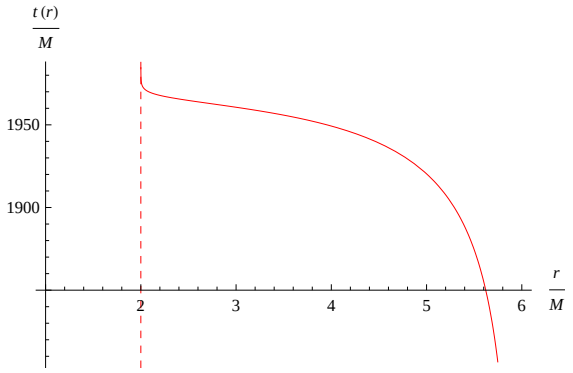

Figure 3.8: Observer's time w.r.t. radial distance from horizon ($\delta = 0.001$)

This behaviour must be reproduced by the code as well, but the machine can calculate and distinguish small numbers only up to a certain finite digit precision[7]. Past this precision, any two very close positions corresponding to two different times will be not distinguished and will be asssigned the same time value. This implies that one can only consider a finite range of time values, despite $t \to +\infty$ at the horizon, and that divisions by zero might occur (such as for any Schwarzschild factor $1 - \frac{2M}{r}$).

In order to prevent these undesirable effects a finite limiting time -called `tcritic` in the code- has been defined, after which instead of relying on the derived expression (3.1.44) for $t(r)$, we switch to a linear relation, such as $t(r^*) = \alpha r^* + \beta$ with α and β to be determined. This is justified by the following argument.

Regge-Wheeler equations (3.1.45) are solved switching to tortoise coordinates, and a numerical routine is used to recover r-values from r^*-values when needed. When this routine fails to distinguish different r^*-values, there the corresponding $t(r)$ is defined as `tcritic`. Then, from the geodesic equations (3.1.5) and following relations one can write

$$\frac{dr^*}{dt} = -\frac{A\sqrt{e}}{R}\frac{l}{\varepsilon}\sqrt{\frac{R}{r}-1}\left(\frac{(e-1)r+R}{er}\right), \tag{3.2.2}$$

with A the amplitude, e the eccentricity, l the specific angular momentum, and ε the specific energy. Close to the BH horizon means $\lim_{r\to 2M}\frac{dr^*}{dt}$. One just needs to be careful in taking the right sign of $\cot(\frac{A\varphi}{2})$, because we are dealing with negative values of φ only, for the infalling branch of the ballistic orbit (3.1.12). The result is that the particle approaches the horizon at the velocity of light, thus it is a good approximation

[7] Using double precision numbers, only differences down to $o(10^{-14})$ can be appreciated, any number smaller than $1e10^{-14}$ is treated as zero.

to consider $\frac{dr^*}{dt} = -1$ for very large negative values of r^*, i.e. close to the horizon, and solving this equation leads to

$$r^* = -t + constant, \tag{3.2.3}$$

whose integration constant can be adjusted directly on the last numerically evaluated point using the usual routines and time relation (3.1.44).

If we now consider the $r \to 2M$ limit for other quantities, like the azimuthal angle φ or radial distance r we see that

$$\lim_{r\to 2M} \frac{dr}{dt} = \lim_{r\to 2M} \frac{dr^*}{dt} \cdot \left(1 - \frac{2M}{r}\right) = 0,$$

as it is expected, since the inverse derivative $\frac{dt}{dr}$ blows up to infinity, meaning that it takes an infinite observer's time to reach the horizon. Instead, if we look at the angle we get

$$\lim_{r\to 2M} \frac{d\varphi}{dr} = \frac{3\sqrt{3}(\delta-1)^2}{(3\delta-4)M\sqrt{2-5\delta+3\delta^2}},$$

a finite value depending on δ. This means that the minor body approaches the horizon at a finite non-trivial angle depending on the beginning distance parameter δ. Of course the time variation of the azimuthal angle is null, because $\lim_{r\to 2M} \frac{d\varphi}{dt} = \lim_{r\to 2M} \frac{d\varphi}{dr} \cdot \frac{dr}{dt} = 0$, meaning that at the horizon every motion ends.

With this we know how μ approaches the horizon and we can use those limits directly. The longer the total time of your observation of the waveform signal is, the bigger the region of spacetime in the light-cone one needs to take into account in the calculation. The relation (3.2.3) may help, but it is not enough. For this reason we develop the approximate behaviour of all the interesting quantities for the near-horizon region.

Such a region can be defined again like the one where numerical routines for the change of coordinates fail to distinguish different points from the horizon. Then we move from the tortoise coordinate definition $r^* = r + 2M \log\left(\frac{r}{2M} - 1\right)$ and make an approximation for an analytical inversion formula. This can be replaced everywhere it is needed and gives approximate expressions for all the other functions in the near-horizon region. Eventually one only needs to switch from the old analytic expressions to the approximate ones every time it is required.

Thus, inverting the tortoise coordinate definition, one gets

$$e^{\frac{r^*-r}{2M}} = \left(\frac{r-2M}{2M}\right),$$

and in the near-horizon region, one can think of $R = r - 2M$ as an infinitesimal quantity. Rephrasing everything in terms of R and then expanding around $R = 0$, that is $r \to 2M$, we get

$$e^{r^*-R-2M} = \left(\frac{R}{2M}\right)^{2M} \sim e^{r^*-2M} \Rightarrow R = 2M\left(e^{\frac{r^*}{2M}-1}\right) \ll 1,$$

and so, for instance, the Schwarzschild factor becomes

$$f(r) = 1 - \frac{2M}{r} \to \frac{R}{2M} = e^{\frac{r^*}{2M}-1},$$

which for very big and negative values of r^* is a very tiny number, but big enough so that its inverse does not blow up to infinity and it can be handled more easily by the code, avoiding the singularity. A complete list of the "near-horizon" expressions is provided in the appendix, here there are some examples

$$\begin{aligned}
&\Lambda(r) \to \lambda + \frac{3}{2}, \quad \varphi(r) \to -\frac{2\arctan\sqrt{\frac{3\delta}{4-6\delta}}}{\sqrt{\frac{\delta}{2-2\delta}}} - \frac{6\sqrt{3(\delta-1)}(\delta-1)}{(3\delta-4)\sqrt{3\delta-2}} e^{\frac{r^*}{2M}-1}, \\
&\bar{V}^l_{ZM}(r^*) \to \frac{l^4+2l^3-l^2-2l+3}{4M^2(l^2+l+1)} e^{\frac{r^*}{2M}-1}, \quad \bar{V}^l_{RW}(r^*) \to \frac{l^2+l-3}{4M^2} e^{\frac{r^*}{2M}-1}.
\end{aligned} \tag{3.2.4}$$

3.2.2 Regge-Wheeler waveforms for the ballistic orbit

After discussing the numerical procedure implemented to solve the RW/ZM-equations, we present in this section the waveforms obtained in this way. The values for the Regge-Wheeler modes $\psi^{lm}_{RW/ZM}$ have been collected at the observer's position in the equatorial plane $r_{obs} = 500M$, sufficiently far from the binary coalescence, as previously argued. The following waveforms represent the time evolution of the $\psi^{lm}_{RW/ZM}$ modes at this fixed location.

To obtain a reliable wave signal for the infall on a ballistic orbit starting close to the ISCO from a quasi-periodic orbit, we consider a Schwarzschild spacetime in which the inspiral of the test mass has produced a continuous set of outgoing gravitational waves. Realistic initial conditions for the angular modes $\psi^{lm}_{RW/ZM}$ are created by letting the test mass μ run on the ISCO for a sufficiently long period that any initial transient waves have passed the point where the observer is located and the wave forms are measured.

Next we set the compact mass on a nearby ballistic orbit, and compute the resulting angular wave modes and metric perturbations. The instantaneous shift in the orbit, even if small, also produces a transient signal (see for instance Fig. 3.7 where the transition from ISCO to ballistic orbit is evident). However, for small e the ballistic orbit has an almost-periodic initial stage during which it runs close to the ISCO for a long time. During this time the original periodic signal is recovered to a very good approximation. In fact, initial transients are common in standard numerical techniques, arising for example from the well-known Gibbs phenomenon [122, 123]. We have checked that changing the initial conditions in various ways, though affecting the transient and the initial signal, does not change the almost-periodic signal during the initial stage of the ballistic orbit (see previous section), nor the development of the signal afterwards. Thus it is confirmed that, as in other numerical works [22, 124], spurious transients appear only in the initial phase of the signal[8] and are followed by numerically stable physical wave forms.

The next figures Fig. 3.9 and Fig. 3.10 show the results for the most relevant RW- and ZM-modes, as calculated for a system with mass ratio $\nu = \mu/M = 10^{-7}$ on a ballistic orbit with $e = 1.5 \times 10^3$, as observed from the equatorial plane. For convenience of representation the amplitudes have been rescaled by the inverse of the mass ratio $1/\nu$.

[8] In previous papers, such as [122, 22], to quote some of them, these initial transients have been named "junk radiation", for they do not represent any physical signal, but just an inevitable numerical feature.

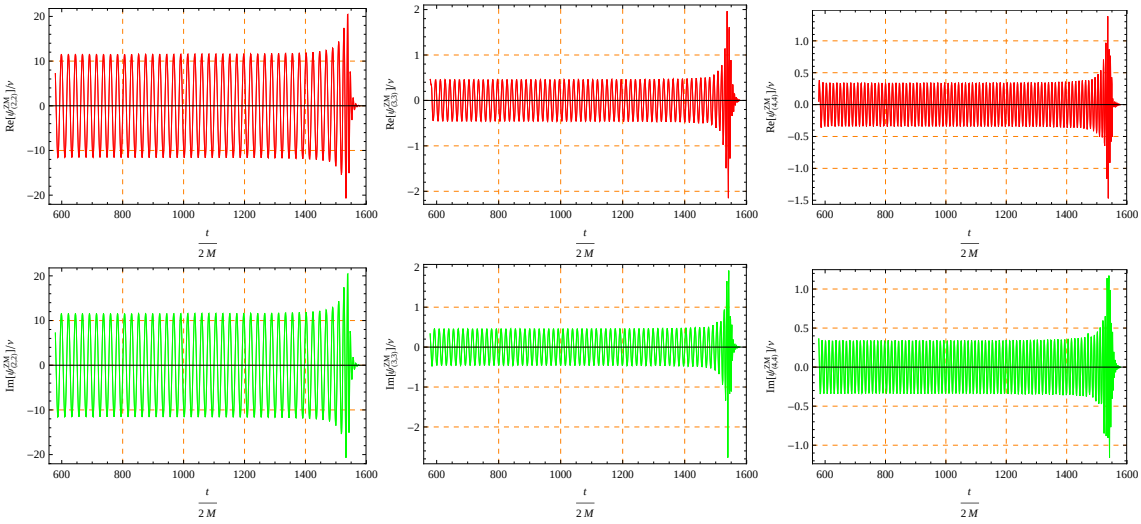

Figure 3.9: Top row: Real parts (red) of the amplitudes ψ^{ll}_{ZM} for $l = 2, 3, 4$, magnified by $1/\nu$. Second row: Imaginary parts (green) of the same amplitudes.

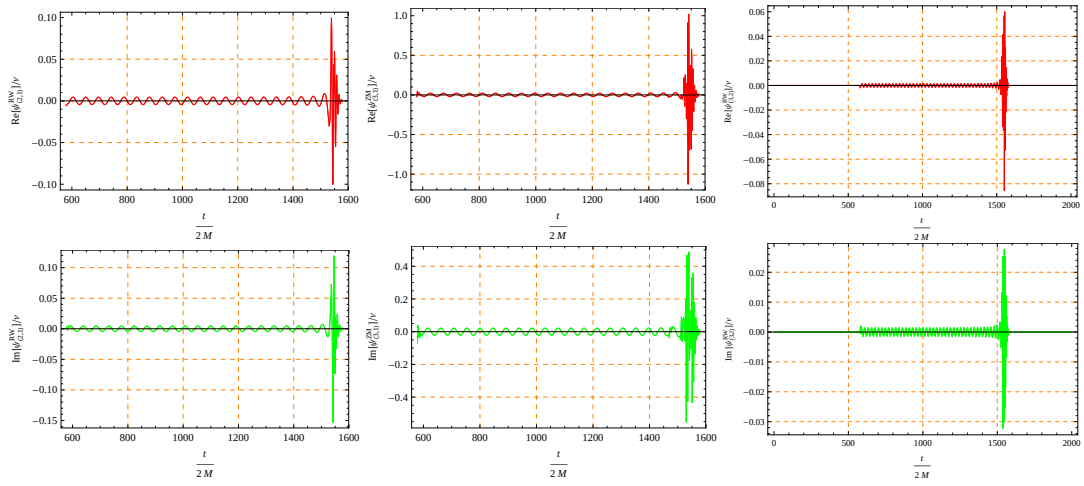

Figure 3.10: Top row: Real parts of the amplitudes ψ^{21}_{RW}/ν, ψ^{31}_{ZM}/ν, and ψ^{32}_{RW}/ν. Second row: Imaginary parts of the amplitudes ψ^{21}_{RW}/ν, ψ^{31}_{ZM}/ν, and ψ^{32}_{RW}/ν.

Both the real and imaginary parts are shown, from the time after the spurious transient signals have disappeared. The mode with $m = l = 2$ dominates all others; the modes with $m = l \geq 3$ are subdominant, representing the most important corrections. The modes with $m < l$ have negligible amplitudes, even for $l = 2$.

As one can see from the plots of the waveforms, the Regge-Wheeler function $\psi^{lm}_{RW/ZM}$ has the same behaviour, independently of the particular mode: a quasi-periodic shape, corresponding to the quasi-circular branch of the ballistic orbit (3.1.12), followed by a chirp emission, with relatively steep increase of amplitude, especially in the non-dominant

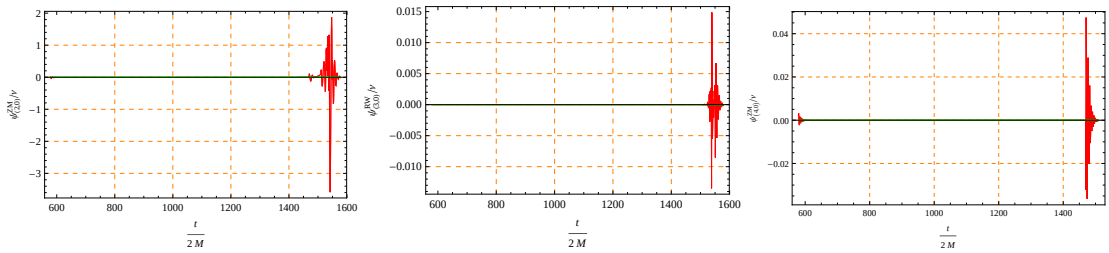

Figure 3.11: Real parts of the $m = 0$ modes, ψ^{20}_{RW}/ν, ψ^{30}_{ZM}/ν, and ψ^{40}_{ZM}/ν.

modes, in the last part, corresponding to the more radial part of the orbit. When the particle reaches the near-horizon region, another shift to the near-horizon orbital functions (3.2.4) in the code causes another Gibbs-like jump in the amplitude, (not shown in the previous plots for practical reasons). After this, the signal basically dies out.

The $\psi^{lm}_{RW/ZM}$ waveforms mirror the properties of the spherical harmonics, in fact the imaginary parts of the $m = 0$ modes are identically null, and there are symmetries among the real and imaginary parts of the l, m-modes, namely

$$\begin{aligned} \mathcal{R}e(\psi^{l,-m}) &= (-1)^m \mathcal{R}e(\psi^{l,m}) \\ \mathcal{I}m(\psi^{l,-m}) &= (-1)^{m+1} \mathcal{I}m(\psi^{l,m}). \end{aligned} \tag{3.2.5}$$

The verification of these properties provide as a consistency check for the solution of the Regge-Wheeler equation (3.1.45) using the LP algorithm.

3.2.3 Physical GW waveforms, energy and angular momentum loss rates

Inserting the results for the $\psi^{lm}_{RW/ZM}$ into the expression (2.2.40) for the GW amplitude produces the waveforms shown in the figures Fig. 3.12, 3.13, as seen from two orthogonal directions in the equatorial plane.

(3.2.6)
$$h_+(r,t,\theta,\phi) - i h_\times(r,t,\theta,\phi) = \frac{1}{r} \sum_{l,m} \left(\psi^{lm}_{ZM}(r^*_{obs}, t) - 2i \int_{-\infty}^{t} \psi^{lm}_{RW}(r^*_{obs}, t') dt' \right) {}_{-2}Y^{lm}(\theta, \phi),$$

Together with the relations for the gravitational waves in the TT-gauge (3.2.6), the Regge-Wheeler functions contain information about the energy and angular momentum loss rates, namely (2.2.45):

(3.2.7)

$$\frac{dE}{dt} = \frac{1}{64\pi}\sum_{l,m}\frac{(l+2)!}{(l-2)!}\left(|\dot{\psi}^{lm}_{ZM}(r,t)|^2 + 4|\dot{\psi}^{lm}_{RW}(r,t)|^2\right),$$

$$\frac{dL}{dt} = 2\Re\left[\frac{i}{128\pi}\sum_{l,m} m\frac{(l+2)!}{(l-2)!}\left(\dot{\psi}^{lm}_{ZM}(r,t)\psi^{*lm}_{ZM}(r,t) + 4\dot{\psi}^{*lm}_{RW}(r,t)\int_{-\infty}^{t}\psi^{*lm}_{RW}(r,t')dt'\right)\right].$$

In order to calculate these quantities, we have used the data sets plotted in Fig. 3.9 and Fig. 3.10 and streamed them to another short C++ code, taking advantage of the symmetries (3.2.5) among the different modes. This code basically implements the previous relations (3.2.6),(3.2.7). The results of this calculation are shown in the following figures.

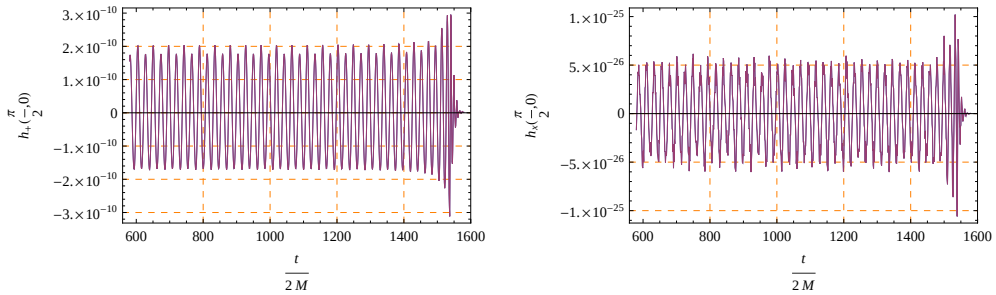

Figure 3.12: $h_+(\frac{\pi}{2},\varphi=0), h_\times(\frac{\pi}{2},\varphi=0)$ polarizations of gravitational waves radiated by a system with mass ratio $\nu = 10^{-7}$ on a ballistic orbit for $e = 0.0015$.

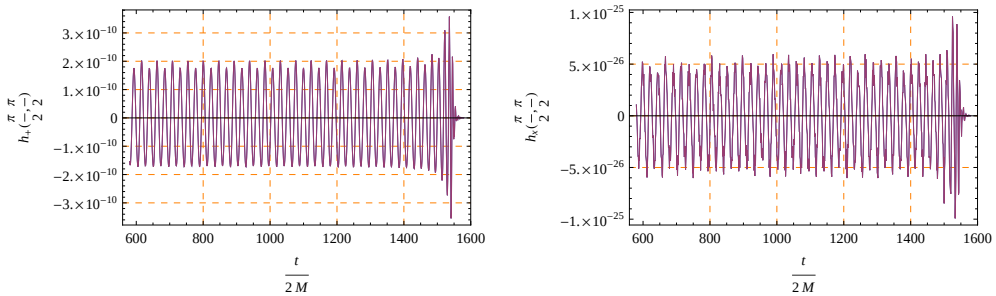

Figure 3.13: $h_+(\frac{\pi}{2},\varphi=\pi/2), h_\times(\frac{\pi}{2},\varphi=\pi/2)$ polarizations of gravitational waves radiated by a system with mass ratio $\nu = 10^{-7}$ on a ballistic orbit for $e = 0.0015$.

The GW polarizations $h_+, h_\times$ depend upon the angle of observation φ; changing it from 0 to π varies the phase of the wave, but the amplitudes stays the same. This reflects the spherical symmetry of the binary system as described by Schwarzschild metric. Notice that most of the contributions, to both the $h_+, h_\times$ polarizations and the power and angular momentum rate, come from the dominant $(2,2)$-mode whose amplitude's contribution overcomes that of the other modes.

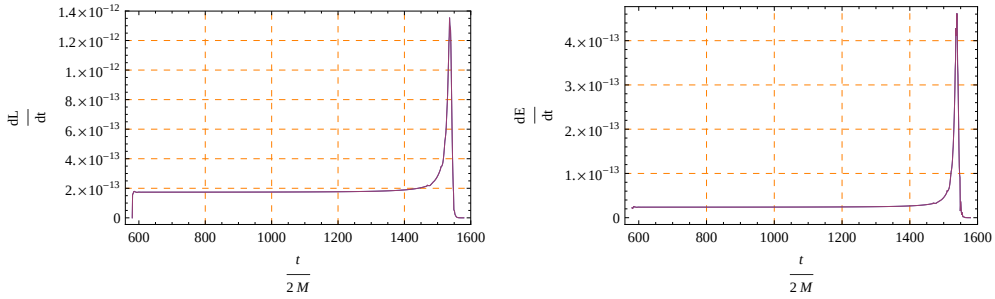

Figure 3.14: Angular momentum loss (left) and energy loss (right) on a ballistic orbit with $e = 0.0015$.

The figures Figs. 3.12, 3.13 confirm that the compact mass μ keeps orbiting for about 20 revolutions quite close to the ISCO, in a quasi-circular motion (see figure Fig. 3.5). However, once it reaches a radial distance $r \simeq 4.4M$ the final stage of direct plunge towards the black hole sets in, during which the radial velocity becomes comparable to the transverse velocity. The signal then increases in amplitude quite fast, until it crosses the light ring at $r = 3M$. After that the gravitational waves red shift and quickly fade. This behaviour was already envisaged in the Regge-Wheeler waveforms, but is even more clear here, looking at the physical gravitational signal.

The change in the GW signal of the ballistic orbit from almost periodic to direct plunge can be identified more easily in the emitted energy and angular momentum, as is clear from Fig. 3.14. The power peaks at time $t = 1536.5M$, shortly before the compact mass crosses the light ring ($r = 3M$). The total energy emitted during the infall on a ballistic orbit is a fraction 0.33×10^{-4} of the original energy of motion of the infalling mass, and most of it is emitted in the last burst before the particle crosses the horizon, at the beginning of the merger phase.

3.3 The connection between ballistic orbits and BH binary coalescences

Once that the gravitational waveforms emitted by a binary system with a central Black Hole M and a smaller companion μ moving on a ballistic orbit (3.1.12) have been presented (see figures Figs. 3.9, 3.10, 3.12 and following), we would like to make a connection between the properties of these waves, from the ballistic orbits, and from other coalescences known in the literature.

3.3.1 Orbital dependence of the emitted gravitational radiation

As it has already been pointed out several times in the previous sections, the Regge-Wheeler function $\psi^{lm}_{RW/ZM}$ undergoes sudden jumps everytime the source terms (3.1.46) change shape and there is a transition from one orbit to another. This happens when passing from data driven only by the initial conditions to source terms containing orbital

terms depending on the ISCO ($r = 6M$, $\dot{\varphi}$ constant...), or on the ballistic orbit (3.1.12), or on the ballistic orbit in the near-horizon region (3.2.4). These chirps in the signal are due to the way the algorithm is conceived and do not have a physical meaning of their own, rather they have to be cut out in order to get the correct contributions to the gravitational radiation, but they do have an utility of their own. They are strongly dependent on user-defined parameters such as the grid step Δ, or the deviation from the ISCO δ, and in this sense they help in defining the part of the signal which is stable.

Following the analysis of this part we have already remarked how the produced gravitational waves can be split into two phases. The first phase is characterized by almost-periodic gravitational radiation, very similar to the waves emitted by a compact mass in orbit on the ISCO. The second phase instead is much shorter and characterized by a burst of gravitational radiation in which the amplitude increases by a factor of two before the mass disappears effectively behind the light ring. The amplitude increases only slightly before this burst of radiation.

These two phases can be immediately accounted for by looking at the properties of the ballistic orbits. First the point mass μ follows an almost-circular orbit, for which $\dot{r} \ll r\dot{\varphi}$; around $r \simeq 4.4M$ the radial and circular velocities become comparable, after which the radial motion dominates. This is clear looking at the plots of the two velocities, Fig. 3.15.

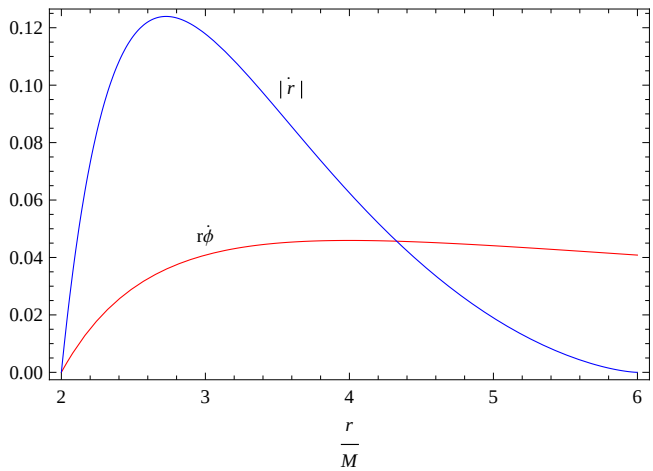

Figure 3.15: Evolution of circular and radial velocities as a function of r for the orbit with $\delta = 0.001$.

This subdivision in the orbit was already recognized in [21], when studying more general cases of black-hole coalescences. Similar studies in the small-mass-ratio limit of the transition from inspiral to plunge can be found in [125, 126, 127]. The similarity of the first phase with the radiation emitted by a body orbiting on the ISCO is justified by the fact that the ballistic orbit starts very close to it. As we have mentioned before, the apastron of such orbits is $R = 6M(1-\delta)$, with δ a small perturbative parameter (3.1.36). This shows that one can tune δ to obtain different ballistic orbits, starting at different distant positions from the ISCO.

It has been shown [21, 128] that the number of revolutions during plunge from the ISCO for coalescences is roughly $(4\nu)^{-1/5}$, where $\nu = \frac{\mu}{M}$ is the mass ratio. The mechanism behind this dependence is the fractional loss of energy by emission of gravitational radiation. As the ballistic orbits are exact geodesics, they do not account for such energy loss, but we can tune δ to make up for this and obtain a realistic approximation. For example, $\nu = 10^{-7}$ corresponds to 19 revolutions and $\delta = 0.0013$. In Fig. 3.16 the mode amplitude for $l = m = 2$ is shown for values of δ matching with $\nu = (10^{-7}, 10^{-5}, 10^{-3})$, respectively. One can see directly that the smaller δ is, the longer the quasi-circular phase is.

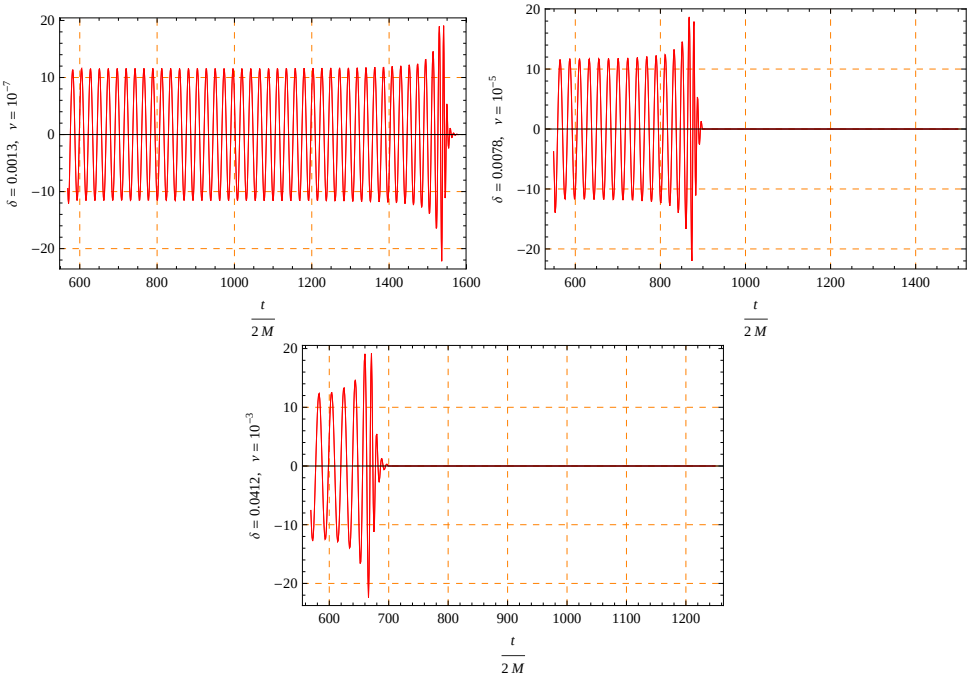

Figure 3.16: $\psi^{(2,2)}_{ZM}/\nu$ amplitudes for $\delta = (0.0013, 0.0078, 0.0412)$, only real parts shown. The values of δ are chosen to match mass ratios $\nu = (10^{-7}, 10^{-5}, 10^{-3})$. The smaller (ν, δ), the longer the near-circular
phase after $\frac{t}{2M} = 550$.

For ballistic orbits in EMR binaries – similar to what is believed to happen for more general cases – the total energy emitted during infall is only a tiny fraction of the initial energy. Therefore in practice we expect the deviation from geodesic motion to be small. Indeed, it has been argued in the literature before [21] that in the particle limit $\nu \to 0$ the motion is driven mainly by the central black hole, leading to quasi-geodesic motion. Moreover, the energy emission is far too weak to exceed the potential barrier created by the Zerilli potential (2.2.21), which shows a maximum in the region close to the light-ring $r \simeq 3M$. Thus the final burst of gravitational waves reaching a distant observer occurs before the compact mass crosses this barrier. No substantial amount of radiation coming from the inner region $r < 3M$ can be transmitted to the outer region [129, 130, 131, 124].

There is clear evidence, also from the plots, that most of the emitted energy ($\sim 98\%$) is in the dominant $(2,2)$-mode.

3.3.2 The universal phase of ballistic EMR

The analysis shows that the ballistic orbit, and therefore the gravitational signal emitted along it, depends strongly on its apastron, the point of closest approach to the ISCO. The number of almost circular revolutions is practically decided by the deviation parameter δ.

Despite this dependence, it is possible to detect a universal behaviour, independent of δ or even the mass ratio ν, for any such ballistic EMR binary. In fact the radial distance r_*/M where the cross-over occurs, and the number of turns during the second phase of radially dominated motion (the change in orbital phase in units of 2π) are virtually independent of δ. These conclusions are illustrated by the numbers in Table 3.1, calculated from our analytic formulae.

$\delta \times 10^3$	r_*/M	n_1	n_2
1.3	4.328	18.71	0.49
3.2	4.328	11.59	0.50
7.8	4.328	7.09	0.50
18.3	4.327	4.29	0.50
41.2	4.323	2.53	0.50

Table 3.1: Circular vs. radial phase on ballistic orbits; r_* is the radial co-ordinate at which the cross-over occurs; n_1 is the number of turns in the orbit before reaching the cross-over; n_2 is the number of turns between cross-over and horizon.

One can calculate from expressions like (3.1.35) the time elapsed during plunge, from the apastron to the horizon $r = 2M$, and this time can vary in a range of values such as $\frac{t}{2M} \in [60, 1000]$ for $\delta \in [10^{-3}, 10^{-1}]$. Obviously this range of values is determined largely by the duration of the nearly-circular phase of the orbit. But already from a comparison of the dominant component of the Regge-Wheeler modes for various values of δ as in Fig. 3.16 shows quite similar final bursts of radiation, whilst the duration of the almost-periodic part of the signal varies considerably [128, 132, 22]. This suggests the idea of a universal phase and behaviour of the binary coalescence, independently of the mass ratio. In fact the deviation from the ISCO δ changes the duration of the quasi-circular part, but not the direct plunge, as the number of revolutions after the transition to this regime (fourth column in table 3.1) is virtually the same.

The analogy does not stop at the number of turns in this spiralling motion, but it extends also forward to the mass ratio. As we mentioned in the previous section, in [21, 128] the number of revolutions during plunge was already related to the mass ratio. The idea behind this is that the smaller the companion body is, the less the motion will deviate from a geodesic path and therefore the quasi-circular phase will be prolonged. As a check on this, one can compare with another result of [21], elaborated in [22] and following papers, stating that the onset of universal behaviour starts inside the ISCO at

co-ordinate distance

$$\frac{r}{M} = 6 - \alpha\nu^{2/5}, \tag{3.3.1}$$

where α is a constant from 2.5PN calculations (see [21]). As the ballistic orbits are geodesic and universal, one should expect the values of δ to scale in the same way: $\delta = \gamma\nu^{2/5}$. We find that this relation holds reasonably well with $\gamma = 0.8$ for small values $\nu \leq 10^{-5}$, beyond which deviations arise of the order of 10% or more. Table 3.2 summarizes the numerical results for this comparison.

$\delta \times 10^3$	ν	$\gamma = \nu^{-2/5}\delta$
1.3	10^{-7}	0.82
3.2	10^{-6}	0.80
7.8	10^{-5}	0.78
18.3	10^{-4}	0.73
41.2	10^{-3}	0.67

Table 3.2: Test of the universality of the dependence of δ on the mass ratio ν.

As one can see from the table, deviations appear for larger mass ratios. There are at least two reasons: the center-of-mass motion and back reaction of the compact object on the Schwarzschild background geometry have been so far neglected, and the kinetic energy of the compact object is overestimated according to Eq. (3.1.28) by a factor $\Delta\varepsilon/\varepsilon = 3\delta/8$. These effects both increase when the smaller companion μ gains relevance.

3.4 Final remarks

The ballistic orbits (3.1.12) are exact solutions of the geodesic equation for Schwarzschild spacetime. They describe the motion of a test mass rising up from the horizon to a maximum radial distance $R < 6M$, before returning to the horizon; for R close to $6M$ this includes a large number of turns around the black hole. As they can come arbitrarily close to the ISCO and are degenerate in energy and angular momentum with stable circular orbits, in the limit of small e they can be used to describe test masses infinitesimally boosted from the ISCO to the infalling part of a ballistic orbit (3.1.28).

For such infalling test masses we have computed the gravitational waves emitted during the infall, using these orbits as basis for the source terms (3.1.46) in the Regge-Wheeler equations (3.1.45) which describe spacetime perturbations of a Schwarzschild background. The equations have been solved numerically through the Lousto-Price algorithm and from its results gravitational radiation has been calculated.

In specific parameter ranges the ballistic orbits can be used as a first approximation to the infall phase of an EMR binary. Comparing the waveforms for ballistic orbits with those computed for direct infall from the ISCO[9], based on Post-Newtonian and

[9]The ISCO is commonly regarded to be the region where the transition from adiabatic inspiral and plunge takes place [21, 128, 124].

Effective One-Body approximations [128, 132, 22, 124], it is easy to see that they share the same qualitative behaviour. The ballistic orbits define also a universal behaviour in the last stages of the plunge, which is independent of the mass ratio and confirms previous expectations from binary coalescences [21, 128]. Finally, we have confirmed earlier calculations showing that the total amount of energy converted into gravitational waves during the plunge phase is small, and that a quasi-geodetic description of this process for EMR binaries seems adequate.

Since the entire treatment is dynamically conservative, and pure geodesic motion does not allow for energy losses through gravitational waves, the results reported here can be improved further. One way is computing perturbative corrections to the orbits by the method of geodesic deviations, as was done for the quasi-periodic motion during the inspiral phase in [17, 18]. This method and its application to the ballistic orbit are the object of the next chapter.

* *

4 Beyond ballistic orbits

* *

In this chapter we generalise the ballistic orbits described and studied in the previous chapter in order to get a more realistic model for the plunge phase of EMR binaries. As we mentioned before, the ballistic orbits (3.1.12) are already a good model for the last stages of a EMR coalescence, but they still have two limitations. Firstly their energy is always bigger than the ISCO energy -the limit orbit between the different regimes of inspiral and plunge- contradicting the general model where the energy of the binary decreases gradually because of gravitational radiation[1]. Secondly, there is no way to include at this stage any backreaction or dissipative effects, as the ballistic orbits are solutions of the geodesic equations in Schwarzschild background.

The idea presented in this chapter is to overcome these two flaws by using geodesic deviation from the ballistic orbits, as we described at the end of chapter 2. New orbits can be built, starting from a general ballistic orbit, that have the correct energy. Moreover we will show that the energy and angular momentum of these new orbits can be adjusted in a continuous fashion in order to fulfill any additional requirement, be it the decrease of energy due to GWs, or other dissipative effects not included in the usual BH perturbation theory.

The outline of the chapter is as follows: in the first section the ballistic orbits are displayed again in the more general context of bound orbits in Schwarzschild spacetime, showing the aforementioned limitations, in the second section the geodesic deviation of these orbits is presented. A non-trivial discussion about consistent initial conditions follows next, and in section 4 the symmetries and properties of the newly found solutions are established, before the concluding remarks are given.

4.1 Associated orbits in Schwarzschild spacetime

Orbits in Schwarzschild spacetime are solutions of the geodesic equations (1.1.3) and can be derived as we did in the previous chapter (3.1.5), but a more convenient way is writing down the Lagrangian for a particle of mass m

$$\mathcal{L} = \frac{m}{2}\left[\left(1-\frac{2M}{r}\right)\left(\frac{dt}{d\tau}\right)^2 - \frac{\left(\frac{dr}{d\tau}\right)^2}{\left(1-\frac{2M}{r}\right)} - r^2\left(\frac{d\theta}{d\tau}\right)^2 - r^2\sin^2\theta\left(\frac{d\varphi}{d\tau}\right)^2\right], \tag{4.1.1}$$

[1] Except from particular situations, for instance when a third body is involved giving a push towards the inner region of the ISCO, see [19].

with the usual conserved quantities, energy and angular momentum

$$E = m\left(1 - \frac{2M}{r}\right)\frac{dt}{d\tau} \qquad L = mr^2 \sin^2\theta \frac{d\varphi}{d\tau}. \tag{4.1.2}$$

The Lagrangian (4.1.1) quadratic in the velocities coincides with the proper time hamiltonian and it is a conserved quantity itself. A compact object orbiting a Black Hole follows a timelike geodesic. Therefore we can rescale the proper time such that $2\mathcal{L} = m$, and rewrite (4.1.1) in terms of the conserved quantities (4.1.2), obtaining

$$\left(\frac{dr}{d\tau}\right)^2 + \left(1 - \frac{2M}{r}\right)\left(1 + \frac{L^2}{r^2}\right) = E^2. \tag{4.1.3}$$

This is equivalent to the normalisation condition of the 4-velocity $u^\mu u_\mu = -1$ in Schwarzschild spacetime. Now, the most natural parametrization for the radial distance is in terms of the azimuthal angle $r = r(\varphi)$. With this and defining $u = \frac{1}{r(\varphi)}$, Eq. (4.1.3) can be rewritten as

$$\left(\frac{du}{d\varphi}\right)^2 = 2Mu^3 - u^2 + \frac{2M}{L^2}u - \frac{1 - E^2}{L^2} = f(u), \tag{4.1.4}$$

together with

$$\frac{d\tau}{d\varphi} = \frac{1}{Lu^2} \qquad \frac{dt}{d\varphi} = \frac{E}{Lu^2(1 - 2Mu)}. \tag{4.1.5}$$

The condition to impose in order to have bound motion is $E^2 < 1$, then, depending on the roots of the equation $f(u) = 0$, one can distinguish different classes of orbits, following the analysis first developed by Darwin [133, 47].

Here we will focus only on the case where $f(u) = 0$ has three real roots, which can be written as

$$u_1 = \frac{1 - \eta}{p}, \qquad u_2 = \frac{1 + \eta}{p}, \qquad u_3 = \frac{1}{2M} - \frac{2}{p}, \tag{4.1.6}$$

such that p is the so-called *semi-latus rectum* and $0 \leq \eta \leq 1$ is the *eccentricity* of the orbits. These names refer to the meaning of these parameters in the most common kind of orbits falling in this category, i.e. elliptic orbits, generally parametrized as

$$\frac{1}{r} = u = \frac{1 + \eta\cos\chi}{p}, \tag{4.1.7}$$

with χ the "relativistic anomaly", a dimensionless parameter describing the motion, not to be confused with the azimuthal angle, given in this case by $\varphi(\chi)$. Elliptic orbits such as (4.1.7) are limited by the mentioned roots (4.1.6), namely $u_1 \leq u \leq u_2$. Simplifying the condition $u_1 \leq u_2 \leq u_3$ leads to the inequality

$$p \geq 2M(3 + \eta), \tag{4.1.8}$$

which defines the "separatrix" in Schwarzschild spacetime for stable orbits (for $\eta = 0$, one obtains the usual ISCO limit). These stable elliptic solutions of the equation (4.1.4) are called [47] orbits of the "first kind".

One can also look for solutions of the "second kind", namely those such that $u \geq u_3$. These orbits differ from those of the first kind in their shape, although still being closed and bound. They do not oscillate between two fixed values, rather they can reach the central singularity in the Schwarzschild Black Hole. In fact a common parametrization for these orbits is

$$u = \left(\frac{1}{2M} - \frac{2}{p}\right) + \left(\frac{1}{2M} - \frac{3+\eta}{p}\right)\tan^2\frac{\xi}{2}, \tag{4.1.9}$$

with the master equation of motion now being the following

$$\left(\frac{d\xi}{d\varphi}\right)^2 = \left(1 - \frac{6p}{M} + \frac{2p\eta}{M}\right)\left(1 - \frac{4p\eta}{M - 6p + 2p\eta}\sin^2\frac{\xi}{2}\right). \tag{4.1.10}$$

Here parameter ξ plays the same role as χ in (4.1.7). These orbits have been called *associated orbits* first [133], because they are in 1-1 correspondence with the orbits of the first kind. The ballistic orbits belong to this group of orbits as well, as we will shortly show, and it is possible to cast them in the form (4.1.9) by a suitable parameter transformation.

More precisely, it is easy to show that for the special case $\eta = 0$ in (4.1.9) the solution to (4.1.10) can be written as

$$\xi = \sqrt{1 - \frac{6p}{M}}(\varphi - \varphi_0), \qquad \text{with} \qquad u = \frac{1}{r} = \frac{1}{p} + \left(\frac{1}{2M} - \frac{3}{p}\right)\frac{1}{\cos^2\xi}. \tag{4.1.11}$$

This orbit (4.1.11) begins for $\varphi = \varphi_0$ at a limited radius $r = \frac{1}{u_3}$ such that $3M \leq \frac{1}{u_3} \leq 6M$, revolving around the black hole several times and then ending in the central singularity. However from the equations of motion written in terms of the parameter ξ,

$$\frac{d\tau}{d\xi} = \frac{1}{Lu^2}\frac{d\varphi}{d\xi}, \qquad \frac{dt}{d\xi} = \frac{E}{Lu^2(1-2Mu)}\frac{d\varphi}{d\xi}, \tag{4.1.12}$$

one notices that the factor $1-2Mu = 1-\frac{2M}{r}$ prevents someone outside the BH horizon to observe the singularity anyway. The ISCO itself $r = 6M$ is a degenerate solution whereby the orbit turns out to be stable and circular, thus it represents the envelope orbit of all such solutions (4.1.11). If one calculates the energy and angular momentum per unit mass for such orbits, one obtains the same value of stable circular orbits of the first kind, with radius equal to the semi-latus rectum parameter p, in this case,

$$\varepsilon^2 = \frac{(p-2M)^2}{p(p-3M)} \qquad \ell^2 = \frac{Mp^2}{p-3M}. \tag{4.1.13}$$

This proves that the associated orbits with $\eta = 0$, are in 1-1 correspondence with circular orbits in the outer region $r \geq 6M$, for the semi-latus rectum p has to obey (4.1.8) anyway. The same energy and angular momentum (4.1.13) have been calculated for the ballistic orbits, in that case[2]

$$p = 6M(1-\delta) = (6-4e) \quad \text{and} \quad \varepsilon^2_{ballistic} = \frac{2(2-e)^2}{9-9e+2e^2} = \frac{2(2-3\delta)^2}{9(1-\delta)(1-2\delta)}. \tag{4.1.14}$$

[2]Be careful not to mistake the eccentricity parameter appearing in the ballistic orbits with the general eccentricity appearing in (4.1.9); for the ballistic orbits $e = \frac{3}{2}\delta$ indicates the initial distance from the ISCO, while for the general associated orbit η is the eccentricity. Ballistic orbits have $\eta = 0$ in the general representation (4.1.9).

Therefore ballistic orbits are associated to outer circular orbits.

Eventually, the energy per unit mass for a generic associated orbit, with $\eta \neq 0$ is the same as for orbits of the first kind,

$$\varepsilon^2 = \frac{p^2 - 4Mp + 4M^2(1-\eta^2)}{p(p-(3+\eta^2)M)} > \frac{8}{9} = \varepsilon^2_{ISCO}, \tag{4.1.15}$$

which is always bigger than the corresponding energy for an associated orbit with $\eta = 0$, with energy (4.1.13). This demonstrates that among all the orbits of the second kind, the ones in correspondence with circular orbits -the ballistic orbits- minimize the energy, just like circular orbits do for elliptic orbits. However the energy of any associated orbit is always bigger than that of the ISCO $\varepsilon^2 = \frac{8}{9}$. In other words,

$$\forall \eta : 0 \leq \eta < 1 \quad \Rightarrow \quad \varepsilon_{associated} \geq \varepsilon_{ballistic} > \varepsilon_{ISCO}. \tag{4.1.16}$$

The interest in associated orbits, and specifically in the ballistic orbits, lies in that they are geodesic solutions apt to describe the last stages of a BH binary, i.e. the quasi-circular transition from the inspiral to plunge and after the plunge itself. They also raise the problem of their energy, being in 1-1 correspondence with outer circular orbits. $\varepsilon_{ballistic}$ is bigger than the ε_{ISCO}, a case which is not realistic as a model for a binary coalescence, unless a third body intervenes while crossing the ISCO or an extra push is given to the infalling body towards the black hole. One way to solve this problem is to generate an orbit which is a geodesic deviation from an original ballistic orbit. This will be addressed in the next sections.

4.2 Ballistic geodesic deviations

Previously the ballistic orbits have been introduced and studied, defined by

$$r = \frac{R}{1 + e\cot^2\left(\frac{A\varphi}{2}\right)}, \tag{4.2.1}$$

with the following relations among the parameters characterizing the orbits,

$$A^2 = \frac{1}{2}\left(\frac{6M}{R} - 1\right) = \xi = \frac{e}{3-2e}, \qquad e = \frac{3}{2}\left(1 - \frac{R}{6M}\right). \tag{4.2.2}$$

The eccentricity e appearing here is not the same eccentricity η defining a general associated orbit (4.1.9); ballistic orbits are in correspondence with outer circular orbits, i.e. they have null eccentricity in (4.1.9). The relation (4.2.1) can be inverted to give

$$\varphi(r) = -\frac{2\arctan\sqrt{\frac{er}{(6-4e)M-r}}}{\sqrt{\frac{e}{3-2e}}}, \tag{4.2.3}$$

in order to have the correct branch of the orbit, with the following limits on the azimuthal angle

$$-\frac{\pi}{\sqrt{\frac{e}{3-2e}}} \leq \varphi \leq -2\frac{\arctan\sqrt{\frac{e}{2-2e}}}{\sqrt{\frac{e}{3-2e}}}. \tag{4.2.4}$$

We have derived the complete solution for ballistic orbits in Schwarzschild spacetime using the radial distance r as independent variable, and the calculation of gravitational waves has been developed accordingly. Now, in order to write the geodesic deviation equations one usually requires the proper time τ to be the independent variable and writes

$$\frac{d^2 n^\mu}{d\tau^2} + 2\Gamma^\mu_{\nu\lambda}\frac{dx^\nu}{d\tau}\frac{dn^\lambda}{d\tau} + \partial_\nu \Gamma^\mu_{\lambda\kappa}\frac{dx^\lambda}{d\tau}\frac{dx^\kappa}{d\tau}n^\nu = 0. \tag{4.2.5}$$

As we explained in chapter 1, solving Eq. (4.2.5) for the deviation vector n^μ will let us build a new orbit of the form

$$x^\mu = x^\mu_{ballistic} + \sigma n^\mu + o(\sigma^2), \tag{4.2.6}$$

with σ the geodesic distance. Developing orbits to the first order in σ is good enough for our purposes of improving the ballistic orbits, as we will show shortly.

The geodesic deviation equation (4.2.5) for the θ-component decouples from the rest, as it is expected in Schwarzschild spacetime, because we keep the spherical symmetry. The simplest way to show this is to introduce a new parametrization for the angle φ, such that

$$\lambda = -\cot\frac{A\varphi}{2}, \qquad 0 \le \lambda \le \sqrt{\frac{2-2e}{e}}, \tag{4.2.7}$$

With the parametrization (4.2.7), the equation for n^θ reads

$$\frac{d^2 n^\theta}{d\lambda^2} + \frac{2\lambda}{1+\lambda^2}\frac{dn^\theta}{d\lambda} = 0, \tag{4.2.8}$$

completely decoupled from the other equations and leading to a simple solution

$$n^\theta = C_1 \arctan(\lambda) + C_2, \tag{4.2.9}$$

depending on two integration constants. This eliminates n^θ among the unknowns. However, we can ask for the motion to stay planar, or that the deviated orbit starts with the same conditions of the ballistic orbits, i.e. $\theta = \frac{\pi}{2}$ and $\dot\theta = 0$, which results in $C_1 = C_2 = 0$ and null θ-deviation $n^\theta = 0$. This can always be asked, for the Schwarzschild metric is spherically symmetric and one can shift coordinates accordingly.

The remaining equations can be cast in a matrix form, renaming the coefficients after functions a_i, b_i, c_i with $i = 1\ldots 4$ at most, which depend on the affine parameter λ and e, M. The Ordinary Differential Equation (ODE) system given by (4.2.5) would read then:

$$-\frac{d^2}{d\lambda^2}\begin{pmatrix} n^t \\ n^r \\ n^\varphi \end{pmatrix} = \begin{pmatrix} a_1\frac{d}{d\lambda} & a_2\frac{d}{d\lambda}, +a_3 & 0 \\ b_1\frac{d}{d\lambda} & b_2\frac{d}{d\lambda} + b_4 & b_3\frac{d}{d\lambda} \\ 0 & c_1\frac{d}{d\lambda} + c_3 & c_2\frac{d}{d\lambda} \end{pmatrix}\begin{pmatrix} n^t \\ n^r \\ n^\varphi \end{pmatrix}. \tag{4.2.10}$$

This ODE system (4.2.10) is linear but has non-constant coefficients, and so there is no trivial way to solve it in closed form. However, one can try different strategies. In

Schwarzschild spacetime energy ε and angular momentum l per unit mass are conserved quantities. Moving from the energy balance Eq. (4.1.3), if now we perform geodesic deviations on a given orbit, shifting from the orbit x^μ to the orbit $x^{\mu\prime} = x^\mu + \sigma n^\mu + o(\sigma^2)$, to first order in the geodesic parameter σ, the previous constants are still conserved, namely

$$\varepsilon_f = \varepsilon_0 + \sigma\varepsilon_1 + o(\sigma^2), \qquad \ell_f = \ell_0 + \sigma\ell_1 + o(\sigma^2), \tag{4.2.11}$$

where ε_0 is the specific energy of the background orbit, ε_f the energy of the final orbit obtained with geodesic deviations, and ε_1 is the correction to first order in σ to the starting energy. The same applies to the angular momentum. Starting from a geodesic orbit, (ε_0, ℓ_0) are natural conserved quantities. In this case they are the energy and angular momentum per unit mass of the ballistic orbit (4.2.1).

If we now perform the expansion in the usual relation for the energy in Schwarzschild metric (2.1.9),

(4.2.12)

$$\begin{aligned}
\varepsilon = \left(1 - \frac{2M}{r}\right)\frac{dt}{d\tau} \quad \Rightarrow \varepsilon &= \left(1 - \frac{2M}{r+\sigma n^r}\right)\left(\frac{dt}{d\tau} + \sigma\frac{dn^t}{d\tau}\right) + o(\sigma^2) \\
&= \left(1 - \frac{2M}{r}\right)\frac{dt}{d\tau} + \sigma\left(\frac{dn^t}{d\tau} + \frac{2M}{r}\left(\frac{n^r}{r} - \frac{dn^t}{d\tau}\right)\right) + o(\sigma^2) \\
&= \varepsilon_0 + \sigma\varepsilon_1 + o(\sigma^2).
\end{aligned}$$

The same can be done for the angular momentum and for the condition of the normalisation of u^μ, i.e.

$$\begin{aligned}
\varepsilon^2 &= \left(\frac{dr}{d\tau}\right)^2 + \left(1 - \frac{2M}{r}\right)\left(1 + \frac{\ell^2}{r^2}\right) \Rightarrow \\
(\varepsilon_0 + \sigma\varepsilon_1)^2 &= \left(\frac{d}{d\tau}(r + \sigma n^r)\right)^2 + \left(1 - \frac{2M}{r+\sigma n^r}\right)\left(1 + \frac{(\ell_0 + \sigma\ell_1)^2}{(r+\sigma n^r)^2}\right) + o(\sigma^2) \Rightarrow \\
\Rightarrow \qquad \varepsilon_0\varepsilon_1 &= \frac{dr}{d\tau}\frac{dn^r}{d\tau} - \frac{n^r}{r^2}\left(\frac{\ell_0^2}{r}\left(1 - \frac{3M}{r}\right) - M\right) + \frac{\ell_0\ell_1}{r^2}\left(1 - \frac{2M}{r}\right);
\end{aligned} \tag{4.2.13}$$

leading to the following three expressions,

$$\begin{aligned}
&\varepsilon_1 = \left(1 - \frac{2M}{r}\right)\frac{dn^t}{d\tau} + \frac{2M}{r^2}\frac{dt}{d\tau}n^r, \\
&\ell_1 = r^2\frac{dn^\varphi}{d\tau} + 2r\frac{d\varphi}{d\tau}n^r, \\
&\left(1 - \frac{2M}{r}\right)\left(\frac{dt}{d\tau}\varepsilon_1 - \frac{d\varphi}{d\tau}\ell_1\right) = \frac{dr}{d\tau}\frac{dn^r}{d\tau} - n^r\left(r\left(\frac{d\varphi}{d\tau}\right)^2\left(1 - \frac{3M}{r}\right) - \frac{M}{r^2}\right).
\end{aligned} \tag{4.2.14}$$

After some straightforward algebra one can prove that ε_1 and ℓ_1 are conserved quantities, because from (4.2.14)

$$\begin{aligned}
\frac{d\varepsilon_1}{d\tau} &= \left(1 - \frac{2M}{r}\right)\left(\frac{D^2n^t}{D\tau^2} - R^t{}_{\nu\lambda\kappa}u^\nu n^\lambda u^\kappa\right) = 0, \\
\frac{d\ell_1}{d\tau} &= r^2\left(\frac{D^2n^\varphi}{D\tau^2} - R^\varphi{}_{\nu\lambda\kappa}u^\nu n^\lambda u^\kappa\right) = 0,
\end{aligned} \tag{4.2.15}$$

which are the geodesic deviation equations for n^t, n^φ in covariant form (2.4.1). This result holds for any geodesic deviation in Schwarzschild spacetime, not just the ones based on ballistic orbits, and proves that, to first order in the parameter σ, the energy and the angular momentum are conserved.

Now the crucial point is that one can treat ε_1 and ℓ_1 as constants of motion to be tuned matching the resulting values $\varepsilon_f = \varepsilon_0 + \sigma\varepsilon_1$ and $\ell_f = \ell_0 + \sigma\ell_1$ with those of a chosen orbit. In this way (ε_1, ℓ_1) are not constants of motion to be found, rather they become necessary to solve the geodesic deviation equations. The system of first integrals (4.2.14) is a simpler ODE, because it is of first order and the third equation shows that n^r is decoupled from the other equations. So, in principle one can solve for n^r from the third equation, and then use this solution in the other two equations and find the missing components with a single quadrature.

The constants ε_1 and ℓ_1 are to be chosen such as to tune the final energy and angular momentum (ε_f, ℓ_f) to the desired values. This means that for every couple of values (ε_1, ℓ_1) one can solve for a different deviation and obtain a different orbit, satisfying the desired requirements. The major problem we are trying to address with ballistic deviations is that the energy (and angular momentum) of the simple ballistic orbit are too big to account for a generic binary coalescence. They refer to special cases, as we have already discussed in the first section. We refer to the next sections for a more detailed discussion about this; for the time being, just consider (ε_1, ℓ_1) constant values such that $(\varepsilon_f = \varepsilon_{ballistic} + \sigma\varepsilon_1, \ell_f = \ell_{ballistic} + \sigma\ell_1)$ are known.

The next most convenient step is to rewrite the first integrals (4.2.14) in terms of the radial variable, obtaining

$$
\begin{aligned}
&\varepsilon_1 = \left(1 - \frac{2M}{r}\right)\left(\frac{dn^t}{dr}\frac{dr}{d\tau} + \frac{2M\varepsilon_0}{r^2}n^r\right),\\
&\ell_1 = r^2\frac{dn^\varphi}{dr}\frac{dr}{d\tau} + \frac{2\ell_0}{r}n^r,\\
&\varepsilon_0\varepsilon_1 - \frac{\ell_0\ell_1}{r^2}\left(1 - \frac{2M}{r}\right) = \left(\frac{dr}{d\tau}\right)^2\frac{dn^r}{d\tau} + \left(\frac{M}{r^2} - \frac{\ell_0^2}{r^3}\left(1 - \frac{3M}{r}\right)\right)n^r.
\end{aligned}
\tag{4.2.16}
$$

Renaming the apastron of a ballistic orbit $R = (6-4e)M$, the following limits can be easily verified

$$
\lim_{r\to R}\frac{dr}{d\tau} = 0, \qquad \lim_{r\to R}\frac{d^2r}{d\tau^2} = \frac{\ell_0^2 M e^2}{R^4},
\tag{4.2.17}
$$

leading to the Taylor expansion in proper time of the radial distance for a ballistic orbit,

$$
r(\tau) = R + \frac{\ell_0^2 M e^2}{R^4}\tau^2 + o(\tau^3).
\tag{4.2.18}
$$

Therefore the radial velocity term $\frac{dr}{d\tau}$ into the third first integral in (4.2.16) is null at $\tau = 0$. This entails that if we now take as initial condition on the deviation component n^r the fact that initially the deviated orbit coincides with the original ballistic orbit, so $n^r(\tau = 0) = 0$, from the third of Eqs.(4.2.16), one gets

$$
\varepsilon_0\varepsilon_1 - \frac{\ell_0\ell_1}{R^2}\left(1 - \frac{2M}{r}\right) = 0 \quad \text{i.e.} \quad \varepsilon_1 = \sqrt{\frac{1-e}{2(3-2e)}}\frac{\ell_1}{(2-e)(3-2e)M},
\tag{4.2.19}
$$

requiring a constraint between the correction values (ε_1, ℓ_1). From now on, we will solve the first integrals (4.2.16) in all generality and then apply the relation between the energy and angular momentum corrections as given in (4.2.19). Notice that both the energy correction and the angular momentum correction share the same sign.

Solving for the radial component $n^r(r)$

The third of the first integrals (4.2.16) can also be written as

$$\begin{aligned}\left(\frac{dr}{d\tau}\right)^2 &= \varepsilon_0\varepsilon_1 - \frac{\ell_0\ell_1}{r^2}\left(1-\frac{2M}{r}\right) - \left(\frac{M}{r^2} - \frac{\ell_0^2}{r^3}\left(1-\frac{3M}{r}\right)\right) n^r \\ &= \left[\varepsilon_0^2 - \left(1-\frac{2M}{r}\right)\left(1+\frac{\ell_0^2}{r^2}\right)\right]\frac{dn^r}{dr},\end{aligned} \tag{4.2.20}$$

where in the second line the hamiltonian constraint (4.1.3) has been used. Now we can define an ad hoc function $g(r)$ such that

$$\frac{dg(r)}{dr} = \frac{d}{dr}\left[\varepsilon_0^2 - \left(1-\frac{2M}{r}\right)\left(1+\frac{\ell_0^2}{r^2}\right)\right] = -2\left(\frac{M}{r^2} - \frac{\ell_0^2}{r^3}\left(1-\frac{3M}{r}\right)\right), \tag{4.2.21}$$

therefore Eq. (4.2.20) becomes

$$h(r) = \varepsilon_0\varepsilon_1 - \frac{\ell_0\ell_1}{r^2}\left(1-\frac{2M}{r}\right) = g(r)\frac{dn^r}{dr} - \frac{1}{2}\frac{dg(r)}{dr}n^r \quad \rightarrow \quad \frac{h(r)}{g(r)\sqrt{g(r)}} = \frac{d}{dr}\left(\frac{n^r}{\sqrt{g(r)}}\right). \tag{4.2.22}$$

The solution for the radial component $n^r(r)$ can be found via a simple quadrature, namely

$$n^r = \sqrt{g(r)}\int \frac{h(r)}{g(r)\sqrt{g(r)}}dr, \quad \text{with} \quad n^r(R) = 0 \quad (\text{equivalent of } n^r(\tau=0)=0\ ). \tag{4.2.23}$$

For the sake of reporting a more detailed calculation, we present are the fundamental steps leading to the solution $n^r(r)$,

$$\int \frac{h(r)}{g(r)\sqrt{g(r)}}dr = (3-4e+e^2)(3-2e)^{3/2}\int \left(\frac{r}{R-r}\right)^{\frac{3}{2}} \frac{a_0 + a_1 r^3 + a_2 r}{(R-(1-e)r)^3}dr,$$

with $a_0 = 4M^2\ell_1(3-2e)$, $a_1 = (2-e)\sqrt{\frac{2(1-e)}{3-2e}}\varepsilon_1$, $a_2 = -2M\ell_1(3-2e)$. Now, the key transformation to do is $s^2 = \frac{r}{R-r}$, which gives

$$\int \frac{h(r)}{g(r)\sqrt{g(r)}}dr = \frac{2}{R^2}(3-4e+e^2)(3-2e)^{3/2}\int \frac{s^4\left(a_0 + b_1 s^2 + b_2 s^4 + b_3 s^6\right)}{(1+s^2)^2(1+es^2)^3}ds,$$

with $b_1 = 3a_0 + Ra_2$, $b_2 = 3a_0 + 2Ra_2$, and $b_3 = a_0 + R^3 a_1 + Ra_2$. The final result is obtained solving this last integral in the dummy variable s and then replacing it with its radial counterpart. Eventually the integral is multiplied by $\sqrt{g(r)}$ and the resulting function gives the radial component of the deviation vector $n^r(r)$ up to an additive constant.

The final result derived from (4.2.23), upon using the relation (4.2.19) for the energy per unit mass ε_1, is

(4.2.24)
$$
\begin{aligned}
n^r(r) = &-\frac{(3-2e)^{3/2}\left(3-4e+e^2\right)\ell_1}{(6-4e)^2(1-e)^3}\sqrt{\frac{(R-r)}{(9-18e+11e^2-2e^3)\,r^3}}(R-(1-e)r)\\
&\cdot\left(\frac{4(1-e)}{M\sqrt{\frac{r}{R-r}}}r-\frac{(1-e)(3-2e)\left(15-44e+13e^2\right)}{e^2\sqrt{\frac{r}{R-r}}(R-(1-e)r)}r\right.\\
&\quad-24(3-e)(3-2e)\arctan\sqrt{\frac{r}{R-r}}+\frac{2(3-e)(1-e)^2(3-2e)}{e^2\left(\frac{r}{(R-r}\right)^{3/2}(R-(1-e)r)^2}r^2\\
&\quad\left.+\frac{3(3-2e)\left(3-15e+37e^2-9e^3\right)}{e^{5/2}}\arctan\sqrt{\frac{er}{R-r}}\right),
\end{aligned}
$$

and it automatically satisfies the requirement $n^r(R)=0$, so there is no need to add an integration constant. The only singular points in the solution (4.2.24) are for $r=\frac{R}{1-e}>R$ which is irrelevant because outside of the domain of the original ballistic orbit, and clearly the origin of Schwarzschild coordinates $r=0$, where $n^r(r)\sim\frac{1}{r}$ for $r\to 0$. Therefore $n^r(r)$ is well-defined and regular at all points $2M\leq r\leq R$.

Solving for the temporal and azimuthal components $n^t(r)$, $n^\varphi(r)$

Once the solution for the radial component (4.2.24) is known, the other two first integrals (4.2.16) give the remaining components by simple quadratures. In fact from the second of (4.2.16) one reads, modulo an additive constant,

$$
\frac{dn^\varphi}{dr}=\left(\frac{\ell_1}{\ell_0}-2\frac{n^r(r)}{r}\right)\frac{d\varphi}{dr}\quad\to\quad n^\varphi(r)=\frac{\ell_1}{\ell_0}\varphi(r)-2\int\frac{d\varphi}{dr}\frac{n^r(r)}{r}dr. \tag{4.2.25}
$$

The integral to be performed is the following

(4.2.26)
$$
\begin{aligned}
\int\frac{n^r(r)}{r}\frac{d\varphi}{dr}dr=&\,c_0\int\left(c_1 r\sqrt{\frac{R-r}{r}}+c_2\frac{\sqrt{r\frac{R-r}{r}}}{R-(1-e)r}+c_3\frac{r^2(\frac{R-r}{r})^{\frac{3}{2}}}{(R-(1-e)r)^2}\right)\frac{dr}{r^3}\\
&+c_0\int\left(c_4\arctan\sqrt{\frac{r}{R-r}}+c_5\arctan\sqrt{\frac{er}{R-r}}\right)\frac{dr}{r^3},
\end{aligned}
$$

with

$$
c_0=\frac{(3-2e)(3-e)M\ell_1}{2(1-e)^2\sqrt{9-18e+11e^2-2e^3}},\ c_1=\frac{4(1-e)}{M},\ c_2=-\frac{(1-e)(3-2e)(15-44e+13e^2)}{e^2},
$$
$$
c_3=\frac{2(3-e)(1-e)^2(3-2e)}{e^2},\ c_4=-24(3-e)(3-2e),\ c_5=\frac{3(3-2e)(3-15e+37e^2-9e^3)}{e^{\frac{5}{2}}}.
$$

The final result of this integration, with the same techniques used in (4.2.23), contributes to the azimuthal component of the deviation vector, $n^{\varphi}(r)$, i.e.

(4.2.27)

$$
\begin{aligned}
n^{\varphi}(r) = &-\frac{\sqrt{(3-2e)\,(3-4e+e^2)}\ell_1}{M(3-2e)(1-e)^2\sqrt{e(9-18e+11e^2-2e^3)R^2}}\arctan\sqrt{\frac{er}{R-r}} \\
&+\frac{(3-2e)(3-e)\ell_1}{2M(1-e)^2\sqrt{9-18e+11e^2-2e^3}R^2}\Bigg[\frac{3\left(18-105e+179e^2-129e^3+43e^4-6e^5\right)}{e^2}\sqrt{\frac{R-r}{r}} \\
&+\frac{3(1-e)\left(9-42e+27e^2-2e^3\right)}{e^2}\left(\frac{R-r}{r}\right)^{\frac{3}{2}}-\frac{4(3-e)(1-e)^3(3-2e)r}{e(R-(1-e)r)}\sqrt{\frac{R-r}{r}} \\
&+14(3-e)(3-2e)\arctan\sqrt{\frac{r}{R-r}}+72(3-e)(3-2e)\frac{R^2-r^2}{r^2}\arctan\sqrt{\frac{r}{R-r}} \\
&+\frac{18-171e+97e^2-3e^3+21e^4-10e^5}{e^{\frac{3}{2}}}\arctan\sqrt{\frac{er}{R-r}} \\
&+\frac{3(3-2e)\left(3-15e+37e^2-9e^3\right)}{e^{\frac{5}{2}}}\frac{R^2-r^2}{r^2}\arctan\sqrt{\frac{er}{R-r}}\Bigg]+n^{\varphi}_{c}.
\end{aligned}
$$

Likewise one can derive the solution for the temporal component $n^t(r)$. Again, from the first equation in (4.2.16),

(4.2.28)

$$
\begin{aligned}
\frac{dn^t}{dr} &= \left(\frac{r^2}{\left(1-\frac{2M}{r}\right)}\frac{\varepsilon_1}{\ell_0}-\frac{2M\varepsilon_0}{\ell_0}n^r\right)\frac{d\varphi}{dr} \\
&\rightarrow n^t(r) = \int\frac{r^2}{\left(1-\frac{2M}{r}\right)}\frac{\varepsilon_1}{\ell_0}\frac{d\varphi}{dr}(r)dr-\int\frac{2M\varepsilon_0}{\ell_0}n^r(r)\frac{d\varphi}{dr}(r)dr,
\end{aligned}
$$

together with an additive constant. These integrals can be performed in the same way as the previous ones, the only difference being in the first term, where the Schwarzschild factor appears. This accounts for the observer's time delay when getting close to the BH horizon $r \to 2M$. In fact the first term in (4.2.28), upon using the relation for the energy and angular momentum (4.2.19) given by $n^r(R) = 0$, looks like

$$
\int\frac{d\varphi}{dr}\frac{r^2\varepsilon_1}{\ell_0\left(1-\frac{2M}{r}\right)}dr = \int\frac{\sqrt{2(3-e)(1-e)}\ell_1R^2s^6}{(6-7e+2e^2)M(1+s^2)^2(1+es^2)(2M+(2M-R)s^2)}ds,
$$

with the dimensionless dummy variable $s^2 = \frac{r}{R-r}$. The term $\frac{1}{(2M+(2M-R)s^2)}$ -taking into account the correct domain for s- gives a $\operatorname{arccoth}\left(\frac{r(R-2M)}{2M(R-r)}\right)$ term in the final solution, which is divergent at the BH horizon.

This being said, the final result for the temporal component of the deviation vector

$n^t(r)$ is the following, up to an additive constant n_c^t:

(4.2.29)

$$
\begin{aligned}
n^t(r) = \frac{\ell_1}{2\sqrt{6-2e}(1-e)^2}\Bigg[& -\frac{(2-e)(3-e)}{(3-2e)^2}\Bigg(\frac{3(1-e)\left(9-42e+27e^2-2e^3\right)}{e^2}\sqrt{\frac{R-r}{r}} \\
& -\frac{2(1-e)^2\left(9-9e+2e^2\right)r}{e(R-(1-e)r)}\sqrt{\frac{R-r}{r}} + 8\left(21-17e+2e^2\right)\arctan\sqrt{\frac{r}{R-r}} \\
& +24\left(9-9e+2e^2\right)\frac{R-r}{r}\arctan\sqrt{\frac{r}{R-r}} + \frac{9-99e-19e^2+75e^3-14e^4}{e^{\frac{3}{2}}}\arctan\sqrt{\frac{er}{R-r}} \\
& -\frac{3(3-2e)\left(3-15e+37e^2-9e^3\right)}{e^{\frac{5}{2}}}\frac{R-r}{r}\arctan\sqrt{\frac{er}{R-r}}\Bigg) \\
& +\frac{(3-e)(1-e)^3}{(2-e)(6-7e+2e^2)M^2}\Bigg(\frac{4\sqrt{2}M^2\,\mathrm{arccoth}\sqrt{\frac{2(1-e)r}{R-r}}}{\sqrt{1-e}} - \frac{2(2-e)M}{1-e}\sqrt{r(R-r)} \\
& +4M^2\frac{22-33e+15e^2-2e^3}{(1-e)^2}\arctan\sqrt{\frac{r}{R-r}} - \frac{8(3-2e)^2M^2}{\sqrt{e}(1-e)^2}\arctan\sqrt{\frac{er}{R-r}}\Bigg)\Bigg].
\end{aligned}
$$

4.3 Criteria for initial conditions

The procedure for solving the geodesic deviation equations (4.2.5) based on ballistic orbits (4.2.1) depends on some global constants. These are the boundary conditions that one can impose on the final orbit. As we have already mentioned, the final orbit will have a conserved energy and angular momentum (ε_f, ℓ_f) to first order in the geodesic deviation $o(\sigma)$, obeying the following relationship

$$
\varepsilon_f = \varepsilon_{ballistic} + \sigma\varepsilon_1, \qquad \ell_f = \ell_{ballistic} + \sigma\ell_1, \tag{4.3.1}
$$

where without loss of generality we can put $\sigma = 1$, by a rescaling of the constants (ε_1, ℓ_1) still to be chosen. These represent the corrections to the energy and angular momentum of the original orbit -the ballistic orbit- such that the resulting final energy and angular momentum comply with a general binary coalescence behaviour, for instance requiring that $\varepsilon_f < \varepsilon_{ISCO}$.

In a generic binary coalescence, after the adiabatic inspiral has ended,[3] there is a first quasi-circular motion, where angular velocity prevails over the radial one, followed by a more direct plunge, a feature which the ballistic orbits likewise agree with. Due to gravitational radiation emission, some energy and angular momentum are lost during these stages and the initial energy (and angular momentum) are anyway less than those of a stable orbit at the ISCO. Ballistic orbits alone do not meet this requirement, but a correction through geodesic deviations can help.

Since we are virtually able to solve the deviation equations (4.2.11) for any couple of values (ε_1, ℓ_1), i.e. we are able to place the smaller companion in the binary coalescence

[3] This happens in the region of the ISCO, depending on the mass ratio $\nu = \mu/M$.

in any inspiralling orbit with any energy, we are left with determining the values of such initial parameters.

The correction to the new orbit, i.e. the geodesic deviation vector n^μ, can make the final parameters (ε_f, ℓ_f) equal to the ISCO ones. These represent an orbit beginning immediately after leaving the ISCO with its same energy and angular momentum. In this case the corrections would be

$$\begin{aligned} \varepsilon_1 &\leq \varepsilon_{ISCO} - \varepsilon_{ballistic} = \frac{2\sqrt{2}}{3} - \frac{\sqrt{2}(2-e)}{\sqrt{9-9e+2e^2}} < 0, \\ \ell_1 &\leq \ell_{ISCO} - \ell_{ballistic} = 2\sqrt{3}M - \frac{2M(3-2e)}{\sqrt{(3-e)(1-e)}} < 0, \end{aligned} \tag{4.3.2}$$

and they would depend only on the eccentricity e of the original ballistic orbit, which we have shown in the previous chapter to be strictly correlated to the mass ratio $\nu = \mu/M$.

Although we are able to find good deviations from the ballistic orbits for any couple (ε_1, ℓ_1) satisfying (4.3.2), we have shown that requiring the deviation n^μ to start at $\tau = 0$, or $r = R = (6-4e)M$, i.e. exactly on the ballistic orbit, puts bounds on the values of energy and angular momentum of the final orbit. In particular (4.2.19) shows that the energy correction required depends on the value of the angular momentum correction, via

$$\varepsilon_1 = \sqrt{\frac{1-e}{2(3-2e)}}\,\frac{\ell_1}{(2-e)(3-2e)M}. \tag{4.3.3}$$

Upon using this constraint one can legitimately ask whether the conditions (4.3.2) are still satisfied. This happens to be the case, because one can always choose freely the angular momentum correction ℓ_1 such that $\ell_f \leq \ell_{ISCO}$, then the energy correction is fixed and the resulting final energy ε_f is automatically less than the ISCO energy. For instance, taking $\ell_1 = \ell_{ISCO} - \ell_{ballistic}$, i.e. the value saturating the inequality (4.3.2) above, the energy is

$$\varepsilon_1 = \frac{2\sqrt{\frac{1-e}{6-4e}}\left(\sqrt{3} - \frac{3-2e}{\sqrt{3-4e+e^2}}\right)}{(2-e)(3-2e)}, \tag{4.3.4}$$

which gives a final energy of the deviated orbit less than the ISCO one. The following plot Fig. 4.1 shows the energy difference w.r.t. different eccentricities to be always positive, meaning that the ISCO energy is the upper limit of the energy of deviated orbits. This limit is reached in the case $e = 0$, whereby the ballistic orbit coincides with the ISCO, and the corresponding deviated orbit has null corrections $\varepsilon_1 = 0 = \ell_1$.

This fixes the problem of the energy of associated orbits raised in (4.1.16), and forces the smaller body to move on a geodesic orbit with the correct requirements. As it was expected the other initial parameters, i.e. n^t_c, n^φ_c, are independent of this energy and angular momentum balance. That is why the deviated ballistic orbit fulfilling (4.3.2) is not unique, but there is a class of orbits, given by a simple initial shift in the observer's time t and the azimuthal angle φ.

In the next section we are going to report in more detail the features of such deviations from ballistic orbits, studying the behaviour of the orbit $x^\mu = x^\mu_{ballistic} + n^\mu$. In

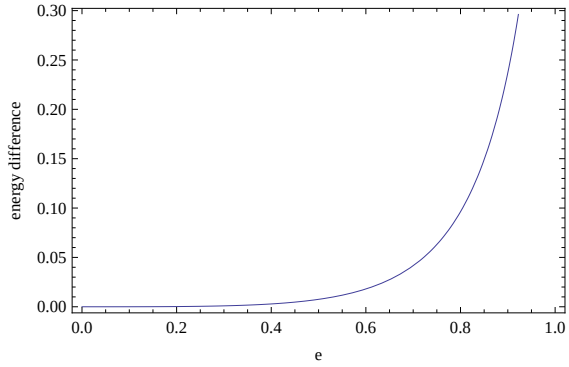

Figure 4.1: Plot of the energy difference per unit mass $\varepsilon_{ISCO} - \varepsilon_f \geq 0$ between the ISCO and the orbit built on the deviation from a ballistic orbit with eccentricity e.

doing so, we will use the conditions (4.3.2),(4.3.3) for the energy and angular momentum corrections.

4.4 Behaviour of the newly built solution

As long as the constraint (4.3.4) is satisfied, any value of ℓ_1 below

$$\ell_1 \leq \ell_{ISCO} - \ell_{ballistic} \qquad \Rightarrow \qquad \ell_1 \leq 2\sqrt{3}M - \frac{2M(3-2e)}{\sqrt{(3-e)(1-e)}} \qquad \forall e \geq 0, \tag{4.4.1}$$

gives a good orbit modeling the plunge of an EMR binary. Once the limit (4.4.1) is violated the final angular momentum (and the energy too) will be bigger than the corresponding ISCO values.

In this section we wish to show the effects of the deviations on the original ballistic orbit. Being small deviations, one does not expect the effect of n^μ to change dramatically the qualitative behaviour of the ballistic orbit, in fact the order of magnitude of the deviation is fixed by ℓ_1 itself. In the limit where $\ell_1 \to 0$ the final energy and angular momentum (ε_f, ℓ_f) are equal to the ISCO ones, the inequality (4.4.1) is saturated and the geodesic deviation $n^\mu = 0$ ceases to exist. One can notice trivially that every component is directly proportional to the angular momentum correction ℓ_1, see Eqs. (4.2.24),(4.2.27),(4.2.29).

Keeping this in mind, the deviation affects the original ballistic orbit mainly in the radial distance and in the observer's time. For the sake of representation, we are using an angular momentum correction $\ell_1 = -4.3388 \cdot 10^{-6}$, which is calculated using the ISCO as reference orbit, so saturating the inequality (4.4.1) for $(e = 0.0015, M = 10)$, the same values used previously for the analysis of ballistic orbits. This means that the particle orbiting the new orbit has the same energy per unit mass as a particle on the ISCO.

The radial component $n^r(r)$ presents an initial local maximum, soon after $r = R$, and it reaches a finite value $n^r(2M) \neq 0$ at the BH horizon, independently of the mass M. A plot of this component over the domain $2M \leq r \leq (6-4e)M$ is shown in Fig. 4.2.

The deviation is working against the fall into the black hole, increasing only at the very beginning the radial distance. This effect is considerably reduced in the limit $e \to 0$,

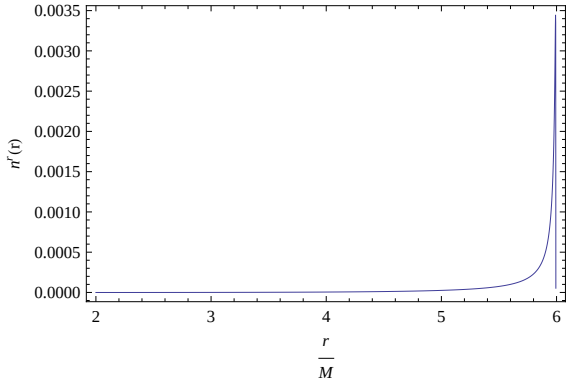

Figure 4.2: Radial component of the deviation vector $n^\mu(r)$, for $(e = 0.0015, M = 10)$. The angular momentum correction used is the one saturating the inequality (4.4.1), which for the given values of eccentricity and mass amounts to $\ell_1 = -4.3388 \cdot 10^{-6}$.

as one can see in Fig. 4.3. The only way to invert this small correction in order to have the minor body fall faster towards the BH with respect to the original ballistic orbit, would be to swap sign in the parameter σ, namely to use $r - n^r$, but this would give an energy and angular momentum always greater than those on the ISCO (4.3.1). This is an indication that one is accelerating the body towards the BH with an extra acceleration and more kinetic energy, a situation which we want to avoid.

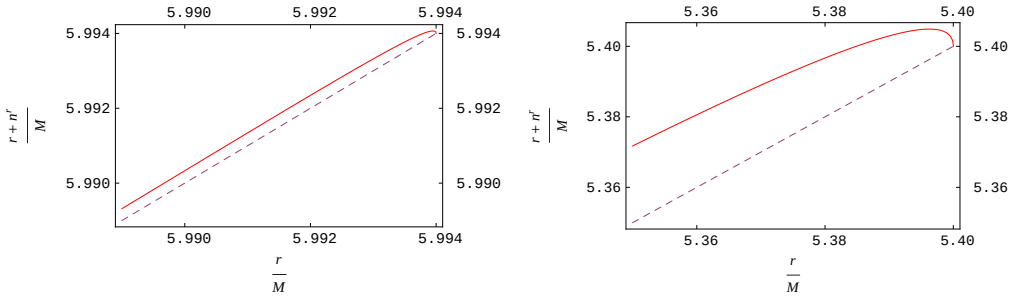

Figure 4.3: Radial coordinate $r + n^r(r)$ (red) against the original radial variable r (dashed line) for different values of (e, ℓ_1), mass $M = 10$. The angular momentum correction is chosen in order to saturate (4.4.1) in all cases. $e = (0.0015, 0.15)$ respectively for the two plots.

Next to the radial motion, one can calculate the corrections n^t, n^φ to the observer's time and azimuthal angle choosing the integration constants in such a way that time $t = 0$ is measured at the beginning of motion -like it was done for the ballistic orbit- and at the same angular position. This can be achieved asking that

$$\lim_{r\to R} t(r) + n^t(r) = 0, \qquad \lim_{r\to R} \varphi(r) + n^\varphi(r) = \varphi_0 = -\sqrt{\frac{3-2e}{e}}\pi, \tag{4.4.2}$$

and fixing the integration constants accordingly. This reduces to the following conditions

(4.4.3)

$$n_c^t = \frac{\ell_1 \pi}{4\sqrt{6-2e}(2-e)^2(1-e)^2 e^{3/2}(3-2e)}\Big(72 - 660e + 1080e^{3/2} + 230e^2 - 1908e^{5/2} + 951e^3 + 1236e^{7/2} - 1060e^4 - 348e^{9/2} + 454e^5 + 36e^{11/2} - 90e^6 + 7e^7\Big),$$

$$n_c^\varphi = \frac{\ell_1 \pi}{12(3-2e)M}\left(\frac{3\,(1-\sqrt{e})\,(3-e)\left(18 + 54\sqrt{e} - 63e - 117e^{3/2} - 11e^2 + 39e^{5/2} + 30e^3 + 10e^{7/2}\right)}{4\,(1+\sqrt{e})^2\, e^{3/2}\sqrt{9 - 18e + 11e^2 - 2e^3}} - 6\sqrt{\frac{9}{e} + 11e - 2e^2 - 18}\right).$$

Once the conditions (4.4.3) have been taken into account, the solution $x^\mu_{ballistic} + n^\mu$ is complete. The variations in the time and angle components are minimal, as Fig. 4.4 shows.

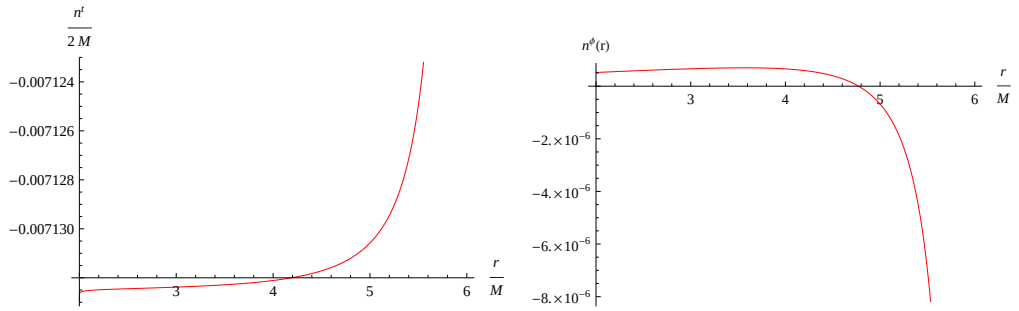

Figure 4.4: Time (left) and angular (right) deviation components for $e = 0.0015, M = 10, \ell_1 = -4.3388 \cdot 10^{-6}$ after applying conditions (4.4.3). The deviations are even at their largest absolute values six or more orders of magnitude smaller than the original orbit ($\frac{t}{2M} \sim 10^3$, and $\varphi \sim 10$).

It is relevant to notice that, although the arccoth()-term in n^t (4.2.29) tends to $-\infty$ working against the time dilation of an observer approaching the BH horizon, this effect is still too small to overcome the time dilation of the original ballistic time at the horizon $r \to 2M$.

Using the deviation vector it is not difficult to compute its effect on the orbital velocities and the difference in the source terms appearing in the Regge-Wheeler equations, thus predicting qualitatively how much the wave solutions could deviate from the ballistic ones. The orbital velocities appearing in the source terms (2.2.32) get contributions

directly proportional to the radial deviation $n^r(r)$ and they read

(4.4.4)

$$u^t = \frac{dt_{ballistic}}{d\tau} + \sigma\frac{dn^t}{d\tau} = \frac{\varepsilon_0}{\left(1-\frac{2M}{r}\right)} + \sigma\left(\frac{\varepsilon_1}{\left(1-\frac{2M}{r}\right)} - \frac{2M\varepsilon_0}{r^2}n^r\right),$$

$$u^\varphi = \frac{d\varphi_{ballistic}}{d\tau} + \sigma\frac{dn^\varphi}{d\tau} = \frac{\ell_0}{r^2} + \sigma\left(\frac{\ell_1}{r^2} - \frac{2\ell_0}{r^3}n^r\right),$$

$$u^r = \frac{dr_{ballistic}}{d\tau} + \sigma\frac{dn^r}{d\tau} =$$

$$\sqrt{\varepsilon_0^2 - \left(1-\frac{2M}{r}\right)\left(1+\frac{\ell_0^2}{r^2}\right)} + \sigma\frac{\varepsilon_0\varepsilon_1 - \frac{\ell_0\ell_1}{r^2}\left(1-\frac{2M}{r}\right) - \left(\frac{M}{r^2} - \frac{\ell_0^2}{r^3}\left(1-\frac{3M}{r}\right)\right)n^r}{\sqrt{\varepsilon_0^2 - \left(1-\frac{2M}{r}\right)\left(1+\frac{\ell_0^2}{r^2}\right)}}.$$

4.5 Discussion

As a first step towards a calculation of gravitational radiation, after checking the modest contribution of the deviation vector to the radial direction, one can investigate the source terms $F^{lm}_{ZM/RW}$ and $G^{lm}_{ZM/RW}$ and what is the order of magnitude of change between the original ballistic orbit and the new more general orbit. For the sake of simplicity we report only the source terms for the dominant mode $(l,m) = (2,2)$ in the following Fig. 4.5. One can notice that the plots overlap with each other almost perfectly, suggesting that any difference is very small and not easy to detect.

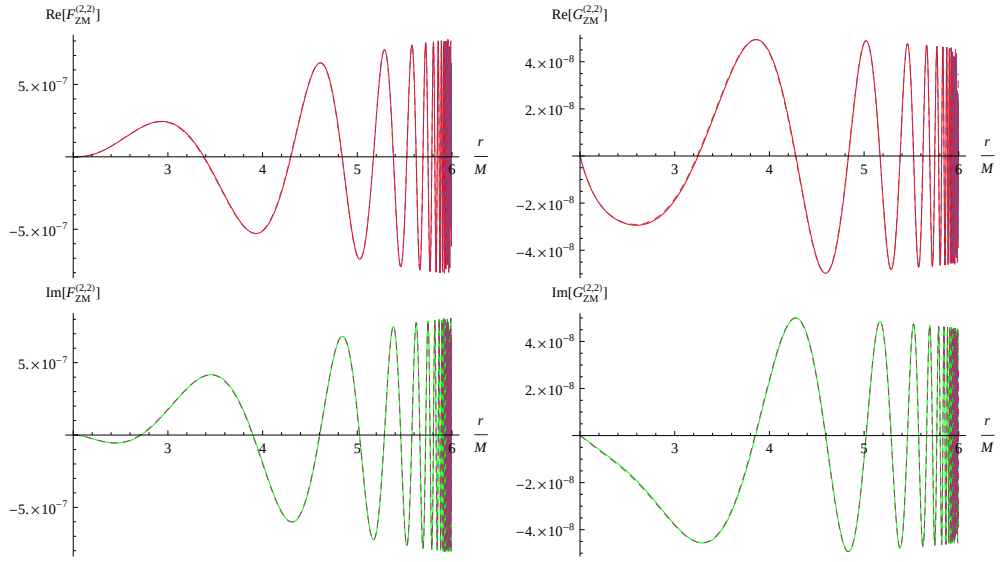

Figure 4.5: Source terms for the dominant mode $(l,m) = (2,2)$, with $e = 0.0015, M = 10, \mu = 10^{-6}$. Comparison between source terms for the original ballistic orbit (dashed lines) and the new deviated orbit (continuous lines). Real parts in red, imaginary ones in green.

In the next plots in Fig. 4.6 one can actually observe that the differences are one to two orders smaller than the magnitude of the source functions for the source term $F^{(2,2)}_{ZM}$. The immediate consequence of this is that one can expect the final waveforms to be pretty close to the original ballistic ones discussed in the previous chapter; see also [19]. In contrast to this, the differences in the $G^{(2,2)}_{ZM}$ are more relevant, specially during the first quasi-circular revolutions around the central black hole.

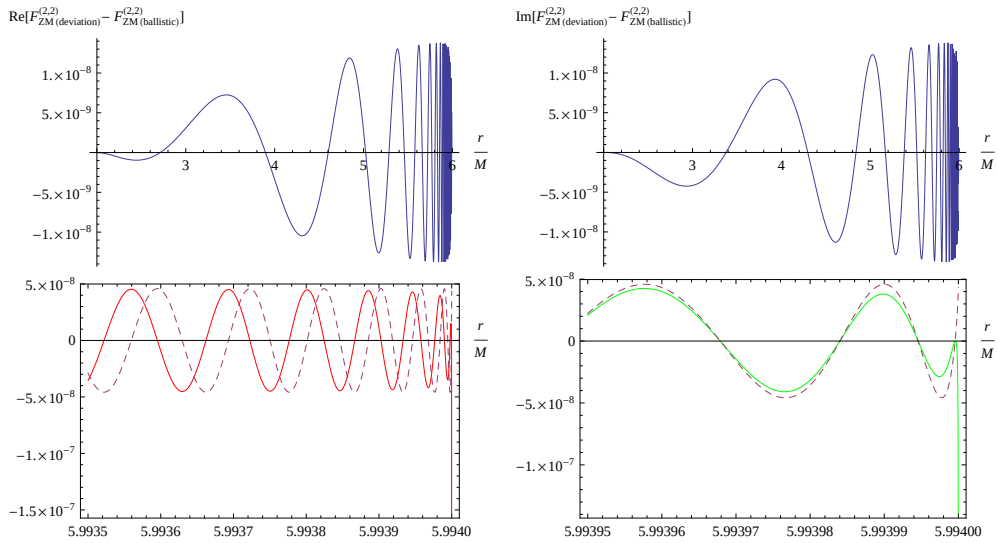

Figure 4.6: Top row: difference for the dominant mode source function $F^{(2,2)}_{ZM}$ between the original ballistic orbit and the new deviated orbit. Real part on the left, imaginary part on the right.
Bottom row: zoom in of the $G^{(2,2)}_{ZM}$ in proximity of the initial position $R = (6 - 4e)M$, where the difference among the deviated orbit (continuous curve) and the original (dashed curve) is greatest. Real parts in red, imaginary ones in green. The same values for eccentricity and BH masses as in Fig. 4.5 have been used.

On a slightly different note, one can also look at the total number of revolutions during the new deviated orbit, as we did already for the ballistic orbits. This is easily evaluated considering the orbital phase change, i.e. the difference in radians between the azimuthal angle at the beginning of motion (which we have put equal to the corresponding one in the ballistic orbit by choosing n^{φ}_{c} (4.4.3)) and the final value reached at the BH horizon, i.e. $\lim_{r\to 2M} \varphi_{ballistic} + n^{\varphi}$.

With these conditions in mind the difference Δn between the number of revolutions following a deviated orbit and following a simple ballistic orbit is then given by the difference of the limits of the orbital phase at the BH horizon between the two orbits, for

the same parameters (e, M). After a straightforward calculation one obtains

(4.5.1)

$$\Delta n = \lim_{r\to 2M} n^{\varphi}(r) = \frac{\ell_1}{4M\pi}\sqrt{\frac{(3-e)(1-e)}{e(3-2e)}}\Bigg[\pi + \frac{72-378e+433e^2-170e^3+19e^4}{2(2-e)(1-e)^2}\sqrt{\frac{1-e}{2e^3}}$$
$$+ 6\sqrt{e}(2-e)^2(1-e)(3-2e)^2(3-e)\arctan\sqrt{\frac{1}{2-2e}}$$
$$- \frac{72-474e+1517e^2-1725e^3+771e^4-113e^5}{4e^2(1-e)^3}\arctan\sqrt{\frac{e}{2-2e}}$$
$$- 2\arctan\sqrt{\frac{e}{2-2e}} - \frac{6+18e^{1/2}-17e-27e^{3/2}-15e^2-5e^{5/2}}{8e\left(1+\sqrt{e}\right)^3}\pi\Bigg].$$

As one can see Eq. (4.5.1) is directly proportional to the ratio of the angular momentum correction over the central BH mass. The angular momentum correction ℓ_1 is also the parameter fixing the order of magnitude of the deviation itself, which cannot be bigger or comparable to the size of the original ballistic orbit, otherwise it is not a slight deviation anymore, but rather a major change in the companion's motion.

So far we have determined limits (4.3.2) on the correction ℓ_1 such that the final energy is not bigger than that of the ISCO. These represent upper limits on the correction parameters. What can be said about the lower limits, if any, of these corrections? Eq. (4.5.1) can help to ascertain how far below the energy of the ISCO we can get with deviations. In fact, if ℓ_1 is too big, two undesired phenomena can happen. First the radial correction, which we described in Fig. 4.2 and 4.3, becomes too big and n^{μ} is not just a simple deviation to the ballistic orbit; it is pushing too much the minor body μ back towards the ISCO, such that in the initial phase of motion, for a given distance r, $r_{ballistic} + n^r > 6M$. This would be counterintuitive, as afterwards the body falls back into the BH anyway. Secondly the number of revolutions could differ significantly from the original one, leading to a different relation between the eccentricity e and the mass ratio $\nu = \mu/M$.

The difference in the number of revolutions (4.5.1) can be rewritten as

(4.5.2)
$$\Delta n = \frac{\ell_1}{4M\pi} f(e),$$

with $f(e)$ a scalar function of e, plotted in Fig. 4.7. In this plot one can notice that for $e < 0.3$ the number of revolutions can only increase, i.e. $\Delta n > 0$, as ℓ_1 is always negative. If we look back at section 3.3.2 in the previous chapter, we see that there is a relation between the number of revolutions and the mass ratio of the EMR binary. From Tables Tab. 3.1 and 3.2 one can see that the mass ratio $\nu = \mu/M$ increases, while the number of revolutions decreases following a power law $\sim (4\nu)^{-1/5}$ [21, 128]. The difference among revolutions corresponding to different mass ratios can be used to set a lower limit on the angular momentum correction.

One needs to calculate for different mass ratios the expected number of revolutions and compare it to the ones that the deviated orbit takes. The deviation n^{μ} will increase the original number given by the ballistic orbit, but this increment cannot be so big as

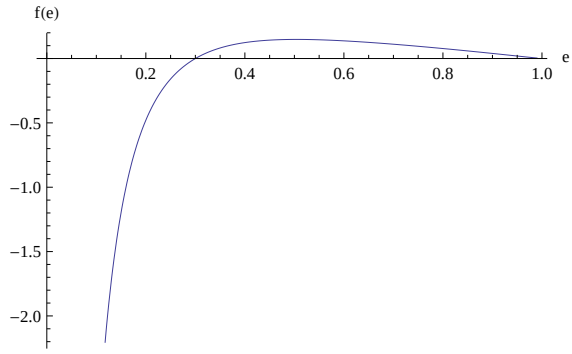

Figure 4.7: Plot of $f(e)$ as defined in (4.5.2). For $e < 0.3$, so for all practical values of e, the curve is always negative.

to reach the number of revolutions needed for the next bigger mass ratio. So, for a given mass ratio ν_0, the corresponding ballistic orbit, following Tab. 3.2, has a specific value of the parameter δ_0 and the eccentricity e_0. For this eccentricity the deviation from the ballistic orbit takes an extra number of revolutions $\Delta n(e_0, \ell_1)$ given by (4.5.1) more than the original ballistic orbit. This cannot be bigger or comparable with the difference in revolutions coming from the next mass ratio ν_1, smaller by one order of magnitude with respect to ν_0. These considerations are summarized in the following table Tab. 4.1. For

ν	$n_{expected}$	$\Delta n_{expected}$	$\delta \times 10^3$	$e \times 10^3$	$\Delta n(e)$
10^{-8}	30.17	10.96	0.5	0.8	-8198.82
10^{-7}	19.21	7.12	1.3	1.9	-2147.91
10^{-6}	12.09	4.50	3.2	4.8	-545.74
10^{-5}	7.59	2.80	7.8	11.7	-137.27

Table 4.1: $n_{expected}$ is the expected number of turns for the corresponding mass ratio ν according to the power law $\sim (4\nu)^{-1/5}$; next $\Delta n_{expected}$ is the difference of turns w.r.t. the next bigger order of magnitude for ν; δ and e the corresponding parameters for the ballistic orbit; $\Delta n(e)$ is the difference of number of revolutions of the deviated orbit w.r.t. the ballistic one, in units of ℓ_1/M.

instance for an EMR binary of mass ratio $\nu \sim 10^{-7}$, such as those studied throughout this dissertation, one expects to have roughly $n_{expected} \sim 19$ turns, ~ 10.96 revolutions less than what comes for the next smaller order of magnitude of mass ratio $\nu \sim 10^{-8}$. The ballistic orbit fulfilling these requirements, in agreement with [21, 128, 19], as discussed in the previous chapter, has a $\delta = 0.0013$ or $e = 0.00195$; with these values the deviated orbit would turn $\Delta n(e) = -2147.91 \frac{\ell_1}{M}$ times more than the original ballistic orbit. Therefore this sets a lower limit for ℓ_1 (or an upper limit for $|\ell_1|$), in fact

$$\Delta n(e)\frac{\ell_1}{M} \ll \Delta n_{expected} \Rightarrow \ell_1 \gg \frac{\Delta n_{expected} M}{\Delta n(e)}, \tag{4.5.3}$$

for $\Delta n(e) < 0$ for this range of values of the eccentricity. Applying this argument (4.5.3)

for the mass ratios reported in the previous table Tab. 4.1, one gets the following lower limits for the angular momentum correction:

ν	$e \times 10^3$	ℓ_1
10^{-7}	1.9	$\gg -0.0051035M$
10^{-6}	4.8	$\gg -0.0130444M$
10^{-5}	11.7	$\gg -0.0328173M$

Table 4.2: Different mass ratios ν correspond to different values of eccentricity e and give different lower limits (third column) for the angular momentum correction ℓ_1.

For instance, the case of $\mu = 10^{-6}, M = 10$, the range of possible values for ℓ_1 is:

$$-0.051035 \ll \ell_1 \leq -4.3388 \cdot 10^{-6}.$$

One is then left with comparing the global magnitude of the deviation with respect to the original orbit, in order to prevent $r > 6M$.

4.6 Concluding remarks

The ballistic orbits (4.2.1) have been very useful in determining an initial model for the plunge phase of an EMR binary coalescence, but by using them one is naturally confronted with the issue of the energy of the body following such orbits. This is always bigger than the corresponding energy for the ISCO orbit, as it happens for every associated orbit (4.1.16). Being the neighbourhood of the ISCO the region where the transition between adiabatic inspiral and plunge occurs, it is necessary for a realistic model of an EMR binary to have continuously decreasing energy and angular momentum as the coalescence evolves in time.

In this chapter we have used the method of geodesic deviations [18] in order to overcome this limit of the model based on ballistic orbits. We have solved the geodesic deviation equations in the radial variable to first order and obtained the deviation vector $n^\mu(r)$ (4.2.24),(4.2.27), and (4.2.29). The energy and angular momentum of the final orbit can be tuned smoothly to any value, as the solutions of the deviation equations depend on the constant values of the energy and angular momentum corrections (ε_1, ℓ_1), provided certain conditions (4.3.2), (4.5.3) are satisfied. This turns the original ballistic orbits into a very diverse tool for modeling the plunge of any EMR coalescence.

We have analysed the effect of the deviation on the original orbit. This results mainly into a delay effect, i.e. causing more revolutions, in the initial quasi-circular stage of the plunge phase. However other consequences on the source terms are very small and any gravitational radiation obtained from that should not differ much qualitatively from the ones obtained originally from the ballistic orbits only. Fig. 4.3 and Fig. 4.5 relate to this.

Clearly solving the Regge-Wheeler equations (2.2.26) with the deviated ballistic orbits would provide the final test on these orbits, and in fact this is the goal of future investigation.

* *

5 Spinning compact objects in EMR binaries

* *

The Schwarzschild metric can give a good account of all the celestial phenomena with spherical symmetry which involve no rotations, or spins, but there is more to that, even just limiting oneself to the binary coalescences. It is well-known that astrophysical black holes do rotate, as one can already deduce from the fact that they originate after the collapse of stars, so if the star was originally rotating, a substantial part of its angular momentum will be transferred to the black hole.

Spinning objects are the most common ones among the observed astrophysical bodies. As far as coalescences are concerned, this entails rotations for both objects involved in their celestial dance. The solution of the Einstein field equations including the spin of the black hole is relatively simple and well-known: it is the Kerr solution [117], and it gives the most complete account for all the tidal phenomena brought about by the addition of spin to a spherical distribution of mass.

Nevertheless it is just as important to know how a generic spinning body behaves in a curved background. Phenomena such as the precession of the spin or Lense-Thirring effects on the orbits of spinning bodies are a current astrophysical reality. Rather than considering how the background is influenced by the rotation of the mass, the question is how a generically curved background, be it Schwarzschild, be it Kerr[1], influences the motion of a spinning object, like a gyroscope, and what its backreaction to the given background metric is. This problem dates back to the founding works of Papapetrou [24] and Pirani [134] and it is related to the analogous situation in quantum mechanics, where these aspects were considered already long before [135] and used for the semi-classical description of elementary particles.

Clearly a spinning compact object such as a neutron star or a planet has an extension, and every attempt to reduce it to a spinning pointlike gyroscope is an approximation, but it is appropriate for an Extreme Mass Ratio coalescence. Here, in fact, the pointlike nature of the companion body is already granted by the assumptions behind the definition itself of an EMR binary. The smaller companion ($\sim 10^6$ orders of magnitude smaller) is regarded as pointlike and its backreaction to the central major body metric is initially neglected. Therefore a spinning body in such a binary is a perfect example of a spinning

[1] Or any other curved background, such as gravitational waves, de Sitter...

particle in a curved background.

In this chapter an analytical and mathematically consistent formalism for a spinning object in any curved background is presented. Even if neglecting the internal structure of the spinning body already allows for many simplifications, this topic is rather involved and the literature about is quite vast (see [136] for a recent review). In the first section a self-contained review of the progress made in the last sixty years will be given, to be followed by the actual formalism we presented in [26]. After that, in the third section, the equations for a worldline deviation expansion are given, including also the spin, up to second order in the worldline deviation. This completes the mathematical framework needed for the application of the methods described in the previous chapter to spinning compact objects. An example of this is already given in the second section of this chapter, but an extended use of these methods to eccentric or ballistic orbits in Schwarzschild background, or in Kerr background, is beyond the scope of this thesis.

5.1 Spinning particles in General Relativity

Studying spinning objects in General Relativity one is confronted with a vast astrophysical phenomenology, ranging from rotating black holes to smaller compact bodies such as neutron stars and white dwarfs. Since the first developments of GR it was clear though [23, 24] that a lot of systems could be conveniently represented by the "spinning-particle model". When one of the moving bodies is significantly smaller than the other, for instance in an EMR binary coalescence, such that its influence on the motion of the other bodies can be neglected, it is called a test particle. A spin can be attached to this particle, so rotational degrees of freedom in the form of an antisymmetric tensor or a vector, making it a *spinning* test particle [137, 138]. Clearly this problem is directly connected to the dynamics of angular momentum in curved spacetime and has been deeply investigated since the early days of GR itself [139, 140, 135, 141, 142, 143].

Historically two approaches [144] have been considered for spinning particles. The first approach [23, 24, 142] builds on the energy-momentum tensor representative of the system, develops a multipole expansion out of it, and finally enforces the conservation law for the energy-momentum tensor $T^{\mu\nu}{}_{;\nu} = 0$. Writing down the covariant and divergence-free energy-momentum tensor of matter has the advantage to possibly account for effects due to the internal structure of the body, and the test-particle limit is reached considering $T^{\mu\nu}$ to be non-null in a sphere of diminishing radius surrounding the spinning particle [24]. In classical electrodynamics [98] one can construct a multipole expansion where the extended body is represented by a set of moments of its current density 4-vector j^{α}; likewise here the system gets represented by a set of "inertial" or "gravitational" moments of $T^{\mu\nu}$, building an expansion commonly referred to as "gravitational skeleton" [23]. In this skeleton the bones representing a spinning particle are the integrals up to the dipole term, in a first approximation. Treating the particle as a single pole accounts for its motion as a pointlike object, the next step is adding the spin, making it a pole-dipole particle [24]. The moments are defined with respect to a representative worldline of the body, namely a point is taken as representative of the whole body.

The second approach assigns directly an overall position, momentum, and spin to the

spinning body, considering it a pointlike object and neglecting any internal structure. Moving from here, an action principle, or a hamiltonian structure, is introduced and equations of motion are derived. This approach focusses on the interaction of the spin with the background and other external fields, leaving room for a semi-classical description of elementary particles as well [145, 146, 147, 148, 149, 28, 150, 151, 152, 153, 154, 155]. The formalism that is presented in this chapter (see the following section) belongs to this family of methods, in that we introduce the dynamical variables describing the spinning particle and the symplectic structure (hamiltonian and Poisson brackets) from which the equations of motion are derived.

Independently of the approach followed to derive them, the equations of motion for a spinning particle in curved background are known as the Mathisson-Papapetrou equations. In their most common form they read

$$\begin{aligned} \frac{DP^\mu}{D\tau} &= \frac{1}{2} R^\mu{}_{\nu\alpha\beta} U^\nu \Sigma^{\alpha\beta}, \\ \frac{D\Sigma^{\mu\nu}}{D\tau} &= P\mu U^\nu - P^\nu U^\nu, \end{aligned} \tag{5.1.1}$$

where P^μ is the total 4-momentum, $\Sigma^{\mu\nu}$ the antisymmetric spin and U^μ is the 4-velocity tangent to the reference worldline $x^\mu(\tau)$. Notice that the relation between 4-velocity and 4-momentum is not as simple as the usual relation, rather

$$P^\mu = MU^\mu + U_\nu \frac{D\Sigma^{\mu\nu}}{D\tau}, \tag{5.1.2}$$

with the extra quantity $U_\nu \frac{D\Sigma^{\mu\nu}}{D\tau}$ usually called "hidden" momentum [156, 136]. As one can easily count, there are extra degrees of freedom and the system of equations is underdetermined (4 unknowns from P^μ, 6 independent components of $\Sigma^{\mu\nu}$, 3 independent components from U^μ, for only 10 equations). Because of this, another condition is usually introduced, commonly referred to as "spin supplementary condition":

$$\Sigma^{\mu\nu} f_\nu = 0, \tag{5.1.3}$$

where f_ν is a timelike vector field defined along x^μ. The choice of the different f^ν gives rise to different supplementary conditions, among which the most common are:

- the Corinaldesi-Papapetrou condition [157] $f^\nu = u^\nu$, with u^ν corresponding to static observers, with zero 3-velocity in the coordinate frame;
- the Mathisson-Pirani condition [134], $f^\nu = U^\nu$, with U^ν corresponding to the 4-velocity of the spinning body;
- the Tulczyjew-Dixon condition [158, 159], $f^\nu = \frac{P^\nu}{m}$, corresponding to an observer in the zero 3-momentum frame.

Different conditions are usually chosen on physical grounds or for mathematical convenience. For a concise review of the different spin conditions (5.1.3) and their consequences, see [160, 161, 136].

Depending on the condition used the covariantly conserved quantities change. For a long time it has not been clear which choice is the most correct one, and several discussions have argued in favour or against particular choices [160], even claiming that some give birth to unphysical motions [25]. However all choices are physically equivalent and reduce to a gauge-fixing procedure [162]. As long as one is consistent within the same framework, one is able to describe the evolution of the spin and its influences on the body's trajectory. The different descriptions have to be physically equivalent.

The reasons for such a plethora of spin conditions lies in the choice of the worldline along which the spinning particle is taken to move. Every condition leads to one of many possible different worldlines, all contained in the minimal worldtube delimited by the worldlines defined for observers that move almost at light speed with respect to the body's rest frame [43, 161]. The presence of spin, in fact, ensures -already in flat spacetime- that the spinning body has a minimal size[2], such that it need not rotate with superluminal speed, recalling again the impossibility of pointlike particles in GR.

On the other hand, in works like [163, 164, 26], descriptions have been devised which avoid any supplementary condition, not introducing extra degrees of freedom, as it will be more clear in the next section. In these models the ambiguity of the worldline choice is shifted from the supplementary condition (5.1.3) to the definition itself of the representative location of the spinning particle. The motion of this point defines the worldline x^μ which is the reference for the multipole expansion in the gravitational skeleton or the position coordinate appearing in the hamiltonian. The equations of motion stemming from these approaches [165, 26] are consistent with the previously mentioned MP-equations (5.1.1), for they entail covariant conservation of the spin tensor $\frac{D\Sigma^{\mu\nu}}{D\tau} = 0$, simplifying considerably the relation between spin and momentum. Therefore the system is no longer underdetermined and there is no need for supplementary conditions.

Although these different approaches have been interpreted as competitive ones for a long time, they are, de facto, equivalent. In order to have an idea of the origin of such differences, one can consider what happens already with the most intuitive choice for a representative point of the spinning body, the center of mass. For instance, taking the CM as representative point means that the observer is comoving with it [161, 136], and the CM is measured in its own rest frame[3], which is nothing else but a result of imposing Pirani condition $\Sigma^{\mu\nu}U_\nu = 0$. However one should not forget that the CM is observer-dependent, Fig. 5.1 below clarifies.

The previous figure shows the intrinsic difficulty in defining a representative point for an extended body in GR. This is actually related to the major fact that there is no such thing as a "rigid body" in relativity, as the mutual distance between any two points of it is observer-dependent. Therefore any definition of the center of mass will depend on the observer's location; centers of mass defined with respect to various timelike observers are also called *centroids*. Angular momentum in a curved background, spins, and rotations clearly suffer from the same ambiguity, for their definitions revolve around an observer-

[2]The argument for the minimal size of a spinning body is worked out in [43], Exercise 5.6. The result is briefly $r_0 \geq \frac{s}{m}$, where $s = \sqrt{g_{\mu\nu}s^\mu s^\nu}$, with $s_\mu = -\frac{1}{2}\varepsilon_{\mu\nu\rho\sigma}U^\nu\Sigma^{\rho\sigma}$ the spin vector w.r.t. the frame with 4-velocity $U^\mu = \frac{p^\mu}{m}$, the 4-velocity of the Centre of Mass, and $m = \sqrt{-p_\sigma p^\sigma}$ its rest mass.

[3]The naturalness of this choice was advocated by Pirani himself [134].

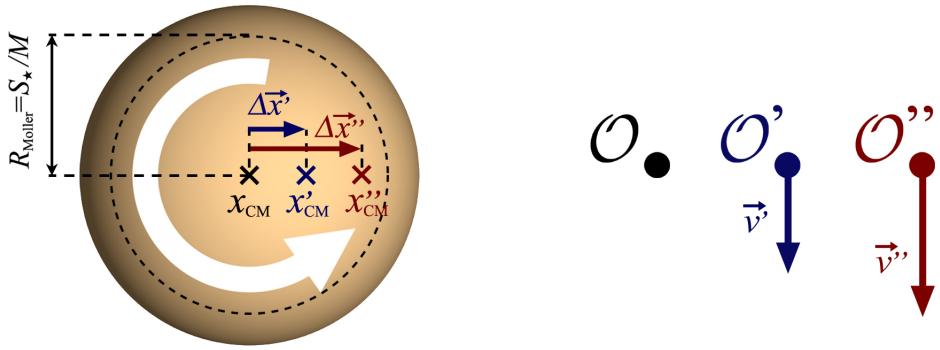

Figure 5.1: An uniform spinning body in flat spacetime, seen from above. The observer $\mathcal{O}$ is at rest w.r.t. the axis of rotation, therefore measures the CM in x_{CM}, coinciding with the geometrical centre of the body. Observers $\mathcal{O}'$ and $\mathcal{O}''$ instead are moving w.r.t. $\mathcal{O}$, opposite to the rotation of the body. The points on the right of the body are perceived as faster than those on the left, then more massive. Therefore the CM measured by these observers shifts to the right to x'_{CM} and x''_{CM} respectively. Figure credit to [136].

dependent reference point. Nevertheless the spin helps define [25, 166, 162] a "mass dipole moment" $(d^u_G)^\alpha$

$$(d^u_G)^\alpha \equiv -\Sigma^{\alpha\beta} f_\beta, \quad \text{and} \quad \Delta x^\alpha = -\frac{\Sigma^{\alpha\beta} f_\beta}{m}, \tag{5.1.4}$$

as measured by an observer of 4-velocity u^α. The vector Δx^α connected to it is instead the displacement of the CM position relative to the reference worldline x^μ. In fact choosing the CM reference frame means that the reference worldline is the one of the CM as measured by the observer [162], the displacement Δx^α is null, and one gets back to the condition $\Sigma^{\alpha\beta} u_\beta = 0$. Thus again it is shown how the choice of representative point, in this case the CM with respect to the observer, selects the condition (5.1.3) and/or the reference worldline x^μ. The mass dipole moment [136] represents an important vector clarifying the physical interpretation of the equations of motion (5.1.1).

Anyway, considering all possible observers, the corresponding centroids fill a circular disc with radius $R_{M\text{øller}} < \frac{|S|}{m}$, the ratio between the spin vector and the rest mass of the spinning body, which is the minimal size of a spinning body as well [161, 136]. In this way the worldlines of all possible centroids define the surface of the minimal worldtube containing all the worldlines x^μ along which the spinning test particle can move.

5.2 Effective hamiltonian formalism

There are various equivalent ways to describe a spinning particle in a curved background, as we have discussed in the previous section. Most of these approaches start from writing the equations of motion for a spinning test mass, to be complemented with supplementary conditions (5.1.3), in order to get rid of extra degrees of freedom and fix the relation between P^μ and U^μ. The internal structure of the body and its backreaction on the

background are completely neglected, since these are the necessary assumptions made at the beginning of the procedure leading to the equations of motion (5.1.1).

In this section we want to introduce a hamiltonian formalism which does not introduce extra degrees of freedom and which can suit different kinds of spinning compact objects, giving at the same time some account for their internal structure. By the end of this section it will be clear why this is, to all intents, an *effective* hamiltonian formalism. Some basic ideas underlying the formalism were formulated first in Khriplovich's paper [163] on the subject, and take into account a vast literature about hamiltonian models for spinning particles [146, 147, 148, 149, 28, 154], even in supersymmetric frameworks [150, 151, 152, 153].

Hamiltonian dynamical systems are specified by three sets of ingredients: the phase space, identifying the dynamical degrees of freedom, the Poisson-Dirac brackets defining a symplectic structure, and the hamiltonian generating the evolution of the system with given initial conditions by specifying a curve in the phase space passing through the initial point. The parametrization of phase space is not unique, as it is familiar from the Hamilton-Jacobi theory of dynamical systems [167]. Changes in the parametrization can be compensated by redefining the brackets and the hamiltonian.

A convenient starting point for models with gauge-field interactions is the use of covariant, i.e. kinetic, momenta rather than canonical momenta [4], in contrast to what was done in preceding works such as [154, 143]. As usual (5.1.1), the spin degrees of freedom are described by an antisymmetric tensor $\Sigma^{\mu\nu}$, which can be decomposed into two spacelike 4-vectors by introducing a timelike unit vector u: $u_\mu u^\mu = -1$, and defining

$$S^\mu = \frac{1}{2\sqrt{-g}}\,\varepsilon^{\mu\nu\kappa\lambda}\,u_\nu\Sigma_{\kappa\lambda}, \qquad Z^\mu = \Sigma^{\mu\nu}u_\nu. \tag{5.2.1}$$

By construction both four-vectors S and Z are spacelike:

$$S^\mu u_\mu = 0, \qquad Z^\mu u_\mu = 0. \tag{5.2.2}$$

In the following we take u to be the proper four-velocity of the particle. Then S is the Pauli-Lubanski pseudo-vector, from which a magnetic dipole moment can be constructed, whilst the components of Z, which will be referred to as the Pirani vector [134], can be used to define an electric or mass dipole moment [25, 136], as we have introduced in (5.1.4). In fact, the same spin tensor can be used for a description of the quantum spin of particles, in which case the vector S is the equivalent of the usual spin vector [169], or it can define the mass dipole moment. The last one is more interesting for our case, as it is related to the description of a classical spin particle (as opposed to a quantum one) and to the problem of defining the Centre of Mass of a rotating body in curved space. Refer back to the previous section for more extended account and references thereof.

One can also define [27] a third space-like vector

$$W^\mu = -\frac{1}{\sqrt{-g}}\,\varepsilon^{\mu\nu\kappa\lambda}u_\nu S_\kappa Z_\lambda = \left(\Sigma^{\mu\nu} - u^\mu Z^\nu\right) Z_\nu, \tag{5.2.3}$$

[4] See [168] and references cited therein for a general discussion, and [163] for the application to spinning particles.

orthogonal to the other ones:

$$W \cdot u = W \cdot S = W \cdot Z = 0. \tag{5.2.4}$$

Thus (u, S, Z, W) form a set of independent vectors, one time-like and three space-like, which can be used to define a frame of basis vectors carried along the particle world-line.

Observe that one can invert the relations (5.2.1) to write

$$\Sigma^{\mu\nu} = -\frac{1}{\sqrt{-g}}\,\varepsilon^{\mu\nu\kappa\lambda}\,u_\kappa S_\lambda + u^\mu Z^\nu - u^\nu Z^\mu. \tag{5.2.5}$$

Therefore, if the Pirani vector[5] vanishes: $Z = 0$, the full spin tensor can be reconstructed from S. However, in non-flat spacetime this is generally not the case. The spin vector S is maybe the easiest to visualize in terms of physical spin. Suppose one has a spinning neutron star or other compact object orbiting around a central black hole. Precession of the spin in the orbit, such as given by the Lense-Thirring effect, is the precession of the S vector, alignment of the spin is the parallelism between this vector and the orbital angular momentum, orthogonal to the plane of the orbit, in a dynamically conservative description of the system. Nevertheless here we deal first with more fundamental quantities, as all the degrees of freedom describing the rotation of the test particle are encapsulated in the spin tensor Σ.

The full set of phase space coordinates of a spinning particle thus consists of the position coordinate x^μ, the covariant momentum π_μ and the spin tensor $\Sigma^{\mu\nu}$. These are the dynamical variables required for the formalism we are introducing. Together with them come the anti-symmetric Dirac-Poisson brackets

$$\begin{aligned}
&\{x^\mu, \pi_\nu\} = \delta^\mu_\nu, \qquad \{\pi_\mu, \pi_\nu\} = \frac{1}{2}\,\Sigma^{\kappa\lambda} R_{\kappa\lambda\mu\nu}, \\
&\{\Sigma^{\mu\nu}, \pi_\lambda\} = \Gamma_{\lambda\kappa}{}^{\mu}\,\Sigma^{\nu\kappa} - \Gamma_{\lambda\kappa}{}^{\nu}\,\Sigma^{\mu\kappa}, \\
&\left\{\Sigma^{\mu\nu}, \Sigma^{\kappa\lambda}\right\} = g^{\mu\kappa}\Sigma^{\nu\lambda} - g^{\mu\lambda}\Sigma^{\nu\kappa} - g^{\nu\kappa}\Sigma^{\mu\lambda} + g^{\nu\lambda}\Sigma^{\mu\kappa}.
\end{aligned} \tag{5.2.6}$$

The brackets imply that π represents the generator of covariant translations, whilst the spin degrees of freedom Σ generate internal rotations and Lorentz transformations. It is straightforward to check that these brackets are closed in the sense that they satisfy the Jacobi identities for triple bracket expressions. Thus they define a consistent symplectic structure on the phase space. Other sets of brackets have been proposed [143] based on a larger set of degrees of freedom, some of which are subsequently removed by supplementary constraints. In this case there is no need for supplementary conditions (5.1.3) to be imposed, as there are no extra degrees of freedom to get rid of. However we like to add that the same set of equations of motion we obtain from the system (5.2.6) coincides with those obtained with the Ohashi-Kyrian-Semerák spin condition [170, 161], where the spin tensor is also covariantly constant and there is no hidden momentum (5.1.2), as we will shortly show.

[5] If $Z = 0$, then the well-known Pirani condition $\Sigma^{\mu\nu}u_\nu = 0$ is enforced, whence the name Pirani vector, which we first adopted in [26].

In order to get a well-defined dynamical system one needs to complete the phase-space structure with a hamiltonian generating the proper-time evolution of the system. In principle a large variety of covariant expressions can be constructed; however if we impose the additional condition that the particle interacts only gravitationally and that in the limit of vanishing spin the motion reduces to geodesic motion, the variety is reduced to hamiltonians

$$H = H_0 + H_\Sigma, \qquad H_0 = \frac{1}{2m}\, g^{\mu\nu}\pi_\mu\pi_\nu, \tag{5.2.7}$$

where $H_\Sigma = 0$ whenever $\Sigma^{\mu\nu} = 0$. By changing the hamiltonian it is possible to obtain different descriptions for different compact objects, possibly taking into account the internal structure of the rotating bodies. In that sense the hamiltonian is an *effective* hamiltonian, suitable to describe the motion of various types of objects in so far as the role of other internal degrees of freedom can be restricted to their effects on overall position, linear momentum and spin. An example of a non-trivial hamiltonian will be given in the next sections, now we focus on deriving the equations of motion.

Eqs. (5.2.6) and (5.2.7) specify a complete and consistent dynamical scheme for spinning particles. The simplest model is obtained by restricting the hamiltonian to the minimal geodesic term H_0. By itself this hamiltonian generates the following set of proper-time evolution equations,

$$\dot{x}^\mu = \{x^\mu, H_0\} \quad \Rightarrow \quad \pi_\mu = m g_{\mu\nu}\dot{x}^\nu, \tag{5.2.8}$$

stating that the covariant momentum π is a vector tangent to the world line, proportional to the proper 4-velocity $u = \dot{x}$. This is quite different from situations where extra quantities such as the hidden momentum appear (5.1.2) and the equations of motion are not sufficient to determine the motion. However in this case no extra supplementary condition is required. Next to (5.2.8) one has

$$\dot{\pi}_\mu = \{\pi_\mu, H_0\} \quad \Rightarrow \quad D_\tau\pi_\mu \equiv \dot{\pi}_\mu - \dot{x}^\lambda \Gamma_{\lambda\mu}{}^\nu \pi_\nu = \frac{1}{2m}\, \Sigma^{\kappa\lambda} R_{\kappa\lambda\mu}{}^\nu\, \pi_\nu, \tag{5.2.9}$$

which specifies how the worldline curves in terms of the evolution of its tangent vector. Finally the rate of change of the spin tensor is

$$\dot{\Sigma}^{\mu\nu} = \{\Sigma^{\mu\nu}, H_0\} \quad \Rightarrow \quad D_\tau\Sigma^{\mu\nu} \equiv \dot{\Sigma}^{\mu\nu} + \dot{x}^\lambda \Gamma_{\lambda\kappa}{}^\mu \Sigma^{\kappa\nu} + \dot{x}^\lambda \Gamma_{\lambda\kappa}{}^\nu \Sigma^{\mu\kappa} = 0. \tag{5.2.10}$$

In these equations the overdot denotes an ordinary derivative w.r.t. proper time τ, whereas D_τ denotes the pull-back of the covariant derivative along the world line $x^\mu(\tau)$. By substitution of Eq. (5.2.8) into Eq. (5.2.9) one finds that

$$D_\tau^2 x^\mu = \ddot{x}^\mu + \Gamma_{\lambda\nu}{}^\mu \dot{x}^\lambda \dot{x}^\nu = \frac{1}{2m}\, \Sigma^{\kappa\lambda} R^\mu{}_{\nu\kappa\lambda}\dot{x}^\nu, \tag{5.2.11}$$

which reduces to the geodesic equation in the limit $\Sigma = 0$. The worldline is the solution of the combined equations (5.2.11) and (5.2.10) satisfying some given initial conditions.

This worldline is a curve in spacetime along which the spin tensor is covariantly constant. It has been remarked by many authors [163, 171, 165, 156] that the spin-dependent force (5.2.9) exerted by the spacetime curvature on the particle is similar to the Lorentz force with spin replacing the electric charge and curvature replacing the electromagnetic field strength[6]. In this analogy the covariant conservation of spin along the worldline is the natural equivalent of the conservation of charge.

Even though the spin tensor is covariantly constant, this does not hold for the Pauli-Lubanski and Pirani vectors S and Z individually. Indeed, due to the gravitational Lorentz force

$$\begin{aligned} D_\tau S^\mu &= \frac{1}{4m\sqrt{-g}}\,\varepsilon^{\mu\nu\kappa\lambda}\Sigma_{\kappa\lambda}\Sigma^{\alpha\beta}R_{\alpha\beta\nu\rho}u^\rho, \\ D_\tau Z^\mu &= \frac{1}{2m}\,\Sigma^{\mu\nu}\Sigma^{\alpha\beta}R_{\alpha\beta\nu\rho}u^\rho, \end{aligned} \tag{5.2.12}$$

where $\Sigma^{\mu\nu}$ is the linear expression in terms of S^μ and Z^μ given in eq. (5.2.5). The rate of change of both spin vectors is of order $\mathcal{O}[\Sigma^2]$. In particular, as Z is not conserved in non-flat spacetimes the condition $Z=0$ cannot be imposed during the complete motion in general. Indeed, the evolution of the system is completely determined by eqs. (5.2.8), (5.2.9), (5.2.10), and leaves no room for additional constraints.

In fact, any condition of the form (5.1.3), like $\Sigma^{\mu\nu}v_\nu = 0$, with v^ν a linear combination of the existing relevant vectors and objects, such as $\Sigma^{\mu\nu}, Z^\mu, \dot{x}^\mu$, would either lead at all times to $v^\nu = 0$ or to a contradiction with the equations of motion (5.2.9),(5.2.10). In fact, suppose that such a vector $v_\mu = \alpha S_\mu + \beta Z_\mu + \gamma\dot{x}_\mu$ exists, with α, β, γ numeric coefficients. Then the covariant derivative of a supplementary condition on v^μ like $\Sigma^{\mu\nu}v_\nu = 0$ would give, by virtue of (5.2.10),

$$\Sigma^{\mu\nu}\frac{Dv_\nu}{D\tau} = 0.$$

From here $\frac{Dv_\mu}{D\tau} = \lambda v_\mu$, with $\lambda \in \mathbb{C}$. We can write down the covariant derivative using Eqs.(5.2.9),(5.2.12) and obtain

$$\begin{aligned} \frac{Dv_\mu}{D\tau} =& \frac{1}{2m}\Sigma^{\alpha\beta}R_{\alpha\beta}{}^{\nu}{}_{\rho}\dot{x}^\rho\left(\frac{\alpha}{2\sqrt{-g}}\varepsilon_{\mu\nu\kappa\lambda}\Sigma^{\kappa\lambda} + \beta\Sigma_{\mu\nu} + \gamma g_{\mu\nu}\right) = \lambda v_\mu \\ &\Rightarrow \frac{1}{2m}\Sigma^{\alpha\beta}R_{\alpha\beta}{}^{\nu}{}_{\rho}\dot{x}^\rho = \lambda\dot{x}^\nu. \end{aligned}$$

Contracting then both members with $\dot{x}_\nu$ it is clear that $\lambda = 0$, because of the anti-symmetry of the Riemann tensor and the normalization condition $\dot{x}_\nu\dot{x}^\nu = -1$ on velocity. Therefore one is left with $\frac{Dv_\mu}{D\tau} = 0$. This leads only to

$$\frac{\alpha}{2\sqrt{-g}}\varepsilon_{\mu\nu\kappa\lambda}\Sigma^{\kappa\lambda} + \beta\Sigma_{\mu\nu} + \gamma g_{\mu\nu} = 0,$$

which can be fulfilled only by $\gamma = 0$ and $\beta Z^\mu = -\alpha S^\mu$. In this way, by its own definition, $v_\mu = 0$ and the whole procedure of introducing such a vector becomes futile, as we advocated.

[6] This is among the basic analogies giving rise to gravitomagnetism phenomena, for an extensive review see [156].

The Pirani vector, which is intimately connected to the mass dipole of the system (5.1.4), indicates the difference between the worldline consistently defined through the hamiltonian system (5.2.6),(5.2.7) and other worldlines defined through different set-ups. In order to show the physical equivalence of the worldline (5.2.8), and the motions described by it, with other worldline, it is necessary to take into account the time-evolution of the Z vector as well. Therefore in our formalism Z^μ is a dynamical variable as necessary for describing the motion as the spin vector S^μ.

5.2.1 Conservation laws

From this formalism one is able to deduce conservation laws. These depend on the specific hamiltonian chosen; here we first give the ones for the minimal hamiltonian, then in the last part of this section we will show what happens adding a non-trivial term to (5.2.7). By construction the time-independent hamiltonian represented by (5.2.7) is a constant of motion for the spinning body, irrespective of the specific geometry of the spacetime manifold. In particular for the minimal geodesic hamiltonian H_0 we have

$$H_0 = -\frac{m}{2}. \tag{5.2.13}$$

Another obvious constant of motion is the total spin, just as it happens in any other equivalent description for spinning bodies in curved backgrounds, as mentioned in the previous section,

$$I = \frac{1}{2}\, g_{\kappa\mu} g_{\lambda\nu} \Sigma^{\kappa\lambda} \Sigma^{\mu\nu} = S_\mu S^\mu + Z_\mu Z^\mu. \tag{5.2.14}$$

Another conserved quantity is the pseudo-scalar product [27]

$$D = \frac{1}{8}\, \sqrt{-g}\, \varepsilon_{\mu\nu\kappa\lambda} \Sigma^{\mu\nu} \Sigma^{\kappa\lambda} = S \cdot Z. \tag{5.2.15}$$

In addition, there exist conserved quantities $J(x, \pi, \Sigma)$ resulting from symmetries of the background geometry, as implied by Noether's theorem [142, 160, 172]. They are solutions of the generic equation

$$\{J, H_0\} = \frac{1}{m}\, g^{\mu\nu} \pi_\nu \left[\frac{\partial J}{\partial x^\mu} + \Gamma_{\mu\lambda}{}^{\kappa}\, \pi_\kappa \frac{\partial J}{\partial \pi_\lambda} + \frac{1}{2}\, \Sigma^{\alpha\beta} R_{\alpha\beta\lambda\mu} \frac{\partial J}{\partial \pi_\lambda} + \Gamma_{\mu\alpha}{}^{\kappa}\, \Sigma^{\lambda\alpha} \frac{\partial J}{\partial \Sigma^{\kappa\lambda}} \right] = 0. \tag{5.2.16}$$

It follows that any constants of motion linear in momentum [172] are of the form

$$J = \alpha^\mu \pi_\mu + \frac{1}{2}\, \beta_{\mu\nu}\, \Sigma^{\mu\nu}, \tag{5.2.17}$$

with

$$\nabla_\mu \alpha_\nu + \nabla_\nu \alpha_\mu = 0, \qquad \nabla_\lambda \beta_{\mu\nu} = R_{\mu\nu\lambda}{}^{\kappa} \alpha_\kappa. \tag{5.2.18}$$

These equations imply that α is a Killing vector on the spacetime, and β is its antisymmetrized gradient:

$$\beta_{\mu\nu} = \frac{1}{2} \left(\nabla_\mu \alpha_\nu - \nabla_\nu \alpha_\mu \right). \tag{5.2.19}$$

Similarly constants of motion quadratic in momentum [173] are of the form

$$J = \frac{1}{2}\,\alpha^{\mu\nu}\pi_\mu\pi_\nu + \frac{1}{2}\beta_{\mu\nu}{}^{\lambda}\,\Sigma^{\mu\nu}\pi_\lambda + \frac{1}{8}\,\gamma_{\mu\nu\kappa\lambda}\Sigma^{\mu\nu}\Sigma^{\kappa\lambda}, \tag{5.2.20}$$

where the coefficients have to satisfy the ordinary partial differential equations

$$\begin{aligned}
&\nabla_\lambda\alpha_{\mu\nu} + \nabla_\mu\alpha_{\nu\lambda} + \nabla_\nu\alpha_{\lambda\mu} = 0,\\
&\nabla_\mu\beta_{\kappa\lambda\nu} + \nabla_\nu\beta_{\kappa\lambda\mu} = R_{\kappa\lambda\mu}{}^{\rho}\alpha_{\nu\rho} + R_{\kappa\lambda\nu}{}^{\rho}\alpha_{\mu\rho},\\
&\nabla_\rho\gamma_{\mu\nu\kappa\lambda} = R_{\mu\nu\rho}{}^{\sigma}\beta_{\kappa\lambda\sigma} + R_{\kappa\lambda\rho}{}^{\sigma}\beta_{\mu\nu\sigma}.
\end{aligned} \tag{5.2.21}$$

Thus α is a symmetric rank-two Killing tensor, and the coefficients (β,γ) satisfy a hierarchy of inhomogeneous Killing-like equations determined by the $\alpha_{\mu\nu}$. In the case of Grassmann-valued spin tensors $\Sigma^{\mu\nu} = i\psi^\mu\psi^\nu$ the coefficient γ is completely antisymmetric and the equations are known to have a solution in terms of Killing-Yano tensors [174].

In fact, one can infer more about the solutions of Eq.(5.2.21), namely α is a Killing tensor and as such it can be written in terms of antisymmetric Killing-Yano tensors $F_{\mu\nu} = -F_{\nu\mu}$, satisfying a Killing-like equation

$$\nabla_\mu F_{\nu\lambda} + \nabla_\nu F_{\mu\lambda} = 0, \tag{5.2.22}$$

and precisely $\alpha_{\mu\nu} = F_{\mu\lambda}F_\nu{}^{\lambda}$ satisfies (5.2.21). Killing-Yano tensors have the property that

$$\nabla_\kappa\nabla_\lambda F_{\mu\nu} = R_{\mu\nu\kappa}{}^{\alpha}F_{\alpha\lambda} + \frac{1}{2}R_{\kappa\mu\lambda}{}^{\alpha}F_{\alpha\nu} - \frac{1}{2}R_{\kappa\nu\lambda}{}^{\alpha}F_{\alpha\mu} - \frac{1}{2}R_{\mu\nu\lambda}{}^{\alpha}F_{\alpha\kappa}, \tag{5.2.23}$$

and using this relation one can find the expression for the tensor β after some straightforward calculations,

$$\beta_{\kappa\lambda}{}^{\mu} = F^{\mu\nu}\nabla_\nu F_{\kappa\lambda} + \frac{1}{2}\left(F_\kappa{}^{\nu}\nabla_\nu F_\lambda{}^{\mu} - F_\lambda{}^{\nu}\nabla_\nu F_\kappa{}^{\mu}\right). \tag{5.2.24}$$

Instead the most complete Ansatz form for $\gamma_{\mu\nu\kappa\lambda}$ can also be written in terms of the Killing-Yano tensor as:

$$\begin{aligned}
4\gamma_{\mu\nu\kappa\lambda} = \;& 4c\nabla^\rho F_{\mu\nu}\nabla_\rho F_{\kappa\lambda} + 2d\left(\nabla^\rho F_{\mu\kappa}\nabla_\rho F_{\nu\lambda} - \nabla^\rho F_{\mu\lambda}\nabla_\rho F_{\nu\kappa}\right)\\
&+ 2e\left(R_{\mu\nu\rho\sigma}F^\rho{}_\kappa F^\sigma{}_\lambda + R_{\kappa\lambda\rho\sigma}F^\rho{}_\mu F^\sigma{}_\nu\right) + 2f\left(R_{\mu\nu\rho\sigma}F^{\rho\sigma}F_{\kappa\lambda} + R_{\kappa\lambda\rho\sigma}F^{\rho\sigma}F_{\mu\nu}\right)\\
&+ g\left(R_{\mu\rho\kappa\sigma}F^\rho{}_\nu F^\sigma{}_\lambda - R_{\mu\rho\lambda\sigma}F^\rho{}_\nu F^\sigma{}_\kappa - R_{\nu\rho\kappa\sigma}F^\rho{}_\mu F^\sigma{}_\lambda + R_{\nu\rho\lambda\sigma}F^\rho{}_\mu F^\sigma{}_\kappa\right)\\
&+ h\left(R_{\mu\rho\kappa\sigma}F^{\rho\sigma}F_{\nu\lambda} - R_{\mu\rho\lambda\sigma}F^{\rho\sigma}F_{\nu\kappa} - R_{\nu\rho\kappa\sigma}F^{\rho\sigma}F_{\mu\lambda} + R_{\nu\rho\lambda\sigma}F^{\rho\sigma}F_{\mu\kappa}\right)\\
&+ m\left(R_{\mu\rho\kappa\sigma}F^\rho{}_\lambda F^\sigma{}_\nu - R_{\mu\rho\lambda\sigma}F^\rho{}_\kappa F^\sigma{}_\nu - R_{\nu\rho\kappa\sigma}F^\rho{}_\lambda F^\sigma{}_\mu + R_{\nu\rho\lambda\sigma}F^\rho{}_\kappa F^\sigma{}_\mu\right)\\
&+ p\left(R_{\mu\nu\kappa\rho}F^\rho{}_\sigma F^\sigma{}_\lambda - R_{\mu\nu\lambda\rho}F^\rho{}_\sigma F^\sigma{}_\kappa + R_{\kappa\lambda\mu\rho}F^\rho{}_\sigma F^\sigma{}_\nu - R_{\kappa\lambda\nu\rho}F^\rho{}_\sigma F^\sigma{}_\mu\right).
\end{aligned} \tag{5.2.25}$$

From the third equation in (5.2.21) one can consider the trace parts, namely

$$\begin{aligned}
4\nabla\gamma_{\kappa\rho\lambda}{}^{\rho} = \;& R_{\mu\nu\kappa}{}^{\rho}\left(2F^{\nu\sigma}\nabla_\sigma F_{\rho\lambda} + F_\lambda{}^{\sigma}\nabla_\sigma F_\rho{}^{\nu} - F_\rho{}^{\sigma}\nabla_\sigma F_\lambda{}^{\nu}\right)\\
&+ R_{\mu\nu\lambda}{}^{\rho}\left(2F^{\nu\sigma}\nabla_\sigma F_{\rho\kappa} + F_\kappa{}^{\sigma}\nabla_\sigma F_\rho{}^{\nu} - F_\rho{}^{\sigma}\nabla_\sigma F_\kappa{}^{\nu}\right),
\end{aligned} \tag{5.2.26}$$

and

$$\nabla_\mu \gamma_{\kappa\lambda}{}^{\kappa\lambda} = R_{\mu\nu\kappa\lambda}\left(F^{\nu\sigma}\nabla_\sigma F^{\kappa\lambda} + F^{\kappa\sigma}\nabla_\sigma F^{\lambda\nu}\right). \tag{5.2.27}$$

By using Bianchi and Ricci identities, and anti-symmetrization of the property (5.2.23) one obtains that

(5.2.28)

$$R_{\mu\nu\kappa\lambda}\left(F^{\nu\sigma}\nabla_\sigma F^{\kappa\lambda} + F^{\kappa\sigma}\nabla_\sigma F^{\lambda\nu}\right) = \frac{1}{4}\nabla_\mu\left(R_{\kappa\lambda\nu\sigma}F^{\nu\sigma}F^{\kappa\lambda}\right) \Rightarrow \gamma_{\kappa\lambda}{}^{\kappa\lambda} = \frac{1}{4}R_{\kappa\lambda\mu\nu}F^{\kappa\lambda}F^{\mu\nu},$$

valid for spacetimes with vanishing Ricci tensor, such as Schwarzschild or Kerr metric. Moreover, considering the complete antisymmetrization of the equation for γ in (5.2.21), one can show that

$$\varepsilon^{\mu\nu\kappa\lambda}\gamma_{\mu\nu\kappa\lambda} = \varepsilon^{\mu\nu\kappa\lambda}\left(\frac{1}{2}R_{\mu\nu\rho\sigma}F^\rho{}_\kappa F^\sigma{}_\lambda + \nabla^\rho F_{\mu\nu}\nabla_\rho F_{\kappa\lambda}\right), \tag{5.2.29}$$

and this together with (5.2.28) constrains the coefficients in the general Ansatz (5.2.25) to obey the following relations:

$$m = 1 + g - 2e, \qquad h = 2f, \qquad 2e + 2f - g = 1. \tag{5.2.30}$$

It follows that the general solution for γ can be further constrained to be as

$$\gamma_{\mu\nu\kappa\lambda} = A_{\mu\nu\kappa\lambda} + \frac{e}{2}B_{\mu\nu\kappa\lambda} + \frac{f}{2}C_{\mu\nu\kappa\lambda}, \tag{5.2.31}$$

with

(5.2.32)

$$\begin{aligned}
A_{\mu\nu\kappa\lambda} = \;& c\nabla^\rho F_{\mu\nu}\nabla_\rho F_{\kappa\lambda} + \frac{d}{2}\left(\nabla^\rho F_{\mu\kappa}\nabla_\rho F_{\nu\lambda} - \nabla^\rho F_{\mu\lambda}\nabla_\rho F_{\nu\kappa}\right) \\
& - \frac{1}{4}\left(R_{\mu\rho\kappa\sigma}F^\rho{}_\nu F^\sigma{}_\lambda - R_{\mu\rho\lambda\sigma}F^\rho{}_\nu F^\sigma{}_\kappa - R_{\nu\rho\kappa\sigma}F^\rho{}_\mu F^\sigma{}_\lambda + R_{\nu\rho\lambda\sigma}F^\rho{}_\mu F^\sigma{}_\kappa\right), \\
B_{\mu\nu\kappa\lambda} = \;& R_{\mu\nu\rho\sigma}F^\rho{}_\kappa F^\sigma{}_\lambda + R_{\kappa\lambda\rho\sigma}F^\rho{}_\mu F^\sigma{}_\nu \\
& + R_{\mu\rho\kappa\sigma}F^\rho{}_\nu F^\sigma{}_\lambda - R_{\mu\rho\lambda\sigma}F^\rho{}_\nu F^\sigma{}_\kappa - R_{\nu\rho\kappa\sigma}F^\rho{}_\mu F^\sigma{}_\lambda + R_{\nu\rho\lambda\sigma}F^\rho{}_\mu F^\sigma{}_\kappa, \\
C_{\mu\nu\kappa\lambda} = \;& R_{\mu\nu\rho\sigma}F^{\rho\sigma}F_{\kappa\lambda} + R_{\kappa\lambda\rho\sigma}F^{\rho\sigma}F_{\mu\nu} \\
& + R_{\mu\rho\kappa\sigma}F^{\rho\sigma}F_{\nu\lambda} - R_{\mu\rho\lambda\sigma}F^{\rho\sigma}F_{\nu\kappa} - R_{\nu\rho\kappa\sigma}F^{\rho\sigma}F_{\mu\lambda} + R_{\nu\rho\lambda\sigma}F^{\rho\sigma}F_{\mu\kappa} \\
& + R_{\mu\rho\kappa\sigma}F^\rho{}_\nu F^\sigma{}_\lambda - R_{\mu\rho\lambda\sigma}F^\rho{}_\nu F^\sigma{}_\kappa - R_{\nu\rho\kappa\sigma}F^\rho{}_\mu F^\sigma{}_\lambda + R_{\nu\rho\lambda\sigma}F^\rho{}_\mu F^\sigma{}_\kappa \\
& + R_{\mu\rho\kappa\sigma}F^\rho{}_\lambda F^\sigma{}_\nu - R_{\mu\rho\lambda\sigma}F^\rho{}_\kappa F^\sigma{}_\nu - R_{\nu\rho\kappa\sigma}F^\rho{}_\lambda F^\sigma{}_\mu + R_{\nu\rho\lambda\sigma}F^\rho{}_\kappa F^\sigma{}_\mu,
\end{aligned}$$

and c, d, e, f still to be determined, depending on the background spacetime.

The constants of motion (5.2.17) linear in momentum are special in that they define a Lie algebra: if J and J' are two such constants of motion, then their bracket is a constant of motion of the same type. This follows from the Jacobi identity

$$\{\{J, J'\}, H_0\} = \{\{J, H_0\}, J'\} - \{\{J', H_0\}, J\} = 0. \tag{5.2.33}$$

Thus, if $\{e_i\}_{i=1}^r$ is a complete basis for Killing vectors

$$\alpha^\mu = \alpha^i e_i^\mu, \qquad e_j^\nu \nabla_\nu e_i^\mu - e_i^\nu \nabla_\nu e_j^\mu = f_{ij}{}^k e_k^\mu,$$

the constants of motion define a representation of the same algebra:

$$J_i = e_i^\mu \pi_\mu + \frac{1}{2} \nabla_\mu e_{i\nu} \Sigma^{\mu\nu} \quad \Rightarrow \quad \{J_i, J_j\} = f_{ij}{}^k J_k. \tag{5.2.34}$$

Such constants of motion are helpful in the analysis of spinning particle dynamics [160, 175, 176].

5.2.2 Application to EMR Schwarzschild Black Hole

The dynamics of spinning bodies can be illustrated by the motion in a static and spherically symmetric Schwarzschild spacetime, for which the hamiltonian H_0 in Droste coordinates is given by

$$2mH_0 = -\frac{1}{1-\frac{2M}{r}} \pi_t^2 + \left(1 - \frac{2M}{r}\right) \pi_r^2 + r^2 \pi_\theta^2 + r^2 \sin^2\theta \, \pi_\varphi^2. \tag{5.2.35}$$

Schwarzschild spacetime admits four Killing vectors, for time-translations and rotations. They give rise to the conservation of kinetic energy

$$-E = \pi_t + \frac{M}{r^2} \Sigma^{tr}, \tag{5.2.36}$$

and angular momentum

$$\begin{aligned} J_1 &= -\sin\varphi \, \pi_\theta - \operatorname{cotan}\theta \cos\varphi \, \pi_\varphi \\ &\quad -r \sin\varphi \, \Sigma^{r\theta} - r \sin\theta \cos\theta \cos\varphi \, \Sigma^{r\varphi} + r^2 \sin^2\theta \cos\varphi \, \Sigma^{\theta\varphi}, \\ J_2 &= \cos\varphi \, \pi_\theta - \operatorname{cotan}\theta \sin\varphi \, \pi_\varphi \\ &\quad +r \cos\varphi \, \Sigma^{r\theta} - r \sin\theta \cos\theta \sin\varphi \, \Sigma^{r\varphi} + r^2 \sin^2\theta \sin\varphi \, \Sigma^{\theta\varphi}, \\ J_3 &= \pi_\varphi + r \sin^2\theta \, \Sigma^{r\varphi} + r^2 \sin\theta \cos\theta \, \Sigma^{\theta\varphi}. \end{aligned} \tag{5.2.37}$$

It is straightforward to check that these satisfy the usual algebra of time-translations and spatial rotations:

$$\{E, J_i\} = 0, \qquad \{J_i, J_j\} = \varepsilon_{ijk} J_k. \tag{5.2.38}$$

As usual, the conservation of total angular momentum and the spherical symmetry of the spacetime geometry allow one to take the angular momentum $\mathbf{J}$ as the direction of the z-axis, such that

$$\mathbf{J} = (0, 0, J). \tag{5.2.39}$$

For spinless particles, for which the angular momentum is strictly orbital, this implies that the orbital motion is in a plane perpendicular to the angular momentum 3-vector; with our choice of the z-axis this is the equatorial plane $\theta = \pi/2$.

In the presence of spin the result no longer holds in general, as the precession of spin can be compensated by precession of the orbital angular momentum, resulting in a non-planar orbit [177]. However, one can ask under which conditions planar motion is still possible. As in that case the directions of orbital and spin angular momentum are separately preserved, it means that necessary conditions for motion in the equatorial plane are

$$J_1 = J_2 = 0, \qquad \pi_\theta = 0, \tag{5.2.40}$$

and therefore also

$$\Sigma^{r\theta} = \Sigma^{\theta\varphi} = 0. \tag{5.2.41}$$

Furthermore the absence of acceleration perpendicular to the equatorial plane expressed by $D_\tau \pi_\theta = 0$ implies that

$$\Sigma^{t\theta} = 0. \tag{5.2.42}$$

Thus planar motion requires alignment of the spin with the orbital angular momentum; it is straighforward to show that the reverse statement also holds [178]. Aligned spin does not precess, a statement confirmed even by more intuitive models [179] and by astrophysical observations as well.

From the definition (5.2.15) it follows that such orbits satisfy the conservation law

$$D = S \cdot Z = 0, \tag{5.2.43}$$

while, in terms of the four-velocity components, one is now left with relevant constants of motion

$$E = m\left(1 - \frac{2M}{r}\right) u^t - \frac{M}{r^2}\,\Sigma^{tr}, \tag{5.2.44}$$

and

$$J = mr^2 u^\varphi + r\Sigma^{r\varphi}, \tag{5.2.45}$$

in addition to the hamiltonian constraint

$$\left(1 - \frac{2M}{r}\right) u^{t\,2} = 1 + \frac{u^{r\,2}}{1 - \frac{2M}{r}} + r^2 u^{\varphi\,2}, \tag{5.2.46}$$

and the conservation of total spin I, or equivalently:

$$\Sigma^{t\varphi\,2} = -\frac{1}{r^2}\frac{I + \Sigma^{tr\,2}}{1 - \frac{2M}{r}} + \frac{\Sigma^{r\varphi\,2}}{\left(1 - \frac{2M}{r}\right)^2}. \tag{5.2.47}$$

These equations show that all the non-vanishing spin components can be calculated from Eqs. (5.2.44), (5.2.45) and (5.2.47), once the orbital velocities are known.

The simplest type of planar orbit is the circular orbit $r = R =$ constant, $u^r = 0$. In this case the symmetry of the orbit implies that (u^t, u^φ) are constant in time, and that $\Sigma^{t\varphi} = 0$. This can be shown as follows. First, absence of radial acceleration $D_\tau u^r = 0$ gives, upon using the conservation laws for E and J,

(5.2.48)
$$\left(1-\frac{2M}{R}\right)\left(2-\frac{3M}{R}\right)mu^{t\,2} - \left(1-\frac{3M}{R}\right)mR^2u^{\varphi\,2} = 2E\left(1-\frac{2M}{R}\right)u^t + \frac{JM}{R}\,u^\varphi,$$

whilst the hamiltonian constraint (5.2.46) simplifies to

$$\left(1-\frac{2M}{R}\right)u^{t\,2} = 1 + R^2u^{\varphi\,2}. \tag{5.2.49}$$

These two equations can be solved for u^t and u^φ in terms of (R, E, J), implying that they are constant. An immediate consequence is that Σ^{tr}, $\Sigma^{r\varphi}$ and $\Sigma^{t\varphi}$ are constant as well, and actually $\Sigma^{t\varphi}$ vanishes. This follows directly from the absence of four-acceleration:

$$\frac{du^t}{d\tau} = \frac{M}{mR}\,u^\varphi\Sigma^{t\varphi} = 0, \qquad \frac{du^\varphi}{d\tau} = \frac{M}{mR^3}\left(1-\frac{2M}{R}\right)u^t\Sigma^{t\varphi} = 0. \tag{5.2.50}$$

Then also the rate of change of $\Sigma^{t\varphi}$ must vanish

(5.2.51)
$$-\frac{M}{R}\left(1-\frac{2M}{R}\right)\frac{d\Sigma^{t\varphi}}{d\tau} = \left(1-\frac{M}{R}\right)\left(1-\frac{3M}{R}\right)mu^tu^\varphi + \frac{JM^2}{R^4}\,u^t - E\left(1-\frac{2M}{R}\right)u^\varphi = 0.$$

Now from Eqs. (5.2.48) and (5.2.49) it follows that

$$\frac{2E}{m}\left(1-\frac{2M}{R}\right)u^t = 2 - \frac{3M}{R} - \frac{JM}{mR}\,u^\varphi + R^2u^{\varphi\,2}. \tag{5.2.52}$$

These equations then allow the elimination of E and u^t, with the result that

$$\frac{JM}{mR^2}\left(\frac{2M}{R} + R^2u^{\varphi\,2}\right) = Ru^\varphi\left[\frac{M}{R} - \left(1-\frac{6M}{R}+\frac{6M^2}{R^2}\right)R^2u^{\varphi\,2}\right]. \tag{5.2.53}$$

As for the total spin, for circular orbits the expression (5.2.47) can be written as

(5.2.54)
$$\begin{aligned} I &= -\Sigma^{tr\,2} + \frac{R^2\Sigma^{r\varphi\,2}}{1-\frac{2M}{R}} \\ &= -\frac{R^4}{M^2}\left[\left(1-\frac{2M}{R}\right)mu^t - E\right]^2 + \frac{1}{\left(1-\frac{2M}{R}\right)^2}\left[J - mR^2u^\varphi\right]^2. \end{aligned}$$

Thus for circular orbits u^φ and u^t are constants which can be expressed in terms of R and J, in turn fixing E and I as well. Solving the relation (5.2.52) gives the modified third Kepler law in the presence of spin. Notice that the spinless case $\Sigma^{\mu\nu} = 0$ gives back the usual Kepler "law of harmonies" for a circular orbit [180]. Suppose in fact that $\Sigma^{\mu\nu} = 0$, then solving together (5.2.49),(5.2.52) for the velocities, one gets

$$u^{\varphi\,2} = \frac{M}{R^3}\frac{1}{1-\frac{3M}{R}} \qquad u^{t\,2} = \frac{1}{1-\frac{3M}{R}}, \tag{5.2.55}$$

and therefore

$$\left(\frac{u^t}{u^\varphi}\right)^2 = \left(\frac{dt}{d\varphi}\right)^2 = \frac{T^2}{4\pi^2} = \frac{R^3}{M}, \tag{5.2.56}$$

that is third Kepler's law for a circular orbit [180, 181].

5.2.3 Application to a non-minimal hamiltonian

So far we focussed on the dynamics generated by the minimal hamiltonian H_0 (5.2.7). However, the purpose of the formalism introduced with (5.2.6) is to build a mathematically consistent description for a spinning test-particle in a curved background. On one side changing the metric $g_{\mu\nu}$ one is able to consider different spacetimes, and we have shown an example of the simple situation of circular orbits in Schwarzschild spacetime. On the other side changing the hamiltonian one is able to describe different types of compact objects in the same background. A gravitational analogue of the Stern-Gerlach force is described by the hamiltonian

$$H_\Sigma = \frac{\kappa}{4} R_{\mu\nu\kappa\lambda}\Sigma^{\mu\nu}\Sigma^{\kappa\lambda}, \tag{5.2.57}$$

including the spin-spin interaction via spacetime curvature. This force has been investigated by Khriplovich [149]. The choice of hamiltonians can be enlarged further by including charges coupling the particle to vector fields like the electromagnetic field [163, 169].

It is straightforward to derive the equations of motion:

$$\begin{aligned}
\dot{x}^\mu = \{x^\mu, H\} \quad &\Rightarrow \quad \pi_\mu = m g_{\mu\nu}\dot{x}^\nu, \\
\dot{\pi}_\mu = \{\pi_\mu, H\} \quad &\Rightarrow \quad D_\tau \pi_\mu = \frac{1}{2m}\Sigma^{\kappa\lambda} R_{\kappa\lambda\mu}{}^{\nu}\pi_\nu - \frac{\kappa}{4}\Sigma^{\kappa\lambda}\Sigma^{\rho\sigma}\nabla_\mu R_{\kappa\lambda\rho\sigma}, \\
\dot{\Sigma}^{\mu\nu} = \{\Sigma^{\mu\nu}, H\} \quad &\Rightarrow \quad D_\tau \Sigma^{\mu\nu} = \kappa\Sigma^{\kappa\lambda}\left(R_{\kappa\lambda}{}^{\mu}{}_{\sigma}\Sigma^{\nu\sigma} - R_{\kappa\lambda}{}^{\nu}{}_{\sigma}\Sigma^{\mu\sigma}\right).
\end{aligned} \tag{5.2.58}$$

Comparing again with the electromagnetic force, the middle equation manifestly describes a gravitational Lorentz force and a gravitational Stern-Gerlach force, coupling spin to the gradient of the curvature. Therefore the coupling parameter κ has been termed the "gravimagnetic ratio" [28, 182]. Like in the electromagnetic case [183] the Pauli-Lubanski and Pirani-vectors are affected by this Stern-Gerlach force:

(5.2.59)

$$D_\tau S^\mu = \frac{1}{4m\sqrt{-g}}\varepsilon^{\mu\nu\kappa\lambda}\Sigma_{\kappa\lambda}\Sigma^{\alpha\beta}\left(R_{\alpha\beta\nu\sigma}u^\sigma - \frac{\kappa}{2}\Sigma^{\rho\sigma}\nabla_\nu R_{\rho\sigma\alpha\beta}\right),$$

$$D_\tau Z^\mu = -\kappa\Sigma^{\kappa\lambda}R_{\kappa\lambda}{}^{\mu}{}_{\nu}Z^\nu + \left(\kappa + \frac{1}{2m}\right)\Sigma^{\mu\nu}\Sigma^{\kappa\lambda}R_{\kappa\lambda\nu\sigma}u^\sigma - \frac{\kappa}{4m}\Sigma^{\mu\nu}\Sigma^{\kappa\lambda}\Sigma^{\rho\sigma}\nabla_\nu R_{\kappa\lambda\rho\sigma}.$$

The second equation simplifies strongly for the special value

$$\kappa = -\frac{1}{2m}. \tag{5.2.60}$$

In that case an initial condition $Z^\mu = 0$ is conserved up to terms of cubic order in spin. For the extended hamiltonian the conditions for the existence of constants of motion are modified. The total spin I defined in (5.2.14) is still conserved, but the conserved hamiltonian now is of course $H = H_0 + H_\Sigma$. Finally the constants of motion J of the form (5.2.17) are preserved under this modification of the hamiltonian. To see this, observe that

$$\{J, H_\Sigma\} = -\kappa \Sigma^{\mu\nu}\Sigma^{\rho\sigma}\left(\frac{1}{4}\,\alpha^\lambda \nabla_\lambda R_{\mu\nu\rho\sigma} + \beta_{\mu\lambda} R^\lambda{}_{\nu\rho\sigma}\right). \tag{5.2.61}$$

For the Killing-vector solutions (5.2.18) the right-hand side takes the form

(5.2.62)

$$\begin{aligned}\Sigma^{\mu\nu}\Sigma^{\rho\sigma}\left(\frac{1}{4}\,\alpha^\lambda \nabla_\lambda R_{\mu\nu\rho\sigma} + \beta_{\mu\lambda} R^\lambda{}_{\nu\rho\sigma}\right) &= \frac{1}{2}\,\Sigma^{\mu\nu}\Sigma^{\rho\sigma}\left(\nabla_\mu\nabla_\rho\nabla_\sigma + \nabla_\rho\nabla_\mu\nabla_\sigma\right)\alpha_\nu \\ &= \frac{1}{2}\,\Sigma^{\mu\nu}\Sigma^{\rho\sigma}\left(\nabla_\mu\nabla_\rho + \nabla_\rho\nabla_\mu\right)\beta_{\sigma\nu} = 0,\end{aligned}$$

due to the antisymmetry of the tensor $\beta_{\sigma\nu}$. Therefore in particular the expressions (5.2.36) and (5.2.37) also define constants of motion in Schwarzschild spacetime in the presence of Stern-Gerlach forces, as described by the non-minimal hamiltonian (5.2.57).

The minimal choice of hamiltonian is the one which describes the geodesic motion of spinless particles. Instead, non-minimal hamiltonians like (5.2.57) can provide more complicated dynamics, as required for example for objects with non-vanishing gravimagnetic ratios [28, 165]. In this case the spin rotates around field-lines of constant curvature. Clearly the brackets (5.2.6) and the conservation laws (5.2.17),(5.2.20) can be extended to other non-minimal hamiltonians of different kind, but restricting to the hamiltonians like the one (5.2.57) we have dealt with, one can already obtain a description of various compact objects simply by tuning the gravimagnetic ratio κ. This could in principle contain information coming from the internal structure of the body, like an equation of state for a neutron star.

In this sense one uses the non-minimal hamiltonian (5.2.57) as an effective approach. In contrast to [163, 28, 165] where κ has a fixed value, here κ is considered as a free parameter to be tuned case by case, inferring it from the specific energy-momentum tensor of the source or from observations.

5.3 Spin worldline deviation

When spin is involved in GR, tidal effects take place and these lead the worldline to diverge from its original path, sometimes even tearing the compact object apart, as it happens to neutron stars approaching a Kerr Black Hole. In order to take such effects into account, deviations from the usual geodesic path can be introduced. Moreover this would also be a way to generalize special solutions, such as the circular orbit described previously, to more general orbits. Therefore we show in this section how the method of geodesic deviations fits in the framework of spinning compact objects in GR.

Suppose one wants to apply this method to a generic orbit for a spinning compact object, one has to consider deviations of the spin tensor (5.2.5) alongside the deviations

of the orbit itself. Since there is also spin involved in the dynamical evolution of the body through spacetime, the motion follows a *worldline*, and therefore we will deal with worldline deviations, rather than geodesic deviations [118]. Such worldline deviations have already been considered, for instance, when attaching Lorentz indices to the body in the framework of a supersymmetric theory, where the spin tensor was composed of more fundamental degrees of freedom such as Grassmann variables [147, 108].

In other works [178, 184] worldline deviations from the Mathisson-Papapetrou equations (5.1.1) have been considered, in a linearised regime, leading to a restriction of the phase space of spin and orbital configurations.

In this section we first describe the effects of worldline deviation for a spinning compact object to first order. Then we continue to derive the equations up to second order in the worldline deviation. The results are derived here for the case of a spinning body, using the same notation of this chapter, but they can also be applied to any non-trivial right-hand side in a geodesic equation, such as the Lorentz term appearing for a charged particle in curved background.

5.3.1 Worldline deviation equations

We first introduce some notation that will be used throughout this chapter. Consider a generic worldline, described in some system of coordinates by $x^\mu(\tau)$, with τ some timelike parametrization for the curve. The velocity is the tangent vector $u^\mu = \frac{dx^\mu}{d\tau} = \frac{Dx^\mu}{D\tau}$, where the last one indicates the covariant derivative [43, 44]. More extensive remarks about the deviation equations have already been described in section 2.4; for the sake of clarity we report here only the main points before applying it to the formalism of spinning bodies.

If one takes the covariant derivative of the velocity u^μ along the same curve x^μ, one gets the so-called "geodesic equation"

$$\frac{D^2x^\mu}{D\tau^2} = \frac{d^2x^\mu}{d\tau^2} + \Gamma^\mu_{\nu\lambda}\frac{dx^\nu}{d\tau}\frac{dx^\lambda}{d\tau} = \begin{cases} 0 & \text{in free space,} \\ f^\mu & \text{with other external force.} \end{cases} \tag{5.3.1}$$

Since we want to find the worldline deviation to the equations (5.2.10), (5.2.11), we will consider the case of a worldline with a non-trivial external force, represented in this case by $f^\mu = \frac{1}{2m}\Sigma^{\kappa\lambda}R^\mu{}_{\nu\kappa\lambda}\,\dot{x}^\nu$. In order to fix the notation, notice that we can also write the left-hand side as

$$\frac{D^2x^\mu}{D\tau^2} = \frac{Du^\mu}{D\tau} = (u\cdot\nabla u)^\mu.$$

Now, given a certain background spacetime, it is possible to parametrize the family of the geodesic curves in such a way that moving from one geodesic to another requires just a change in this parameter. To make a simple example with a known metric: in Schwarzschild spacetime consider the family of all the circular orbits which are solutions of the geodesic equations (3.1.5). These are parametrized by their radial distance R and moving from one geodesic to another means changing the radius of the orbit. Nevertheless more complicated situations can be built, with non-trivial displacements from one geodesic to the other. The theory about the geodesic deviation is well-known [43] and it gives insight in the meaning of the Riemann tensor as well.

Without loss of generality one can consider a family of worldlines described by a timelike parameter for moving along the worldline τ, and another parameter for moving between worldlines within the same family. Be this new parameter σ. Then one can define the rate, at fixed value of τ, of moving from one geodesic to the other inside the same family to be

$$n^\mu = \left.\frac{dx^\mu}{d\sigma}\right|_{\sigma=0} = \frac{Dx^\mu}{D\sigma}, \tag{5.3.2}$$

this is the *first order worldline deviation vector*. The name is due to the following Taylor expansion at the same fixed value of the timelike parameter τ

$$x^\mu = x_0^\mu + \sigma \left.\frac{dx^\mu}{d\sigma}\right|_{\sigma=0} + \frac{\sigma^2}{2!}\left.\frac{d^2x^\mu}{d\sigma^2}\right|_{\sigma=0} + \frac{\sigma^3}{3!}\left.\frac{d^3x^\mu}{d\sigma^3}\right|_{\sigma=0} + o(\sigma^4) \tag{5.3.3}$$

where x_0^μ is a well-known worldline which is the starting point of the worldline deviation expansion. Moving among members of the family of worldlines one can go from this one to another one $x^\mu(\tau;\sigma)$.

Nevertheless this is not a covariant expression and in order to handle it at different points in spacetimes one has to rewrite the expansion (5.3.3) in terms of covariant quantities such as n^μ in (5.3.2). For this reason one defines the *second order worldline deviation vector*

$$k^\mu = \left.\frac{D^2x^\mu}{D\sigma^2}\right|_{\sigma=0} = \left.\frac{Dn^\mu}{D\sigma}\right|_{\sigma=0} = \frac{d^2x^\mu}{d\sigma^2} + \Gamma^\mu_{\nu\lambda}\frac{dx^\lambda}{d\sigma}\frac{dx^\nu}{d\sigma} \tag{5.3.4}$$

so that the Taylor deviation expansion becomes

$$x^\mu = x_0^\mu + \sigma n^\mu + \frac{\sigma^2}{2!}(k^\mu - \Gamma^\mu_{\nu\lambda}n^\nu n^\lambda) + o(\sigma^3). \tag{5.3.5}$$

The deviation vector (5.3.2) changes along the curve itself, i.e. its rate of change with respect to the timelike parameter τ is:

$$\begin{aligned}\frac{Dn^\mu}{D\tau} &= \frac{D^2x^\mu}{D\tau D\sigma} = (u\cdot\nabla n)^\mu \\ &= \frac{dn^\mu}{d\tau} + \Gamma^\mu_{\nu\lambda}\frac{dx^\lambda}{d\tau}\frac{dx^\lambda}{d\sigma} = \frac{d^2x^\mu}{d\tau d\sigma} + \Gamma^\mu_{\nu\lambda}\frac{dx^\lambda}{d\tau}\frac{dx^\nu}{d\sigma}.\end{aligned} \tag{5.3.6}$$

From this last expression one can see there is symmetry in the derivatives with respect to τ and σ, thanks to Schwarz's theorem, so $\frac{du^\mu}{d\sigma} = \frac{dn^\mu}{d\tau}$ or stated differently that

$$(u\cdot\nabla n)^\mu = u_\nu\nabla^\nu n^\mu = n^\nu\nabla_\nu u^\mu = (n\cdot\nabla u)^\mu \Rightarrow u\cdot\nabla n = n\cdot\nabla u, \tag{5.3.7}$$

a property which we are going to use extensively in the following proofs. A first application is given by the covariant expression for the geodesic "acceleration" term, which we derive here for the most general case, namely when the right-hand side of (5.3.1) is not trivially

zero.

$$\begin{aligned}\frac{D^2n^\mu}{D\tau^2} &= u^\nu\nabla_\nu(u^\tau\nabla_\tau n^\mu) = u^\nu\nabla_\nu(n^\tau\nabla_\tau u^\mu)\\ &= u^\nu\nabla_\nu n^\tau\nabla_\tau u^\mu + u^\nu n^\tau\nabla_\nu\nabla_\tau u^\mu = n^\nu\nabla_\nu u^\tau\nabla_\tau u^\mu + u^\nu n^\tau\nabla_\nu\nabla_\tau u^\mu\\ &= n^\nu\nabla_\nu(u^\tau\nabla_\tau u^\mu) - n^\nu u^\tau\nabla_\nu\nabla_\tau u^\mu + n^\tau u^\nu\nabla_\nu\nabla_\tau u^\mu\\ &= n^\nu\nabla_\nu(u^\tau\nabla_\tau u^\mu) + n^\tau u^\nu(\nabla_\nu\nabla_\tau - \nabla_\tau\nabla_\nu)u^\mu\\ &= n^\nu\nabla_\nu(u^\tau\nabla_\tau u^\mu) + n^\tau u^\nu R^\mu{}_{\nu\tau\kappa}u^\kappa\\ &= R^\mu{}_{\nu\tau\kappa}u^\nu n^\tau u^\kappa + f^\mu{}_{;\nu}n^\nu\end{aligned} \tag{5.3.8}$$

where $R^\mu{}_{\nu\tau\kappa}$ is the Riemann tensor associated with the background metric. This is the usual geodesic deviation equation (2.4.1) with an extra term associated to the background fields. For instance a particle with charge q and mass m follows the worldline equation

$$\frac{D^2x^\mu}{D\tau^2} = \frac{q}{m}F^\mu{}_\nu\frac{dx^\nu}{d\tau} = f^\mu, \tag{5.3.9}$$

and the corresponding first order worldline deviation equation is

$$\frac{D^2n^\mu}{D\tau^2} = R^\mu{}_{\nu\tau\kappa}u^\nu n^\tau u^\kappa + \frac{q}{m}F^\mu{}_{\lambda;\nu}n^\nu u^\lambda + \frac{q}{m}F^\mu{}_\lambda\frac{Dn^\lambda}{D\tau}. \tag{5.3.10}$$

We can already apply the result (5.3.8) for the first-order worldline deviation equation with background fields to the spinning particle case. In this case one takes the equation of motion (5.2.11), which we recall here to be

$$\frac{D^2x^\mu}{D\tau^2} = \frac{1}{2m}\Sigma^{\kappa\lambda}R^\mu{}_{\nu\kappa\lambda}u^\nu = f^\mu, \tag{5.3.11}$$

and then from (5.3.8) after some straightforward algebra one derives the first order worldline deviation equation with the Stern-Gerlach term as background field

$$\frac{D^2n^\mu}{D\tau^2} = R^\mu{}_{\kappa\nu\lambda}u^\kappa u^\lambda n^\nu + \frac{\Sigma^{\kappa\lambda}}{2m}R^\mu{}_{\nu\kappa\lambda}\frac{Dn^\nu}{D\tau} + \frac{1}{2m}\left(\Sigma^{\kappa\lambda}R^\mu{}_{\nu\kappa\lambda;\rho}u^\nu n^\rho + J^{\kappa\lambda}R^\mu{}_{\nu\kappa\lambda}u^\nu\right). \tag{5.3.12}$$

In this equation we have introduced the antisymmetric tensor $J^{\kappa\lambda}$. This is the spin counterpart of n^μ. In fact, together with the worldline deviation itself, one has to consider the spin deviation, or

$$J^{\kappa\lambda} = \frac{D\Sigma^{\kappa\lambda}}{D\sigma}. \tag{5.3.13}$$

The worldline deviation equations for a spinning particle would not be complete without the deviation equations for the spin tensor, as this is a dynamical degree of freedom as well. This implies a Taylor expansion of the spin tensor Σ like (5.3.3):

$$\Sigma^{\mu\nu} = \Sigma_0^{\mu\nu} + \sigma\frac{d\Sigma^{\mu\nu}}{d\sigma}\bigg|_{\sigma=0} + \frac{\sigma^2}{2!}\frac{d^2\Sigma^{\mu\nu}}{d\sigma^2}\bigg|_{\sigma=0} + \frac{\sigma^3}{3!}\frac{d^3\Sigma^{\mu\nu}}{d\sigma^3}\bigg|_{\sigma=0} + \mathcal{O}(\sigma^4). \tag{5.3.14}$$

Once the definition for the spin first-order deviation tensor (5.3.13) has been given, one can proceed to write down the deviation equation. First observe that, by the definition of the Riemann tensor in torsion-less spacetimes [43], one can write

$$[\nabla_\mu, \nabla_\nu]\Sigma^{\kappa\lambda} = R_{\mu\nu}{}^{[\kappa}{}_{\rho}\Sigma^{\rho\lambda]} = R_{\mu\nu}{}^{\kappa}{}_{\rho}\Sigma^{\rho\lambda} - R_{\mu\nu}{}^{\lambda}{}_{\rho}\Sigma^{\rho\kappa} = [R_{\mu\nu}, \Sigma]^{\kappa\rho}. \tag{5.3.15}$$

Finally, the first order deviation equation for the spin term $J^{\kappa\lambda}$ reads

$$\frac{DJ^{\mu\nu}}{D\tau} = -R_{\kappa\lambda}{}^{[\mu}{}_{\rho}\Sigma^{\rho\nu]}u^\kappa n^\lambda = [R_{\kappa\lambda}, \Sigma]^{\mu\nu}u^\kappa n^\lambda. \tag{5.3.16}$$

Summarizing, to first order in the Taylor expansions (5.3.3), (5.3.14), the worldline deviations for a spinning test-particle are given by the vector n^μ and the tensor $J^{\kappa\lambda}$, whose evolution equations [108] are

$$\begin{aligned}
&\frac{D^2n^\mu}{D\tau^2} = R^\mu{}_{\kappa\nu\lambda}u^\kappa u^\lambda n^\nu + \frac{\Sigma^{\kappa\lambda}}{2m}R^\mu{}_{\nu\kappa\lambda}\frac{Dn^\nu}{D\tau} + \frac{1}{2m}\left(\Sigma^{\kappa\lambda}R^\mu{}_{\nu\kappa\lambda;\rho}u^\nu n^\rho + J^{\kappa\lambda}R^\mu{}_{\nu\kappa\lambda}u^\nu\right),\\
&\frac{DJ^{\kappa\lambda}}{D\tau} = [R_{\mu\nu}, \Sigma]^{\kappa\lambda}u^\mu n^\nu.
\end{aligned}$$

5.3.2 Second order worldline deviation

The next step is to derive the second order deviation equation, that is the equations concerning k^μ and its spin analog. The second order deviation vector has already been defined in (5.3.4), while the spin counterpart is $K^{\mu\nu}$, i.e. the second order covariant derivative of the spin tensor

$$\frac{D^2\Sigma^{\mu\nu}}{D\sigma^2} = \frac{DJ^{\mu\nu}}{D\sigma} = K^{\mu\nu}. \tag{5.3.17}$$

With this definition, one can write down the worldline expansion in the spin (5.3.14) in covariant terms as

$$\begin{aligned}
\Sigma^{\mu\nu} = \Sigma_0^{\mu\nu} &+ \sigma\left(J^{\mu\nu} - \Gamma^\mu_{\kappa\lambda}\Sigma^{\kappa\nu}n^\lambda - \Gamma^\nu_{\kappa\lambda}\Sigma^{\mu\kappa}n^\lambda\right)\\
&+ \frac{\sigma^2}{2!}\Bigg(K^{\mu\nu} - \Gamma^\mu_{\kappa\lambda,\rho}\Sigma^{\kappa\nu}n^\rho n^\lambda - \Gamma^\nu_{\kappa\lambda,\rho}\Sigma^{\mu\kappa}n^\rho n^\lambda - \left(\Gamma^\mu_{\kappa\lambda}\Sigma^{\kappa\nu} + \Gamma^\nu_{\kappa\lambda}\Sigma^{\mu\kappa}\right)\left(k^\lambda - \Gamma^\lambda_{\rho\tau}n^\rho n^\tau\right)\\
&\quad - \Gamma^\mu_{\kappa\lambda}n^\lambda\left(J^{\kappa\nu} - \Gamma^\kappa_{\rho\tau}\Sigma^{\rho\nu}n^\tau - \Gamma^\nu_{\rho\tau}\Sigma^{\kappa\rho}n^\tau\right) - \Gamma^\nu_{\kappa\lambda}n^\lambda\left(J^{\mu\kappa} - \Gamma^\kappa_{\rho\tau}\Sigma^{\mu\rho}n^\tau - \Gamma^\mu_{\rho\tau}\Sigma^{\kappa\rho}n^\tau\right)\Bigg)\\
&+ \mathcal{O}(\sigma^3).
\end{aligned} \tag{5.3.18}$$

Unlike (5.3.12) which are second order differential equations, the Eq. (5.3.16) for $J^{\mu\nu}$ is

of the first order, so one can expect the equation for $K^{\mu\nu}$ to be of the same order,

(5.3.19)

$$\begin{aligned}
\frac{DK^{\kappa\lambda}}{D\tau} &= u\nabla(n\nabla J^{\kappa\lambda}) \\
&= u\cdot\nabla(n\cdot\nabla J^{\kappa\lambda}) + (n\cdot\nabla u)\nabla J^{\kappa\lambda} - (u\cdot\nabla n)\nabla J^{\kappa\lambda} \\
&= u\cdot\nabla(n\cdot\nabla J^{\kappa\lambda}) + n\cdot\nabla(\frac{DJ^{\kappa\lambda}}{D\tau}) - u^\mu n^\nu\nabla_\nu\nabla_\mu J^{\kappa\lambda} \\
&\qquad - u\cdot\nabla(n\cdot\nabla J^{\kappa\lambda}) + u^\mu n^\nu\nabla_\mu\nabla_\nu J^{\kappa\lambda} \\
&= n\cdot\nabla(\frac{DJ^{\kappa\lambda}}{D\tau}) + (\nabla_\mu\nabla_\nu J^{\kappa\lambda} - \nabla_\nu\nabla_\mu J^{\kappa\lambda})u^\mu n^\nu \\
&= n\cdot\nabla(\frac{DJ^{\kappa\lambda}}{D\tau}) + [R_{\mu\nu}, J]^{\kappa\lambda}u^\mu n^\nu \Rightarrow \\
\frac{DK^{\kappa\lambda}}{D\tau} &= [R_{\mu\nu;\rho}, \Sigma]^{\kappa\lambda}u^\mu n^\nu n^\rho + 2[R_{\mu\nu}, J]^{\kappa\lambda}u^\mu n^\nu + [R_{\mu\nu}, \Sigma]^{\kappa\lambda}(\frac{Dn^\mu}{D\tau}n^\nu + k^\nu u^\mu).
\end{aligned}$$

The following equalities have been used

$$\begin{aligned}
u\cdot\nabla(n\cdot\nabla J^{\kappa\lambda}) &= (u\cdot\nabla n)\cdot\nabla J^{\kappa\lambda} + u^\mu n^\nu\nabla_\mu\nabla_\nu J^{\kappa\lambda}, \\
[\nabla_\mu, \nabla_\nu]J^{\kappa\lambda} &= [R_{\mu\nu}, J]^{\kappa\lambda}, \\
n\cdot\nabla(\frac{DJ^{\kappa\lambda}}{D\tau}) &= n^\rho\nabla_\rho(u^\mu\nabla_\mu J^{\kappa\lambda}) \\
&= n^\rho\nabla_\rho([R_{\mu\nu}, \Sigma]^{\kappa\lambda}u^\mu n^\nu) \\
&= [R_{\mu\nu;\rho}, \Sigma]^{\kappa\lambda}u^\mu n^\nu n^\rho + [R_{\mu\nu}, J]^{\kappa\lambda}u^\mu n^\nu + [R_{\mu\nu}, \Sigma]^{\kappa\lambda}(\frac{Dn^\mu}{D\tau}n^\nu + k^\nu u^\mu) \\
(u^\mu n^\nu)_{;\rho}n^\rho &= n\cdot\nabla(u^\mu n^\nu) \\
&= n\cdot\nabla u^\mu n^\nu + n\cdot\nabla n^\nu u^\mu \\
&= \frac{Dn^\mu}{D\tau}n^\nu + k^\nu u^\mu \\
n\cdot\nabla n^\nu &= k^\nu.
\end{aligned}$$

We are left with the equation for k^μ in the presence of a non-trivial external force, as the Stern-Gerlach term in (5.3.11). While it is relatively easy to find the geodesic deviation equations in GR textbooks, and even the generalizations to non-trivial background fields have already been considered in the literature [118, 108, 178, 184], performing it to the second order is a more involved task. An easy way to find out this equation is employing a different formalism than the one used so far. We rely heavily on the vector formalism established in [107], whose basic elements are recalled here.

So, be X, Z two vectors tangent to two different curves in the curved spacetime and be $[X, Z] = \nabla_X Z - \nabla_Z X$ their Lie derivative. As it is well-known the curvature is expressed by the Riemann tensor, whose definition would read, using these vectors,

$$R(X, Z)Y = [\nabla_X, \nabla_Z]Y - \nabla_{[X,Z]}Y,$$

and the interpretation of the covariant derivatives in the usual symbols leads to

$$\nabla_W(\nabla_X Y^\mu) = W^\alpha(Y^\mu{}_{;\nu}X^\nu)_{;\alpha}.$$

As check one can derive again the first order worldline deviation equation; just by making the following replacements

$$\begin{aligned} X &\to n^\mu, \\ Z &\to u^\mu, \\ &\Rightarrow \nabla_Z Z = u^\mu u^\lambda_{;\mu} = f^\lambda, \\ u\cdot\nabla n = n\cdot\nabla u &\Rightarrow \nabla_X Z = \nabla_Z X \text{ and } [X,Z]=0, \end{aligned}$$

$$[\nabla_\alpha,\nabla_\beta]n^\alpha u^\beta u = R(n,u)u \Rightarrow [\nabla_X,\nabla_Z]Z = R(X,Z)Z,$$

one obtains the first order worldline deviation equation (5.3.8)

$$\begin{aligned} \frac{D^2 n^\mu}{D\tau^2} &= u^\nu (u^\lambda n^\mu{}_{;\lambda})_{;\nu} = \nabla_Z(\nabla_Z X) = \nabla_Z(\nabla_X Z) \\ &= \nabla_Z(\nabla_X Z) - \nabla_X(\nabla_Z Z) + \nabla_X(\nabla_Z Z) \\ &= R(Z,X)Z + \nabla_X(\nabla_Z Z) = R^\mu{}_{\alpha\beta\gamma} u^\alpha n^\beta u^\gamma + f^\mu{}_{;\nu} u^\nu. \end{aligned} \tag{5.3.20}$$

Before moving to the second order geodesic deviation equation, an important observation is necessary. Be Y a so-called *Jacobi-field* such that $[Y,Z]=0=[X,Z]$, then, through Jacobi identity one deduces that $[[Y,X],Z]=0$. Be $W=[Y,X]$, also W is a Jacobi field whose Lie derivative along the curve tangent to Z is null as well. This implies the following identities which will be useful later on. The first one is

$$\begin{aligned} \nabla_Z(\nabla_Z W) &= \nabla_Z^2([X,Y]) = R(Z,[X,Y])Z + \nabla_{[X,Y]}(\nabla_Z Z) \\ &= \nabla_Z^2(\nabla_X Y - \nabla_Y X) = R(Z,\nabla_X Y - \nabla_Y X)Z + \nabla_{[X,Y]}(\nabla_Z Z) \\ &= \nabla_Z^2(\nabla_X Y) - \nabla_Z^2(\nabla_Y X) = R(Z,\nabla_X Y)Z - R(Z,\nabla_Y X)Z + \nabla_{[X,Y]}(\nabla_Z Z), \end{aligned}$$

implying that

$$\nabla_Z(\nabla_Z(\nabla_Y X)) - R(Z,\nabla_Y X)Z = \nabla_Z(\nabla_Z(\nabla_X Y)) - \nabla_{[X,Y]}(\nabla_Z Z) - R(Z,\nabla_X Y)Z. \tag{5.3.21}$$

One can always exchange the order between the couples (X,Y), (Y,Z) and (X,Z) since these are all Jacobi fields. Keeping this in mind, we take the covariant derivative of the left-hand side of the equation above and get

$$\begin{aligned} \nabla_Z(\nabla_Z(\nabla_X Y)) &= \nabla_Z(\nabla_Z(\nabla_X Y) - \nabla_X(\nabla_Z Y)) + \nabla_Z(\nabla_X(\nabla_Z Y)) \\ &= \nabla_Z(R(Z,X)Y) + \nabla_Z(\nabla_X(\nabla_Z Y)) \\ &= (\nabla_Z R)(Z,X)Y + R(\nabla_Z Z,X)Y + R(Z,\nabla_Z X)Y \\ &\quad + R(Z,X)\nabla_Z Y + \nabla_Z(\nabla_X(\nabla_Z Y)). \end{aligned}$$

This equality helps in the evaluation of $\nabla_Z^2(\nabla_Y X) - R(Z,\nabla_Y X)Z$, which is the crucial calculation to get to the second order worldline deviation equation. In fact, one can notice that

$$\begin{aligned} \nabla_Z^2(\nabla_Y X) - R(Z,\nabla_Y X)Z &= (\nabla_Z R)(Z,X)Y + R(\nabla_Z Z,X)Y + R(Z,\nabla_Z X)Y \\ &\quad + R(Z,X)\nabla_Z Y + \nabla_Z(\nabla_X(\nabla_Z Y)) - \nabla_{[X,Y]}(\nabla_Z Z) - R(Z,\nabla_X Y)Z. \end{aligned} \tag{5.3.22}$$

Now, since

$$\nabla_X R((Z,Y)Z) = (\nabla_X R)(Z,Y)Z + R(\nabla_X Z, Y)Z + R(Z, \nabla_X Y)Z + R(Z,Y)\nabla_X Z$$

one can rewrite (5.3.22) in the following way

$$\begin{aligned}\nabla_Z^2(\nabla_Y X) - R(Z,\nabla_Y X)Z = {} & (\nabla_Z R)(Z,X)Y + R(\nabla_Z Z, X)Y + R(Z,\nabla_Z X)Y + R(Z,X)\nabla_Z Y \\ & + \nabla_Z(\nabla_X(\nabla_Z Y)) - \nabla_{[X,Y]}(\nabla_Z Z) + (\nabla_X R)(Z,Y)Z \\ & + R(\nabla_X Z, Y)Z + R(Z,Y)\nabla_X Z - \nabla_X(R(Z,Y)Z) \\ \\ = {} & R(\nabla_Z Z, X)Y - \nabla_{[X,Y]}(\nabla_Z Z) \\ & + (\nabla_Z R)(Z,X)Y + R(Z,X)\nabla_Z Y \\ & + (\nabla_X R)(Z,Y)Z + R(Z,Y)\nabla_X Z \\ & + R(Z,\nabla_Z X)Y + R(\nabla_X Z, Y)Z - \nabla_X(R(Z,Y)Z) \\ & + \underbrace{\nabla_Z(\nabla_X(\nabla_Z Y)) - \nabla_X(\nabla_Z(\nabla_Z Y))}_{R(Z,X)\nabla_Z Y} + \nabla_X(\nabla_Z(\nabla_Z Y)).\end{aligned}$$

From now on take into account only the last six terms (last two rows of the equation above), which can be rewritten as five

$$R(Z,X)\nabla_Z Y + R(Z,\nabla_Z X)Y + \nabla_X(\nabla_Z(\nabla_Z Y)) + R(\nabla_X Z, Y)Z - \nabla_X(R(Z,Y)Z).$$

Now we exchange the order of X, Z in covariant derivatives, since their Lie derivative is null

$$R(Z,X)\nabla_Z Y + R(Z,\nabla_X Z)Y + \nabla_X(\nabla_Z(\nabla_Y Z)) + R(\nabla_X Z, Y)Z - \nabla_X(R(Z,Y)Z),$$

and then subtract and add the same term

$$\begin{aligned}R(Z,X)\nabla_Z Y + R(Z,\nabla_X Z)Y + & \underbrace{\nabla_X(\nabla_Z(\nabla_Y Z)) - \nabla_X(\nabla_Y(\nabla_Z Z))}_{\nabla_X(R(Z,Y)Z)} + \nabla_X(\nabla_Y(\nabla_Z Z)) \\ & + R(\nabla_X Z, Y)Z - \nabla_X(R(Z,Y)Z).\end{aligned}$$

Third and fourth term give another covariant derivative of the Riemann tensor term which annihilates with the last term, leaving only

$$R(Z,X)\nabla_Z Y + \nabla_X(\nabla_Y(\nabla_Z Z)) + R(Z,\nabla_X Z)Y + R(\nabla_X Z, Y)Z. \tag{5.3.23}$$

Thanks to Bianchi identity $R(U,V)W + R(V,W)U + R(W,U)V = 0$ the last two terms can be replaced with $-R(Y,Z)\nabla_X Z = R(Z,Y)\nabla_X Z$ and one can now collect all the terms together obtaining the so longed equation

$$\begin{aligned}\nabla_Z^2(\nabla_Y X) - R(Z,\nabla_Y X)Z = {} & \overbrace{R(\nabla_Z Z, X)Y - \nabla_{[X,Y]}(\nabla_Z Z) + \nabla_X(\nabla_Y(\nabla_Z Z))}^{\text{terms disappearing if } Z \text{ is geodesic tangent vector}} \\ & + (\nabla_Z R)(Z,X)Y + (\nabla_X R)(Z,Y)Z \\ & + 2R(Z,X)\nabla_Z Y + 2R(Z,Y)\nabla_X Z.\end{aligned} \tag{5.3.24}$$

Notice that the first three terms on the right-hand side would all vanish if considering a geodesic curve, so with $\nabla_Z Z = 0$. In order to retrieve from this very general expression the worldline deviation one needs the following replacements

$$\begin{aligned} &X = Y \to n^\mu, \\ &Z \to u^\mu, \\ &\quad \Rightarrow \nabla_Z Z = \nabla_u u^\mu = f^\mu, \\ &\qquad \nabla_Y X = \nabla_X X = \frac{Dn^\mu}{D\sigma} = k^\mu. \end{aligned}$$

Finally one obtains

$$\begin{aligned} \nabla_u^2(\nabla_n n) - R(u, \nabla_n n)u = {} & R(\nabla_u u, n)n - \nabla_{[n,n]}(\nabla_u u) \\ & + \nabla_u(\nabla_n(\nabla_u u)) + (\nabla_u R)(u,u)n \\ & + (\nabla_n R)(u,n)u + 2R(u,n)\nabla_u n + 2R(u,n)\nabla_n u. \end{aligned} \tag{5.3.25}$$

or

$$\begin{aligned} &\frac{D^2 k^\mu}{D\tau^2} + R^\mu(k,u)u = \\ &\qquad R^\mu(f,n)n + \frac{D}{D\tau}\frac{Df^\mu}{D\sigma} + \frac{DR^\mu}{D\tau}(u,n)n + \frac{DR^\mu}{D\sigma}(u,n)u + 4R^\mu(u,n)\frac{Dn}{D\tau}. \end{aligned} \tag{5.3.26}$$

Stated differently, one can say that everytime there is a worldline equation of the type $\frac{D^2 x^\mu}{D\tau^2} = f^\mu$, the second-order worldline deviation equation is

$$\begin{aligned} &\frac{D^2 k^\mu}{D\tau^2} + R_{\nu\rho\sigma}{}^\mu k^\nu u^\rho u^\sigma = \\ &\qquad R_{\nu\rho\sigma}{}^\mu n^\rho n^\sigma f^\nu + \frac{D}{D\tau}\frac{Df^\mu}{D\sigma} + u^\lambda u^\nu n^\rho n^\sigma \left(R_{\nu\rho\sigma}{}^\mu{}_{;\lambda} - R_{\rho\nu\lambda}{}^\mu{}_{;\sigma} + 4R_{\nu\rho\sigma}{}^\mu u^\nu n^\rho \frac{Dn}{D\tau} \right). \end{aligned} \tag{5.3.27}$$

This is the second-order worldline deviation equation for the vector k^μ. The non-trivial right-hand side of the equation of motion (5.3.11) has to be replaced instead of f^μ in order to obtain the worldline deviation equation coupled to (5.3.19).

Summarizing, the second-order worldline-deviation equations, describing the proper-time evolution of the second-order deviation vector k^μ and tensor $K^{\mu\nu}$, are respectively:

$$\begin{aligned} &\frac{D^2 k^\mu}{D\tau^2} + R_{\nu\rho\sigma}{}^\mu k^\nu u^\rho u^\sigma = \\ &\qquad R_{\nu\rho\sigma}{}^\mu n^\rho n^\sigma f^\nu + \frac{D}{D\tau}\frac{Df^\mu}{D\sigma} + u^\lambda u^\nu n^\rho n^\sigma \left(R_{\nu\rho\sigma}{}^\mu{}_{;\lambda} - R_{\rho\nu\lambda}{}^\mu{}_{;\sigma} + 4R_{\nu\rho\sigma}{}^\mu u^\nu n^\rho \frac{Dn^\sigma}{D\tau} \right), \end{aligned} \tag{5.3.28}$$

$$\frac{DK^{\kappa\lambda}}{D\tau} = [R_{\mu\nu;\rho}, \Sigma]^{\kappa\lambda} u^\mu n^\nu n^\rho + 2[R_{\mu\nu}, J]^{\kappa\lambda} u^\mu n^\nu + [R_{\mu\nu}, \Sigma]^{\kappa\lambda}\left(\frac{Dn^\mu}{D\tau} n^\nu + K^\nu u^\mu\right). \tag{5.3.29}$$

5.4 Concluding remarks

The notion of pointlike mass in GR is troublesome, because any mass has a corresponding Schwarzschild radius $r_S = \frac{2GM}{c^2}$, indicating the minimal size of the body as defined by its corresponding horizon [43]. On top of this for a spinning mass there is the minimal size [185] typified by its Møller radius $r_M = \frac{S}{m}$. These two define the scale of the approximation for a compact body rotating in curved spacetime. The body has to be considerably smaller than the radius of curvature of the background in order to be considered a spinning test-particle [186, 176].

Once these conditions are fulfilled, a representative point can be chosen for the spinning compact object, and much effort has been put in the literature to define such a position variable, which is not unique. The result is that different worldlines correspond to physically equivalent descriptions of the same system [23, 25, 166, 136]. These different choices can be enforced through different spin supplementary conditions (5.1.3) or directly in the definition of the position variable x^μ appearing in the hamiltonians and actions describing the system [149, 165, 26, 27]. An important role in connecting different choices is played by the mass dipole moment (5.1.4) or the Pirani vector (5.2.1). In particular, the closed set of Dirac-Poisson brackets (5.2.6) provides a unique and unambiguous starting point for the derivation of equations of motion for any representation of the spin degrees of freedom, allowing for a large class of physical implementations as fixed by the choice of hamiltonian. Two such choices, a minimal and a non-minimal one, have been presented and analyzed in the second section of this chapter.

The equations of motion (5.1.1), (5.2.9), (5.2.10) show that the spin-orbit coupling makes the motion of the test mass non-geodetic. Geodetic motion for spinless particles is retrieved with the minimal hamiltonian (5.2.7), for spinning particles this provides covariant conservation of the spin tensor (5.2.10). Other constants of motion can be introduced (5.2.13), (5.2.14), (5.2.17), (5.2.20), even for non-minimal hamiltonians considering a gravimagnetic ratio κ [165]. This formalism gives the opportunity to take into account other effects, such as internal structure of the spinning body, by tuning this parameter, making (5.2.7) an effective hamiltonian. The question which effective hamiltonian to use for which physical system now becomes a matter of phenomenology. One should either derive the correct effective hamiltonian from first principles [182, 28], connecting the formalism to the specific energy-momentum tensor, or determine it from experiments or observations. For the particular case of rotating black holes it could presumably be measured by observing gravitational waves from Extreme-Mass-Ratio binary systems involving a stellar-mass black hole.

An example is given by the Schwarzschild geometry, where the minimal hamiltonian case has been analyzed and the correspondence between aligned spin, i.e. non-precessing, and circular orbits has been reestablished and confirmed. Small deviations from this motion have shown little precession of the orbit in a confined region of spacetime [177, 178] in a linearised regime. In order to use fully General Relativity one needs to provide the formal worldline deviation expansions, as well for the orbit as for the spin degrees of freedom. This formalism has been further extended, providing the mathematical proofs for any curved background in all generality, in the last section of this chapter.

* *

6 Conclusion

* *

In this work two aspects of the dynamics of Extreme Mass Ratio (EMR) binary systems have been investigated. First we established a model for the "plunge" phase within Black-Hole perturbation theory, and the gravitational radiation coming from it has been calculated. The limits and possibilities of this method have been discussed and further extended using geodesic deviations. Secondly, spin has been added to the minor companion of the binary, exploring the dynamics of a spinning particle in curved background by establishing a new effective formalism and with applications, for instance to circular orbits in Schwarzschild spacetime.

During the last stages of an EMR binary, the orbit of the minor companion is considerably less eccentric than it was during the previous long inspiral stage. The plunge phase and the following merger start in the proximity of the Innermost Stable Circular Orbit (ISCO) and we have devised a geodesic solution of the Schwarzschild background (assuming for convenience that the central major black hole is non-rotating) that begins for $r < 6M$ in the inner region and ends on the BH horizon $r = 2M$. This is an example of the so-called "ballistic orbits", a special subclass of Darwin's associated orbits [133, 47]. We have analysed their properties, thanks to the fact that these orbits are known analytically and in closed form. They are a valuable model for the plunge phase of an EMR binary as they reproduce a quasi-circular motion first, followed by a more direct spiralling drive towards the horizon.

The ballistic orbits are exact solutions of the geodesic equation for Schwarzschild spacetime, they have their apastron at $r = R = (6 - 4e)M$, with e being an "eccentricity" parameter for the orbits. For R close to $6M$ the quasi-circular phase includes a large number of turns around the central black hole. They can come arbitrarily close to the ISCO and are degenerate in energy and angular momentum with outer stable circular orbits, those with radius $r_c > 6M$. This implies that their energy and angular momentum are slightly higher than those of the ISCO, so in the limit of small e they can be used to describe test masses infinitesimally boosted from the ISCO and then falling into the black hole. Following a ballistic orbit the test mass μ orbits first along an almost-circular orbit, for which $\dot{r} \ll r\dot{\varphi}$. Then near $r = 4.3M$ the radial and circular velocities become equal, and after this cross-over the radial motion dominates. This subdivision in the orbit is a

well-known fact, already recognized when studying more general cases of BH coalescences [21, 22]. As far as the initial revolutions are concerned, one can account for their number using power laws of the mass-ratio $\nu = \frac{\mu}{M}$, valid in the regime of Extreme Mass Ratio (for $\nu \sim 10^{-4}$ the relation breaks down). These considerations also mark the presence of a "universal phase", independent of the mass ratio, starting with the transition from quasi-circular to more radial motion.

For the infalling test mass we have computed the gravitational waves emitted during the infall. This has been done within Regge-Wheeler perturbation theory, exploiting the spherical symmetry of the Schwarzschild background. The implicit assumption made here is that the backreaction of the test mass and the waves on the background metric may be neglected. The Regge-Wheeler equations then have been solved numerically through the Lousto-Price algorithm implemented in C++ code. The behaviour of the waves obtained in this way confirms the kinematics of the orbit, in that the waves slowly and smoothly increase in amplitude and frequency throughout the quasi-circular phase, then a sudden increase with a final burst occurs (with amplitudes increasing by a factor of 2), followed by a damped and dying signal. Whereas the initial slow increase is strongly dependent on the parameters of the ballistic orbit, like the distance between its apastron and the ISCO, or the mass ratio, the final burst is virtually independent and in analogy with the second part of the ballistic orbit.

In specific parameter ranges the ballistic orbits can then be used as a first approximation to the infall phase of an EMR binary. The waveforms obtained in this way reproduce qualitatively known results. One is left with the issue of energy and angular momentum being higher than the corresponding ISCO values. In order to obtain a more realistic model for the plunge phase of EMR binaries, we have applied the technique of geodesic deviations to the ballistic orbits. We have been able to find an analytic solution of the geodesic deviation equations discovering first integrals of the equations, and eventually to perturb the original orbit. The deviation is not large and it affects mainly the radial motion. Our calculations have shown that in this way one can increase the number of revolutions in the quasi-circular phase, leaving the universal phase practically untouched. The main advantage though comes from the possibility of tuning the parameters of the deviation, the energy and angular momentum corrections ε_1, ℓ_1. This allows to shape the final orbit with any desired energy and angular momentum, provided certain reasonable constraints are satisfied. Clearly, in this way the energy of the test particle can be reduced to that of the ISCO or to lower values, which reflects a more realistic behaviour for a general EMR binary, where energy is continuously decreasing due to emission of GWs.

As far as EMR binaries are concerned, there is also the possibility to include spin into this framework. The simplest situation is when the minor body rotates, as in Neutron Star - Black Hole binaries. This can be described by a test particle with attached a classical spin vector moving in the curved background of the central major body. The equations for a spinning particle, where the effects of spin are taken up to dipole order and again the backreaction on the background metric is neglected, are long-known [136]. The spin degrees of freedom are included in an antisymmetric spin-tensor $\Sigma^{\mu\nu}$ and in the

common procedure one introduces reasonable "supplementary conditions" to get rid of the extra degrees of freedom, thus defining the worldline of the representative point of the spinning test-particle. The canonical momentum does not coincide with the product $m\dot{x}^\mu$, but it includes the spin as well. Instead in our case we have introduced a covariant formalism with a built-in worldline, i.e. the representative position x^μ is defined as the one satisfying the equations of motion derived from an appropriate set of Poisson-Dirac brackets. In this case the equality $\pi^\mu = m\dot{x}^\mu$ is restored. Within this formalism, we have derived again the equations of motion for a spinning test-particle, established the constants of motion, and under which conditions they are conserved. Afterwards we have provided an application to circular orbits in Schwarzschild spacetime and a non-minimal hamiltonian, showing that the applications are independent of the chosen hamiltonian.

The Poisson-Dirac brackets used in our derivation were partly investigated already by Khriplovich [163], but with a different meaning and interpretation. Here we used the hamiltonian as an effective one, namely one can change the hamiltonian with the one best fitting the particular object under study. In this way the information relative to the internal structure of the body represented by the test-particle is included into extra terms and factors in the hamiltonian. For the minimal hamiltonian $H = \frac{1}{2m} g_{\mu\nu}\pi^\mu\pi^\nu$ the usual equations of motion are retrieved. One can then include other effects such as Stern-Gerlach terms and electromagnetic fields.

Together with the brackets we have introduced conserved quantities, such as the total spin, energy, and total angular momentum, but also a system of orthogonal 4-vectors (u, W, S, Z) forming a basis of independent vectors defining a frame to be carried along the particle worldline. One of these, the Pirani vector Z^μ, is the "mass dipole moment", defining the connection between the particle's worldline and the center-of-mass worldline. On top of this, we have investigated the conserved quantities quadratic in the momenta π^μ, establishing the relations to be satisfied in terms of Killing-Yano tensors. All these results are general and valid for any background metric.

As an application of the formalism we have considered the Schwarzschild metric for convenience and we have shown how to build circular orbits in the equatorial plane, finding deviations from Kepler's third law. Another application has been realized with a non-minimal hamiltonian made by Stern-Gerlach terms, which still preserve constants of motion to first order in the gravimagnetic ratio κ. Finally, we have extended the geodesic deviation equations to spinning particles, up to second order in the deviation parameter σ, thus laying down the foundations for a worldline deviation method including spin.

The spin formalism discussed in this thesis can be further investigated, especially in the relation with the other equivalent decriptions requiring the use of supplementary conditions. Changing these conditions is like making a gauge choice, therefore it should be possible to reduce the differences between orbital descriptions, the position of the center of mass with respect to the body's worldline, the spin vectors, and so on, to a transformation from a worldline to another, as a coordinate change. The results obtained about spinning compact objects are useful for EMR binaries, as these naturally satisfy the test-particle requirements, and have found further application through worldline deviations for circular

orbits in Schwarzschild and Reissner-Nordstrøm backgrounds [27], determining also how the ISCO changes due to spin effects. Further improvements can be done in this direction, beyond planar motions or to other metrics, like Kerr.

The extension to Kerr metric is important because of the significance of this metric in modelling astrophysical pheonomena, namely any black hole can be represented by a Kerr BH. The problem can be tackled first along the equatorial plane, for convenience of calculation. This is valid for the spin as for the geodesic deviation in general. In this case the ballistic orbits can be employed again for the plunge phase.

Another interesting application is to explore to which extent the ballistic orbits can be matched to previous stages in the EMR coalescence. Through deviations one could devise orbits matching directly the eccentric orbits before the ISCO, so with a higher energy, and in this way complete the picture of inspiral/quasi-circular transition/direct plunge and merger of the binary coalescence. Gravitational radiation has been extracted from a ballistic orbit, but it can be compared to the corresponding one from the deviated ballistic orbit or to backreaction effects, as the deviations allow to adjust the orbit in order to take even those into account.

All these possible directions aim at a better understanding of the EMR dynamics and the gravitational radiation emitted by their binaries. Confirmation of the existence of gravitational waves came this year from the ground-based detector of second generation aLIGO, which can detect in the range of comparable-mass-ratio binaries, as GW150914 was. This should be a stronger drive to search also for EMR binaries as sources of GWs and it will even further increase the interest in eLISA, scheduled to be launched in 2034. Gravitational waveforms for EMR binaries will be ready by that time, if their dynamics will have been explored sufficiently. GW detection is a considerable step forward and the beginning of a new era; all the combined efforts in waveform prediction and GW detection will provide us with stronger tests of General Relativity and most of all, with a new instrument to look at the sky and investigate the properties of astrophysical objects.

* *

A Near-horizon source terms

* *

Here below are reported the $F^{lm}_{ZM/RW}, G^{lm}_{ZM/RW}$ source functions and similar expressions evaluated near the black-hole horizon, for a small body of mass μ moving on a ballistic orbit (3.1.12). These are needed for the implementation of the Lousto-Price algorithm when the test-particle is approaching the BH horizon, as it is discussed in section 3.2.1.

A superscript (h) indicates that these are the same terms appearing in the Regge-Wheeler equations, but evaluated close to the horizon by using the approximation for the infinitesimal quantity $R = r - 2M$. Expanding around $R = 0$, that is $r \to 2M$, one gets

$$e^{r^*-R-2M} = \left(\frac{R}{2M}\right)^{2M} \sim e^{r^*-2M} \Rightarrow R = 2M\left(e^{\frac{r^*}{2M}-1}\right) \ll 1,$$

and so, for instance, the Schwarzschild factor becomes

$$f(r) = 1 - \frac{2M}{r} \to \frac{R}{2M} = e^{\frac{r^*}{2M}-1},$$

A subscript p indicates a quantity calculated along the particle's orbit. The following are results of Taylor expansions around $R = 0$ to second order in the difference $R = r = 2M$, for the terms appearing in the source integral in the Lousto-Price algorithm expression (2.3.7).

Auxiliary functions:

$$\begin{aligned}
\Lambda^{(h)}(r) &= \lambda + \frac{3}{2}, \\
\bar{V}^{l(h)}_{ZM}(r^*) &= \frac{l^4 + 2l^3 - l^2 - 2l + 3}{4M^2(l^2 + l + 1)} e^{\frac{r^*}{2M}-1}, \\
\bar{V}^{l(h)}_{RW}(r^*) &= \frac{l^2 + l - 3}{4M^2} e^{\frac{r^*}{2M}-1}, \\
\varphi^{(h)}_p(r^*) &= -\frac{2\arctan\sqrt{\frac{3\delta}{4-6\delta}}}{\sqrt{\frac{\delta}{2-2\delta}}} - \frac{6\sqrt{3(\delta-1)}(\delta-1)}{(3\delta-4)\sqrt{3\delta-2}} e^{\frac{r^*}{2M}-1}, \\
\dot{r}_p(r^*) &= -1 - \frac{9(1-\delta)(4-5\delta)}{4M(4-3\delta)\sqrt{\frac{2-3\delta}{(2-\delta)(1-\delta)}}\sqrt{4-12\delta+11\delta^2-3\delta^3}} e^{\frac{r^*}{2M}-1}.
\end{aligned} \tag{A.0.1}$$

Odd modes (Regge-Wheeler):

(A.0.2)

$$\frac{F_{RW}^{lm(h)}(r_p,t)}{f^2(r_p)} = -\frac{288\pi\mu(1-\delta)^2\sqrt{2-3\delta+\delta^2}}{M\left(16-44\delta+36\delta^2-9\delta^3\right)}\frac{(l-2)!}{(l+2)!}W_{\varphi\varphi}^{*lm}\left(\frac{\pi}{2},\varphi_p\right) + \frac{864\pi\mu(1-\delta)^2\sqrt{2-3\delta+\delta^2}}{M\left(16-44\delta+36\delta^2-9\delta^3\right)}\frac{(l-2)!}{(l+2)!}W_{\varphi\varphi}^{*lm}\left(\frac{\pi}{2},\varphi_p\right)e^{\frac{r^*}{2M}-1}+o\left(R^2\right),$$

(A.0.3)

$$\frac{\partial}{\partial r}\left(\frac{F_{RW}^{lm(h)}(r_p,t)}{f(r_p)}\right) = -\frac{144\pi\mu(1-\delta)^3}{M^2(4-3\delta)(2-3\delta)\sqrt{2-3\delta+\delta^2}}\frac{(l-2)!}{(l+2)!}W_{\varphi\varphi}^{*lm}\left(\frac{\pi}{2},\varphi_p\right) + \frac{1152\pi\mu(1-\delta)^3}{M^2(4-3\delta)(2-3\delta)\sqrt{2-3\delta+\delta^2}}\frac{(l-2)!}{(l+2)!}W_{\varphi\varphi}^{*lm}\left(\frac{\pi}{2},\varphi_p\right)e^{\frac{r^*}{2M}-1}+o\left(R^2\right),$$

(A.0.4)

$$\begin{aligned}\frac{G_{RW}^{lm(h)}(r_p,t)}{f(r_p)} = &-\frac{288\pi\mu(1-\delta)^2\sqrt{2-3\delta+\delta^2}}{M^2\left(16-44\delta+36\delta^2-9\delta^3\right)}\frac{(l-2)!}{(l+2)!}W_{\varphi\varphi}^{*lm}(\frac{\pi}{2},\varphi_p)\\ &+\frac{2016\pi\mu(1-\delta)^2\sqrt{2-3\delta+\delta^2}}{M^2\left(16-44\delta+36\delta^2-9\delta^3\right)}\frac{(l-2)!}{(l+2)!}W_{\varphi\varphi}^{*lm}(\frac{\pi}{2},\varphi_p)e^{\frac{r^*}{2M}-1}\\ &-\frac{8\pi\mu\sqrt{3}\pi(1-\delta)\sqrt{\frac{2-\delta}{2-3\delta}}}{l(l+1)M^2(2-\delta)}X_{\varphi}^{*lm}(\frac{\pi}{2},\varphi_p)\\ &+\frac{12\pi\mu(1-\delta)\sqrt{\frac{6-9\delta}{2-\delta}}\left(28-63\delta+33\delta^2\right)}{l(l+1)M^2(2-3\delta)^2(4-3\delta)}X_{\varphi}^{*lm}(\frac{\pi}{2},\varphi_p)e^{\frac{r^*}{2M}-1}+o\left(R^2\right).\end{aligned}$$

Even modes (Zerilli-Moncrief):

(A.0.5)

$$\begin{aligned}&\frac{F_{ZM}^{lm(h)}(r_p,t)}{f^2(r_p)} =\\ &\frac{96\pi\mu(4-5\delta)\sqrt{2-3\delta+\delta^2}}{l\left(1+2l+2l^2+l^3\right)(4-8\delta+3\delta^2)}Y^{*lm}\left(\frac{\pi}{2},\varphi_p\right)\\ &-\frac{288\pi\mu\left(-8+8l(1-\delta)^2+8l^2(1-\delta)^2+16\delta-7\delta^2\right)\sqrt{2-3\delta+\delta^2}}{l(l+1)\left(1+l+l^2\right)^2\left(16-44\delta+36\delta^2-9\delta^3\right)}Y^{*lm}\left(\frac{\pi}{2},\varphi_p\right)e^{\frac{r^*}{2M}-1},\end{aligned}$$

(A.0.6)

$$\begin{aligned}&\frac{\partial}{\partial r}\left(\frac{F_{ZM}^{lm(h)}(r_p,t)}{f(r_p)}\right) = -\frac{48\pi\mu(1-\delta)(4-5\delta)}{l(l+1)\left(l^2+l+1\right)M(2-3\delta)\sqrt{2-3\delta+\delta^2}}Y^{*lm}\left(\frac{\pi}{2},\varphi_p\right)\\ &+\frac{96\pi\mu(1-\delta)\left(8-16\delta+6\delta^2-l\left(l+1\right)\left(40-80\delta+39\delta^2\right)\right)}{l(1+l)\left(l^2+l+1\right)^2M(4-3\delta)(2-3\delta)\sqrt{2-3\delta+\delta^2}}Y^{*lm}\left(\frac{\pi}{2},\varphi_p\right)e^{\frac{r^*}{2M}-1}\\ &+o\left(R^2\right),\end{aligned}$$

(A.0.7)

$$\frac{G_{ZM}^{lm(h)}(r_p,t)}{f(r_p)} = g_1 Y^{*lm}\left(\frac{\pi}{2},\varphi_p\right) + g_2 Z_{\varphi}^{*lm}\left(\frac{\pi}{2},\varphi_p\right) + g_3 U_{\varphi\varphi}^{*lm}\left(\frac{\pi}{2},\varphi_p\right) + g_4 V_{\varphi\varphi}^{*lm}\left(\frac{\pi}{2},\varphi_p\right) + o\left(R^2\right),$$

with

$$\begin{aligned}
g_1 = {} & \frac{8\pi\mu\sqrt{2-3\delta+\delta^2}\left(68-153\delta+81\delta^2-3l\left(l^3+2l^2-l-2\right)\left(4-9\delta+5\delta^2\right)\right)}{l(l+1)\left(l^2+l+1\right)^2 M(2-\delta)(1-\delta)(2-3\delta)} \\
& + \frac{8\pi\mu\sqrt{2-3\delta+\delta^2}e^{\frac{r^*}{2M}-1}}{l(l+1)\left(l^2+l+1\right)^3 M(2-\delta)(1-\delta)(4-3\delta)(2-3\delta)}\Bigg[296-888\delta+783\delta^2-207\delta^3 \\
& - l\left(1144-3432\delta+3369\delta^2-1089\delta^3\right)+12l^4\left(-16+48\delta-47\delta^2+15\delta^3\right) \\
& - 9l^5\left(-40+120\delta-119\delta^2+39\delta^3\right)-3l^6\left(-40+120\delta-119\delta^2+39\delta^3\right) \\
& + 3l^3\left(-328+984\delta-971\delta^2+315\delta^3\right)+4l^2\left(-424+1272\delta-1251\delta^2+405\delta^3\right)\Bigg], \\
g_2 = {} & \frac{64\pi\mu(1-\delta)\sqrt{\frac{6-9\delta}{2-\delta}}}{l(l+1)M\left(l^2+l+1\right)(2-3\delta)} \\
& - \frac{32\pi\mu\sqrt{3}(1-\delta)\left(20-45\delta+27\delta^2+\left(l^2+l\right)\left(68-153\delta+81\delta^2\right)\right)e^{\frac{r^*}{2M}-1}}{l(l+1)\left(l^2+l+1\right)^2 M(4-3\delta)(2-3\delta)\sqrt{4-8\delta+3\delta^2}}, \\
g_3 = {} & -\frac{288\pi\mu(1-\delta)^3 e^{\frac{r^*}{2M}-1}}{l(l+1)\left(l^2+l+1\right)M(4-3\delta)(2-3\delta)\sqrt{2-3\delta+\delta^2}}, \\
g_4 = {} & -\frac{576\pi\mu(1-\delta)^3}{M(4-3\delta)(2-3\delta)\sqrt{2-3\delta+\delta^2}}\frac{(l-2)!}{(l+2)!} \\
& + \frac{1728\pi\mu(1-\delta)^3}{M(4-3\delta)(2-3\delta)\sqrt{2-3\delta+\delta^2}}\frac{(l-2)!}{(l+2)!}e^{\frac{r^*}{2M}-1}.
\end{aligned}$$

* *

Summary

* *

"On September 14, 2015 at 09:50:45 UTC the two detectors of the Laser Interferometer Gravitational-Wave Observatory simultaneously observed a transient gravitational-wave signal" such is the beginning of the first paper in Gravitational Wave (GW) astronomy ever, issued on 12 February 2016 [4], exactly a hundred years after the first prediction of GWs by Einstein himself [30]. The detection of gravitational waves has been a long awaited event[1], it is the result of long-lasting efforts, and contributes to make our epoch a very exciting one. This discovery is of a fundamental importance not only because it fully confirms the current theory of the gravitational interaction -General Relativity (GR)- in regions which we have never been able to test before, but also because it represents the first of a series of other similar observations which altogether will give us a completely new view on the universe.

The detection of Gravitational Waves

Two detectors are involved in this discovery, one in Hanford, Washington and the other at Livingston, Louisiana, in the US. Both these *interferometers* are part of the LIGO experiment, and their data, including the mentioned formidable detection, have been analysed by the joint collaboration of LIGO and Virgo (another interferometer experiment situated in Italy, soon starting to take data too). In simple terms, an interferometer is a big experimental set-up with laser and mirrors, where the laser beams travel along two orthogonal arms and then recombine together. The purpose of the experiment is that if a gravitational-wave signal passes by the interferometer, then the laser undergoes tiny deformations that can be noticed when the laser beams recombine. The principle is not different from similar optical set-ups, but what makes it incredible is the precision that has to be reached in order to hear a gravitational wave. To give an idea, the inteferometer has to be so sensitive to measure a variation of distance smaller than an atom over a total path the size of the distance Earth-Sun!

It takes long time and technological progress and efforts to reach such sensitivities, and this is all justified by the quest for gravitational waves. These have been first theoretically predicted, but what truly convinced scientists to invest their time and energy into gravitational waves' hunt was the collection of indirect proofs of their existence that we

[1] The detection event itself has been named GW150914, with obvious referral to the date.

kept gathering until nowadays. The most notorious one was the observation of a binary pulsar[2] (a couple of rotating neutron stars emitting a beam of electromagnetic radiation) whose behaviour could only be explained with gravitational wave emission. This discovery in 1974 was worth a Nobel prize to in 1993. Forty years later we observed GW150914, a binary system of black holes emitting gravitational waves.

Before GW150914 we were able to see the sky only thanks to electromagnetic radiation, be it light (from our naked eye looking up above on a clear night to the powerful telescopes of remote observatories), be it other non-visible radiation (caught by huge antennas such as in radiotelescopes or other devices). Now we can "hear" the universe with a different tool, interferometers, and this is just like going from old silent films to present-day movies: a whole new pack of information is now available to us. Moreover the first detection of gravitational waves brings along other discoveries relevant on their own, namely the detected waveforms come from a system of two black holes inspiraling and then merging together. This is a confirmation of the existence of black-hole binaries and also the first detection ever of a black-hole merger. Physicists have many good reasons for being excited.

General Relativity as the theory of Gravity

All these fascinating phenomena, gravitational waves and black holes, stem out of the theory of General Relativity, which we owe mainly to Einstein's work, and that constitutes the best explanation we currently have experimentally tested for gravity. Without this theory, we would have not predicted these astrophysical wonders and therefore not even observed them. Since the first experiments by Galilei on free fall, and Newton's law of universal gravitation explaining Kepler's empirical laws for the motion of planets, to nowadays satellites and GPS system, we have come a long way. In Einstein's general relativity picture space and time are not independent, but coupled together into a new entity: spacetime. While with Newtonian gravity the Earth is attracted by the gravitational force of the Sun, in the new general-relativistic picture the Earth is moving freely, but in a geometry curved by the mass of the Sun, therefore it is not following a straight-line path, but rather an elliptic orbit around the Sun. The usual image of spacetime provided by GR is that of a carpet extending throughout space and time where astrophysical objects move according to its curvature, its bendings. In this pictorial representation gravitational waves are ripples, vibrations of the carpet itself, propagating along spacetime, and black holes are holes, sinks, engulfing whatever comes too close to them, beyond the so-called "event horizon" of the black hole. Even light does not escape from them, therefore they are black.

However, black holes move and by doing so the spacetime carpet gets wrinkled and the ripples propagate: moving black holes, or more generally moving masses, generate gravitational waves in spacetime. We have built specific "antennas" -the interferometers- to feel these waves and we recently succeeded. This would have not been possible if we

[2]The pulsar is named PSR B1913+16, or more commonly known as the Hulse-Taylor binary pulsar, from the names of its discoverers. After this pulsar, similar others have been found.

had not first developed predictions and models for the signal to be detected and for the black holes generating it.

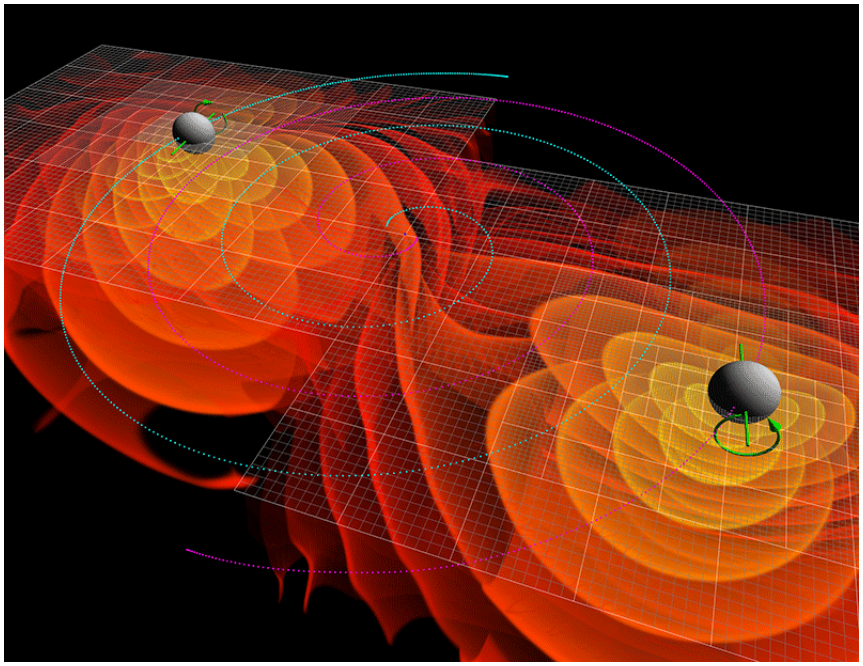

Numerical simulations of the gravitational waves (in red/orange) produced by inspiraling black holes. The blue and purple curves represent their orbits, while the green arrows their spins. Simulation credit to C. Henze/NASA Ames Research Center.

The thesis

This thesis is concerned with the study of pairs of compact objects -binary systems- that can be black holes or other kind of astrophysical objects, such as neutron stars[3]. In particular this thesis is devoted to models for the orbit of these objects and to the effect of other parameters, such as the spin (the content of the second part of this dissertation), in order to make predictions for the emitted gravitational radiation. For instance, a black-hole binary is a system of two black holes orbiting around each other for very long time and eventually merging into a unique final black hole. This whole process is commonly called "coalescence", from Latin *coalescere*, that is literally joining together. The kind of coalescence and its behaviour are strictly dependent on the masses of the two black holes and their spins. The black holes in the binary detected in GW150914 have masses respectively of 36 and 29 $M_\odot$, so they have comparable masses[4]. Whenever the mass

[3]Neutron stars are the densest and smallest stars known to exist in the Universe and are composed almost entirely of neutrons; gravitational waves from neutron star systems can help us define better their inner structure.

[4]$M_\odot = (1.98855 \pm 0.00025) \times 10^{30}$ kg is the solar mass, the mass of the Sun.

ratio of the two objects is smaller than 1 in 100000, that is one of the two has a mass at least 10^5 times bigger than the other, the binary is an Extreme Mass Ratio binary (EMR). Usually in order to justify such big masses the only possibility is that the heavier body is a Supermassive Black Hole, with a mass $\sim 10^6 M_\odot$. This distinction between comparable-mass binaries and EMR binaries is crucial in identifying the time scale of the phenomena at hand, the frequency of the emitted gravitational waves, and the techniques that can be employed to describe these systems. Extreme-mass-ratio binaries[5] are the main topic of investigation of this thesis.

Despite these distinctions, the qualitative behaviour of different-mass-ratio binaries is the same: the first, long part consists of the two objects orbiting around each other in slowly shrinking orbits, in the second part they spiral towards each other. This happens because during their motion they lose energy through emission of gravitational waves. After this phase, called *inspiral*, the two bodies rapidly accelerate their motion, the amplitude and frequency of the emitted radiation increases: the two components are merging -*merger* phase- and one is left with the end result of the coalescence, a final massive object. Next comes the *ringdown* phase where most of the energy has been radiated away and the system is stabilising into a new-born star, or more commonly a new-born black hole. For an extreme-mass-ratio binary the center of gravity of this motion is practically inside the major body, so it is more intuitive to describe everything as the minor body orbiting around its companion (which can always be done with the appropriate coordinate system). One sees then that the orbit of the minor body turns from an eccentric one to a more circular one during the inspiral, until the Last Stable Orbit is reached. Afterwards the motion is more radial and this stage is commonly referred to as *plunge*, because the minor body is like plunging into the other before merging.

As one can already understand from the title of this dissertation, the study of extreme-mass-ratio binaries has mostly focused on this last stage of the coalescence, after the last stable orbit, by employing a special kind of orbits developed to this aim, the *ballistic* orbits. We named them ballistic because they can be used to represent a body shot from the black hole towards the outer space, and then coming back to it. With some mathematical modifications they offer unique features good to describe the last phase of the EMR binary. This is contained in [19] and chapter 3 of this thesis. A way to address some problems raised by these orbits by using other clever methods of orbit perturbation (geodesic deviation's method) is discussed in chapter 4, turning the ballistic orbit into a very versatile tool for binary coalescences.

Moreover, in the second part of the thesis we introduced a new formalism to treat the spin, namely the rotation, of the minor body. This is also an old topic in the scientific literature dedicated to general relativity, for which different approaches have been developed, and it is of vital importance to describe the effects of spin of the components of a binary, see [26, 27] or chapter 5 of this thesis. Usual compact objects involved in binary systems, such as neutron stars or black holes, rotate and therefore have spin. This affects the orbital motion and the gravitational waves emitted by the binary. Therefore it is important to include the spin into the description of binary coalescences.

[5] Sometimes people refer to EMRI's, EMR Inspirals, rather than simply EMR binaries, but the *inspiral* is only one phase of the coalescence of a binary system, not the whole evolution.

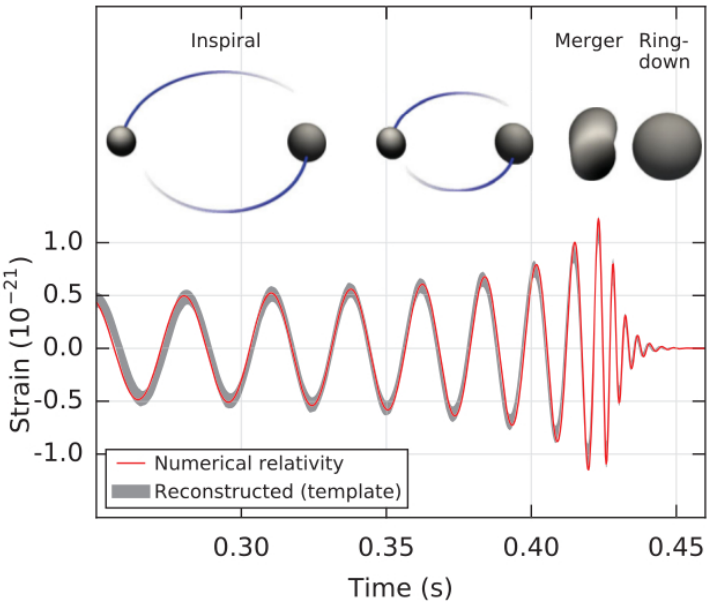

Image from the GW150914 discovery paper [4]. The panel shows the reconstructed gravitational wave together with the corresponding different stages of the black-hole binary coalescence, represented by the two black shapes.

The future

As we already mentioned, the black holes detected by the gravitational-wave interferometer LIGO have comparable mass, while the ones involved in EMR binaries have a big mass difference. The ground-based interferometers such as LIGO, Virgo, and the coming ones in Japan and India are not big enough to detect the lower frequencies of gravitational waves emitted by extreme-mass-ratio binaries. We need longer arms, we need less background noise, therefore we need to go into space. This is the reason why we are now building a space-based interferometer, made up of three satellites orbiting above the Earth: eLISA (from *evolving* LISA, current upgrade of the previous experiment). The international collaboration supporting this experiment managed so far to send into space some part of it, the Lisa Pathfinder, but the full completion and launch of the mission is scheduled by 2034. Hopefully by that time we will detect also the extreme-mass-ratio binaries and other softer gravitational sounds from the universe.

Before that though, we need to study the possible sources of gravitational waves and get prepared making predictions of the signal. The research contained in this thesis is another step in that direction, and surely more needs to be done. Moreover we can consider ourselves lucky, because the detections coming from the ground-based interferometers will provide us more information and help us also with understanding EMR binaries. As we said, the era of gravitational-wave astronomy has just begun.

The study of binary coalescences, the detection of gravitational waves, and the tech-

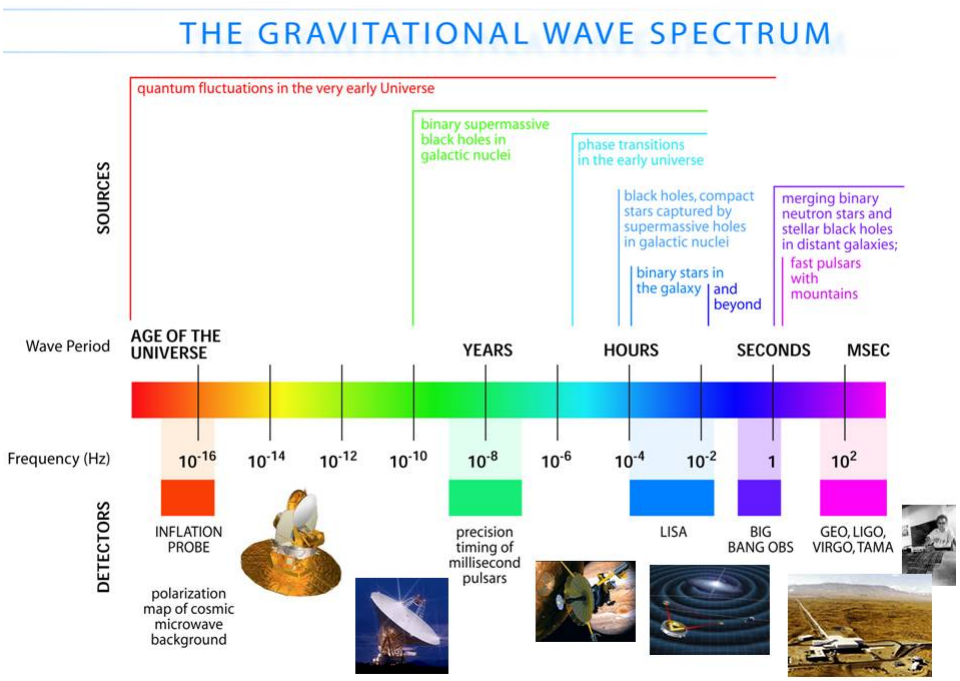

The gravitational wave spectrum. Today we have access only to the far right of the spectrum; eLISA will provide us information from supermassive black holes and extreme-mass-ratio binaries.

nological advancement are all part of the same scientific quest aimed at explaining the most common of the physical interactions in our everyday life: gravity. It should be clear by now that GWs were not a casual discovery, one of those serendipitous events like the discovery of penicillin by A. Fleming, but rather the fruit of decades-long efforts and many-people collaboration. This discovery, as the content of this thesis, fit in the framework of general relativity. It is in this theory that gravitational waves were first predicted. It is with this paradigm of the gravitational interaction that black holes and compact binaries were born and the quest for experimental confirmation started. General Relativity, Einstein's creature, has proven once again to be a successful explanation for the gravitational interaction. Although we know that we need to reconcile it with quantum mechanics somehow, since there are still many open problems lurking at microscopic scales, maybe we will already learn new fundamental facts with gravitational-wave astronomy[6]. After all, beforehand we could only see it, but now we can even hear it: the universe is out there to be explored.

[6]For instance the discovery GW150914 already allowed us to put bounds on the mass of the graviton: we do not know yet if it exists, but suppose it exists, it cannot be heavier than $1.2 \times 10^{-22} eV/c^2$.

The success of a paradigm -whether Aristotle's analysis of motion, Ptolemy's computations of planetary positions, Lavoisier's application of the balance, or Maxwell's mathematization of the electromagnetic field- is at the start largely a promise of success discoverable in selected and still incomplete examples. Normal science consists in the actualization of that promise, an actualization achieved by extending the knowledge of those facts that the paradigm displays as particularly revealing, by increasing the extent of the match between those facts and the paradigm's predictions, and by further articulation of the paradigm itself.
Few people who are not actually practicioners of a mature science realize how much mop-up work of this sort a paradigm leaves to be done or quite how fascinating such work can prove in the execution.

-T.S. Kuhn, The Structure of Scientific Revolutions

* *

Bibliography

* *

[1] C. M. Will, "The Confrontation between General Relativity and Experiment," *Living Rev.Rel.* **17** (2014) 4, arXiv:1403.7377 [gr-qc].

[2] M. Maggiore, *Gravitational waves. Volume 1: theory and experiments.* Oxford Univ. Press, Oxford, 2008.

[3] T. Damour, "1974: the discovery of the first binary pulsar," arXiv:1411.3930 [gr-qc].

[4] B. Abbott *et al.*, "Observation of Gravitational Waves from a Binary Black Hole Merger,"*Phys. Rev. Lett.* **116** (Feb, 2016) 061102. http://link.aps.org/doi/10.1103/PhysRevLett.116.061102.

[5] E. Berti, A. Buonanno, and C. M. Will, "Estimating spinning binary parameters and testing alternative theories of gravity with LISA," *Phys.Rev.* **D71** (2005) 084025, arXiv:gr-qc/0411129 [gr-qc].

[6] C. F. Sopuerta and N. Yunes, "Extreme and Intermediate-Mass Ratio Inspirals in Dynamical Chern-Simons Modified Gravity," *Phys.Rev.* **D80** (2009) 064006, arXiv:0904.4501 [gr-qc].

[7] B. Sathyaprakash and B. Schutz, "Physics, Astrophysics and Cosmology with Gravitational Waves," *Living Rev.Rel.* **12** (2009) 2, arXiv:0903.0338 [gr-qc].

[8] **Virgo, LIGO Scientific** , B. P. Abbott *et al.*, "Tests of general relativity with GW150914," arXiv:1602.03841 [gr-qc].

[9] S. B. Giddings, "Gravitational wave tests of quantum modifications to black hole structure," arXiv:1602.03622 [gr-qc].

[10] **Virgo Collaboration** , T. Accadia *et al.*, "Calibration and sensitivity of the Virgo detector during its second science run," *Class.Quant.Grav.* **28** (2011) 025005, arXiv:1009.5190 [gr-qc].

[11] **KAGRA Collaboration** , K. Somiya, "Detector configuration of KAGRA: The Japanese cryogenic gravitational-wave detector," *Class.Quant.Grav.* **29** (2012) 124007, arXiv:1111.7185 [gr-qc].

[12] **eLISA Collaboration** , P. A. Seoane *et al.*, "The Gravitational Universe," arXiv:1305.5720 [astro-ph.CO].

[13] E. Berti *et al.*, "Testing General Relativity with Present and Future Astrophysical Observations," *Class. Quant. Grav.* **32** (2015) 243001, arXiv:1501.07274 [gr-qc].

[14] K. Riles, "Gravitational Waves: Sources, Detectors and Searches," *Prog.Part.Nucl.Phys.* **68** (2013) 1–54, arXiv:1209.0667 [hep-ex].

[15] S. Babak, J. R. Gair, and R. H. Cole, "Extreme mass ratio inspirals: perspectives for their detection," arXiv:1411.5253 [gr-qc].

[16] T. Regge and J. A. Wheeler, "Stability of a Schwarzschild singularity," *Phys.Rev.* **108** (1957) 1063–1069.

[17] G. Koekoek and J. van Holten, "Epicycles and Poincaré Resonances in General Relativity," *Phys.Rev.* **D83** (2011) 064041, arXiv:1011.3973 [gr-qc].

[18] G. Koekoek and J. van Holten, "Geodesic deviations: modeling extreme mass-ratio systems and their gravitational waves," *Class.Quant.Grav.* **28** (2011) 225022, arXiv:1103.5612 [gr-qc].

[19] G. d'Ambrosi and J. van Holten, "Ballistic orbits in Schwarzschild space-time and gravitational waves from EMR binary mergers," *Class.Quant.Grav.* **32** (2015) no. 1, 015012, arXiv:1406.4282 [gr-qc].

[20] C. O. Lousto and R. H. Price, "Understanding initial data for black hole collisions," *Phys.Rev.* **D56** (1997) 6439–6457, arXiv:gr-qc/9705071 [gr-qc].

[21] A. Buonanno and T. Damour, "Transition from inspiral to plunge in binary black hole coalescences," *Phys.Rev.* **D62** (2000) 064015, arXiv:gr-qc/0001013 [gr-qc].

[22] S. Bernuzzi and A. Nagar, "Binary black hole merger in the extreme-mass-ratio limit: a multipolar analysis," *Phys.Rev.* **D81** (2010) 084056, arXiv:1003.0597 [gr-qc].

[23] M. Mathisson, "Neue mechanik materieller systemes," *Acta Phys.Polon.* **6** (1937) 163–2900.

[24] A. Papapetrou, "Spinning test particles in general relativity. 1.," *Proc.Roy.Soc.Lond.* **A209** (1951) 248–258.

[25] L. F. O. Costa, C. A. Herdeiro, J. Natario, and M. Zilhao, "Mathisson's helical motions for a spinning particle: Are they unphysical?," *Phys.Rev.* **D85** (2012) 024001, arXiv:1109.1019 [gr-qc].

[26] G. d'Ambrosi, S. Satish Kumar, and J. W. van Holten, "Covariant hamiltonian spin dynamics in curved spacetime," *Phys. Lett.* **B743** (2015) 478–483, arXiv:1501.04879 [gr-qc].

[27] G. d'Ambrosi, S. Satish Kumar, J. van de Vis, and J. van Holten, "Spinning bodies in curved spacetime," *Phys. Rev.* **D93** (2016) no. 4, 044051, arXiv:1511.05454 [gr-qc].

[28] I. Khriplovich and A. Pomeransky, "Equations of motion of spinning relativistic particle in external fields," *Surveys High Energ.Phys.* **14** (1999) 145–173, arXiv:gr-qc/9809069 [gr-qc].

[29] S. Weinberg, *Gravitation and Cosmology: Principles and Applications of the General Theory of Relativity*. Wiley New York, New York, 1972.

[30] A. Einstein, "Die Grundlagen der Allgemeinen Relativitätstheorie. (German) [The foundations of the Theory of General Relativity]," *Annalen der Physik* **354** (1916) no. 7, 769–822.

[31] U. J. J. Le Verrier, "Détermination de l'orbite de Mercure et de ses perturbations," *Comptes Rendues de l'Académie des Sciences* **16** (1843) 1054–1065.

[32] A. Einstein, "Erklärung der Perihelbewegung des Merkur aus der allgemeinen Relativitätstheorie. (German) [Explanation of the perihelical motion of Mercury from the General Theory of Relativity]," *Sitzungsberichte der Preussischen Akademie der Wissenschaften zu Berlin* (1915) 831–839.

[33] A. Calaprice, *The new quotable Einstein*. Princeton Univ. Press, Princeton, 2000.

[34] S. Refsdal, "The gravitational lens effect," *Mon.Not.Roy.Astron.Soc.* **128** (1964) 295–306.

[35] R. V. Pound and G. A. Rebka, "Apparent weight of photons," *Phys. Rev. Lett.* **4** (Apr, 1960) 337–341. http://link.aps.org/doi/10.1103/PhysRevLett.4.337.

[36] R. A. Hulse and J. H. Taylor, "Discovery of a pulsar in a binary system," *The Astrophysical Journal Letters* **195** (1975) L51–L53.

[37] G. Galilei, *Discorsi e dimostrazioni mathematiche intorno a due nuove scienze. (Italian) [Two new sciences]*. Elsevier, Leiden, the Netherlands, 1638.

[38] E. Fischbach, G. T. Gillies, D. E. Krause, J. G. Schwan, and C. Talmadge, "Non-newtonian gravity and new weak forces: an index of measurements and theory," *Metrologia* **29** (1992) no. 3, 213–260. http://stacks.iop.org/0026-1394/29/i=3/a=001.

[39] "MICROSCOPE project home page, CNES,". https://microscope.cnes.fr/fr.

[40] E. Di Casola, S. Liberati, and S. Sonego, "Nonequivalence of equivalence principles," *Am. J. Phys.* **83** (2015) 39, arXiv:1310.7426 [gr-qc].

[41] A. Einstein, "Zur Elektrodynamik bewegter Körper. (German) [On the electrodynamics of moving bodies]," *Annalen der Physik (1900) (series 4)* **322** (1905) no. 10, 891–921.

[42] D. W. Sciama, "The physical structure of general relativity,"*Rev. Mod. Phys.* **36** (Jan, 1964) 463–469. http://link.aps.org/doi/10.1103/RevModPhys.36.463.

[43] C. W. Misner, K. S. Thorne, and J. A. Wheeler, *Gravitation*. 1973.

[44] B. Schutz, *Geometrical methods for mathematical physics*. Cambridge University Press, Cambridge, 1980.

[45] F. W. Hehl, "Gauge Theory of Gravity and Spacetime," arXiv:1204.3672 [gr-qc].

[46] A. Einstein, "Die Feldgleichungen der Gravitation. (German) [The field equations of gravitation]," *Sitzungsberichte der Preussischen Akademie der Wissenschaften zu Berlin* (1915) 844–847.

[47] S. Chandrasekhar, *The mathematical theory of black holes*. Oxford classic texts in the physical sciences. Oxford Univ. Press, Oxford, 2002.

[48] E. Poisson, *A relativist's toolkit*. Cambridge University Press, 2004.

[49] **LIGO Scientific Collaboration** , J. Aasi *et al.*, "Advanced LIGO," *Class. Quant. Grav.* **32** (2015) 074001, arXiv:1411.4547 [gr-qc].

[50] L. D. Landau and E. M. Lifshitz, *The classical theory of fields*. Pergamon Press Ltd., Headington Hill Hall, Oxford, 1971.

[51] E. Poisson and C. M. Will, *Gravity: Newtonian, Post-Newtonian, Relativistic*. Cambridge University Press, Cambridge, 2014.

[52] S. Mirshekari, *Gravitational Waves and Inspiraling Compact Binaries in Alternative Theories of Gravity*. PhD thesis, Washington U., St. Louis, 2013. arXiv:1308.5240 [gr-qc]. https://inspirehep.net/record/1250753/files/arXiv:1308.5240.pdf.

[53] L. Blanchet, "Gravitational Radiation from Post-Newtonian Sources and Inspiralling Compact Binaries," *Living Rev. Relativity* **17** (2014) . http://www.livingreviews.org/lrr-2014-2.

[54] J. Weber, *General Relativity and Gravitational Waves*. Wiley Interscience, New York, 1961.

[55] S. Burke-Spolaor, "Gravitational-Wave Detection and Astrophysics with Pulsar Timing Arrays," arXiv:1511.07869 [astro-ph.IM].

[56] K. Belczynski, S. Repetto, D. Holz, R. O'Shaughnessy, T. Bulik, E. Berti, C. Fryer, and M. Dominik, "Comparison of LIGO/Virgo upper limits with predicted compact binary merger rates," arXiv:1510.04615 [astro-ph.HE].

[57] **LIGO Scientific Collaboration** , J. Aasi *et al.*, "Gravitational waves from known pulsars: results from the initial detector era," *Astrophys. J.* **785** (2014) 119, arXiv:1309.4027 [astro-ph.HE].

[58] A. Vilenkin and E. P. S. Shellard, *Cosmic Strings and other topological defects*. Cambridge Monographs on Mathematical Physics. Cambridge Univ. Press, Cambridge, 2000.

[59] X. Siemens, V. Mandic, and J. Creighton, "Gravitational wave stochastic background from cosmic (super)strings," *Phys. Rev. Lett.* **98** (2007) 111101, arXiv:astro-ph/0610920 [astro-ph].

[60] **BICEP2 Collaboration** , P. Ade *et al.*, "Detection of B-Mode Polarization at Degree Angular Scales by BICEP2," *Phys.Rev.Lett.* **112** (2014) 241101, arXiv:1403.3985 [astro-ph.CO].

[61] **BICEP2, Planck collaborations** , P. Ade *et al.*, "Joint Analysis of BICEP2/Keck Array and Planck Data," *Phys. Rev. Lett.* **114** (2015) 101301, arXiv:1502.00612 [astro-ph.CO].

[62] L. Blanchet, S. Detweiler, A. Le Tiec, and B. F. Whiting, "High-order post-Newtonian fit of the gravitational self-force for circular orbits in the Schwarzschild geometry," *Phys. Rev. D* **81** (2010) 084033. http://link.aps.org/doi/10.1103/PhysRevD.81.084033.

[63] B. Bruegmann, "Numerical relativity in (3+1)-dimensions," *Annalen Phys.* **9** (2000) 227–246, arXiv:gr-qc/9912009 [gr-qc].

[64] G. B. Cook, "Initial Data for Numerical Relativity," *Living Rev. Relativity* **3** (2000) 5. http://www.livingreviews.org/lrr-2000-5.

[65] M. Alcubierre and B. Bruegmann, "Simple excision of a black hole in (3+1)-numerical relativity," *Phys.Rev.* **D63** (2001) 104006, arXiv:gr-qc/0008067 [gr-qc].

[66] M. Alcubierre, B. Bruegmann, D. Pollney, E. Seidel, and R. Takahashi, "Black hole excision for dynamic black holes," *Phys.Rev.* **D64** (2001) 061501, arXiv:gr-qc/0104020 [gr-qc].

[67] P. Galaviz, B. Bruegmann, and Z. Cao, "Numerical evolution of multiple black holes with accurate initial data," *Phys.Rev.* **D82** (2010) 024005, arXiv:1004.1353 [gr-qc].

[68] M. Hannam, S. Husa, F. Ohme, D. Muller, and B. Bruegmann, "Simulations of black-hole binaries with unequal masses or nonprecessing spins: Accuracy, physical properties, and comparison with post-Newtonian results," *Phys.Rev.* **D82** (2010) 124008, arXiv:1007.4789 [gr-qc].

[69] A. Buonanno and T. Damour, "Effective one-body approach to general relativistic two-body dynamics," *Phys.Rev.* **D59** (1999) 084006, arXiv:gr-qc/9811091 [gr-qc].

[70] E. Barausse and A. Buonanno, "An Improved effective-one-body Hamiltonian for spinning black-hole binaries," *Phys.Rev.* **D81** (2010) 084024, arXiv:0912.3517 [gr-qc].

[71] Y. Pan, A. Buonanno, M. Boyle, L. T. Buchman, L. E. Kidder, *et al.*, "Inspiral-merger-ringdown multipolar waveforms of nonspinning black-hole binaries using the effective-one-body formalism," *Phys.Rev.* **D84** (2011) 124052, arXiv:1106.1021 [gr-qc].

[72] A. Taracchini, Y. Pan, A. Buonanno, E. Barausse, M. Boyle, *et al.*, "Prototype effective-one-body model for nonprecessing spinning inspiral-merger-ringdown waveforms," *Phys.Rev.* **D86** (2012) 024011, arXiv:1202.0790 [gr-qc].

[73] S. Teukolsky, "Rotating black holes - separable wave equations for gravitational and electromagnetic perturbations," *Phys.Rev.Lett.* **29** (1972) 1114–1118.

[74] L. Barack, "Gravitational self force in extreme mass-ratio inspirals," *Class.Quant.Grav.* **26** (2009) 213001, arXiv:0908.1664 [gr-qc].

[75] B. Wardell, "Self-force: Computational Strategies," arXiv:1501.07322 [gr-qc].

[76] K. Schwarzschild, "Über das Gravitationsfeld eines Massenpunktes nach der Einsteinschen Theorie," *Sitzungsberichte der Königlichen Prussischen Akademie der Wissenschaften* **7** (1916) 189–196.

[77] A. Strominger and C. Vafa, "Microscopic origin of the Bekenstein-Hawking entropy," *Phys. Lett.* **B379** (1996) 99–104, arXiv:hep-th/9601029 [hep-th].

[78] R. Emparan and H. S. Reall, "Black Holes in Higher Dimensions," *Living Rev. Rel.* **11** (2008) 6, arXiv:0801.3471 [hep-th].

[79] O. Aharony, S. S. Gubser, J. M. Maldacena, H. Ooguri, and Y. Oz, "Large N field theories, string theory and gravity," *Phys. Rept.* **323** (2000) 183–386, arXiv:hep-th/9905111 [hep-th].

[80] H. Nastase, "Introduction to AdS-CFT," arXiv:0712.0689 [hep-th].

[81] P. Townsend, "Black holes: Lecture notes," arXiv:gr-qc/9707012 [gr-qc].

[82] L. Ferrarese and H. Ford, "Supermassive black holes in galactic nuclei: Past, present and future research," *Space Sci.Rev.* **116** (2005) 523–624, arXiv:astro-ph/0411247 [astro-ph].

[83] **Perimeter Institute for Theoretical Physics** , A. E. Broderick *et al.*, "The Event Horizon of M87," arXiv:1503.03873 [astro-ph.HE].

[84] R. Penrose, "Gravitational collapse: The role of general relativity," *Riv. Nuovo Cim.* **1** (1969) 252–276. [Gen. Rel. Grav.34,1141(2002)].

[85] A. Petrov, "Classification of spaces defined by gravitational fields," *Sci. Nat. Kazan State University* **114** (1954) 55–69.

[86] F. Pirani, "Invariant formulation of gravitational radiation theory," *Phys.Rev.* **105** (1957) 1089–1099.

[87] G. Birkhoff, *Relativity and Modern Physics*. Harvard Univ. Press, Cambridge, Massachussets, 1923.

[88] Lemaître, Georges, "L'Univers en expansion," *Annales de la Societé scientifique de Bruxelles* **A53** 51–85.

[89] W. G. Unruh, "Universal coordinates for Schwarzschild black holes," `arXiv:1401.3393 [gr-qc]`.

[90] D. Finkelstein, "Past-Future Asymmetry of the Gravitational Field of a Point Particle," *Phys.Rev.* **110** (1958) 965–967.

[91] M. Kruskal, "Maximal extension of Schwarzschild metric," *Phys.Rev.* **119** (1960) 1743–1745.

[92] F. Zerilli, "Gravitational field of a particle falling in a Schwarzschild geometry analyzed in tensor harmonics," *Phys.Rev.* **D2** (1970) 2141–2160.

[93] V. Moncrief, "Gravitational perturbations of spherically symmetric systems. I. The exterior problem.," *Annals Phys.* **88** (1974) 323–342.

[94] O. Sarbach and M. Tiglio, "Gauge invariant perturbations of Schwarzschild black holes in horizon penetrating coordinates," *Phys. Rev.* **D64** (2001) 084016, `arXiv:gr-qc/0104061 [gr-qc]`.

[95] K. Martel and E. Poisson, "Gravitational perturbations of the Schwarzschild spacetime: A Practical covariant and gauge-invariant formalism," *Phys.Rev.* **D71** (2005) 104003, `arXiv:gr-qc/0502028 [gr-qc]`.

[96] P. Ritter, *Ondes gravitationnelles et calcul de la force propre pour un astre compact en mouvement autour d'un trou noir super-massif*. PhD thesis, Université d'Orléans, Orléans, 2013.

[97] K. Martel, *Particles and black holes: time-domain integration of the equations of black-hole perturbation theory*. PhD thesis, Guelph, 2004.

[98] J. D. Jackson, *Classical Electrodynamics*. John Wiley and Sons, New York, 1962.

[99] R. A. Isaacson, "Gravitational Radiation in the Limit of High Frequency. II. Nonlinear Terms and the Effective Stress Tensor," *Phys. Rev.* **166** (1968) 1272–1279.

[100] S. Chandrasekhar and S. Detweiler, "The quasi-normal modes of the Schwarzschild black hole," *Proc.Roy.Soc.Lond. A* **344** (1975) 441–452.

[101] A. Nagar and L. Rezzolla, "Gauge-invariant non-spherical metric perturbations of Schwarzschild black-hole spacetimes," *Class.Quant.Grav.* **22** (2005) R167, `arXiv:gr-qc/0502064 [gr-qc]`.

[102] S. Hadar and B. Kol, "Post-innermost stable circular orbit ringdown amplitudes in extreme mass ratio inspiral," *Phys. Rev. D* **84** (Aug, 2011) 044019. http://link.aps.org/doi/10.1103/PhysRevD.84.044019.

[103] Y. Décanini, A. Folacci, and M. Ould El Hadj, "Waveforms produced by a scalar point particle plunging into a Schwarzschild black hole: Excitation of quasinormal modes and quasibound states," *Phys. Rev.* **D92** (2015) no. 2, 024057, arXiv:1506.09133 [gr-qc].

[104] P. Ritter, A. D. Spallicci, S. Aoudia, and S. Cordier, "Fourth order indirect integration method for black hole perturbations: Even modes," *Class.Quant.Grav.* **28** (2011) 134012, arXiv:1102.2404 [gr-qc].

[105] G. Koekoek, *The Geodesic Deviation Method and Extreme Mass-Ratio Systems. Theoretical methods and application to the calculation of gravitational waves.* PhD thesis, Vrije U., Amsterdam, 2011. https://inspirehep.net/record/1081429/files/Thesis-2011-Koekoek.pdf.

[106] K. Martel and E. Poisson, "One-parameter family of time-symmetric initial data for the radial infall of a particle into a Schwarzschild black hole," *Phys. Rev. D* **66** (Oct, 2002) 084001. http://link.aps.org/doi/10.1103/PhysRevD.66.084001.

[107] R. Kerner, J. van Holten, and J. Colistete, R., "Relativistic epicycles: Another approach to geodesic deviations," *Class.Quant.Grav.* **18** (2001) 4725–4742, arXiv:gr-qc/0102099 [gr-qc].

[108] J. van Holten, "Worldline deviations and epicycles," *Int.J.Mod.Phys.* **A17** (2002) 2764, arXiv:hep-th/0201083 [hep-th].

[109] C. Cutler, D. Kennefick, and E. Poisson, "Gravitational radiation reaction for bound motion around a Schwarzschild black hole," *Phys.Rev.* **D50** (1994) 3816–3835.

[110] J. B. Hartle, *Gravity.* Addison Wesley, San Francisco, 2003.

[111] R. Fujita and W. Hikida, "Analytical solutions of bound timelike geodesic orbits in Kerr spacetime," *Classical and Quantum Gravity* **26** (2009) no. 13, 135002. http://stacks.iop.org/0264-9381/26/i=13/a=135002.

[112] Hackmann, Eva and Lämmerzahl, Claus and Kagramanova, Valeria and Kunz, Jutta, "Analytical solution of the geodesic equation in Kerr-(anti-) de Sitter space-times," *Phys. Rev. D* **81** (Feb, 2010) 044020. http://link.aps.org/doi/10.1103/PhysRevD.81.044020.

[113] T. Futamase and Y. Itoh, "The post-Newtonian approximation for relativistic compact binaries," *Living Rev. Relativity* **10** (2007) 2. http://www.livingreviews.org/lrr-2007-2.

[114] S. Chandrasekhar *Notes and Records of the Royal society of London* **30** (1976) 249–260.

[115] W. Sullivan, *Black Holes.* Anchor Press, Doubleday, Garden City, New York, 1979.

[116] P. Fromholz, E. Poisson, and C. M. Will, "The Schwarzschild metric: It's the coordinates, stupid!," *Am.J.Phys.* **82** (2014) 295, arXiv:1308.0394 [gr-qc].

[117] R. P. Kerr, "Gravitational field of a spinning mass as an example of algebraically special metrics," *Phys.Rev.Lett.* **11** (1963) 237–238.

[118] A. Balakin, J. van Holten, and R. Kerner, "Motions and worldline deviations in Einstein-Maxwell theory," *Class.Quant.Grav.* **17** (2000) 5009–5024, arXiv:gr-qc/0009016 [gr-qc].

[119] P. P. Fiziev, "Exact solutions of Regge-Wheeler equation," *J.Phys.Conf.Ser.* **66** (2007) 012016, arXiv:gr-qc/0702014 [GR-QC].

[120] S. Mano, H. Suzuki, and E. Takasugi, "Analytic solutions of the Regge-Wheeler equation and the postMinkowskian expansion," *Prog. Theor. Phys.* **96** (1996) 549–566, arXiv:gr-qc/9605057 [gr-qc].

[121] T. Damour and A. Nagar, "Binary black hole merger waveforms in the extreme mass ratio limit," arXiv:gr-qc/0612151 [gr-qc].

[122] A. Nagar, T. Damour, and A. Tartaglia, "Binary black hole merger in the extreme mass ratio limit," *Class.Quant.Grav.* **24** (2007) S109–S124, arXiv:gr-qc/0612096 [gr-qc].

[123] S. Hopper and C. R. Evans, "Gravitational perturbations and metric reconstruction: Method of extended homogeneous solutions applied to eccentric orbits on a Schwarzschild black hole," *Phys.Rev.* **D82** (2010) 084010, arXiv:1006.4907 [gr-qc].

[124] T. Damour, A. Nagar, and S. Bernuzzi, "Improved effective-one-body description of coalescing nonspinning black-hole binaries and its numerical-relativity completion," *Phys.Rev. D* **87** (2013) 084035.

[125] A. Ori and K. S. Thorne, "The Transition from inspiral to plunge for a compact body in a circular equatorial orbit around a massive, spinning black hole," *Phys. Rev.* **D62** (2000) 124022, arXiv:gr-qc/0003032 [gr-qc].

[126] O'Shaughnessy, R., "Transition from inspiral to plunge for eccentric equatorial Kerr orbits,"*Phys. Rev. D* **67** (Feb, 2003) 044004. http://link.aps.org/doi/10.1103/PhysRevD.67.044004.

[127] Sundararajan, Pranesh A., "Transition from adiabatic inspiral to geodesic plunge for a compact object around a massive Kerr black hole: Generic orbits,"*Phys. Rev. D* **77** (Jun, 2008) 124050. http://link.aps.org/doi/10.1103/PhysRevD.77.124050.

[128] T. Damour and A. Nagar, "Faithful effective-one-body waveforms of small-mass-ratio coalescing black-hole binaries," *Phys.Rev.* **D76** (2007) 064028, arXiv:0705.2519 [gr-qc].

[129] M. Davis, R. Ruffini, W. Press, and R. Price, "Gravitational radiation from a particle falling radially into a Schwarzschild black hole," *Phys.Rev.Lett.* **27** (1971) 1466–1469.

[130] E. Berti, V. Cardoso, J. A. Gonzalez, U. Sperhake, M. Hannam, *et al.*, "Inspiral, merger and ringdown of unequal mass black hole binaries: A Multipolar analysis," *Phys.Rev.* **D76** (2007) 064034, arXiv:gr-qc/0703053 [GR-QC].

[131] S. Bernuzzi, A. Nagar, and A. Zenginoglu, "Binary black hole coalescence in the extreme-mass-ratio limit: testing and improving the effective-one-body multipolar waveform," *Phys.Rev.* **D83** (2011) 064010, arXiv:1012.2456 [gr-qc].

[132] M. A. Scheel, M. Boyle, T. Chu, L. E. Kidder, K. D. Matthews, *et al.*, "High-accuracy waveforms for binary black hole inspiral, merger, and ringdown," *Phys.Rev.* **D79** (2009) 024003, arXiv:0810.1767 [gr-qc].

[133] C. Darwin, "The Gravity Field of a Particle. II," *Proc.Roy.Soc. A* **263** (1961) no. 1312, 39–50. http://www.jstor.org/stable/2414136.

[134] F. Pirani, "On the Physical significance of the Riemann tensor," *Acta Phys.Polon.* **15** (1956) 389–405.

[135] J. Frenkel, "Die Elektrodynamik des rotierenden Elektrons," *Z.Phys.* **37** (1926) 243–262.

[136] L. F. Costa and J. Natário, "Center of mass, spin supplementary conditions, and the momentum of spinning particles," arXiv:1410.6443 [gr-qc].

[137] R. M. Wald, "Gravitational spin interaction," *Phys.Rev.* **D6** (1972) 406–413.

[138] R. Plyatsko, "Ultrarelativistic circular orbits of spinning particles in a Schwarzschild field," *Class.Quant.Grav.* **22** (2005) 1545–1551, arXiv:gr-qc/0507023 [gr-qc].

[139] W. de Sitter, "Einstein's theory of gravitation and its astronomical consequences, First Paper," *Mon.Not.Roy.Astron.Soc.* **76** (1916) 699–728.

[140] L. Thomas, "The motion of a spinning electron," *Nature* **117** (1926) 514.

[141] V. Fock and D. Ivanenko, "Über eine mögliche geometrische Deutung der relativistischen Quantentheorie," *Z.Phys.* **54** (1929) 798–802.

[142] W. Dixon, "Dynamics of extended bodies in general relativity. I. Momentum and angular momentum," *Proc.Roy.Soc.Lond.* **A314** (1970) 499–527.

[143] A. J. Hanson and T. Regge, "The Relativistic Spherical Top," *Annals Phys.* **87** (1974) 498.

[144] I. Bailey and W. Israel, "Lagrangian Dynamics of Spinning Particles and Polarized Media in General Relativity," *Commun.Math.Phys.* **42** (1975) 65–82.

[145] A. O. Barut, *Electrodynamics and classical theory of fields and particles.* Mac Millan, New York, 1964.

[146] C. Duval, H. H. Fliche, and J. M. Souriau, "Un modèle de particule à spin dans le champ gravitationnel et électromagnétique," *C. R. Acad. Sci. Paris.* **274** (1972) 1082.

[147] L. Brink, P. Di Vecchia, and P. S. Howe, "A Lagrangian Formulation of the Classical and Quantum Dynamics of Spinning Particles," *Nucl.Phys.* **B118** (1977) 76.

[148] A. O. Barut and N. Zanghi, "Classical model of the Dirac electron," *Phys. Rev. Lett.*. **52** (1984) .

[149] I. Khriplovich and A. Pomeransky, "Gravitational interaction of spinning bodies, center-of-mass coordinate and radiation of compact binary systems," *Phys.Lett.* **A216** (1996) 7, `arXiv:gr-qc/9602004 [gr-qc]`.

[150] A. Barducci, R. Casalbuoni, and L. Lusanna, "Supersymmetries and the Pseudoclassical Relativistic electron," *Nuovo Cim.* **A35** (1976) 377.

[151] F. Berezin and M. Marinov, "Particle Spin Dynamics as the Grassmann Variant of Classical Mechanics," *Annals Phys.* **104** (1977) 336.

[152] P. Salomonson, "Supersymmetric Actions for Spinning Particles," *Phys.Rev.* **D18** (1978) 1868–1880.

[153] R. Rietdijk and J. van Holten, "Spinning particles in Schwarzschild space-time," *Class.Quant.Grav.* **10** (1993) 575–594.

[154] E. Barausse, E. Racine, and A. Buonanno, "Hamiltonian of a spinning test-particle in curved spacetime," *Phys.Rev.* **D80** (2009) 104025, `arXiv:0907.4745 [gr-qc]`.

[155] W. Guzmán Ramírez, A. A. Deriglazov, and A. M. Pupasov-Maksimov, "Frenkel electron and a spinning body in a curved background," *JHEP* **1403** (2014) 109, `arXiv:1311.5743 [hep-th]`.

[156] L. F. O. Costa, J. Natário, and M. Zilhao, "Spacetime dynamics of spinning particles - exact gravito-electromagnetic analogies," `arXiv:1207.0470 [gr-qc]`.

[157] E. Corinaldesi and A. Papapetrou, "Spinning test particles in general relativity. 2.," *Proc.Roy.Soc.Lond.* **A209** (1951) 259–268.

[158] W. Tulczyjew, "Motion of multipole particles in General Relativity theory," *Acta Phys. Pol.* **18** (1959) 393.

[159] W. Dixon, "A covariant multipole formalism for extended test bodies in general relativity," *Il Nuovo Cimento* **34** (1964) no. 2, 317–339. http://dx.doi.org/10.1007/BF02734579.

[160] O. Semerak, "Spinning test particles in a Kerr field. I.," *Mon.Not.Roy.Astron.Soc.* **308** (1999) 863–875.

[161] K. Kyrian and O. Semerak, "Spinning test particles in a Kerr field. II.," *Mon.Not.Roy.Astron.Soc.* **382** (2007) 1922–1932.

[162] J. Steinhoff, "Spin gauge symmetry in the action principle for classical relativistic particles," arXiv:1501.04951 [gr-qc].

[163] I. Khriplovich, "Particle with internal angular momentum in a gravitational field," *Sov.Phys.JETP* **69** (1989) 217–219.

[164] A. Pomeransky, R. Senkov, and I. Khriplovich, "Spinning relativistic particles in external fields," *Phys.Usp.* **43** (2000) 1055–1066.

[165] I. Khriplovich, "Spinning Relativistic Particles in External Fields," arXiv:0801.1881 [gr-qc].

[166] L. F. O. Costa, J. Natário, and M. Zilhao, "Mathisson's helical motions demystified," *AIP Conf.Proc.* **1458** (2011) 367–370, arXiv:1206.7093 [gr-qc].

[167] A. Goldstein, *Classical Mechanics*. Pearson Education, 2002.

[168] J. W. van Holten, "Covariant Hamiltonian dynamics," *Phys.Rev.* **D75** (2007) 025027, arXiv:hep-th/0612216 [hep-th].

[169] J. W. van Holten, "On the electrodynamics of spinning particles," *Nucl.Phys.* **B356** (1991) 3–26.

[170] A. Ohashi, "Multipole particle in relativity," *Phys. Rev. D* **68** (2003) 044009. http://link.aps.org/doi/10.1103/PhysRevD.68.044009.

[171] J. W. van Holten, "Relativistic dynamics of spin in strong external fields," arXiv:hep-th/9303124 [hep-th].

[172] Rüdiger, R., "Conserved quantities of spinning test particles in General Relativity I," *Proc.Roy.Soc. Series A* **375** (1981) no. 1761, 185–193.

[173] Rüdiger R., "Conserved quantities of spinning test particles in General Relativity II," *Proc.Roy.Soc. Series A* **385** (1983) no. 1788, 229–239.

[174] G. Gibbons, R. Rietdijk, and J. van Holten, "SUSY in the sky," *Nucl.Phys.* **B404** (1993) 42–64, arXiv:hep-th/9303112 [hep-th].

[175] J. W. Van Holten, "Gravitational waves and black holes: An introduction to general relativity," *Fortsch.Phys.* **45** (1997) 439–516, arXiv:gr-qc/9704043 [gr-qc].

[176] R. Plyatsko, O. Stefanyshyn, and M. Fenyk, "Mathisson-Papapetrou-Dixon equations in the Schwarzschild and Kerr backgrounds," *Class.Quant.Grav.* **28** (2011) 195025, arXiv:1110.1967 [gr-qc].

[177] D. Bini, F. de Felice, A. Geralico, and R. T. Jantzen, "Spin precession in the Schwarzschild spacetime: Circular orbits," *Class.Quant.Grav.* **22** (2005) 2947–2970, arXiv:gr-qc/0506017 [gr-qc].

[178] D. Bini, A. Geralico, and R. T. Jantzen, "Spin-geodesic deviations in the Schwarzschild spacetime," *Gen.Rel.Grav.* **43** (2011) 959, arXiv:1408.4946 [gr-qc].

[179] N. Hari Dass, "Freeman Dyson and Gravitational Spin Precession," arXiv:1312.4738 [gr-qc].

[180] I. Kepler, *Harmonices mundi.* Johan Planck, Linz (Austria), 1619.

[181] I. Newton, *Philosophiae naturalis principia mathematica.* 1st ed. Streater, London, 1687.

[182] I. Khriplovich and A. Pomeransky, "Equations of motion of spinning relativistic particle in external fields," *J.Exp.Theor.Phys.* **86** (1998) 839–849, arXiv:gr-qc/9710098 [gr-qc].

[183] K. Heinemann, "On Stern-Gerlach forces allowed by special relativity and the special case of the classical spinning particle of Derbenev-Kondratenko," arXiv:physics/9611001 [physics].

[184] D. Bini and A. Geralico, "Spin-geodesic deviations in the Kerr spacetime," *Phys.Rev.* **D84** (2011) 104012, arXiv:1408.4952 [gr-qc].

[185] Møller, C., "Sur la dynamique des systèmes ayant un moment angulaire interne," *Ann. Inst. H. Poincaré* **11** (1949) 251–278. http://www.numdam.org/item?id=AIHP_1949__11_5_251_0.

[186] E. Poisson, "The Motion of point particles in curved space-time," *Living Rev.Rel.* **7** (2004) 6, arXiv:gr-qc/0306052 [gr-qc].